

**APPLICATION OF NEURAL NETWORK FOR  
TWO PHASE FLOW THROUGH CHOKES**

BY

**Mohammed Abdul Jaleel Al-Khalifa**

A Thesis Presented to the  
DEANSHIP OF GRADUATE STUDIES

**KING FAHD UNIVERSITY OF PETROLEUM & MINERALS**

DHAHRAN, SAUDI ARABIA

In Partial Fulfillment of the  
Requirements for the Degree of

**MASTER OF SCIENCE**

In

**PETROLEUM ENGINEERING**

JUNE, 2009

**KING FAHD UNIVERSITY OF PETROLEUM & MINERALS**

**DHAHRAN 31261, SAUDI ARABIA**

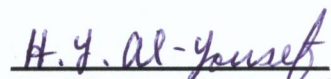
**DEANSHIP OF GRADUATE STUDIES**

This thesis written by Mohammed AbdulJaleel Al-Khalifa under the direction of his thesis advisor and approved by his thesis committee, has been presented to and accepted by the Dean of Graduate Studies, in partial fulfillment of the requirements for the degree of MASTER OF SCIENCE in Petroleum Engineering.

Thesis Committee



Dr. Muhammad Al-Marhoun  
Thesis Advisor



Dr. Hasan Al-Yousef  
Member



Dr. Mahmoud Doklah  
Member



Dr. Sidqi AbuKhamzin  
Department Chairman



Dr. Salam A. Zummo  
Dean of Graduate Studies

28/10/09

Date

# **Acknowledgment**

Praise is due to the creator of the universe and his prophet Mohammed peace be upon him, his family and faithful companions.

Acknowledgment is due to King Fahd University of Petroleum & Minerals for supporting this research, to Professor Muhammad Al-Marhoun for his continuous support, advices and for being my major advisor. I also would like to extend my thanks and appreciation to Dr. Hasan Al-Yousef and Dr. Mahmoud Doklah for being in my thesis committee. I also appreciate and would like to thank AbdulAzeem Al-Towailib, Assad Al-Towailib and Abdullah Al-Dahhan of Saudi Aramco and Dr. Sidqi Abu-Khamsin the chairman of petroleum engineering department at KFUPM for their advices and encouragement.

Special recognition and appreciation to my family for their continuous support encouragements and prayers

# **DEDICATION**

To My Parents & Grand Parents



## خلاصة الرسالة

اسم الطالب: محمد عبدالجليل عبدالله الخليفة

عنوان الدراسة: إستخدام الشبكة العصبية لتقدير تدفق الغاز و الزيت عبر صمامات التحكم

التخصص: هندسة البترول

تاريخ الشهادة: يونيو 2009 م

في السنوات الأخيرة, بدأت الشبكة العصبية الاصطناعية بالشيوع في تطبيقات هندسة البترول المختلفة. فقد تناول العديد من المؤلفين تطبيقات الشبكة العصبية الاصطناعية في تطبيقات هندسة البترول المختلفة, إلا إن أي من الباحثين السابقين لم يتناول تطبيق الشبكة العصبية لتدفق الغاز و الزيت عبر صمامات التحكم. هذه الدراسة تبين استخدام الشبكة العصبية الاصطناعية كأداة هندسية سهلة للتنبؤ بمعدل تدفق الزيت و بمقدار فتح صمامات التحكم. فقد تم تطوير نموذجين بناءً على 4031 نقطة بياناته مقسمة على النحو التالي 80% للتدريب و 10% للمصادقة و 10% للاختبار.

و بعد مراجعة و تطبيق المعادلات الرياضية الأخرى و من ثم مقارنتها مع النموذج المطور باستخدام المقاييس الإحصائية و الرسوم البيانية. أثبتت النماذج الجديدة تفوقها على النماذج الموجودة حالياً بأقل معدل نسبي مطلق للأخطاء بحوالي 3.7% للتنبؤ بفتحة الصمام و 6.7% للتنبؤ بمعدل تدفق الزيت.

درجة الماجستير في العلوم

جامعة الملك فهد للبترول و المعادن

الظهران-المملكة العربية السعودية

يونيو 2009 م

# **Thesis Abstract**

**Student Name: Mohammed Abdul-Jaleel Al-Khalifa**

**Title of Study: Application of Neural Network for Two Phase Flow  
Through Chokes**

**Major Field: Petroleum Engineering**

**Date of Degree: June 2009**

In recent years, neural network have gained popularity in the oil industry. Many authors discussed the applications of neural network in petroleum engineering applications; never the less, none of the researcher studied the application of neural networks for two phase flow through chokes. This study shows the utilization of Artificial Neural Network (ANN) as a simple engineering tool for estimating flow rate and the choke size. Two models were developed based on 4031 data points and a ratio of 80%, 10%, 10% for training, validation and testing respectively.

In this study the existing choke correlations available in the literature were reviewed, evaluated and compared with the new ANN models using statistical and graphical analysis technique. The new models were found to outperform all the existing correlations and have provided the lowest error with average absolute percent error of 3.7% for the choke size prediction and 6.7% for the flow rate estimation.

**MASTER OF SCIENCE DEGREE**

**KING FAHD UNIVERSITY OF PETROLEUM & MINERALS**

**Dhahran-Saudi Arabia**

**Date: June 2009**

## **List of Contents**

Acknowledgment .....	III
Dedication .....	IV
Abstract – In Arabic .....	V
Abstract – In English .....	VI
List of Contents.....	VII
List of Figures.....	X
List of Tables.....	XXVI

### **CHAPTER 1**

<b>Introduction.....</b>	<b>1</b>
1.1 Background.....	1
1.2 Thesis Objectives.....	3
1.3 Approach.....	3

### **CHAPTER 2**

<b>Literature Review.....</b>	<b>4</b>
2.1 Tangren et al. Analysis.....	4
2.2 Gilbert Correlation.....	5
2.3 Poettman and Beck Correlation.....	7
2.4 Omana Correlation.....	12
2.5 Fortunati Analysis.....	13
2.6 Ashford and Peirce Study.....	15
2.7 Schadeva et al. Analysis.....	18
2.8 Osman and Dokla Correlation.....	19

2.9 Surbey et al. Correlation.....	25
2.10 Towailib and Marhoun Correlation.....	29
2.11 Attar and Abdul Majeed Correlation.....	30
2.12 Elgibaly and Nashawi Correlation.....	31
2.13 Perkins Approach.....	33
2.14 Safran and Kelker Equation.....	39
2.15 Rumah and Bizanti Correlation.....	41
2.16 Bizanti and Mansouri Correlation.....	42
2.17 Pilehvari Correlation.....	42

## **CHAPTER 3**

<b>Current Study Data Acquisition.....</b>	<b>44</b>
3.1 Data Description.....	44
3.1.1 Flow Rates.....	44
3.1.2 Tubing wellhead pressure and Temperature.....	45
3.1.3 Choke Sizes.....	45
3.1.4 Production Test Data.....	45
3.1.5 Fluid Properties Data.....	45
3.1.6 Data Screening.....	46

## **CHAPTER 4**

<b>Model Development.....</b>	<b>48</b>
4.1 Artificial Neural Network.....	48
4.1.1 Introduction.....	48
4.1.2 Network Learning.....	50
4.1.3 Network Architecture.....	50

4.1.4 Transfer Function.....	51
4.2 Data Handling.....	58
4.3 Model Development.....	58
4.3.1 Selection of Independent Variables.....	59
4.3.2 Model Architecture and Optimization.....	60
4.3.3 Description of Trained Neural Network Model.....	77
4.3.3.1 Choke Size Prediction.....	77
4.3.3.2 Flow Rate Estimation.....	79
<b>CHAPTER 5</b>	
<b>Results &amp; Discussion.....</b>	82
5.1 Statistical Analysis.....	82
5.1.1 Literature Correlation.....	83
5.1.2 Newly Developed ANN Model.....	91
5.2 Graphical Analysis.....	92
5.2.1 Choke Size.....	92
5.2.2 Flow Rate.....	94
5.3 Incremental Analysis .....	98
5.3.1 Choke Size.....	98
5.3.2 Flow Rate.....	99
<b>CHAPTER 6</b>	
<b>Conclusions.....</b>	226
References.....	227
Vitae.....	230

## List of Figures

<b>Figure No.</b>	<b>Figure Title</b>	<b>Page No.</b>
Figure 2.1	Poettman & Beck Chart for 20 API.....	9
Figure 2.2	Poettman & Beck Chart for 30 API.....	10
Figure 2.3	Poettman & Beck Chart for 40 API.....	11
Figure 2.4	Guzhov and Medviediev Experimental Curve.....	16
Figure 2.5	Osman & Dokla nomograph for the First Equation.....	21
Figure 2.6	Osman & Dokla nomograph for the Second Equation...	22
Figure 2.7	Osman & Dokla nomograph for the Third Equation...	23
Figure 2.8	Osman & Dokla nomograph for the Fourth Equation....	24
Figure 2.9	Procedure Used in Surbey et al. Study.....	28
Figure 2.10	Perkins computer program logic flow diagram.....	38
Figure 4.1	Artificial Neuron (After Freeman <sup>16</sup> ).....	49
Figure 4.2	Supervised Learning Model (After Simon Haykin <sup>20</sup> )....	52
Figure 4.3	Architecture of Neural Network with Two Hidden Layers (After Simon Haykin <sup>20</sup> ).....	53
Figure 4.4	Threshold Function (After Simon Haykin <sup>20</sup> ).....	55
Figure 4.5	Piecewise linear Function (After Simon Haykin <sup>20</sup> ).....	56
Figure 4.6	Sigmoid Function (After Simon Haykin <sup>20</sup> ).....	57
Figure 4.7	Choke Size Neural Network Model.....	62
Figure 4.8	Flow Rate Neural Network Model.....	63
Figure 4.9	Impact of Neurons in First Hidden Layer on Absolute Error of Choke Size Prediction.....	64
Figure 4.10	Impact of Neurons in First Hidden Layer on Correlation Coefficient of Choke Size Prediction.....	65



Figure 4.11	Impact of Neurons in Second Hidden Layer on Absolute Error of Choke Size Prediction.....	66
Figure 4.12	Impact of Neurons in Second Hidden Layer on Correlation Coefficient of Choke Size Prediction.....	67
Figure 4.13	Impact of Neurons in Third Hidden Layer on Absolute Error of Choke Size Prediction.....	68
Figure 4.14	Impact of Neurons in Third Hidden Layer on Correlation Coefficient of Choke Size Prediction.....	69
Figure 4.15	Impact of Neurons in First Hidden Layer on Absolute Error of Flow Rate Prediction.....	70
Figure 4.16	Impact of Neurons in First Hidden Layer on Correlation Coefficient of Flow Rate Prediction.....	71
Figure 4.17	Impact of Neurons in Second Hidden Layer on Absolute Error of Flow Rate Prediction.....	72
Figure 4.18	Impact of Neurons in Second Hidden Layer on Correlation Coefficient of Flow Rate Prediction.....	73
Figure 4.19	Impact of Neurons in Third Hidden Layer on Absolute Error of Flow Rate Prediction.....	74
Figure 4.20	Impact of Neurons in Third Hidden Layer on Correlation Coefficient of Flow Rate Prediction.....	75
Figure 5.1	Statistical Accuracy of Choke Size Prediction using Empirical Correlation Original Coefficients.....	84
Figure 5.2	Statistical Accuracy of Choke Size Prediction using Empirical Correlation after Regression & Robust fit....	86
Figure 5.3	Statistical Accuracy of Flow Rate Estimation using Empirical Correlation Original Coefficients.....	88

Figure 5.4	Statistical Accuracy of Flow Rate Estimation using Empirical Correlation after Regression & Robust fit....	90
Figure 5.5	Correlation Coefficients of Empirical Correlation for Choke Size Prediction.....	96
Figure 5.6	Correlation Coefficients of Empirical Correlation for Flow Rate Estimation.....	97
Figure 5.7	Accuracy of Correlation for Choke Size Prediction for Different Flow Rate ranges. (Absolute Average Percent Relative Error).....	101
Figure 5.8	Accuracy of Correlation for Choke Size Prediction for Different Flow Rate ranges. (Root Mean Square Error).	102
Figure 5.9	Accuracy of Correlation after Regression for Choke Size Prediction for Different Flow Rate ranges. (Absolute Average Percent Relative Error).....	103
Figure 5.10	Accuracy of Correlation after Regression for Choke Size Prediction for Different Flow Rate ranges. (Root Mean Square Error).....	104
Figure 5.11	Accuracy of Correlation after Robust fit for Choke Size Prediction for Different Flow Rate ranges. (AAPE).....	105
Figure 5.12	Accuracy of Correlation after Robust fit for Choke Size Prediction for Different Flow Rate ranges. (RMSE).....	106
Figure 5.13	Accuracy of Correlation for Flow Rate Estimation for Different Flow Rate ranges. (Absolute Average Percent Relative Error).....	107
Figure 5.14	Accuracy of Correlation for Flow Rate Estimation for	

	Different Flow Rate ranges (Root Mean Square Error)..	108
Figure 5.15	Accuracy of Correlation after Regression for Flow Rate Estimation for Different Flow Rate ranges (Absolute Average Percent Relative Error).....	109
Figure 5.16	Accuracy of Correlation after Regression for Flow Rate Estimation for Different Flow Rate ranges. (Root Mean Square Error).....	110
Figure 5.17	Accuracy of Correlation after Robust fit for Flow Rate Estimation for Different Flow Rate ranges. (Absolute Average Percent Relative Error).....	111
Figure 5.18	Accuracy of Correlation after Robust fit for Flow Rate Estimation for Different Flow Rate ranges. (Root Mean Square Error).....	112
Figure 5.19	Error Distribution Plot of Choke Size Prediction for Testing set (ANN model).....	113
Figure 5.20	Error Distribution Plot of Choke Size Prediction for Validation set (ANN model).....	114
Figure 5.21	Error Distribution Plot of Choke Size Prediction for Training set (ANN model).....	115
Figure 5.22	Cross Plot of Choke Size Prediction for Testing set (ANN model).....	116
Figure 5.23	Cross Plot of Choke Size Prediction for Validation set (ANN model).....	117
Figure 5.24	Cross Plot of Choke Size Prediction for Training set (ANN model).....	118

Figure 5.25	Scatter and Overlay Plot of Choke Size Prediction for Testing set (ANN model).....	119
Figure 5.26	Scatter and Overlay Plot of Choke Size Prediction for Validation set (ANN model).....	120
Figure 5.27	Scatter and Overlay Plot of Choke Size Prediction for Training set (ANN model).....	121
Figure 5.28	Error Distribution Plot of Flow Rate Estimation for Testing set (ANN model).....	122
Figure 5.29	Error Distribution Plot of Flow Rate Estimation for Validation set (ANN model).....	123
Figure 5.30	Error Distribution Plot of Flow Rate Estimation for Training set (ANN model).....	124
Figure 5.31	Cross Plot of Flow Rate Estimation for Testing set (ANN model).....	125
Figure 5.32	Cross Plot of Flow Rate Estimation for Validation set (ANN model).....	126
Figure 5.33	Cross Plot of Flow Rate Estimation for Training set (ANN model).....	127
Figure 5.34	Scatter & Overlay Plot of Flow Rate Estimation for Testing set (ANN model).....	128
Figure 5.35	Scatter & Overlay Plot of Flow Rate Estimation for Validation set (ANN model).....	129
Figure 5.36	Scatter & Overlay Plot of Flow Rate Estimation for Training set (ANN model).....	130
Figure 5.37	Cross, Histogram, Scatter and Overlay plots for Ashford Empirical correlation (Choke Size Prediction).	131

Figure 5.38	Cross, Histogram, Scatter and Overlay plots for Ashford Empirical correlation after regression. (Choke Size Prediction).....	132
Figure 5.39	Cross, Histogram, Scatter and Overlay plots for Ashford Empirical correlation after robust fit. (Choke Size Prediction).....	133
Figure 5.40	Cross, Histogram, Scatter and Overlay plots for Bizanti & Mansouri Empirical correlation. (Choke Size Prediction).....	134
Figure 5.41	Cross, Histogram, Scatter and Overlay plots for Bizanti & Mansouri Empirical correlation after regression. (Choke Size Prediction).....	135
Figure 5.42	Cross, Histogram, Scatter and Overlay plots for Bizanti & Mansouri Empirical correlation after robust fit. (Choke Size Prediction).....	136
Figure 5.43	Cross, Histogram, Scatter and Overlay plots for Elgibaly & Nashawi Empirical correlation. (Choke Size Prediction).....	137
Figure 5.44	Cross, Histogram, Scatter and Overlay plots for Elgibaly & Nashawi Empirical correlation after regression. (Choke Size Prediction).....	138
Figure 5.45	Cross, Histogram, Scatter and Overlay plots for Elgibaly & Nashawi Empirical correlation after robust fit. (Choke Size Prediction).....	139
Figure 5.46	Cross, Histogram, Scatter and Overlay plots for Pilehvari Empirical correlation after regression. (Choke	

	Size Prediction).....	140
Figure 5.47	Cross, Histogram, Scatter and Overlay plots for Pilehvari Empirical correlation after robust fit. (Choke Size Prediction).....	141
Figure 5.48	Cross, Histogram, Scatter and Overlay plots for Secen Empirical correlation. (Choke Size Prediction).....	142
Figure 5.49	Cross, Histogram, Scatter and Overlay plots for Secen Empirical correlation after regression. (Choke Size Prediction).....	143
Figure 5.50	Cross, Histogram, Scatter and Overlay plots for Secen Empirical correlation after robust fit. (Choke Size Prediction).....	144
Figure 5.51	Cross, Histogram, Scatter and Overlay plots for Omana Empirical correlation. (Choke Size Prediction).....	145
Figure 5.52	Cross, Histogram, Scatter and Overlay plots for Omana Empirical correlation after regression. (Choke Size Prediction).....	146
Figure 5.53	Cross, Histogram, Scatter and Overlay plots for Omana Empirical correlation after robust fit. (Choke Size Prediction).....	147
Figure 5.54	Cross, Histogram, Scatter and Overlay plots for Towailib & Marhoun Empirical correlation. (Choke Size Prediction).....	148
Figure 5.55	Cross, Histogram, Scatter and Overlay plots for Towailib & Marhoun Empirical correlation after regression. (Choke Size Prediction).....	149



Figure 5.56	Cross, Histogram, Scatter and Overlay plots for Towailib & Marhoun Empirical correlation after robust fit. (Choke Size Prediction).....	150
Figure 5.57	Cross, Histogram, Scatter and Overlay plots for Rumah & Bizanti Empirical correlation. (Choke Size Prediction).....	151
Figure 5.58	Cross, Histogram, Scatter and Overlay plots for Rumah & Bizanti Empirical correlation after regression. (Choke Size Prediction).....	152
Figure 5.59	Cross, Histogram, Scatter and Overlay plots for Rumah & Bizanti Empirical correlation after robust fit. (Choke Size Prediction).....	153
Figure 5.60	Cross, Histogram, Scatter and Overlay plots for Poettman & Beck Empirical correlation. (Choke Size Prediction).....	154
Figure 5.61	Cross, Histogram, Scatter and Overlay plots for Poettman & Beck Empirical correlation after regression. (Choke Size Prediction).....	155
Figure 5.62	Cross, Histogram, Scatter and Overlay plots for Poettman & Beck Empirical correlation after robust fit. (Choke Size Prediction).....	156
Figure 5.63	Cross, Histogram, Scatter and Overlay plots for Attar & Abdul-Majeed Empirical correlation. (Choke Size Prediction).....	157
Figure 5.64	Cross, Histogram, Scatter and Overlay plots for Attar & Abdul-Majeed Empirical correlation after	

	regression. (Choke Size Prediction).....	158
Figure 5.65	Cross, Histogram, Scatter and Overlay plots for Attar & Abdul-Majeed Empirical correlation after robust fit. (Choke Size Prediction).....	159
Figure 5.66	Cross, Histogram, Scatter and Overlay plots for Surbey Empirical correlation. (Choke Size Prediction).....	160
Figure 5.67	Cross, Histogram, Scatter and Overlay plots for Surbey Empirical correlation after regression. (Choke Size Prediction).....	161
Figure 5.68	Cross, Histogram, Scatter and Overlay plots for Surbey Empirical correlation after robust fit. (Choke Size Prediction).....	162
Figure 5.69	Cross, Histogram, Scatter and Overlay plots for Gilbert Empirical correlation. (Choke Size Prediction).....	163
Figure 5.70	Cross, Histogram, Scatter and Overlay plots for Gilbert Empirical correlation after regression. (Choke Size Prediction).....	164
Figure 5.71	Cross, Histogram, Scatter and Overlay plots for Gilbert Empirical correlation after robust fit. (Choke Size Prediction).....	165
Figure 5.72	Cross, Histogram, Scatter and Overlay plots for Achong Empirical correlation. (Choke Size Prediction).....	166
Figure 5.73	Cross, Histogram, Scatter and Overlay plots for Achong Empirical correlation after regression. (Choke Size Prediction).....	167

Figure 5.74	Cross, Histogram, Scatter and Overlay plots for Achong Empirical correlation after robust fit. (Choke Size Prediction).....	168
Figure 5.75	Cross, Histogram, Scatter and Overlay plots for Baxendaell Empirical correlation. (Choke Size Prediction).....	169
Figure 5.76	Cross, Histogram, Scatter and Overlay plots for Baxendaell Empirical correlation after regression. (Choke Size Prediction).....	170
Figure 5.77	Cross, Histogram, Scatter and Overlay plots for Baxendaell Empirical correlation after robust fit. (Choke Size Prediction).....	171
Figure 5.78	Cross, Histogram, Scatter and Overlay plots for Ros Empirical correlation. (Choke Size Prediction).....	172
Figure 5.79	Cross, Histogram, Scatter and Overlay plots for Ros Empirical correlation after regression. (Choke Size Prediction).....	173
Figure 5.80	Cross, Histogram, Scatter and Overlay plots for Ros Empirical correlation after robust fit. (Choke Size Prediction).....	174
Figure 5.81	Cross, Histogram, Scatter and Overlay plots for Osman & Dokla Empirical correlation. (Choke Size Prediction).....	175
Figure 5.82	Cross, Histogram, Scatter and Overlay plots for Osman & Dokla Empirical correlation after regression. (Choke Size Prediction).....	176

Figure 5.83	Cross, Histogram, Scatter and Overlay plots for Osman & Dokla Empirical correlation after robust fit. (Choke Size Prediction).....	177
Figure 5.84	Cross, Histogram, Scatter and Overlay plots for Ashford Empirical correlation. (Flow Rate Prediction)..	178
Figure 5.85	Cross, Histogram, Scatter and Overlay plots for Ashford Empirical correlation after regression. (Flow Rate Prediction).....	179
Figure 5.86	Cross, Histogram, Scatter and Overlay plots for Ashford Empirical correlation after robust fit. (Flow Rate Prediction).....	180
Figure 5.87	Cross, Histogram, Scatter and Overlay plots for Bizanti & Mansouri Empirical correlation. (Flow Rate Prediction).....	181
Figure 5.88	Cross, Histogram, Scatter and Overlay plots for Bizanti & Mansouri Empirical correlation after regression. (Flow Rate Prediction).....	182
Figure 5.89	Cross, Histogram, Scatter and Overlay plots for Bizanti & Mansouri Empirical correlation after robust fit. (Flow Rate Prediction).....	183
Figure 5.90	Cross, Histogram, Scatter and Overlay plots for Elgibaly & Nashawi Empirical correlation. (Flow Rate Prediction).....	184
Figure 5.91	Cross, Histogram, Scatter and Overlay plots for Elgibaly & Nashawi Empirical correlation after regression. (Flow Rate Prediction).....	185

Figure 5.92	Cross, Histogram, Scatter and Overlay plots for Elgibaly & Nashawi Empirical correlation after robust fit. (Flow Rate Prediction).....	186
Figure 5.93	Cross, Histogram, Scatter and Overlay plots for Pilehvari Empirical correlation. (Flow Rate Estimation)	187
Figure 5.94	Cross, Histogram, Scatter and Overlay plots for Pilehvari Empirical correlation after regression. (Flow Rate Prediction).....	188
Figure 5.95	Cross, Histogram, Scatter and Overlay plots for Pilehvari Empirical correlation after robust fit. (Flow Rate Prediction).....	189
Figure 5.96	Cross, Histogram, Scatter and Overlay plots for Secen Empirical correlation. (Flow Rate Prediction).....	190
Figure 5.97	Cross, Histogram, Scatter and Overlay plots for Secen Empirical correlation after regression. (Flow Rate Prediction).....	191
Figure 5.98	Cross, Histogram, Scatter and Overlay plots for Secen Empirical correlation after robust fit. (Flow Rate Prediction).....	192
Figure 5.99	Cross, Histogram, Scatter and Overlay plots for Omana Empirical correlation. (Flow Rate Prediction).....	193
Figure 5.100	Cross, Histogram, Scatter and Overlay plots for Omana Empirical correlation after regression. (Flow Rate Prediction).....	194
Figure 5.101	Cross, Histogram, Scatter and Overlay plots for Omana Empirical correlation after robust fit. (Flow Rate	

	Prediction).....	195
Figure 5.102	Cross, Histogram, Scatter and Overlay plots for Towailib & Marhoun Empirical correlation. (Flow Rate Prediction).....	196
Figure 5.103	Cross, Histogram, Scatter and Overlay plots for Towailib & Marhoun Empirical correlation after regression. (Flow Rate Prediction).....	197
Figure 5.104	Cross, Histogram, Scatter and Overlay plots for Towailib & Marhoun Empirical correlation after robust fit. (Flow Rate Prediction).....	198
Figure 5.105	Cross, Histogram, Scatter and Overlay plots for Rumah & Bizanti Empirical correlation. (Flow Rate Prediction).....	199
Figure 5.106	Cross, Histogram, Scatter and Overlay plots for Rumah & Bizanti Empirical correlation after regression. (Flow Rate Prediction).....	200
Figure 5.107	Cross, Histogram, Scatter and Overlay plots for Rumah & Bizanti Empirical correlation after robust fit. (Flow Rate Prediction).....	201
Figure 5.108	Cross, Histogram, Scatter and Overlay plots for Poettman & Beck Empirical correlation. (Flow Rate Prediction).....	202
Figure 5.109	Cross, Histogram, Scatter and Overlay plots for Poettman & Beck Empirical correlation after regression. (Flow Rate Prediction).....	203
Figure 5.110	Cross, Histogram, Scatter and Overlay plots for	204



	Poettman & Beck Empirical correlation after robust fit. (Flow Rate Prediction).....	
Figure 5.111	Cross, Histogram, Scatter and Overlay plots for Attar & Abdul-Majeed Empirical correlation. (Flow Rate Prediction).....	205
Figure 5.112	Cross, Histogram, Scatter and Overlay plots for Attar & Abdul-Majeed Empirical correlation after regression. (Flow Rate Prediction).....	206
Figure 5.113	Cross, Histogram, Scatter and Overlay plots for Attar & Abdul-Majeed Empirical correlation after robust fit. (Flow Rate Prediction).....	207
Figure 5.114	Cross, Histogram, Scatter and Overlay plots for Surbey Empirical correlation. (Flow Rate Prediction).....	208
Figure 5.115	Cross, Histogram, Scatter and Overlay plots for Surbey Empirical correlation after regression. (Flow Rate Prediction).....	209
Figure 5.116	Cross, Histogram, Scatter and Overlay plots for Surbey Empirical correlation after robust fit. (Flow Rate Prediction).....	210
Figure 5.117	Cross, Histogram, Scatter and Overlay plots for Gilbert Empirical correlation. (Flow Rate Prediction).....	211
Figure 5.118	Cross, Histogram, Scatter and Overlay plots for Gilbert Empirical correlation after regression. (Flow Rate Prediction).....	212
Figure 5.119	Cross, Histogram, Scatter and Overlay plots for Gilbert Empirical correlation after robust fit. (Flow Rate	213

	Prediction).....	
Figure 5.120	Cross, Histogram, Scatter and Overlay plots for Achong Empirical correlation. (Flow Rate Prediction)..	214
Figure 5.121	Cross, Histogram, Scatter and Overlay plots for Achong Empirical correlation after regression. (Flow Rate Prediction).....	215
Figure 5.122	Cross, Histogram, Scatter and Overlay plots for Achong Empirical correlation after robust fit. (Flow Rate Prediction).....	216
Figure 5.123	Cross, Histogram, Scatter and Overlay plots for Baxendaell Empirical correlation. (Flow Rate Prediction).....	217
Figure 5.124	Cross, Histogram, Scatter and Overlay plots for Baxendaell Empirical correlation after regression. (Flow Rate Prediction).....	218
Figure 5.125	Cross, Histogram, Scatter and Overlay plots for Baxendaell Empirical correlation after robust fit. (Flow Rate Prediction).....	219
Figure 5.126	Cross, Histogram, Scatter and Overlay plots for Ros Empirical correlation. (Flow Rate Prediction).....	220
Figure 5.127	Cross, Histogram, Scatter and Overlay plots for Ros Empirical correlation after regression. (Flow Rate Prediction).....	221
Figure 5.128	Cross, Histogram, Scatter and Overlay plots for Ros Empirical correlation after robust fit. (Flow Rate Prediction).....	222

Figure 5.129	Cross, Histogram, Scatter and Overlay plots for Osman & Dokla Empirical correlation. (Flow Rate Prediction).....	223
Figure 5.130	Cross, Histogram, Scatter and Overlay plots for Osman & Dokla Empirical correlation after regression. (Flow Rate Prediction).....	224
Figure 5.131	Cross, Histogram, Scatter and Overlay plots for Osman & Dokla Empirical correlation after robust fit. (Flow Rate Prediction).....	225

## List of Tables

<b>Table No.</b>	<b>Table Title</b>	<b>Page No.</b>
Table 2.1	Coefficients Values for Various Researchers.....	7
Table 3.1	Production Data Summary.....	47
Table 3.2	PVT Data Summary.....	47
Table 4.1	Impact of Neurons in First Hidden Layer on Absolute Error and Correlation Coefficient of Choke Size Prediction.....	76
Table 4.2	Impact of Neurons in Second Hidden Layer on Absolute Error and Correlation Coefficient of Choke Size Prediction.....	76
Table 4.3	Impact of Neurons in Third Hidden Layer on Absolute Error and Correlation Coefficient of Choke Size Prediction.....	76
Table 4.4	Impact of Neurons in First Hidden Layer on Absolute Error and Correlation Coefficient of Flow Rate Prediction.....	76
Table 4.5	Impact of Neurons in Second Hidden Layer on Absolute Error and Correlation Coefficient of Flow Rate Prediction.....	77
Table 4.6	Impact of Neurons in Third Hidden Layer on Absolute Error and Correlation Coefficient of Flow Rate Prediction.....	77
Table 4.7	The Mean and Standard Deviation Values for Training Data.....	78
Table 4.8	Summary of Choke Size Neural Network Model.....	79

Table 4.9	Summary of Flow Rate Neural Network Model.....	81
Table 5.1	Statistical Accuracy of Choke Size Prediction using Empirical Correlation Original Coefficients.....	83
Table 5.2	Statistical Accuracy of Choke Size Prediction using Empirical Correlation after Regression.....	85
Table 5.3	Statistical Accuracy of Choke Size Prediction using Empirical Correlation after Robust fit.....	85
Table 5.4	Statistical Accuracy of Flow Rate Estimation using Empirical Correlation Original Coefficients.....	87
Table 5.5	Statistical Accuracy of Flow Rate Estimation using Empirical Correlation after Regression.....	87
Table 5.6	Statistical Accuracy of Flow Rate Estimation using Empirical Correlation after Robustfit.....	89
Table 5.7	Statistical Accuracy of Choke Size Prediction of the Newly Developed Model Using ANN.....	91
Table 5.8	Statistical Accuracy of Flow Rate Estimation of the Newly Developed Model Using ANN.....	91
Table 5.9	Choke Size Ranges Used in Incremental Analysis....	100
Table 5.10	Flow Rate Ranges Used in Incremental Analysis.....	100

# CHAPTER 1

## INTRODUCTION

### 1.1 Background:

Wellhead choke is a wellhead assembly component that precisely controls the flow of oil or gas to achieve a carefully calculated rate of production. Chokes come in two basic types: adjustable and positive. Adjustable chokes are often used during completion operations to allow the operator to clean and flow test the well. Once the optimum flow rate is determined, the adjustable choke is usually replaced with a positive choke for production. A positive choke is commonly calibrated in 64ths of an inch, from zero to full bore opening.

Wellhead chokes are widely used in the oil and gas industry to

- Control the well stream;
- Produce the reservoir at the most optimum rate;
- Prevent water or gas coning;
- Maintain back pressure;
- Protect formation and surface equipment from abnormal pressure fluctuation.

Accurate correlation for estimating multiphase flow rate is important for quick evaluation of well performance. The behavior of oil and gas flow through chokes has two types, critical and sub-critical. Critical flow occur



when the velocity is equal or greater than the sound velocity, for this condition to exist, downstream or line pressure must be approximately 0.55 of the tubing or upstream pressure. In critical flow the rate depends on the upstream pressure and gas oil ratio only, thus, the changes in the flow line pressure doesn't impact the flow rate. Nodal analysis which is usually utilized for well performance evaluation, eliminate modeling the flow behavior in choke by assuming the flow is always critical and empirical correlations are usually utilized for all well condition. While this is an acceptable solution most of the time, it simply doesn't always provide an accurate model of surface choke behavior.

Several studies on (liquid-gas) two phase flow through choke were conducted. These studies focused on finding relationship between choke size, flow rate and other wellhead parameters. These theories and correlations describe two phase flow through restrictions and are used to determine the most optimum size of the choke or to estimate flow rate using wellhead parameters. These empirical correlations were based on certain range of parameters involved in the correlation. To determine the strength and weakness of these correlations, statistical analyses are usually utilized.

In recent years, neural network which is a parallel-distributed information processing models that can recognize highly complex patterns within available data have gained popularity in petroleum applications. Many authors discussed the applications of neural network in different petroleum engineering subjects such as PVT, reservoir characterization, reservoir simulation and others. Never the less, none of the researchers studied the application of neural networks for two phase flow through chokes.

## **1.2 Thesis Objectives**

The purpose of this study is to review theories and correlations available in the literature and to develop new Artificial Neural Network for two phase flow through chokes, using data from several fields and reservoirs.

## **1.3 Approach**

Two Artificial neural network models will be develop using Matlab software; the models topology will be optimized to determine the best architecture in terms of number of hidden layers and number of neurons in each hidden layer. The input layer will consists of variables involved in the process. The output layer will contain the estimated flow rate for one model and the choke size in the other model.

In addition, Production data from Middle East oil wells will be collected and utilized to evaluate the new and existing correlations. Different statistical analyses will then be carried out on the existing empirical correlations and the newly developed ANN models for comparison purposes. The model with the lowest average absolute percent error will be recommended for industry future utilization.

# **CHAPTER 2**

## **LITERATURE REVIEW**

### **2.1 Tangeren et al. Analysis<sup>1</sup> (1949)**

Tangeren et al. (1949) were among the first to publish significant findings on multiphase flow through chokes. The importance of their research was that it demonstrated that for a compressible mixture, there exists a critical flow velocity above which pressure fluctuations cannot be transmitted upstream. In their study they applied the basic laws of continuity, momentum, energy and ideal gas equation of state to a mixture in such a way to derive an equation of state and an equation of motion for the mixture. To simplify their analysis the following assumptions were made:

1. The liquid is an incompressible fluid and effects due to viscosity, surface tension, and vapor pressure are unimportant.
2. The gas is an ideal gas, with negligible viscosity, constant specific heat and is insoluble in the liquid.
3. The mixture is "homogeneous" in the sense that the bubbles of gas are so small and uniformly distributed that an arbitrary small sample contains the same mass ratio of gas to liquid as the whole mixture.
4. The gas and liquid are always at the same temperature and the flow is insulated (e.g. adiabatic).

5. The flow is one-dimensional, laminar, and expands or compresses slowly enough that inertial transient may be ignored.
6. A slowly varying pressure change or signal is transmitted through the mixture with a definite critical velocity, as distinguished from the irregular distribution and decrease of high frequency pressure waves.

Tangeren et al derived an equation of state, applied Newton equation of motion, and utilized Bernoulli equation for an incompressible fluid to come up with a dimensionless form of the velocity equation as follow:

$$\rho_f \left( \frac{u^2}{2} \right) P_0 = - f_0 (\ln P/P_0) + 1 - P/P_0 \quad (2.1)$$

$$f_0 = \mu \rho_f / \rho_{g0} \quad (2.2)$$

$\rho_f$ : density of fluid mixture slug/ft<sup>3</sup>.

$u$ : velocity, ft/second.

$P_0$ : pressure under initial condition lb/ft<sup>2</sup>.

$P$ : pressure lb/ft<sup>2</sup>.

$\rho_{g0}$ : Gas density at initial condition, slug/ft<sup>3</sup>.

## 2.2 Gilbert Correlation <sup>2</sup> (1954)

Gilbert (1954) developed an empirical correlation based on daily production data of a Californian oil field that relates the liquid flow rate, the gas-liquid ratio, the choke diameter, and the upstream pressure. Using his formula any one of the four parameters can be found when the other parameters are known. The choke size of his data ranges from 6 to 18 sixty fourth of an inch and the oil gravity from 25 to 40° API. Gilbert (1954) assumed that the mixture velocity is higher than the sound

velocity. Thus the formula is valid only when the upstream pressure is more than 1.7 times the downstream pressure ( $P_{ds} / P_{us} < 0.55$ ). He also noted that the formula was extremely sensitive to the choke diameter: errors of 1/128ths of an inch in the choke diameter can cause an error of 5 to 20% in the flowing wellhead pressure estimate.

$$P_{us} = (Q_L 435 R_p^{0.546}) / (S^{1.89}) \quad (2.3)$$

Where

$Q_L$  = gross liquid rate, STBD

$P_{us}$  = flowing wellhead (Upstream) pressure, psia

$P_{ds}$  = downstream pressure, psia

$S$  = bean diameter, 64ths of an inch

$R_p$  = producing gas-liquid ratio, MSCF/STB

If the gas-liquid ratio is considered constant, then the flowing wellhead pressure and the gross liquids production are linearly proportional to each other as:

$$P_{us} = K Q_L \quad (2.4)$$

Where

$$K = 435 R_p^{0.5} S^{1.89} \quad (2.5)$$

Gilbert's (1954) work was followed by several researchers making modifications to his formula. The researchers included Baxendall (1957), Ros (1959), and Achong (1961). All of the formulas kept the same basic form of

$$P_{us} = A R_p^B Q S^C \quad (2.6)$$

Where only the constants were changed; the values for the coefficients for the various researchers are listed in Table 2.1. Baxendall's revision (1957) of the Gilbert equation was simply an update of the coefficients based on incremental data. Ros (1959) extended the theoretical work of Tangeren (1949) and in the process formulated his own version of the Gilbert (1954) equation to match the particular data he was working with. Achong (1961) modified the Gilbert (1954) equation to match the performance of 104 wells in the Lake Maracaibo Field of Venezuela.

Table 2.1 Coefficients Values for Various Researchers (After Gilbert)

Table 4.1: Empirical Coefficients for Two-Phase Critical Flow Correlations.			
Correlation	A	B	C
Gilbert (1954)	10.00	0.546	1.89
Baxendall (1957)	9.56	0.546	1.93
Ros (1959)	17.40	0.500	2.00
Achong (1961)	3.82	0.650	1.88

### 2.3 Poettman and Beck Correlation <sup>6</sup> (1963)

To make Ros equation available for oil field personal, it has been converted to oil field units and reduced to graphical form. In their construction of graph, Borden and Rzasa correlation was used for oil gravities of 20, 30 and 40° API. A gas gravity of 0.6 was assumed in constructing the charts. The effect of variation in gas gravity on ultimate results is small and can be neglected. Figures 2.1, 2.2 and 2.3 show their developed chart for the 20, 30 and 40° API gravity oil respectively. The 20° API chart should be used for gravities ranging from 15-24° API. Similarly, the 30° API chart should be used for gravities ranging from 25 to 34° API, and the 40° API chart, for gravities from 35° and higher. The charts are not valid if there is water production with the oil. Poettman and

Beck have also reduced its graphical form, resulting in the following expression:

$$Q = 88992 A / (5.61 \rho_{ls} + 0.0765 \gamma_g R_s) \\ [9273.6 P / (VL (1+0.5 mL))]^{0.5} \\ [0.4513 (R+0.766)^{0.5} / (R+0.5663)] \quad (2.7)$$

$$R = 0.00504 T Z (R_s - S_s) / (P B_o) \quad (2.8)$$

$$mL = 1 / (1+R \rho_g / \rho_L) \quad (2.9)$$

$$VL = mL / \rho_L \quad (2.10)$$

Where:

Q: barrels of stock tank oil/day.

A: Cross sectional area of throat in square feet.

$\rho_{ls}$ : density of crude in lb/ft<sup>3</sup> at 60° F and 14.7 psia.

$\gamma_g$ : gas gravity referred to air at 60° F and 14.7 psia.

$R_s$ : Solution gas oil ratio in scf of gas per barrel of stock tank oil.

P: upstream or tubing pressure in lb per square foot.

$\rho_g$ : density of gas at pressure P and 85° F, in pound-mass / cu. Ft.

$\rho_L$ : density of crude at pressure P and 85° F, in pound-mass / cu. Ft.

T: Tubing Temperature (Absolute) in Rankin

Z: Compressibility factor of gas at tubing pressure and 85° F.

$S_s$ : Solubility of gas in crude at tubing pressure and 85° F, scf/bbl.

$B_o$ : formation volume factor of crude at tubing pressure and 85° F.

VL: volume of liquid per unit mass of total fluid, cu ft./ lb.

mL: mass of liquid per unit mass of total fluid, dimensionless.

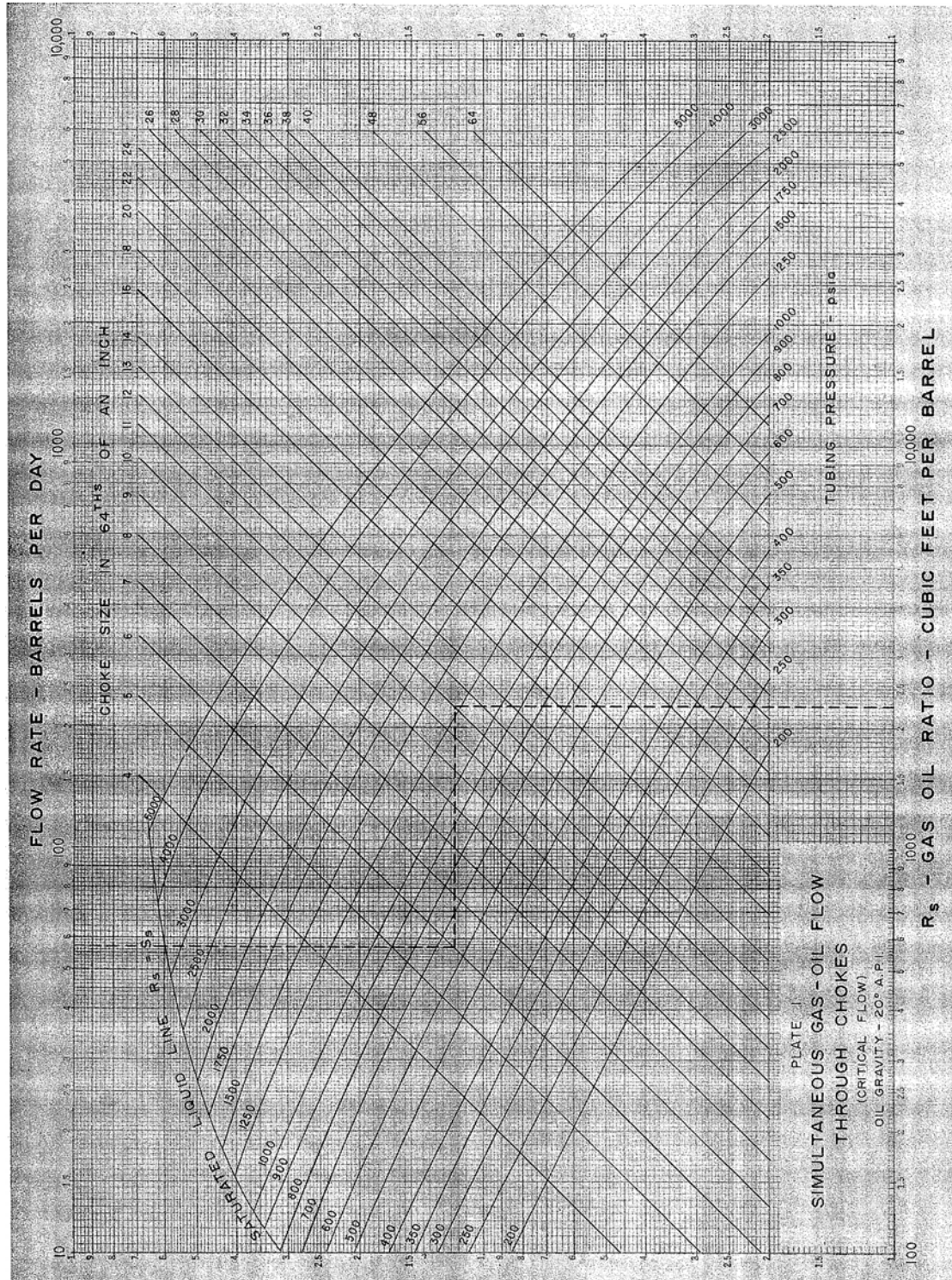


Figure 2.1: Poettman & Beck Chart for 20° API (After Poettman & Beck <sup>6</sup>)



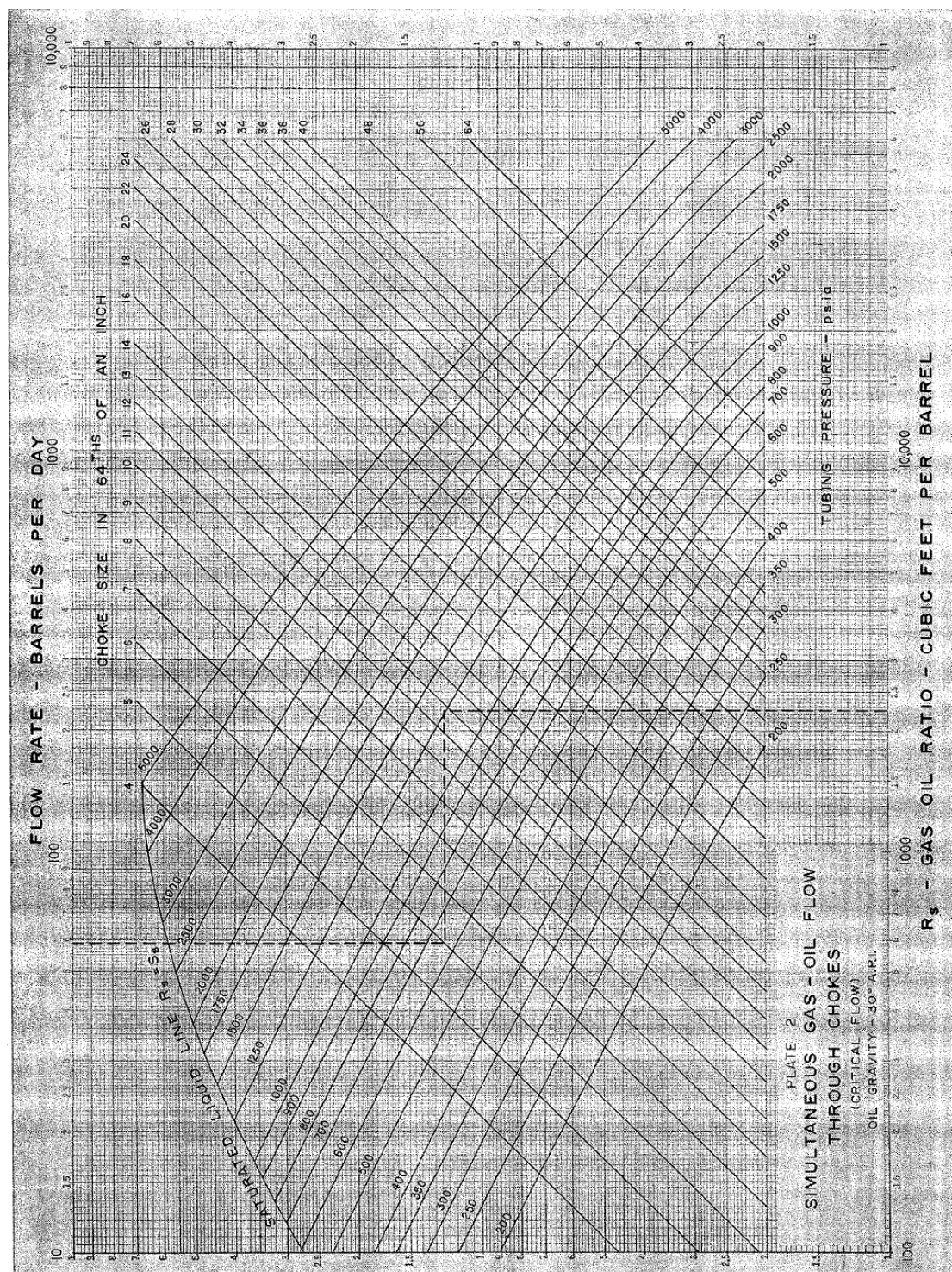


Figure 2.2: Poettman & Beck Chart for 30° API (After Poettman & Beck <sup>6</sup>)

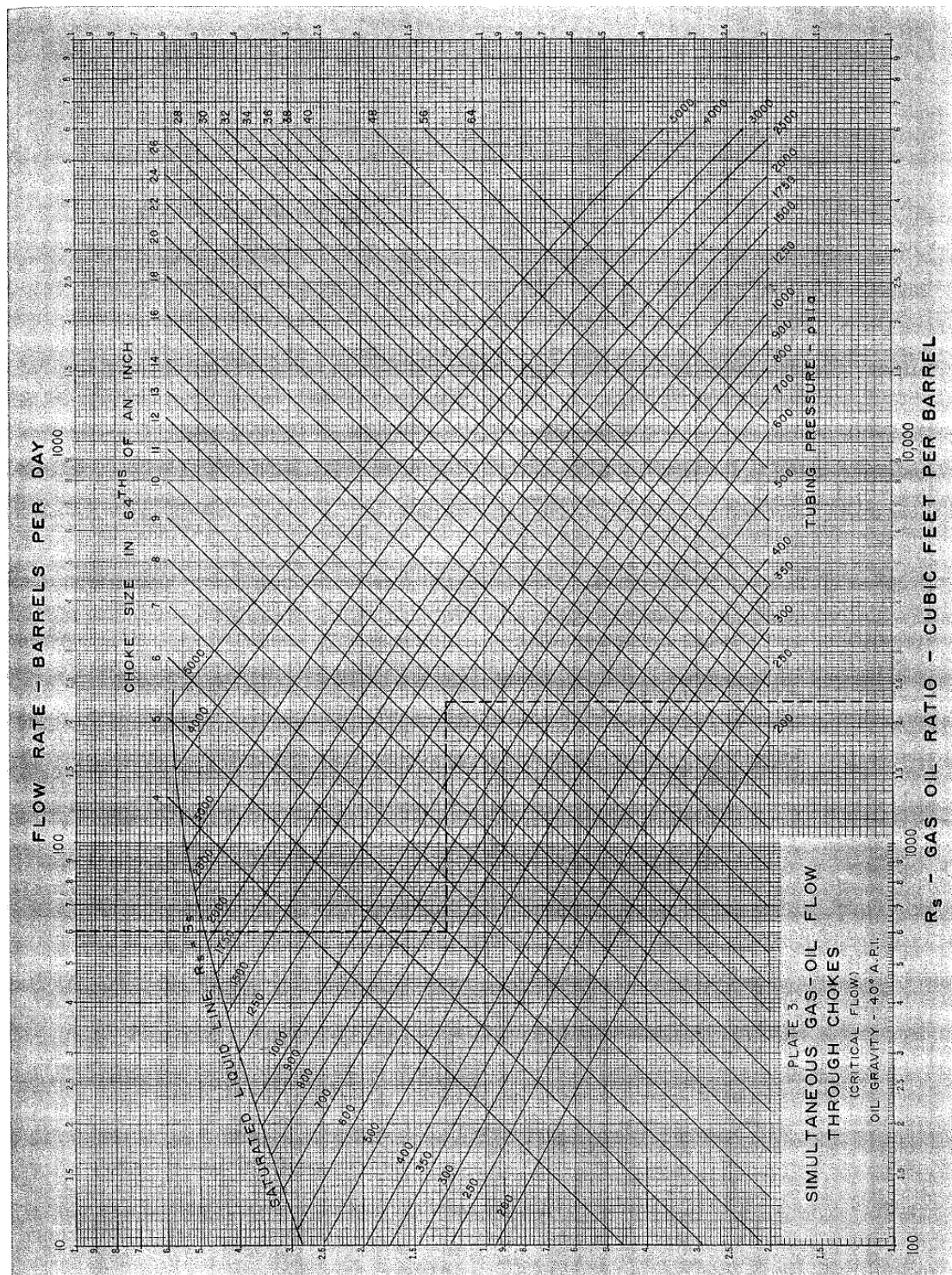


Figure 2.3: Poettman & Beck Chart for 40° API (After Poettman & Beck <sup>6</sup>)

## 2.4 Omana Correlation <sup>7</sup> (1968)

In 1968 Omana conducted experimental field tests to study multiphase flow of gas and liquid through small sized chokes in a vertical position. He developed an empirical correlation using experimental data to relate flow rate [Gas and water], upstream pressure, gas liquid ratio, and choke size. The correlation has a limited range of application and is valid for critical flow conditions. Dimensional analysis was applied and the following correlation was obtained:

$$N_{ql} = 0.263 N_p^{-3.49} N_{pl}^{3.19} Q_d^{0.67} N_d^{1.8} \quad (2.11)$$

Where the dimensionless parameters are defined as follows:

$$N_{ql} = 1.84 Q_L (\rho_L / \sigma)^{1.25} \quad (2.12)$$

$$N_p = c / \rho_L \quad (2.13)$$

$$N_{pl} = 0.0174 P_{us} / \sqrt{\rho_L \sigma} \quad (2.14)$$

$$Q_d = 1 / (1 + R_s) \quad (2.15)$$

$$N_d = 0.01574 D_{64} \sqrt{\rho_L \sigma} \quad (2.16)$$

And where,  $Q_L$ : liquid flow rate, bbl/day.

$P_{us}$ : Upstream or wellhead pressure, psig

$\rho_g$ : gas density, lb/ft<sup>3</sup>.

$\rho_L$ : Liquid density, lb/ft<sup>3</sup>.

$\sigma$ : Liquid surface tension, dyn/cm.

$R_s$ : Actual volumetric gas liquid ratio at upstream conditions.

$D_{64}$ : Choke diameter, 64<sup>th</sup> of an inch.

The application of Omana correlation is limited to the following ranges:

Upstream pressure: 400 – 1000 psig

Maximum Flow rate: 800 bbl/day

Choke Size: 4/64 to 14/64.

## 2.5 Fortunati Analysis <sup>8</sup> (1972)

Fortunati presented a formula for calculating the rates through wellhead chokes, covering both critical and sub-critical flow fluids. When two phase flow occurs, he assumes that there is no slippage between the phases, although he recognized that slippage exists even for immiscible liquids. Two conditions were required for this assumption to be valid:

1. The mixture velocity must be greater than 10 m/sec (32.78 ft/sec).
2. The Froude number ( $V^2/gd$ ) of the mixture must be greater than 600.

In a real simulation, these conditions were believed to be satisfied if the downstream pressure,  $P_{ds}$  is less than  $1.5 \text{ kg/cm}^2$ .

For critical flow conditions, Fortunati derived the following:

$$P_{ds} = \frac{q_o^o}{F_t} \sqrt{(R_{si} - R_s) (\rho_o + \rho_g R_{si})} \frac{P_0 Z T}{T_0} \quad (2.17)$$

$F_t$ : Cross Sectional Area of the choke,  $\text{m}^2$

$P_{ds}$ : Downstream pressure,  $(\text{N/cm}^2)$

$q_o^o$ : oil rate at standard condition,  $\text{m}^3/\text{sec}$ ; STO;

$R_{si}$ : total gas in solution,  $\text{m}^3/\text{m}^3$

$R_s$ : remaining gas in solution at  $P_2$  and  $T$ ,  $\text{m}^3/\text{m}^3$

$\rho_o$ : oil density,  $\text{kg/m}^3$

$\rho_g$ : gas density, kg/m<sup>3</sup>

$P_0$ : reference pressure

$Z$ : gas compressibility factor; dimensionless;

$T$ : working temperature, K

$T_0$ : reference temperature, K

$V$ : mixture velocity at  $P_{ds}=0.137 \text{ N/m}^2$ , as read on figure (2.4) - m/sec.

$g$ : gravity acceleration =  $9.81 \text{ m/sec}^2$ .

$D$ : Choke Size, m.

For sub-critical flow, Fortunati developed his correlation for a downstream pressure of  $0.137 \text{ MN/m}^2$  (19.8 psia) using the curves (Figure 2.4) generated from the experimental work performed by Guzhov and Medviediev. Following is the correlation for sub critical flow:

$$q_L = A_B (1 - \lambda_{g2}) C_D v_{m2F} \{ [P_2 / P_{2F}]^{0.5} \}^\eta / B_o \quad (2.18)$$

Where:

$A_B$ : Choke cross sectional area, m<sup>2</sup>.

$Q_L$ : Liquid volumetric flow rate at in-situ conditions, m<sup>3</sup>/sec.

$C_D$ : Discharge coefficient

$P_2$ : Downstream pressure,  $10^6 \text{ N/m}^2$ .

$P_{2F}$ :  $0.137 * 10^6 \text{ N/m}^2$ , Fortunati Downstream pressure

$v_{m2F}$ : mixture velocity, m/sec.

$B_o$ : Oil Formation Volume Factor

$$\eta = [1 - \lambda_{g2}]^{0.38} \quad (2.19)$$

$$\lambda_{g2} = q_g / (q_L + q_g) \quad (2.20)$$

The Discharge coefficients recommended by Fortunati for sub-critical flow vary from 1.02 to 1.035, depending on the choke size. The model

also assumes isothermal flow and that the fluid physical properties are calculated at downstream conditions.

## 2.6 Ashford and Peirce Study <sup>9</sup> (1974)

In 1974 Ashford and Peirce developed correlation for calculating the pressure drop and flow capacities for multiphase flow through chokes. The model estimates both critical and sub-critical conditions flow behavior, their work is an extension of Ros work. Four assumptions were made by Ashford and Peirce, these are:

1. Adiabatic expansion of the gas;
2. No Slippage occurs between the phases;
3. Friction losses are insignificant;
4. Liquid is incompressible.

For sub-critical flow the above assumptions were derived and used to calculate the oil rate flowing through the orifice:

$$q_o = 3.51 C_D d_B^2 \alpha_{10} \beta_{10} \quad (2.21)$$

where:

$$\alpha_{10} = [B_o + F_{wo}]^{-0.5} \quad (2.22)$$

and

$$\beta_{10} = [ (1/b) T_1 z_1 (R_1 - R_s) (1-X_b) + 198.6 P_1 (1-x) ] / [198.6 + T_1 z_1 / P_1 (R_1 - R_s) X^{(-1/k)}] \cdot [\gamma_o + 0.000217 \gamma_g R_s + F_{wo} \gamma_w]^{1/2} / [\gamma_o + 0.000217 \gamma_g R_1 + F_{wo} \gamma_w] \quad (2.23)$$

$B_o$ : oil formation volume factor

$F_{wo}$ : water oil ratio,

$b$  : coefficient defined by  $(k-1)/k$

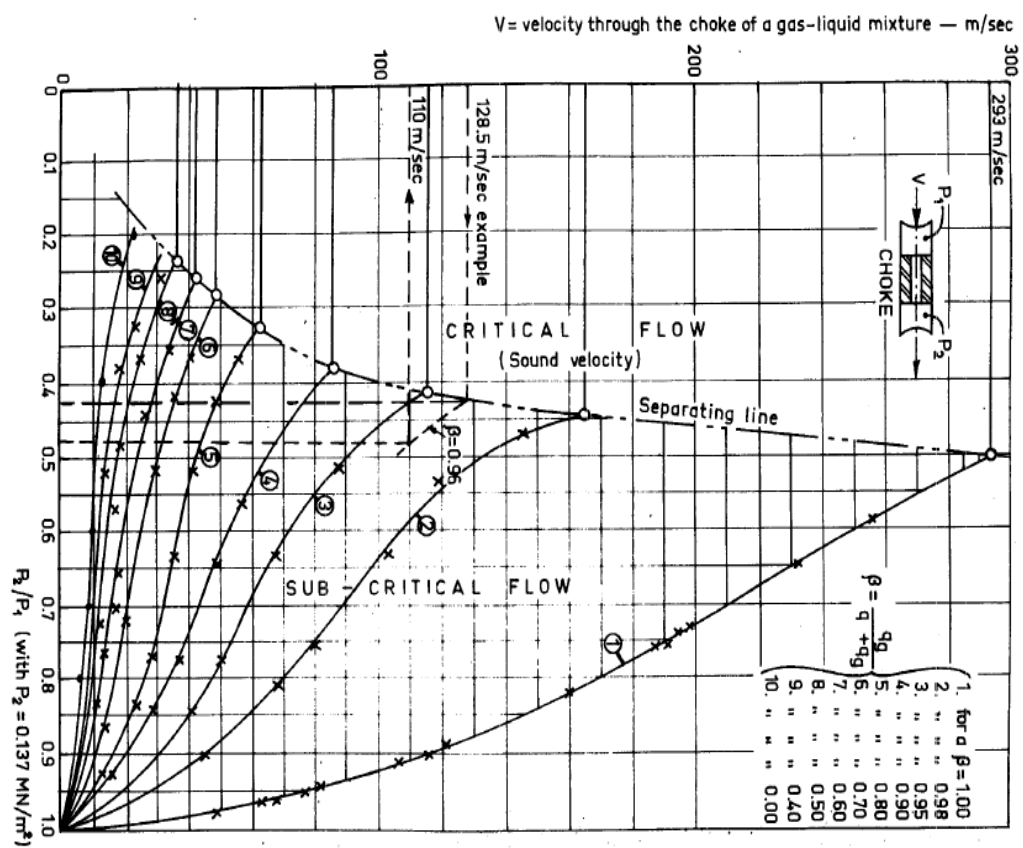


Figure 2.4: Guzhov & Medviediev Experimental Curve (After Fortunati)<sup>8</sup>

k: specific heat ratio, cp/cv

T<sub>1</sub>: Temperature at upstream condition

Z<sub>1</sub>: Gas compressibility factor at upstream condition

R<sub>1</sub>: In situ gas liquid ratio at upstream condition

R<sub>s</sub>: solution gas liquid ratio

X<sub>b</sub>=P<sub>2</sub>/P<sub>1</sub>

P<sub>1</sub>: upstream pressure

X=P<sub>2</sub>/P<sub>1</sub>

γ<sub>o</sub>: oil specific gravity

γ<sub>g</sub>: gas specific gravity

γ<sub>w</sub>: Water specific gravity

d<sub>B</sub>: choke diameter, 64th of an inch

For critical flow conditions, Ashford and Peirce <sup>(9)</sup> developed a multiphase flow equation describing the behavior of orifice flow. The new equation can be used to evaluate well performance using choke size, upstream pressure, choke temperature, production and solution gas oil ratio, gas oil and water gravities, and a discharge coefficient. The developed equation is shown below:

$$q_o = \frac{1.53 C D_c^2 P_1}{(B_o + F_{wo})^{1/2}} \times \frac{\{[T_1 Z_1 (R - R_s) + 151 P_1] (\gamma_o + 0.000217 \gamma_g R_s + F_{wo} \gamma_w)\}^{1/2}}{[T_1 Z_1 (R - R_s) + 111 P_1] (\gamma_o + 0.000217 \gamma_g R + F_{wo} \gamma_w)} \quad (2.24)$$

Where:

d<sub>B</sub> = choke diameter, 64th of an inch

P<sub>1</sub>: upstream pressure, psia

R<sub>p</sub>: production GOR, scf/STB

R<sub>s</sub>: solution GOR, scf/STB at P<sub>1</sub>

C<sub>D</sub>: flow coefficient



$q_o$  : oil production rate, STB/D

Ashford checked his correlation against 14 wells and found the discharge coefficient necessary to estimate measured production rates ranged from 0.642 to 1.218.

Ashford data summary is as follow:

Choke size (64 <sup>th</sup> of an inch):	16 to 40
Production Gas Oil Ratio (scf/STB):	102 to 1065
Pressure (psia):	100 to 1265
Flow Rate (STBD):	190 to 4,728

## 2.7 Schadeva et al. Analysis<sup>12</sup> (1986)

Schadeva et al. in 1986 studied two-phase flow through wellhead chokes, including both critical, sub-critical flow and the boundary between them. His Data were gathered for air-water and air-kerosene flows through five choke diameters from 1/4 to 1/2 inch. A new theoretical model for estimating flow rates and the critical-sub critical flow boundary was tested against these data. The final expression of their data is shown below:

$$G = C_D \{2 g_c 144 P_{us} \rho_{m2}^2 * [(1-x_1) (1-y) / \rho_L + x_1 k / (k-1) (V_{G1} - y V_{G2})]\}^{0.5} \quad (2.25)$$

$$G_2 = (M_{G2} + M_{L2}) / A_c \quad (2.26)$$

$$V_{G2} = 1 / \rho_{G2} \quad (2.27)$$

$$V_{G1} = 1 / \rho_{G1} \quad (2.28)$$

$$Y = P_2 / P_1 \quad (2.29)$$

$P_{us}$  : upstream pressure, psia  
 $g_c$  : gravitational constant  
 $G$  : Mass flux, lbm/ft<sup>2</sup>/sec  
 $C_D$ : flow coefficient  
 $\rho_{m2}$ : mixture density at downstream condition, lbm/ft<sup>3</sup>.  
 $\rho_G$  : gas density, lbm/ft<sup>3</sup>.  
 $x_1$ : gas quality at upstream condition.  
 $A_c$ : Choke Area, ft<sup>2</sup>.  
 $()_2$ : Downstream  
 $()_1$ : Upstream

The data summary is shown below:

Maximum wellhead pressure:	1230 psia
Maximum gas flow rate:	136.6 MSCFD
Maximum liquid flow rate:	1340 STBD
Choke Size range:	16: 32 64 <sup>th</sup> of an inch.

## **2.8 Osman and Dokla Correlation <sup>14</sup> (1990)**

Osman and Dokla in 1990 developed some empirical correlations describing gas condensate behavior through chokes. Four forms of correlations were evaluated against field data. The data were collected from eight different wells producing from gas condensate reservoirs in the Middle East. One of the forms is to correlate the upstream pressure with liquid production rate, gas liquid ratio and choke size. The second form was developed using gas production rate instead of the liquid production rate in the previous form. The other form is developed by using the pressure drop across the choke instead of upstream pressure. These correlations are also presented in graphical form. The four forms of equation are presented using nomograph shown in Figure 2.5 to 2.8. In

their study, it was found that the correlation is most accurate when using pressure drop instead of using the upstream pressure. Never the less, according to them any one of the forms will give reasonable values and can be used when needed. The four forms of equation are as follow:

$$P_{us} = 829.7 R_p^{0.4344} Q_L S^{-1.8478} \quad (2.30)$$

$$P_{us} = 767.2 R_p^{0.5598} Q_g S^{-1.8298} \quad (2.31)$$

$$\Delta P = 310.01 R_p^{0.5919} Q_L S^{-1.8628} \quad (2.32)$$

$$\Delta P = 302 R_p^{0.4038} Q_g S^{-1.8587} \quad (2.33)$$

Where:

$Q_L$  = gross liquid rate, STBD

$Q_g$  = Gas flow rate, MSCFD

$P_{us}$  = flowing wellhead pressure, psia

$\Delta P$  = pressure drop across the choke, psia

$S$  = bean diameter, 64ths of an inch

$R_p$  = producing gas-liquid ratio, MSCF/STB.

Their ranges of data are as follow:

Choke Size (64th of an inch): 28 to 72

Upstream pressure (psia): 2950 to 5200

Condensate flow rate (B/D): 592.6 to 3823.3

Water flow rate (B/D): 0 to 1002.6

Gas flow rate (MMSCFD): 3.91 to 101.33

Wellhead Temperature (°C): 40 to 98.9

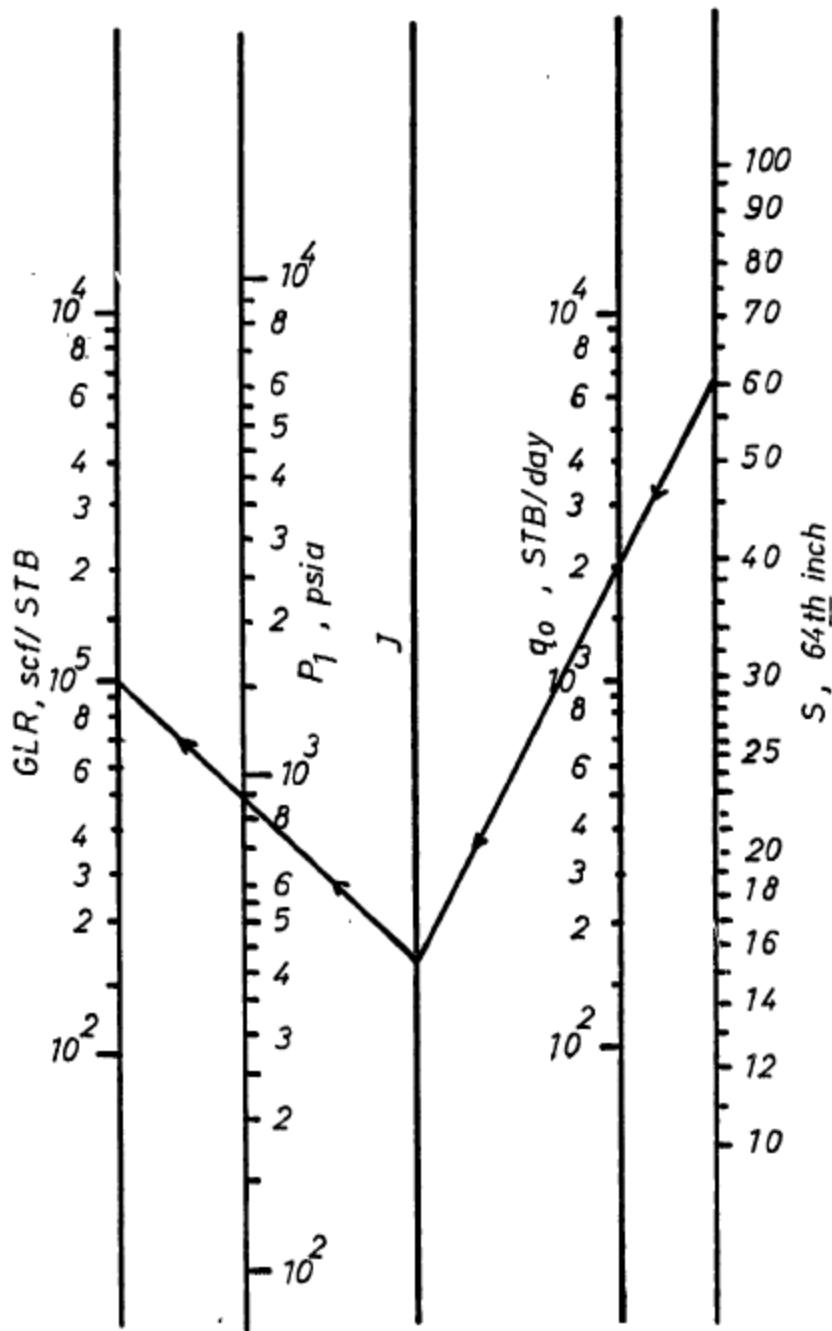


Figure 5: Correlation chart for choke upstream pressure (Eqn. 9.a)  
 Example: for  $S = 60$ ,  $q_0 = 2000$  bal/day and  
 $GLR = 1000$  scf/STB,  $P_1 = 860$  psia

Figure 2.5: Osman & Dokla nomograph for the First Equation (After Osman and Dokla <sup>14</sup>)

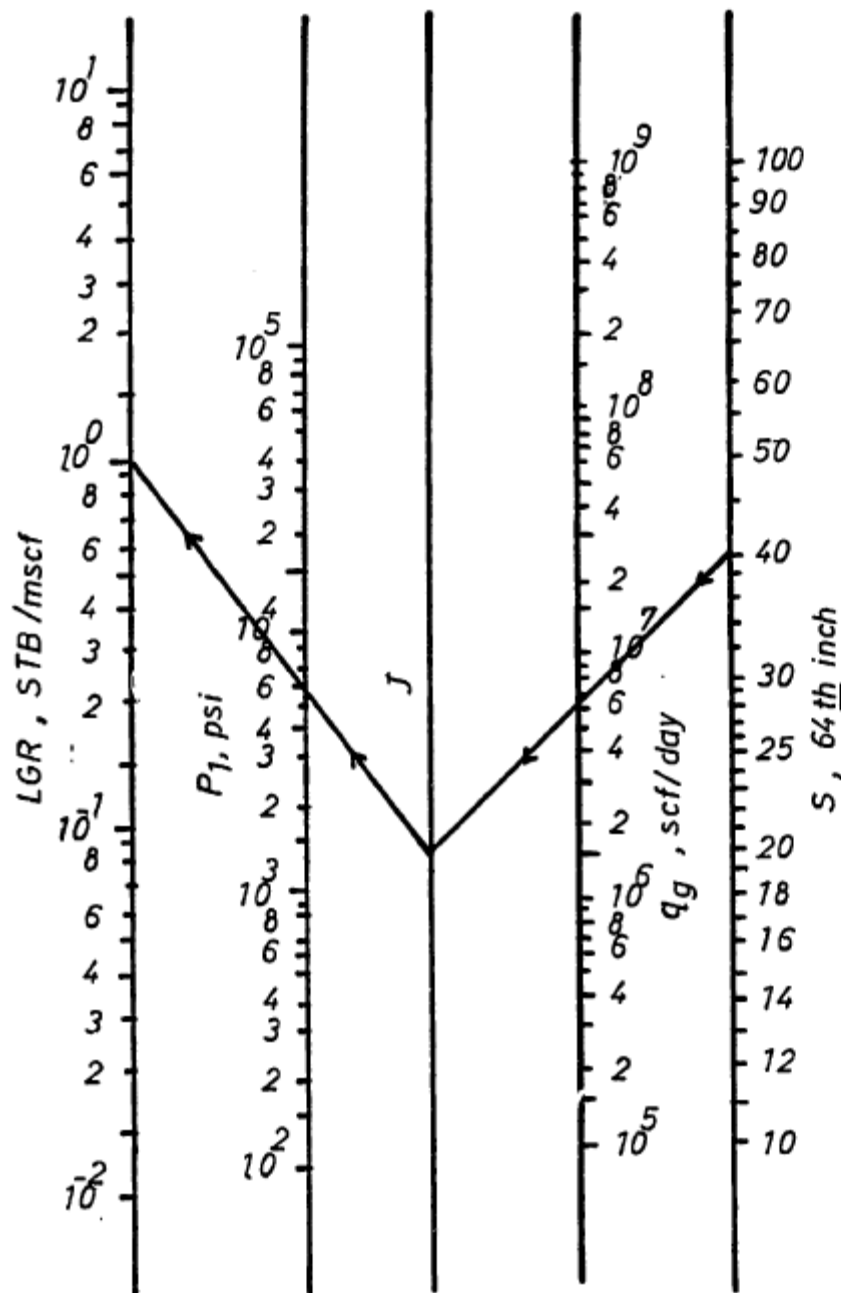


Figure 6: Correlation chart for choke upstream pressure (Eqn. 9.b)  
 Example: for  $S = 40$ ,  $q_g = 6 \times 10^6$  scf/day and  
 $LGR = 1$  STB/mscf,  $P_1 = 5390$  psia

Figure 2.6: Osman & Dokla nomograph for the Second Equation (After Osman and Dokla<sup>14</sup>)

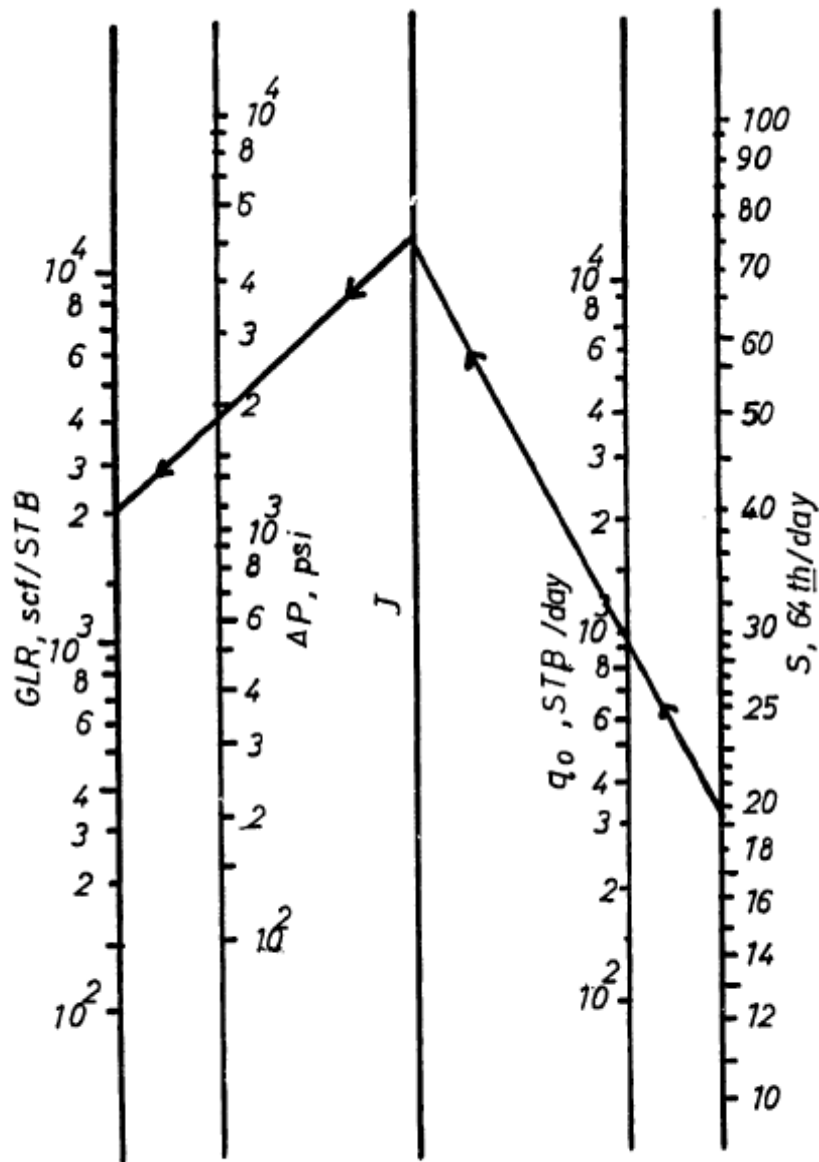


Figure 7: Correlation chart for pressure drop across the choke (Eqn. 9.c). Example: for  $S = 20$ ,  $q_o = 1000$  STB/day and  $GLR = 2000$  scf/STB,  $\Delta P = 1760$  psia

Figure 2.7: Osman & Dokla nomograph for the Third Equation (After Osman and Dokla<sup>14</sup>)

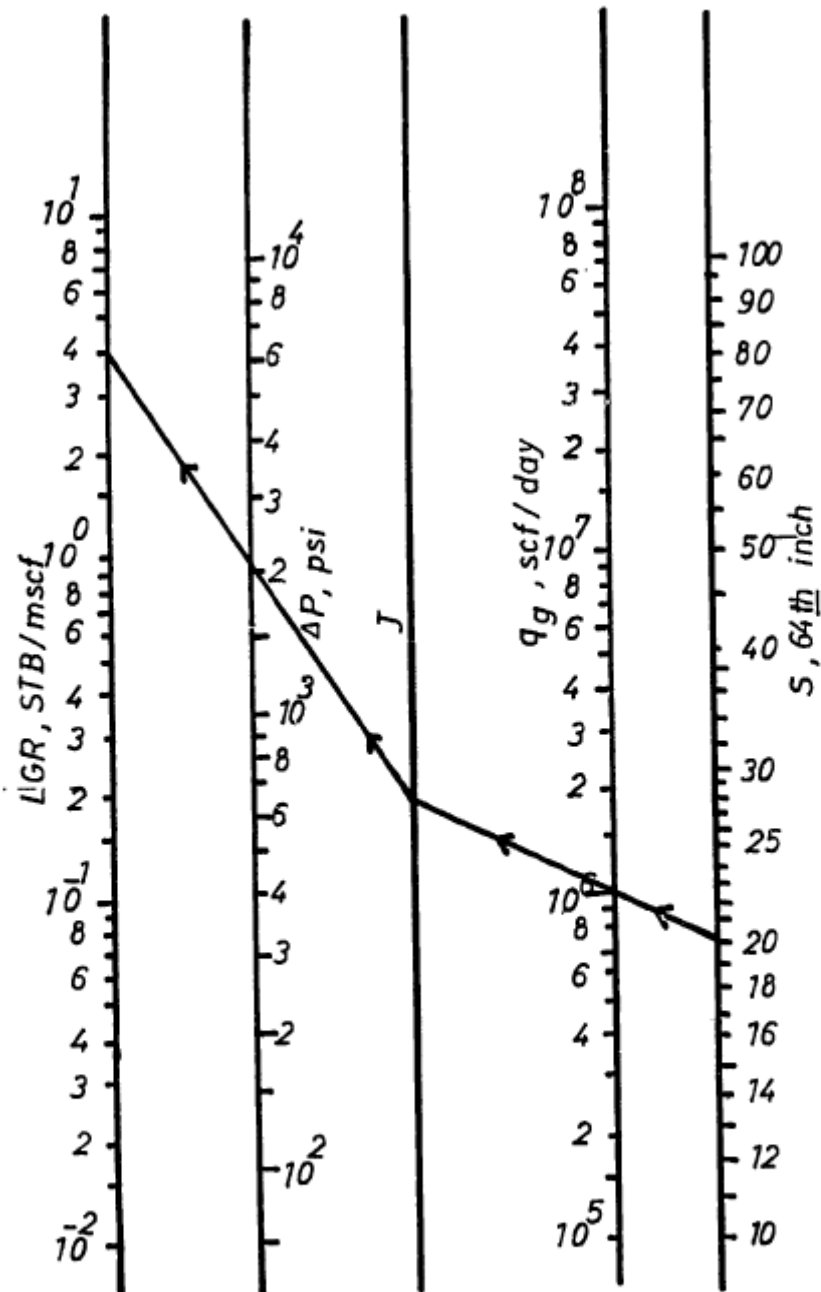


Figure 8: Correlation chart for pressure drop across the choke (Eqn. 9.d). Example: for  $S = 20$ ,  $q_g = 10^6$  scf/day and  $LGR = 4$  STB/mscf,  $\Delta P = 2020$  psia

Figure 2.8: Osman & Dokla nomograph for the Fourth Equation (After Osman and Dokla <sup>14</sup>)

## 2.9 Surbey et al. Correlation<sup>15</sup> (1989)

Surbey, Kelker and Brill in 1989 investigated the use of multiple-orifice-valve (MOV) choke in critical flow region. Experimental data were collected for a high-pressure air/water system show that conventional relationships are not successful in analyzing the experimental data for MOV chokes. A new relationship based on the sonic velocity of two phase homogeneous mixture is developed for the estimation of the critical flow transition.

In their study the experimental data were divided into two groups, sub-critical and critical flow, on the basis of a comparison of the upstream to downstream pressure ratio to literature correlation. When all three correlations estimated a given data point to be in critical region, that point was considered to be in the critical region. All other tests were classified in the sub-critical region. This procedure was important since direct identification of two phase flow was not possible owing to the design of the test facilities. The overall range of experimental data is shown below:

Choke setting (Degree):	90 to 27
Liquid Flow Rate (B/D):	3,550 to 450
Gas Flow Rate (MMSCFD):	2.5 to 0.4
Gas Liquid Ratio (SCF/STB):	5200 to 140
Upstream Pressure (psig):	950 to 85
Temperature (°F):	132 to 48

Surbey et al. used Gilbert type correlation to correlate the critical flow data; the major advantage of the relationship is that it doesn't require the downstream pressure. To compare this correlation with the existing



correlation and due to the noncircular flow passage in the MOV choke the following expression were developed to find the equivalent diameter for the MOV choke:

$$d_e = (4 A_c / \pi)^{1/2} \quad (2.34)$$

In addition to the comparison with the literature correlation a new correlation was developed as shown below:

$$P_1 = 0.2797 (R_p)^{0.3955} q_L^{0.5917} A_c^{-0.4664} \quad (2.35)$$

Where:

$A_c$  = Cross sectional area, in<sup>2</sup>

$q_L$  = volumetric flow rate at standard condition, STBD

$P_1$  = flowing wellhead pressure, psia

$R_p$  = producing gas-liquid ratio, SCF/STB.

For sub critical flow, Surbey et al. developed an iterative procedure that provide a better estimate of the pressure drop (upstream/downstream) which causes the critical velocity. The procedure used in this study for MOV choke is shown in Figure 2.9 below. The iterative procedure converges when the throat pressure is equal to the vapor pressure. Following is the equation used in their iterative procedure:

$$V_{tp} = [(\rho_l f_l + \rho_g f_g) ( f_l / (\rho_l v_l^2) + f_g / (\rho_g v_g^2))]^{-1/2} \quad (2.36)$$

and

$$q_m = v_{tp} A_c \rho_m \quad (2.37)$$

Where:

$v_{tp}$  : critical velocity, ft/sec

$\rho$ : density, Ibm/ft<sup>3</sup>

$f$  : no slip hold up volume fraction.

$v_l$  : liquid choking velocity, ft/sec

$v_g$  : gas sonic velocity, ft/sec

$q_m$  : Mixture flow rate, STBD

$A_c$  : Choke cross section area, square inch

$\rho_m$  : mixture density, Ibm / ft<sup>3</sup>

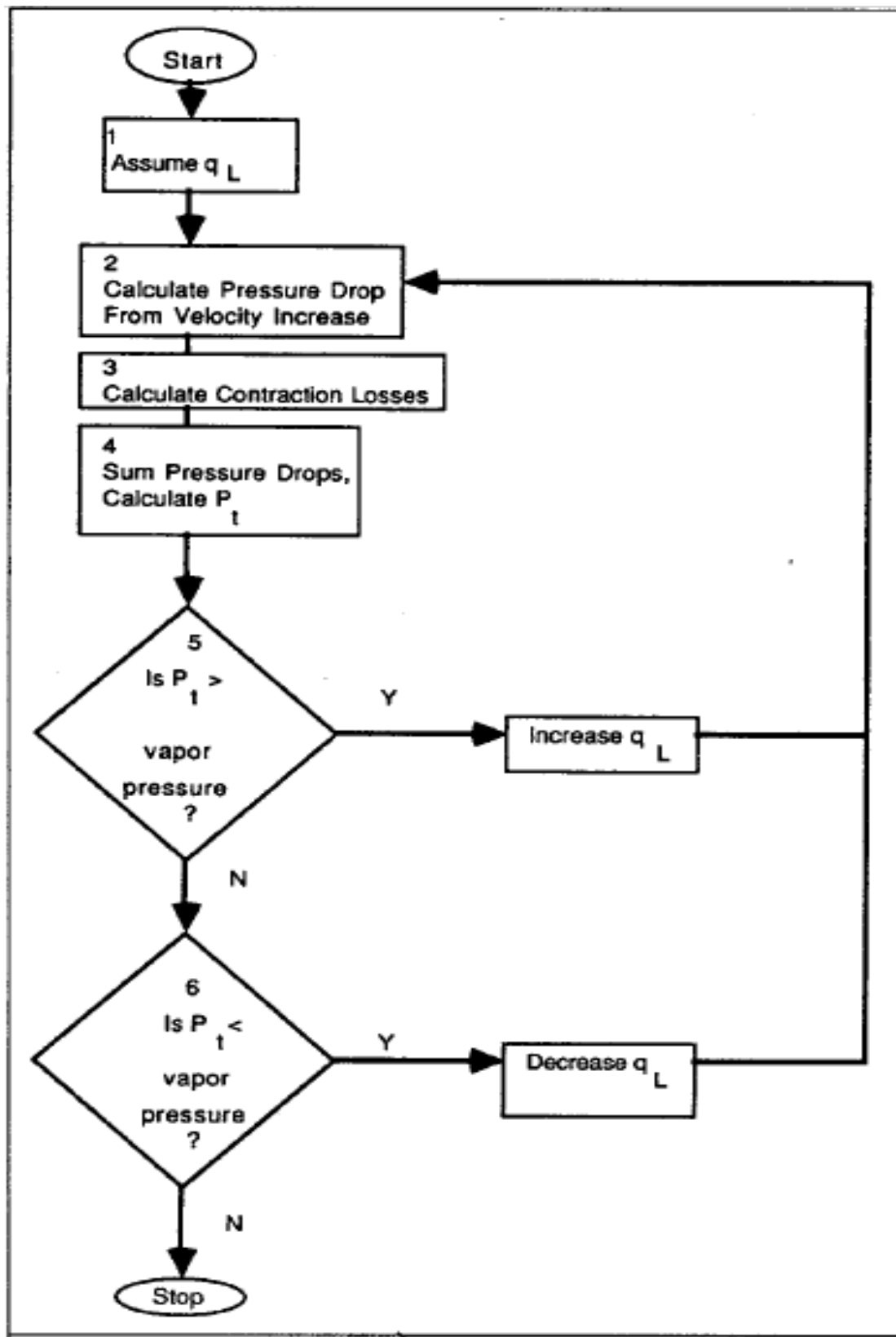


Figure 2.9: Procedure Used in Surbey et al. Study (After Surbey et al <sup>15</sup>)

## 2.10 Towailib and Marhoun Correlation <sup>17</sup> (1992)

Towailib and Marhoun developed an empirical correlation that relates the choke to other parameters. The correlation covered a wide range of flow rates and choke sizes. It was based on 3554 production test data from ten fields in the Middle East. The correlation applies for critical flow conditions, which makes it useful for choke design purposes.

Towailib and Marhoun utilized nonlinear multiple regression and found out that the choke size to be a function of oil flow rate, upstream wellhead pressure, and the mixture relative density. The only difference between this model and Gilbert is the gas oil ratio was replaced by the mixture relative density. The final form of their developed correlation is as follow:

$$S = 20.696 \frac{q_o^{0.483} \gamma_m^{0.707}}{P_{us}^{0.474}} \quad (2.38)$$

where,

$$\gamma_m = \gamma_o + 2.18 \times 10^{-4} R_p \gamma_g \quad (2.39)$$

and,

S: choke size, 64th of an inch

$q_o$  : Oil flow rate, STBD

$P_{us}$  : Upstream wellhead pressure, psig

$\gamma_o$  : Oil relative density (water=1)

$\gamma_g$  : Gas relative density (air=1)

$R_p$  : Producing gas oil ratio, SCF/STB

$\gamma_m$  : Mixture relative density (water=1)

A summary of the data used in their correlation development is shown below:

Oil flow rate, STBD:	172 to 33847
Producing gas oil ratio, SCF/STB:	12 to 5026
Upstream tubing pressure, psig:	97 to 1880
Downstream tubing pressure, psig:	10 to 980
Choke size, 64th of an inch:	16 to 160
API gravity:	27 to 40
Reservoir oil viscosity, cp:	0.29 to 4.6
Formation volume factor, RB/STB:	1.16 to 1.6
Bubble Point pressure, psig:	300 to 3136
Reservoir temperature, °F:	160 to 240
Gas Relative Density (air=1):	0.65 to 0.91

### **2.11 Attar and AbdulMajeed Correlation <sup>13</sup> (1988)**

Attar and AbdulMajeed in 1988 developed two correlations that best fit the production data from East Bagdad Oil field. The first correlation is similar to Gilbert correlation but with different constants and the other is also similar to Gilbert correlation but the API gravity is included. The two correlations are shown below:

$$q_o = 0.016266 P_{wh}^{0.831} S^{1.63} R^{-0.471} \quad (2.40)$$

$$q_o = 0.033567 P_{wh}^{0.8756} S^{1.796} R^{-0.2693} g^{-0.43957} \quad (2.41)$$

Where:

g: API gravity

$q_o$ : oil flow rate, STBD

$P_{wh}$ : wellhead pressure, psig

S: Choke size, 1/64 inch

R: gas liquid ratio, Mscf/STB

### 2.12 Elgibaly and Nashawi Correlation <sup>20</sup> (1996)

Elgibaly and Nashawi developed a new Omana-type correlation that is best suited for the Middle East oil wells and investigated the effect of incorporating various PVT correlations of the produced fluids into different models of critical two phase flow. Their study highlighted the linear relationship between the flow rates and upstream pressure for critical flow.

The newly developed correlation is based on 174 data points for critical flow, least square method, and dimensional analysis and belongs to Omana type correlation. The new correlation is as follow:

$$N_{ql} = 520.5655 N_p^{-0.43624} N_{pl}^{0.6987} Q_d^{0.82502} N_d^{1.50198} \quad (2.42)$$

Where the dimensionless parameters are defined as follows:

$$N_{ql} = 1.84 Q_L (\rho_L / \sigma)^{1.25} \quad (2.43)$$

$$N_p = c / \rho_L \quad (2.44)$$

$$N_{pl} = 0.0174 P_{us} / (\rho_L \sigma)^{1/2} \quad (2.45)$$

$$Q_d = 1 / (1 + Rs) \quad (2.46)$$

$$N_d = 0.01574 D_{64} (\rho_L / \sigma)^{1/2} \quad (2.47)$$

And where:

$Q_L$ : liquid flow rate, bbl/day.

$P_{us}$ : Upstream or wellhead pressure, psig

$\rho_g$ : gas density, lb/ft<sup>3</sup>.

$\rho_L$ : Liquid density, lb/ft<sup>3</sup>.

$\sigma$ : Liquid surface tension, dyne/cm.

$R_s$ : Actual volumetric gas liquid ratio at upstream conditions.

$D_{64}$ : Choke diameter, 64<sup>th</sup> of an inch.

In their study they have also proposed 4-parameter correlation that confirms the concept of linear relationship between flow rate and upstream pressure; the 4-parameter correlation is as shown below:

$$q_o = 0.40133 S^{1.6287} P^{0.7061} R_p^{-1.089} \quad (2.48)$$

Where:

$q_o$ : oil flow rate, STBD

$P$ : wellhead pressure, psig

$S$ : Choke size, 1/64 inch

$R_p$ : Producing gas liquid ratio, scf/STB

Elgibaly and Nashawi have also concluded that estimation of gas oil surface tension (using the Baker and Swerdloff experimental results), use of different gas compressibility factor have only a little impact on the result accuracy. Similarly the combination of various correlations of PVT properties (oil volume factor and solution GOR) with critical two phase flow correlation has showed no major impact on the result accuracy except for Ashford, Sachdeva et al., and Omana et al. correlations.

### 2.13 Perkins Approach<sup>18</sup> (1993)

Perkins in 1993 derived equations describing the isentropic flow of multiphase mixture through chokes; the equations were derived from the general energy equation. These flow equations are valid for both critical and sub-critical flow. Equation, physical property, correlations for oil/water/gas systems, and a computer method that can handle both flow regimes were described. The procedure determines whether flow is critical or sub-critical regime. He tested the method by comparing measured and calculated flow rates of 1,432 sets of literature data comprising both critical and sub-critical air/water, air/kerosene, natural gas, natural gas/oil, natural gas/water and water flows. An average discharge coefficient of 0.826 gave a negligible average error with a 15.4% standard deviation.

Figure 2-11 shows the computer program logic flow diagram. The computing method is as follows:

1. Input data needed to define the problem adequately will include the upstream pipe diameter, the choke diameter, the downstream pipe diameter, upstream pressure and temperature, downstream pressure, gas gravity, oil gravity, GOR and WOR.
2. On the basis of upstream pressure and temperature and of 1 lbm of total material flowing, determine gas compressibility and density; ratio of heat capacity,  $F$ , for the gas; heat capacity of the gas,  $(C_v)$ ; heat capacity of the oil  $(C_{v_o})$ ; mass of flowing oil; oil FVF; flowing oil density; mass of gas dissolved in water; mass of flowing water; water FVF; flowing water density; mass of flowing gas; polytropic expansion exponent,  $n$ .

$$C_v = z R/[M(F-1)] \quad (2.49)$$



$$\frac{(f_g F C_{vg} + f_o C_{vo} + f_w C_{vw})}{(f_g C_{vg} + f_o C_{vo} + f_w C_{vw})} \quad (2.51)$$

3. Assume the value of  $P_r = P_2/P_1$
4. Determine  $T_2$  at the choke throat;

$$(T_2 + 460) = (T_1 + 460) P_r^{(n-1)/n} \quad (2.52)$$

5. determine the average pressure and temperature upstream of the choke throat:

$$P_{\text{Average}} = (P_1 + P_2)/2 \quad (2.53)$$

$$\text{And } T_{\text{Average}} = (T_1 + T_2)/2 \quad (2.54)$$

6. Recalculate the polytropic expansion exponent,  $n$  at the average pressure  $P_{\text{Average}}$  and temperature  $T_{\text{Average}}$ .
7. Iterate on  $P_r$  until the following equation (After Perkins<sup>(20)</sup>) converges:

$$\begin{aligned} & \{2\lambda[1 - p_r^{(n-1)/n}] + 2\alpha_1(1 - p_r)\} \left\{ \left[ 1 - \left( \frac{A_2}{A_1} \right)^2 \left( \frac{f_g + \alpha_1}{f_g p_r^{-1/n} + \alpha_1} \right)^2 \right] \right. \\ & \left. \left[ \frac{f_g}{n} p_r^{-(1+n)/n} \right] + \left( \frac{A_2}{A_1} \right)^2 \frac{f_g (f_g + \alpha_1)^2 p_r^{-(1+n)/n}}{(f_g p_r^{-1/n} + \alpha_1)^2} \right\} \\ & = \left[ 1 - \left( \frac{A_2}{A_1} \right) \left( \frac{f_g + \alpha_1}{f_g p_r^{-1/n} + \alpha_1} \right)^2 \right] (f_g p_r^{-1/n} + \alpha_1) \\ & \times \left[ \lambda \left( \frac{n-1}{n} \right) p_r^{-1/n} + \alpha_1 \right]. \end{aligned} \quad (2.55)$$

8. Calculate  $P_3$ .

$$P_3 = P_1 - [(P_1 - P_4) / (1 - (d_c/d_d)^{1.85})] \quad (2.56)$$

9. If  $P_3 < P_2$  then flow is critical; use  $P_r = P_2/P_1$  in the following equation to calculate isentropic mass flow rate:

$$w_i = A_2 \sqrt{288 g_c P_1} \sqrt{1 - \frac{\lambda \left[ 1 - p_r^{(n-1/n)} \right] + \alpha_1 (1 - p_r)}{\left[ 1 - \left( \frac{A_2}{A_1} \right)^2 \left( \frac{f_g + \alpha_1}{f_g p_r^{-1/n} + \alpha_1} \right)^2 \right] (f_g p_r^{-1/n} + \alpha_1)^2}} \quad (2.57)$$

10. If  $P_3 > P_2$ , then flow is sub-critical; use  $P_r = P_3/P_1$  and the following equation is used to calculate the isotropic mass flow rate.

$$w_i = A_2 \sqrt{288 g_c P_1} \sqrt{1 - \frac{\lambda \left[ 1 - p_r^{(n-1/n)} \right] + \alpha_1 (1 - p_r)}{\left[ 1 - \left( \frac{A_2}{A_1} \right)^2 \left( \frac{f_g + \alpha_1}{f_g p_r^{-1/n} + \alpha_1} \right)^2 \right] (f_g p_r^{-1/n} + \alpha_1)^2}} \quad (2.58)$$

11. If flow rate is measured, calculate discharge coefficient.

12. If the actual flow rate is unknown, use average value for the discharge coefficient to estimate flow rates:

$$w_c = K w_i \quad (2.59)$$

where:

A: Area, ft square

$C_p$ : heat capacity at constant pressure, (ft-lb<sub>f</sub>)/(lb<sub>m</sub>-°F)

$C_v$ : heat capacity at constant volume, (ft-lb<sub>f</sub>)/(lb<sub>m</sub>-°F)

$d_c$ : Choke diameter, ft

$d_d$ : Pipe diameter downstream of the choke, ft

$$\alpha_1 = \frac{1}{v_1} \left( \frac{f_o}{\rho_o} + \frac{f_w}{\rho_w} \right) \quad (2.60)$$

$f$ : Weight fraction in the flowing stream,

$$F = C_p / C_v \quad (2.61)$$

$g_c = 32.2$  (lbm-ft)

$\rho$ : Density, lb<sub>m</sub>/ft<sup>3</sup>

$K=w_a/w_i$ = discharge coefficient

M: Molecular weight, m

P: pressure, psia

T: temperature,

$\bar{P}$ : Average Pressure, psia

$\bar{T}$ : Average Temperature, °F

$$\lambda = f_g + \left[ (f_g C_{vg} + f_o C_{vo} + f_w C_{vw}) M / zR \right] \quad (2.62)$$

Q: Heat transfer to flowing stream, (ft-lbf)/lb<sub>m</sub>

R: Universal gas constant, , (ft-lbf)/(lb<sub>m</sub> -mol-°R)

R<sub>s</sub>: solubility of gas in oil, scf/bbl

R<sub>sw</sub>: solubility of gas in water, scf/bbl

T<sub>r</sub>: reduced temperature,

v: specific volume, ft<sup>3</sup>/lb<sub>m</sub>

V: velocity, ft/sec

w<sub>a</sub>: actual mass flow rate, lb<sub>m</sub>/sec

w<sub>c</sub>: calculated mass flow rate, lb<sub>m</sub>/sec

w<sub>i</sub>: isentropic mass flow rate, lb<sub>m</sub>/sec

w<sub>o</sub>: observed mass flow rate, lb<sub>m</sub>/sec

W: work done by the flowing system, ft- lb<sub>f</sub>/lb<sub>m</sub>

z: gas compressibility factor

$\gamma_o$ : oil specific gravity, (Water=1)

$\gamma_a$ : gas specific gravity, (air=1)

$\gamma_{oa}$ : oil gravity, API

$\gamma_w$ : water specific gravity, (Water=1)

$\rho_r$ : reduced density

and the subscripts are

g: gas

o: oil

w: water

1= upstream of the choke

2 = at the choke throat

3 = condition just downstream of the choke throat if flow is sub-critical

4 = recovered condition downstream of polytropic compression

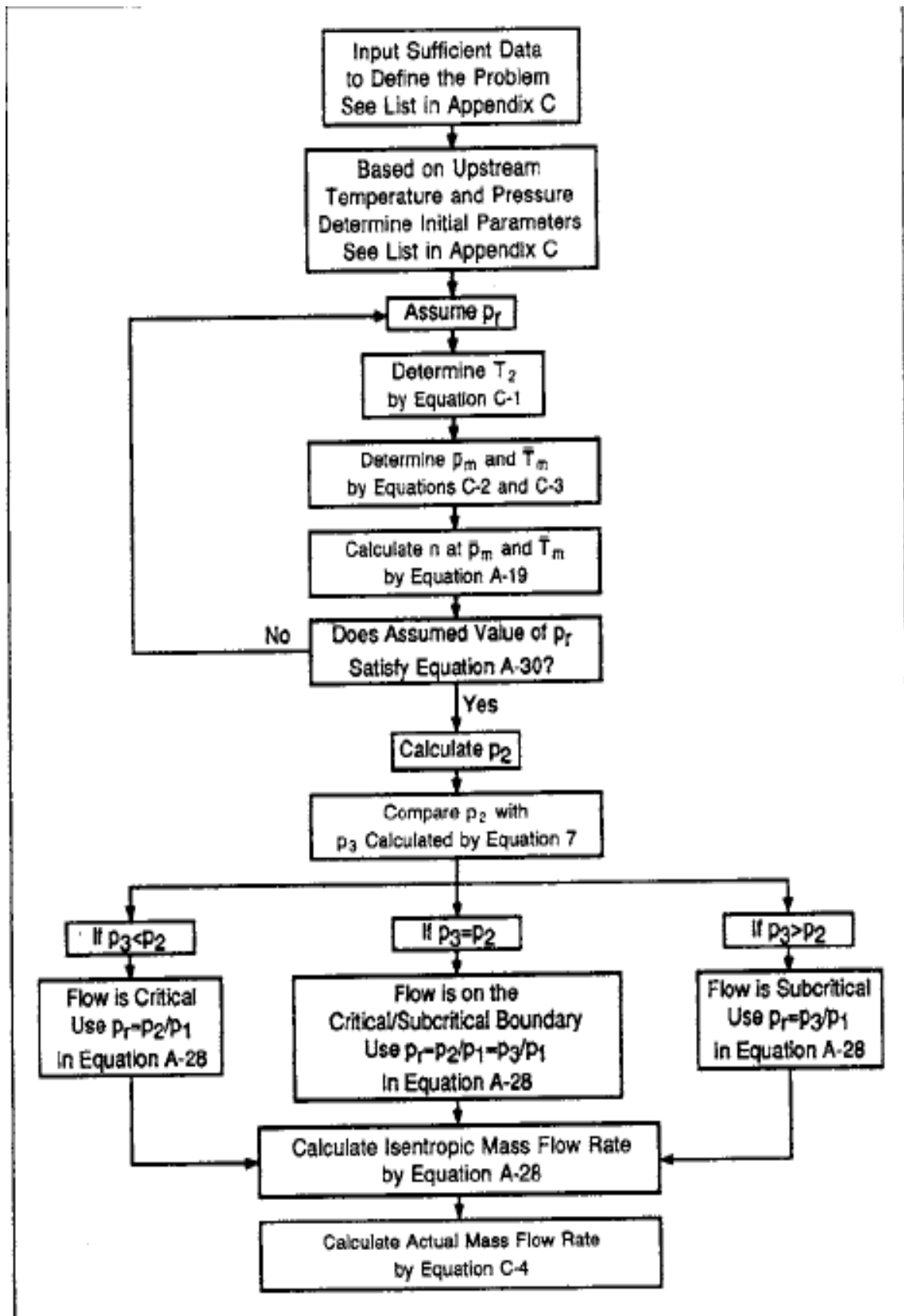


Figure 2.10: Perkins computer program logic flow diagram (After Perkins

### 2.14 Safran and Kelker Equation<sup>27</sup> (2007)

Safran and Kelker developed a theoretical model for two phases through chokes. Their model accounts for slippage between the liquid and gas phases as they pass through the choke. The theoretical basis of the model is based on the following assumptions:

1. Flow is one dimensional;
2. Acceleration is the predominant pressure term;
3. Quality is constant (Frozen flow);
4. Liquid phase is incompressible;
5. Gas phase expands polytropically;
6. Slippage occurs at choke throat;

The present slip model is capable of estimating the critical/sub-critical flow boundary and the critical and sub-critical mass flow rates. The final form of the critical sub-critical flow boundary equation is presented as follow:

$$(r_c)^{1-\frac{1}{n}} = \frac{\alpha(1-r_c) + \frac{n}{n-1}}{\frac{n}{n-1} + \frac{n}{2} \left\{ 1 + \alpha r_c^{1/n} \right\}^2} \quad (2.63)$$

This equation is an implicit equation and requires an iteration to be solved.

Where:

$$n = \frac{x_g k C_{vg} + (1-x_g) C_L}{x_g C_{vg} + (1-x_g) C_L} \quad (2.64)$$

$$\alpha = \frac{R(1-x_g)v_L}{x_g v_{g1}} \quad (2.65)$$

Where:

$r_c$ : critical pressure ratio ( $P_2/P_1$ )

$n$ : polytropic gas expansion exponent

$k$ : gas specific heat ratio

$C_v$ : gas at specific heat at constant volume, (KJ/KG/K)

$C_L$ : Liquid specific heat constant

$X_g$ : gas quality

$v_g$ : gas specific volume

$v_L$ : Liquid specific volume

$R$ : slip ratio ( $u_g/u_L$ )

The final form of the total mass flow rate equation is as follow:

$$\dot{m} = \frac{CA_2^2 p_1 \left[ \alpha(1-r) + \frac{n}{n-1} \left( 1 - r^{\frac{n-1}{n}} \right) \right]}{x_g v_{g1} \left[ r^{\frac{-1}{n}} + \alpha \right]^2 \left[ x_g + \frac{1}{R} (1 - x_g) \right]} \quad (2.66)$$

Where:

$A_2$ : Choke cross sectional area, meter square

$P_1$ : upstream pressure

$C$ : constant that change depending the units used ( $C=2000C_D$  for SI units, and  $C=2 * C_D^2 * g_c * 144$ ).

$C_D=0.75$ .

In the case of critical flow,  $r_c$  is used in the equation above, while in the sub-critical flow  $r$  is used to calculate the sub-critical total mass flow rate.

For critical flow

$$R = \sqrt{1 + x_g \left( \frac{\rho_L}{\rho_g} - 1 \right) \left[ 1 + 0.6e^{-5.0x_g} \right]} \quad (2.67)$$

In which  $\rho$  : density

For Sub-critical flow

$$R = a_0 \left( \frac{1 - x_g}{x_g} \right)^{a_1 - 1} \left( \frac{\rho_L}{\rho_g} \right)^{(a_2 + 1)} \left( \frac{\mu_L}{\mu_g} \right)^{a_3} \quad (2.68)$$

In which:  $\mu$  : phase viscosity and the constant values of  $a_0=1$ ,  $a_1=1$ ,  $a_2=-0.83$  and  $a_3=0$ .

### 2.15 Rumah and Bizanti Correlation<sup>24</sup> (2007)

Rumah and Bizanti in 2007 utilized actual production test data from Sabriyah field in Kuwait to establish a new generalized multiphase flow choke correlation that estimates flow rate as a function of flowing wellhead pressure, gas liquid ratio, and surface wellhead choke size. The purposed correlation based on regression analysis for Sabriyah field is as follow:

$$q_L = \frac{p_{wh}^{0.96614} d_c^{1.946479}}{188 R_{GL}^{0.06322}} \quad (2.69)$$

Where:

$q_L$  : Liquid Flow rate, STBD

$d_c$  : Choke size diameter, 1/64<sup>th</sup> of an inch

$R_{GL}$  : Gas Liquid Ratio, MSCF/STB

$p_{wh}$  : Wellhead pressure, psi

Their correlation was based on 621 data points collected for 73 completions in 63 vertical oil wells, each test of different choke size, from Sabriyah field in Kuwait.



### 2.16 Bizanti and Mansouri Correlation<sup>28</sup>

Bizanti and Mansouri developed a generalized correlation that best fit and describes the multiphase flow through wellhead chokes for offshore Bouri oil field, based on 62 actual production tests from five six vertical oil wells and 73 production tests gathered from horizontal wells in the same field. The new correlation estimates flow rates as a function of flowing wellhead pressure, gas liquid ratio, and surface wellhead choke size.

Following is their proposed model for vertical wells:

$$Q_L = 0.0564 P_{wh}^{1.6785} GLR^{-0.0947} DC^{1.431} \quad (2.70)$$

For horizontal wells:

$$Q_L = 1389.65 P_{wh}^{-0.565} GLR^{-0.00172} DC^{1.132} \quad (2.71)$$

Where:

$Q_L$ : Gross liquid rate, STBD

$P_{wh}$ : wellhead pressure, psig

GLR: gas liquid ratio, SCF/STB

$D_C$ : choke size, 64<sup>th</sup> of an inch

### 2.17 Pilehvari Correlation<sup>12</sup> (1981)

Pilehvari in 1981 conducted an experimental study to develop a method for estimating liquid flow rates for critical flow when air and water flow simultaneously through wellhead chokes.

He applied linear regression technique to 200 data points from his experiment and developed a new correlation. He decided to use the same

model as Gilbert, relating upstream pressure, liquid flow rate, gas liquid ratio, and the diameter of the choke. During regression analysis he found out that tests with high gas liquid ratio didn't fit the model. The 32 data points with gas liquid ratio above 1000 SCF/STB were eliminated and regression analysis was applied to the remaining 168 data points. The resulting new correlation is as shown below:

$$p_1 = \frac{46.666q_L R_p^{0.313}}{d^{2.111}} \quad (2.72)$$

Where:

$p_1$  : Upstream pressure, psig

$q_L$  : Liquid volumetric flow rate at in situ conditions, B/D

$R_p$  : Producing gas liquid ratio, SCF/STB

$d$  : Choke size diameter, 64<sup>th</sup> of an inch

## CHAPTER 3

### CURRENT STUDY DATA ACQUISITION

In this study data from twenty seven (27) different fields were collected to develop an artificial neural network model that covers a wide range of field production data. These data include choke size, production gas oil ratio, upstream tubing pressure, upstream tubing temperature, and oil and gas flow rates. More than five thousands points were collected; these points were screened and filtered before being utilized in order to remove invalid points and outliers. This was done by minimizing the effect of outliers using the robust fit method. The points that were found outliers in all the modeled correlations after robust regression were removed. Four thousands and thirty one (4031) point remained after the screening and filtrations.

#### **3.1 Data description:**

##### 3.1.1. Flow Rates:

The gas and oil flow rates are measured at the wellsite using portable test traps designed for well testing or multiphase flow meters (MPFM) that are calibrated continuously and have an accuracy of  $\pm 10\%$ . Although the test traps and MPFM operate at different pressure and temperature, the final reported data were all calibrated to surface conditions by the field

engineers using the knowledge of PVT data of the fluids and previous production tests done in the laboratory or in the field to describe the behavior of the fluids when changed from the separator conditions to the standard atmospheric conditions.

### 3.1.2 Tubing wellhead pressure and Temperature:

Pressures and temperatures are measured using mechanical springs gauges or electronic devices that have a high accuracy. But sometimes these gauges get stuck resulting in wrong readings; however this happen very rarely as these gauges are frequently inspected.

### 3.1.3 Choke Sizes

Both adjustable and positive chokes were used in the tested wells.

### 3.1.4 Production Test Data

The data were collected from two different sources. The first data set was collected from well tests conducted by well test engineers using portable separators and as a result these data points are very accurate. The second data set was collected from well tests using Multiphase flow meters (MPFM) and this set of data has a lower accuracy than the first set because of the MPFM accuracy which requires continuous calibration and validation.

### 3.1.5 Fluid Properties Data:

The production test data were collected from different fields and accordingly the PVT data of these fields were gathered. Table 3.2 shows the range of these fluid properties.

The table shows the diversity of the PVT properties studied. All these PVT properties were obtained from laboratory analysis of many either

downhole or/and surface fluids sample collected. PVT properties of each individual field were taken to be an average properties of the sample obtained from that field.

#### 3.1.6 Data Screening:

Most of the data utilized in this study were from well tests conducted using portable separators; as a result they have very high accuracy. But the second set of data has a lower accuracy, therefore; the first sets of data in addition to the modeled correlations and the robust fit function in Matlab (that minimizes the effect of outliers) were utilized to discover the outliers in the second set of data. Points that were found outliers in all the modeled correlations were removed. Table 3.1 shows the range of the production tests data after screening and filtrations.

The final number of well tests that were used in the model development was four thousands and thirty one (4031) points.

Table 3.1: Production Data Summary

Description	Minimum	Maximum
Oil Flow Rate, STBD	268	26400
Gas Oil Ratio, SCF/STB	10	5812
Upstream Tubing Pressure, psia	38	3141
Choke Size, 64th of inch	12	172

Table 3.2: PVT Data Summary

Description	Minimum	Maximum
Oil Relative Density (Water=1)	0.765	0.997
Oil Viscosity at reservoir condition, cp	0.09	0.95
Formation Volume Factor, bbl/STB	1.05	2.29
Bubble Point Pressure, psia	125	5913
Reservoir Temperature, °F	141	326
Gas Relative Density (Air=1)	0.708	1.4

# CHAPTER 4

## Model Development

In this chapter a background about artificial neural network (ANN) will be provided. After that, the data handling in terms of preprocessing and post processing will be illustrated; and then finally, the model development methodology and results will be discussed.

### **4.1 Artificial Neural Network**

#### **4.1.1 Introduction**

An artificial neural network is a mathematical model that can acquire artificial intelligence. It is similar to the brain in acquiring knowledge through learning process and storing knowledge through assigning inter-neuron connection strengths known as weights. Artificial Neural Network has a simple arrangement of nodes, called neurons (Figure 4.1), used for the pattern recognition, modeled after a simplistic representation of living brain.

In human brain there are almost 100 billion neurons, some connected to other neurons; whereas in artificial neural network there are several to tens of neurons connected to each other (Figure 4.3). These neurons discover data features and patterns, through the training and learning stage and store it through assigning weights to each neuron.

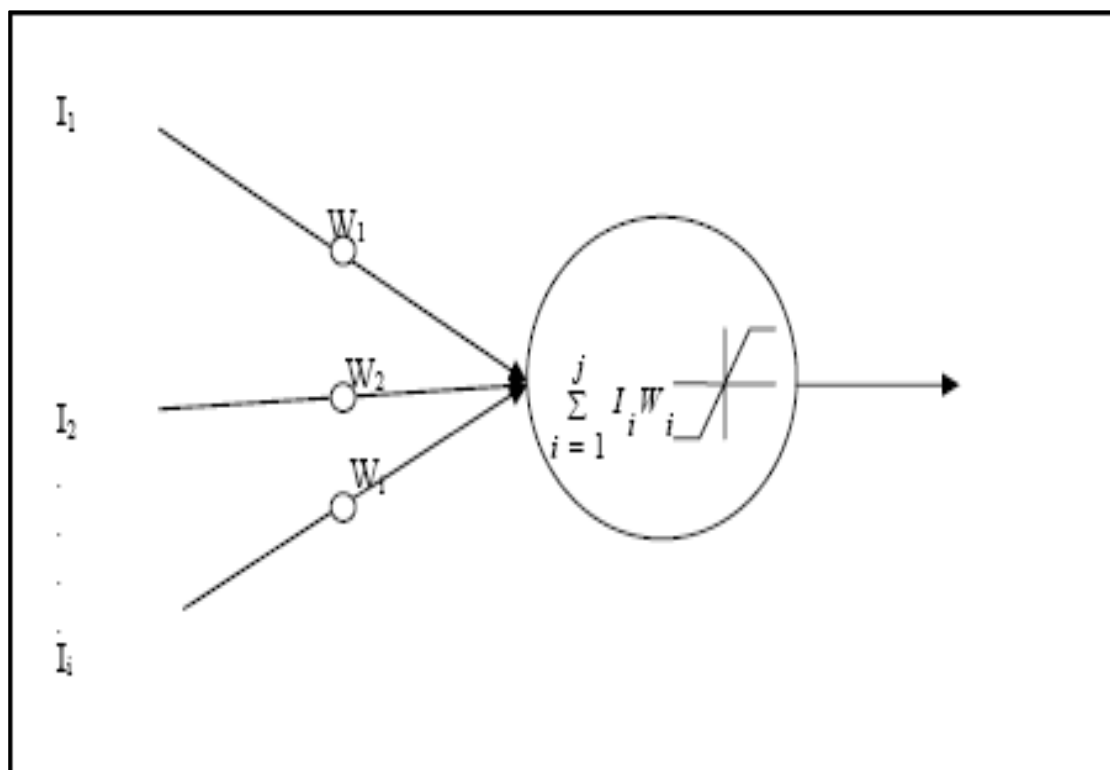


Figure 4.1: Artificial Neuron (After Freeman<sup>16</sup>)



#### 4.1.2 Network Learning:

There are two types of neural network training: supervised learning and unsupervised learning. In supervised learning, (Figure 4.2) the input and output are provided and the error between the real output from the neural network and the desirable output is calculated and used by the algorithm to adjust the weight of the neurons. If the difference is within the acceptable limits, there will be no weight changes, otherwise the weights will be returned (Back propagated) to be adjusted. Thus, the neural network learns under the supervision of the desirable output. After that, the weights will be fixed for the feed forward cycle utilized in the test sets. On the other hand, in unsupervised learning the neural network has to discover the pattern by itself, without the feedback loop indicating if the neural network outputs are correct.

#### 4.1.3 Network Architecture:

Another important element in designing a neural network is the architecture. Neural network consists of neurons arranged normally in layers. They usually consists of one input layer and two or more hidden layers including the output. The input layer consists of a neuron for every input variable, and similarly in the output layer, each output variable is represented by a neuron. On the other hand, the optimum number of hidden layers and neurons in each layer are usually determined by a trial and error process. Different numbers of layers and neurons in each layer has to be attempted before finding the optimum one. Based on the interconnection between the neurons and layers, the neural network can be categorized into two main categories: feed-forward and cascade-forward. In feed forward, the input sweeps directly to the output layer and doesn't allow internal feedback of information. Whereas, the cascade

forward allows internal feedback of information, which makes it better for dynamic models. Internal feedback is recommended as it involves all the history of input and output.

#### 4.1.4 Transfer Function:

To transfer the output of each neuron and layer from one to another, a transfer function is normally assigned to pass the signals after it is being processed inside the neuron. These transfer functions are mathematical functions that come in three main types, namely: threshold, Piecewise-linear and sigmoid functions. In threshold function, the output of the neuron is transmitted either as one, if the output isn't negative, or zero otherwise (Figure 4.4).

$$\varphi(v) = \begin{cases} 1 & \text{if } v \geq 0 \\ 0 & \text{if } v < 0 \end{cases} \quad (4.1)$$

Whereas, Piecewise linear function is an approximation of nonlinear function that is usually reduced to threshold function if the output is very large. (Figure 4.5)

$$\varphi(v) = \begin{cases} 1, & v \geq +\frac{1}{2} \\ v, & +\frac{1}{2} > v > -\frac{1}{2} \\ 0, & v \leq -\frac{1}{2} \end{cases} \quad (4.2)$$

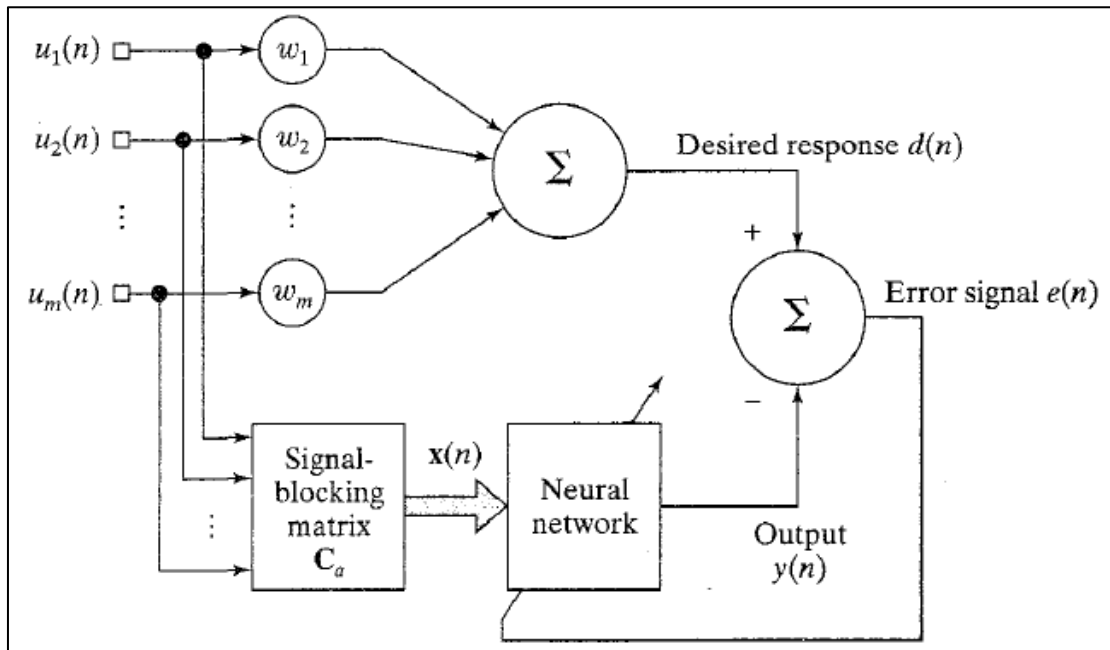


Figure 4.2: Supervised Learning Model (After Simon Haykin<sup>21</sup>)

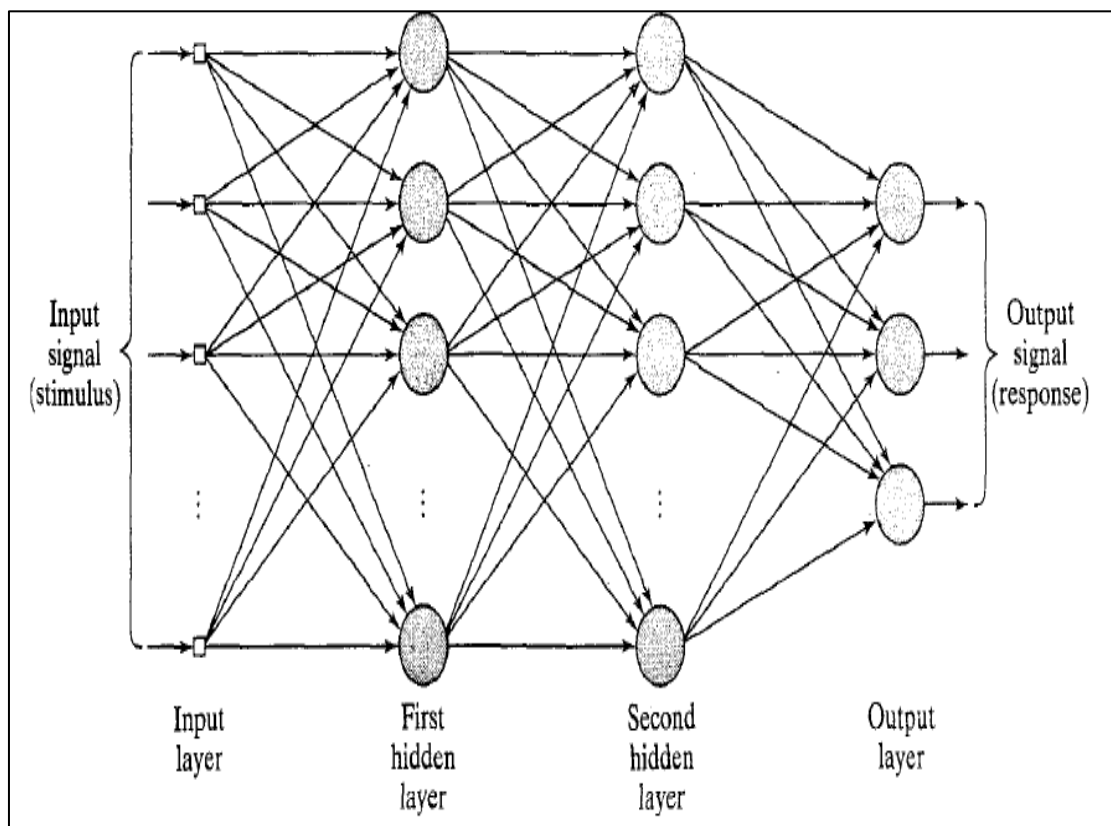


Figure 4.3: Architecture of Neural Network with Two Hidden Layers (After Simon Haykin<sup>21</sup>)

On the other hand, sigmoid functions are the most common transfer function used in developing artificial neural network. It's unlike threshold function which assumes a value of one or zero; the output values in sigmoid function covers all the range from zero to one (Figure 4.6). In addition to that, sigmoid functions are differentiable, which is an important feature in developing an artificial neural network, as it helps in correcting the weight of each neuron. Examples of sigmoid functions are: hyperbolic tangent sigmoid and Log-sigmoid.

Hyperbolic tangent sigmoid function:

$$\mathbf{tansig(n) = 2/(1+exp(-2*n))-1} \quad (4.3)$$

Log-sigmoid function:

$$\mathbf{logsig(n) = 1 / (1 + exp(-n))} \quad (4.4)$$

For both the threshold and sigmoid function, if it is desirable to have the range from minus one to plus one; the transfer function assumes an antisymmetric form with respect to the origin.

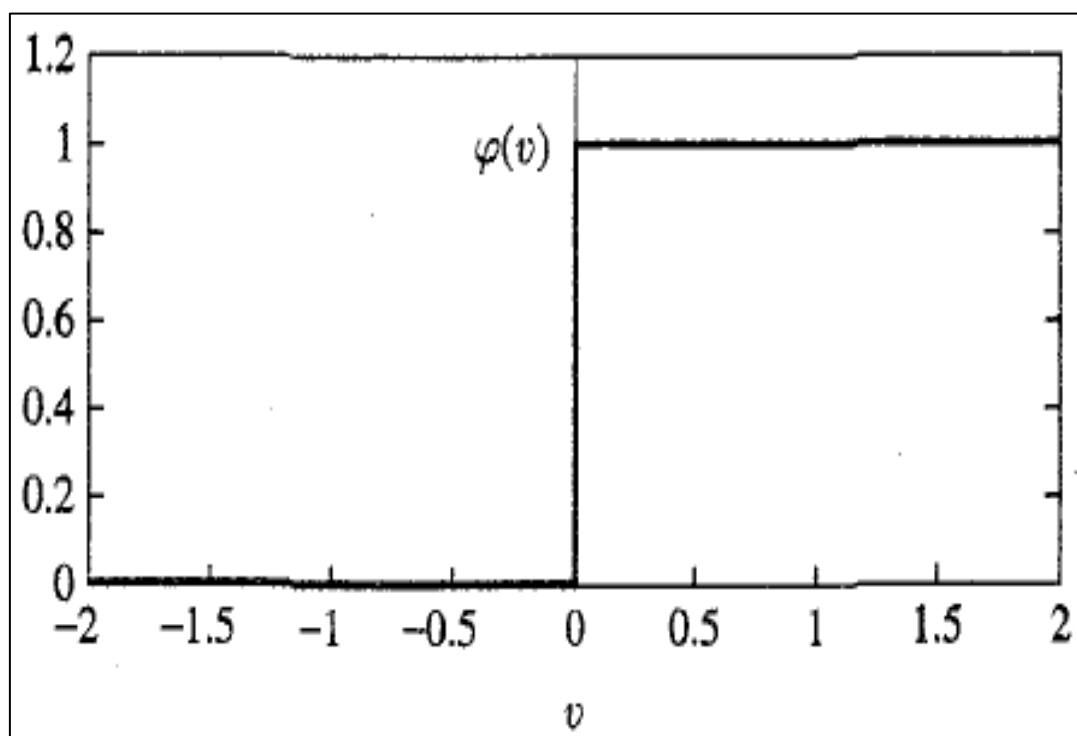


Figure 4.4: Threshold Function (After Simon Haykin<sup>21</sup>)

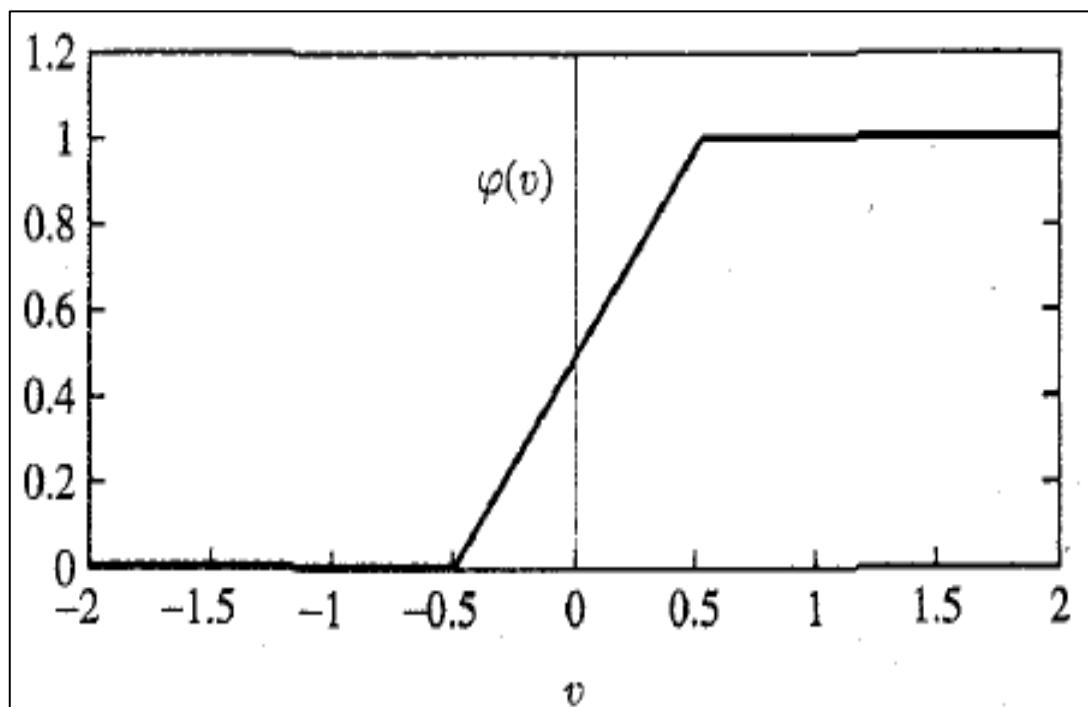


Figure 4.5: Piecewise linear Function (After Simon Haykin<sup>21</sup>)

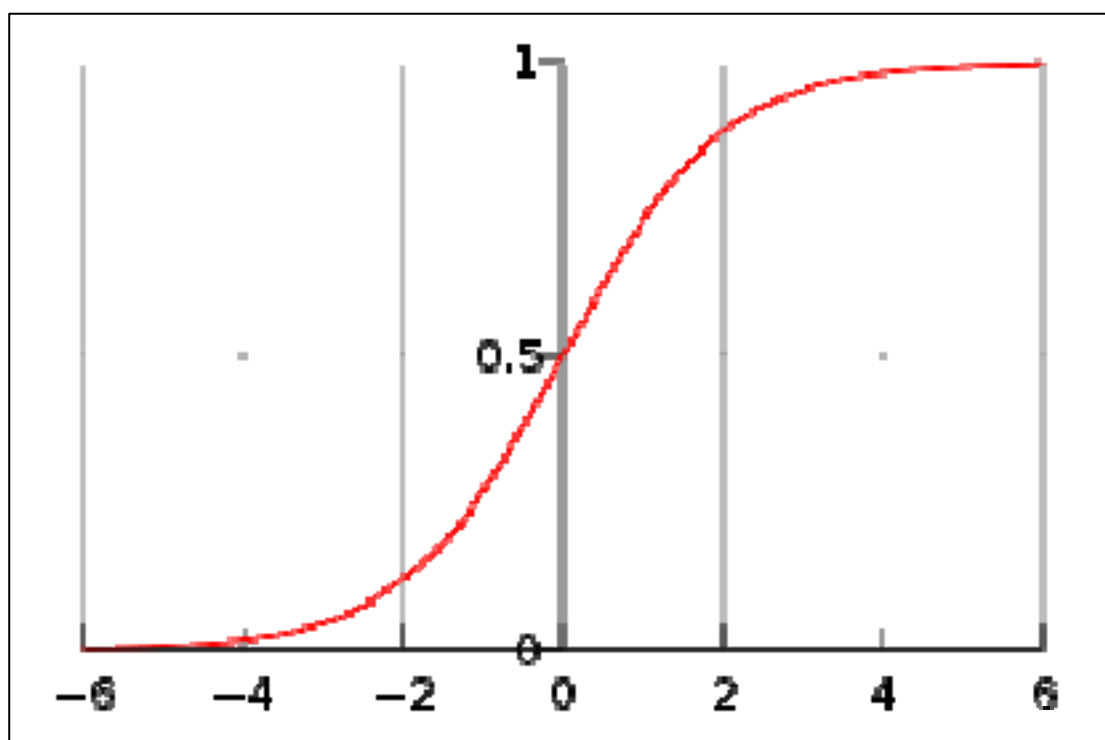


Figure 4.6: Sigmoid Function



## **4.2 Data Handling**

After the collected data were screened and filtered, they were normalized, processed in the neural network, and finally, denormalized. Normalizing the data means, so that if the data were sorted and plotted against their frequency, the mean and standard deviation will equal to zero and one respectively. On the other hand, denormalizing the data means, returning them into their original meaningful format after being processed by the neural network. These steps are very essential to ensure a successful development of neural network.

Another important step before using the data was partitioning the data into training, validation and testing. Training data are used to adjust the weight of the neurons. Validation data are used to ensure the generalization of the network during the training stage, and the testing data are used to examine the network after being finalized. To ensure the data distribution in the training, validation and testing sets covers all the ranges in the data, they were randomly distributed. The partitioning ratio used in this study was 80% training, 10% validation and 10% testing. This ratio was utilized as it has provided the best result compared to other ratios like 2:1:1 and 3:1:1.

## **4.3 Model Development**

Artificial neural network was used to develop both the choke size and flow rate models. This section discusses the model development methodology, in terms of selecting the independent variable, model architecture, and optimization.

#### 4.3.1 Selection of Independent Variables:

The independent variables were selected for critical flow based on the Bernoulli and the gas law equations. Bernoulli equation was considered to describe the fluid flowing through orifice of a reduced area, while keeping in mind, in critical flow the rate depends on the upstream condition only, thus, the changes in the flow line pressure doesn't impact the flow rate. In addition to that, gas oil ratio and the Gas law equation were also considered, because of the importance of considering the gas behavior in two phase flow.

Bernoulli equation is a function of flow rate ( $q$ ), orifice size ( $A_1$ ), pipeline size ( $A_2$ ), fluid density ( $\rho$ ), and the upstream and downstream pressures ( $p_1$  and  $p_2$ ). But the most important parameters for critical flow are the choke size, fluid density and the upstream pressure. The downstream pressure and pipeline size are not as important because of the critical flow condition.

##### Bernoulli equation:

$$q = A_2 [2(p_1 - p_2) / \rho (1 - (A_2 / A_1)^2)]^{1/2} \quad (4.5)$$

Gas law equation on the other hand, is a function of pressure ( $P$ ), molecular weight ( $M$ ), compressibility factor ( $Z$ ) (function of pressure, temperature ( $T$ ) and gas density ( $\rho_g$ ), gas density, the gas constant ( $R$ ) and temperature.

##### Gas Law Equation:

$$\rho_g = P M / (Z R T) \quad (4.6)$$

For this reason, the following parameters were considered while developing the neural network model: Wellhead pressure ( $P_{WH}$ ) and temperature ( $T_{WH}$ ), choke size ( $D_c$ ), flow rate ( $Q_o$ ), oil and gas relative

densities ( $\gamma_o$  and  $\gamma_g$ ), in addition to the production gas oil ratio ( $R_p$ ). These parameters were also found to be in agreement with the parameters used in the literature.

#### 4.3.2 Model Architecture and Optimization

The model architecture in terms of number of neurons, layers and the type of interconnection function were determined based on a trial and error process. It was found to be the most successful criteria in developing the model. During development, the design started with a minimum number of neurons and was increased gradually while monitoring the performance for every case, using absolute average percent error, correlation coefficient in addition to other statistical and graphical analysis techniques such as average percent error, root mean square error. In addition to that, several learning functions were tested and monitored using the same approach in selecting the number of neurons.

Finding the optimum model architecture was not an easy task, it involved many steps such as testing different number of neurons, layers, interconnection function, transfer function, objective function, and different combinations of these parameters.

While developing the model the following optimization steps were followed. The model started with three (3) neurons which were increased till the optimum number was found. Different transfer functions were tested while changing the number of neurons but the best was the log sigmoid. A similar approach was followed after increasing the number of layers from two to three and from three to four. The number of neurons

was increased gradually till the optimum was found and different transfer functions were tested to find the best one.

On the other hand, the best learning algorithm for training the neural network was found to be the cascade-forward for both the choke size and flow rate estimation, with the mean absolute error as an objective function.

In addition to that, a serious problem was encountered while training the model. The model was found to be trapped at certain point and caused the training to be stopped before being finalized. After investigating the problem, it was found to be related to the local minimum. The main reasons for this was found to be the error function being the superposition of nonlinear transfer function which might have minima at different points. Certain design criteria were modified to solve this problem; the maximum number of validation failures has been increased from the default of 5 to 750.

Figures (4.9: 4.20) and Tables (4.1: 4.6) show the results of the optimization study and the final selected model. The choke size prediction model consisted of three hidden layers with five (5), nine (9) and five (5) neurons, in addition to the output layer with one neuron. The transfer functions used in the three hidden layers were log sigmoid and the pure line for the output layer. For the flow rate estimation, the neural network model consisted of three hidden layers with nine (9), five (5) and eight (8) neurons, in addition to the output layer with one neuron. The best transfer function for the three hidden layers was found to be the log sigmoid and for the pure line for the output layer.

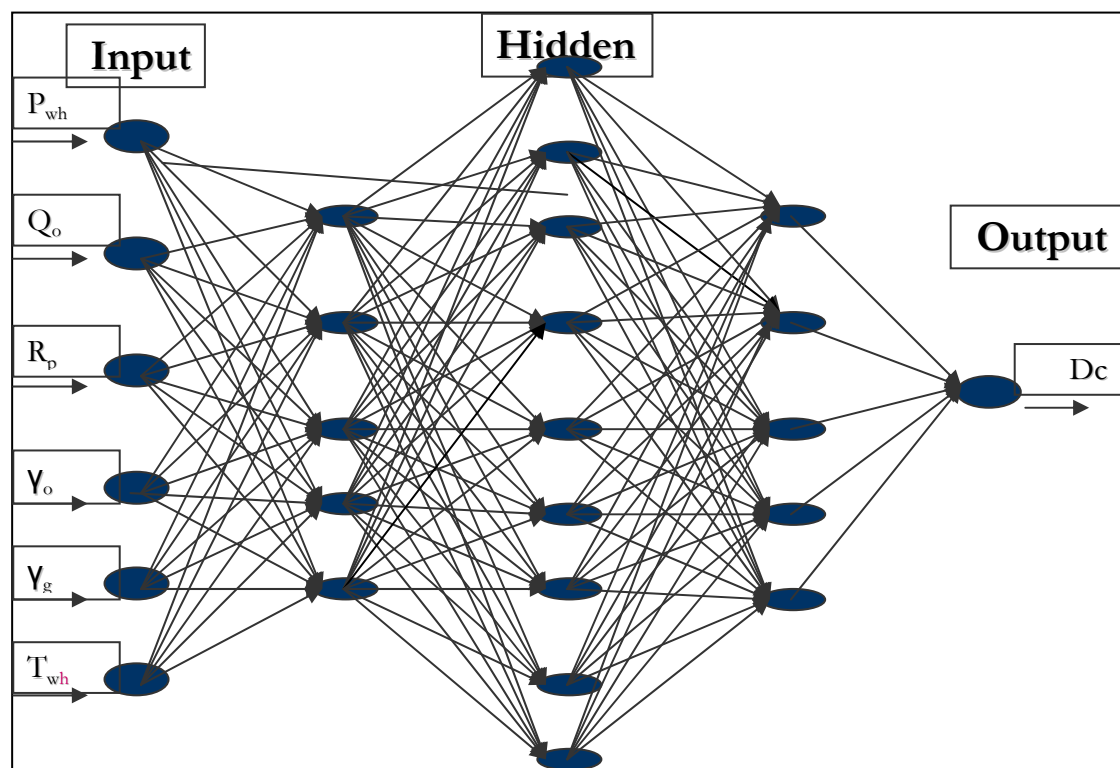


Figure 4.7: Choke Size Neural Network Model

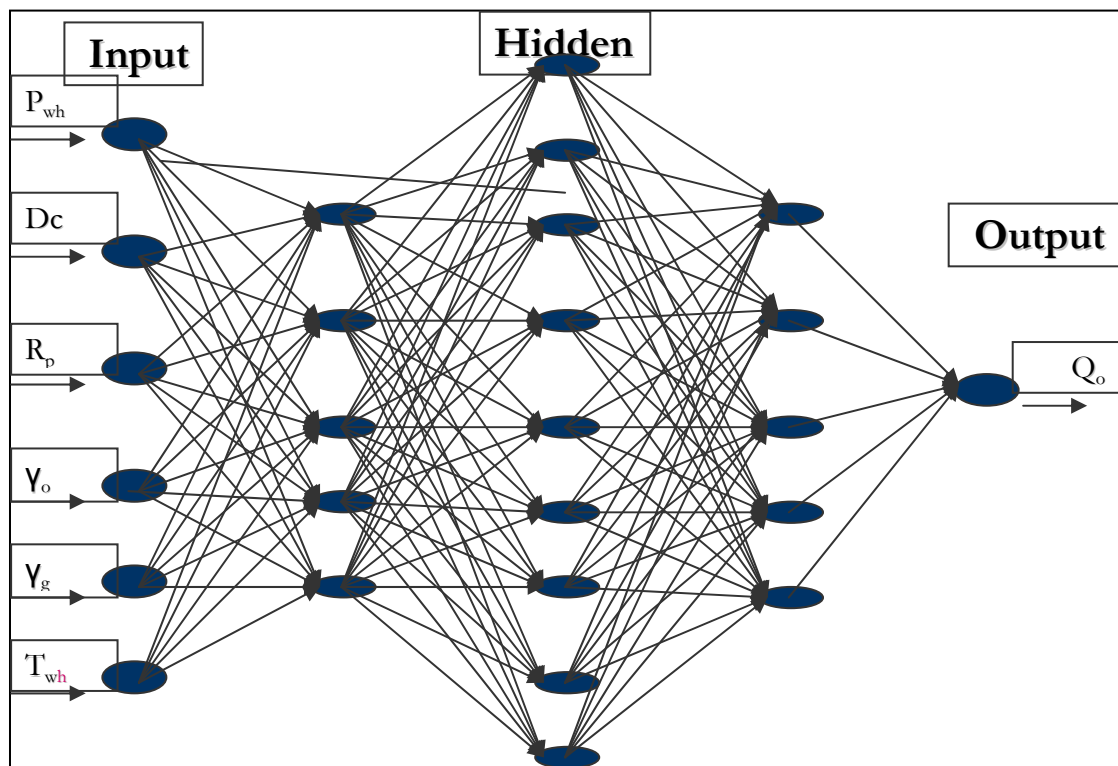


Figure 4.8: Flow Rate Neural Network Model

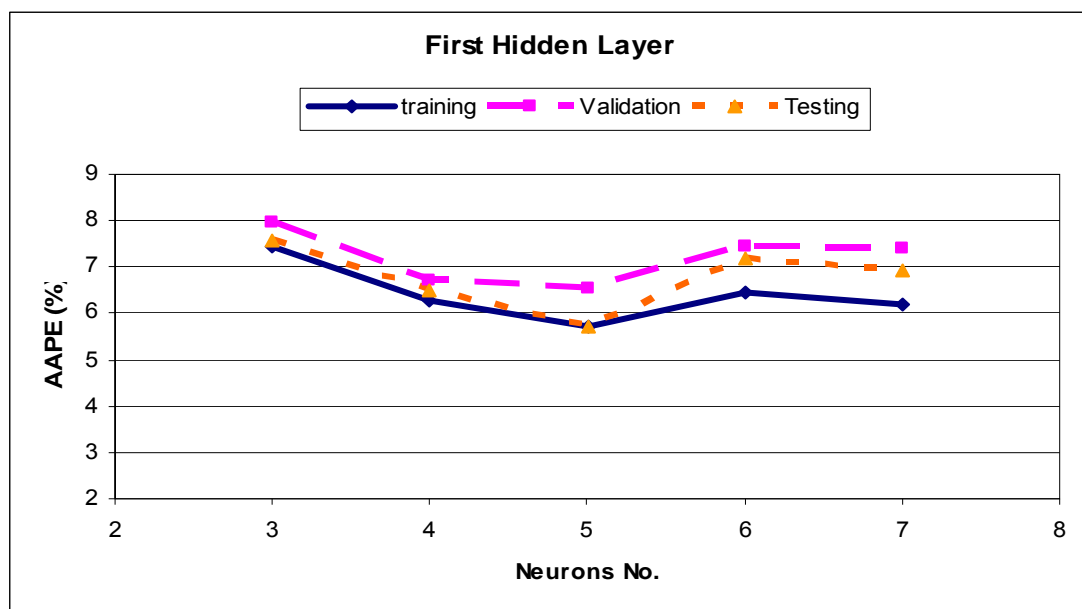


Figure 4.9: Impact of Neurons in First Hidden Layer on Absolute Error of Choke Size Prediction

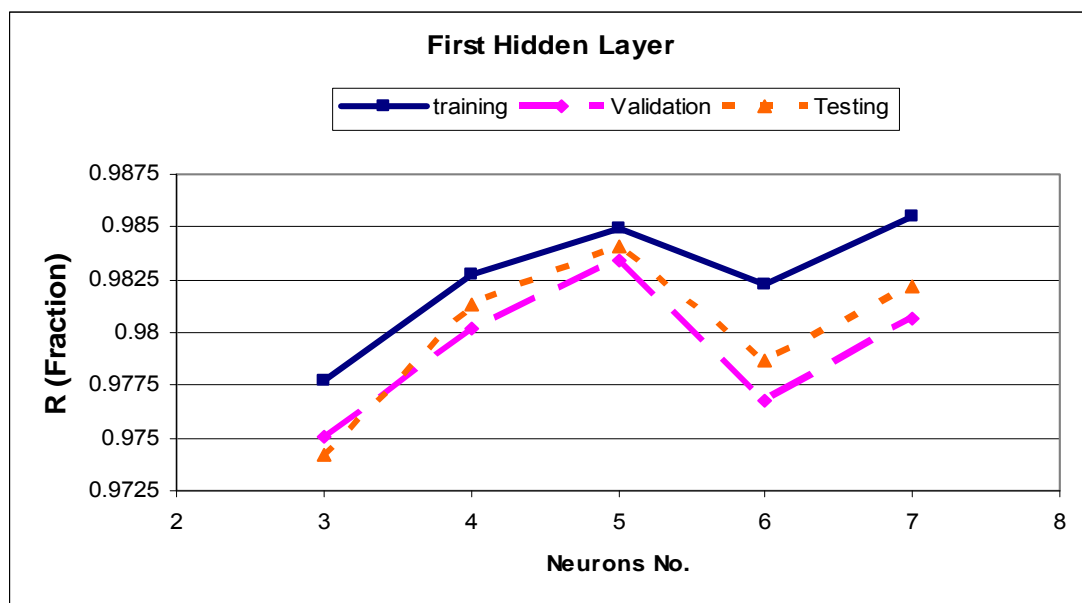


Figure 4.10: Impact of Neurons in First Hidden Layer on Correlation Coefficient of Choke Size Prediction



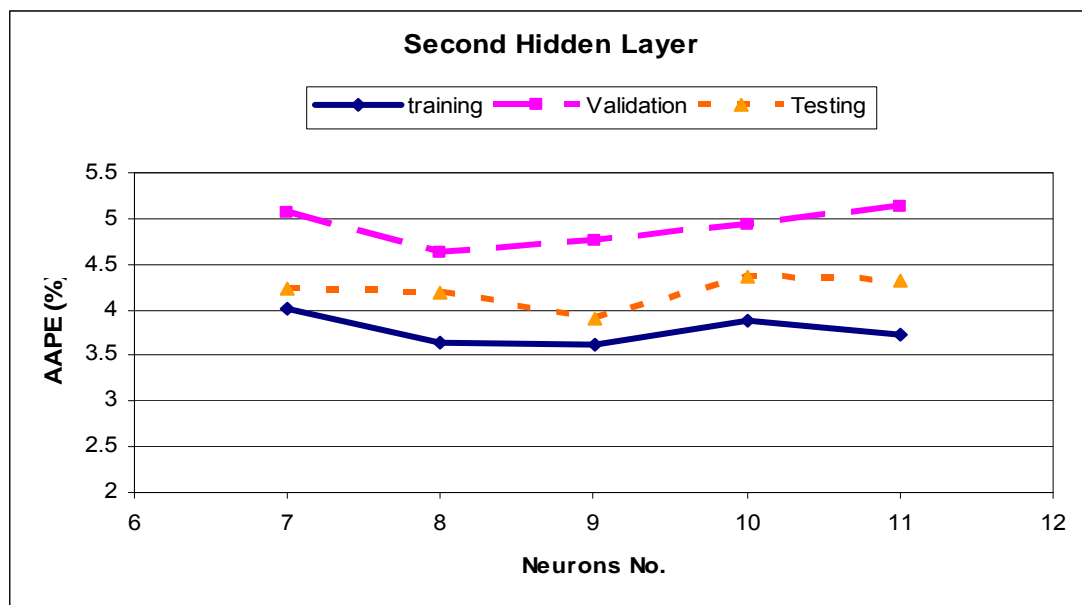


Figure 4.11: Impact of Neurons in Second Hidden Layer on Absolute Error of Choke Size Prediction

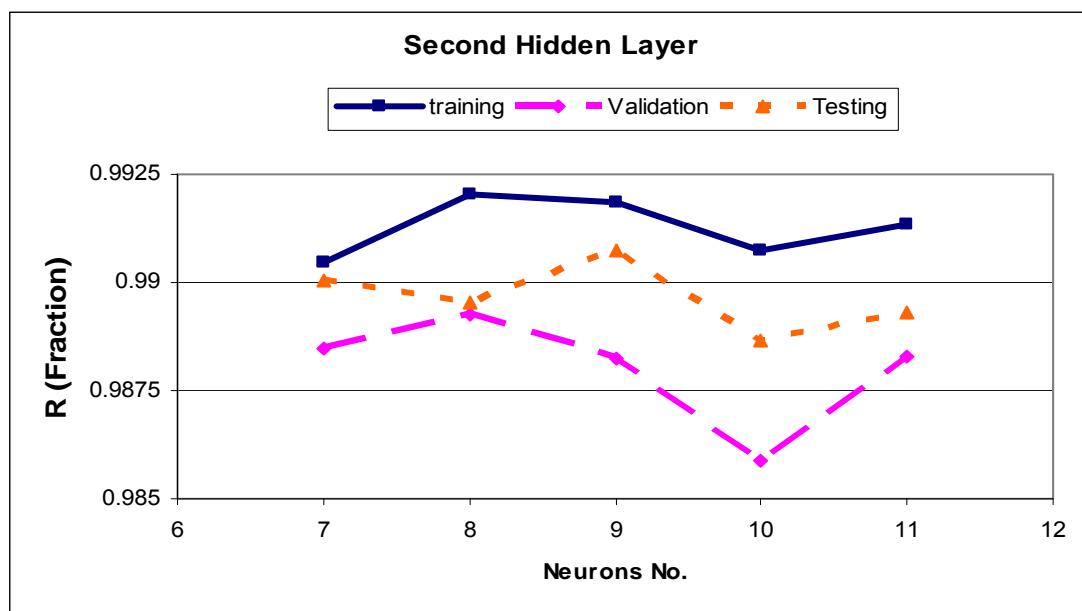


Figure 4.12: Impact of Neurons in Second Hidden Layer on Correlation Coefficient of Choke Size Prediction

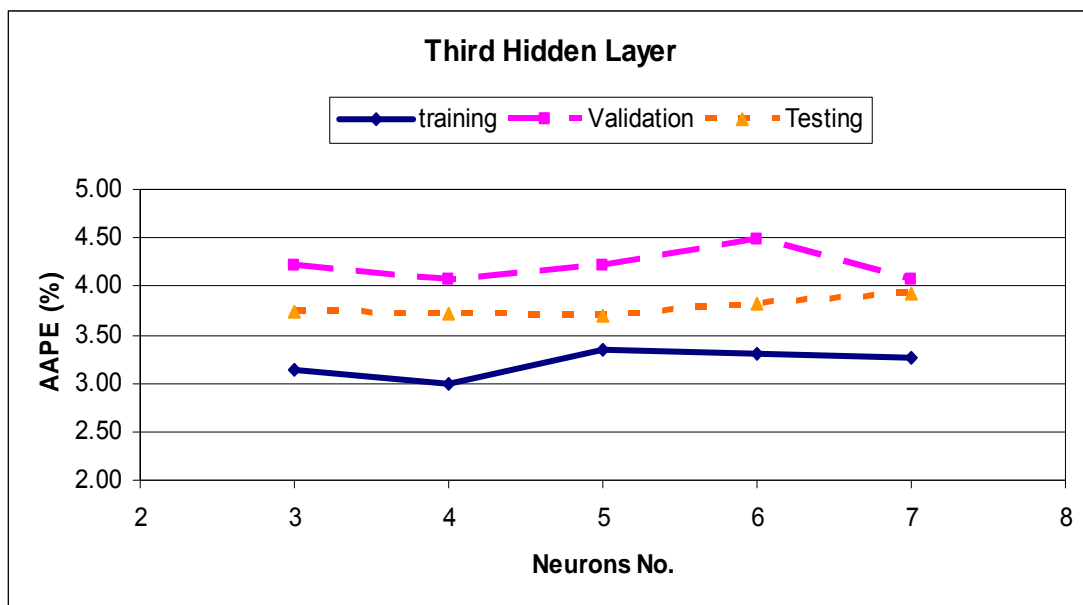


Figure 4.13: Impact of Neurons in Third Hidden Layer on Absolute Error of Choke Size Prediction

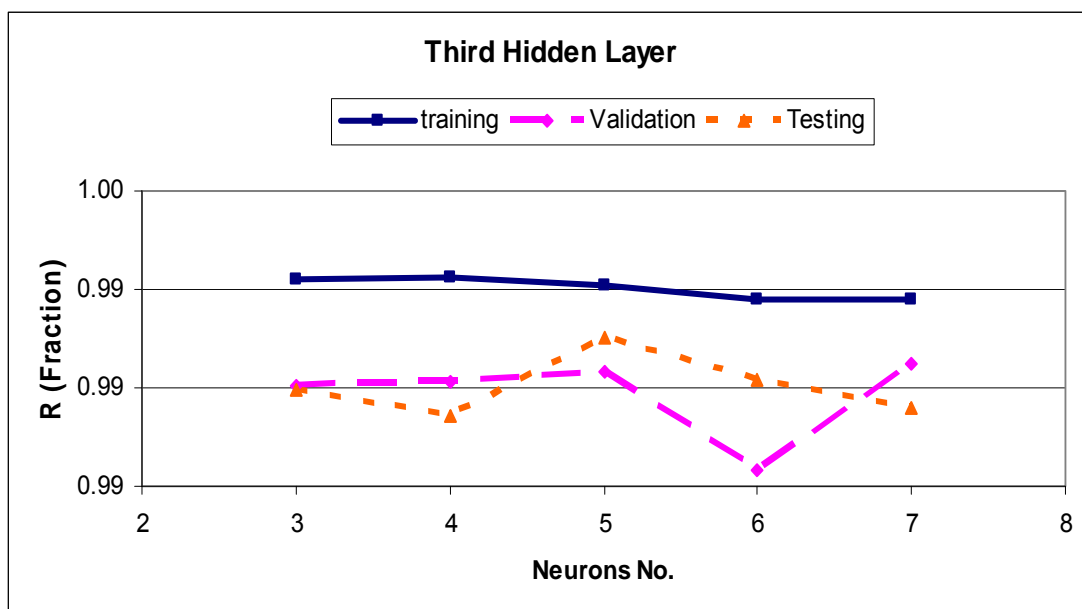


Figure 4.14: Impact of Neurons in Third Hidden Layer on Correlation Coefficient of Choke Size Prediction

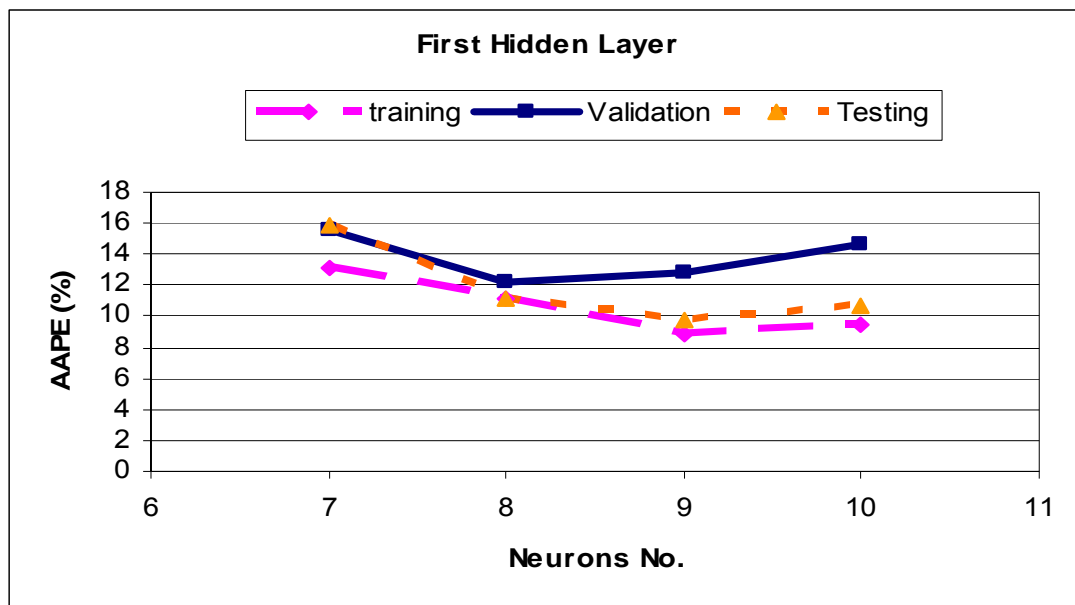


Figure 4.15: Impact of Neurons in First Hidden Layer on Absolute Error of Flow Rate Prediction

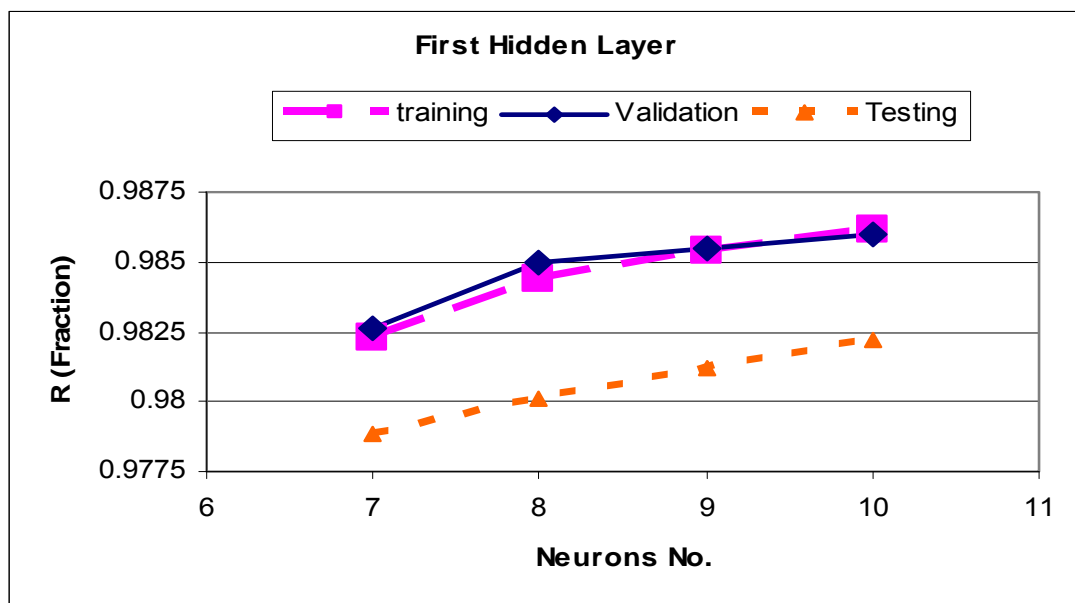


Figure 4.16: Impact of Neurons in First Hidden Layer on Correlation Coefficient of Flow Rate Prediction

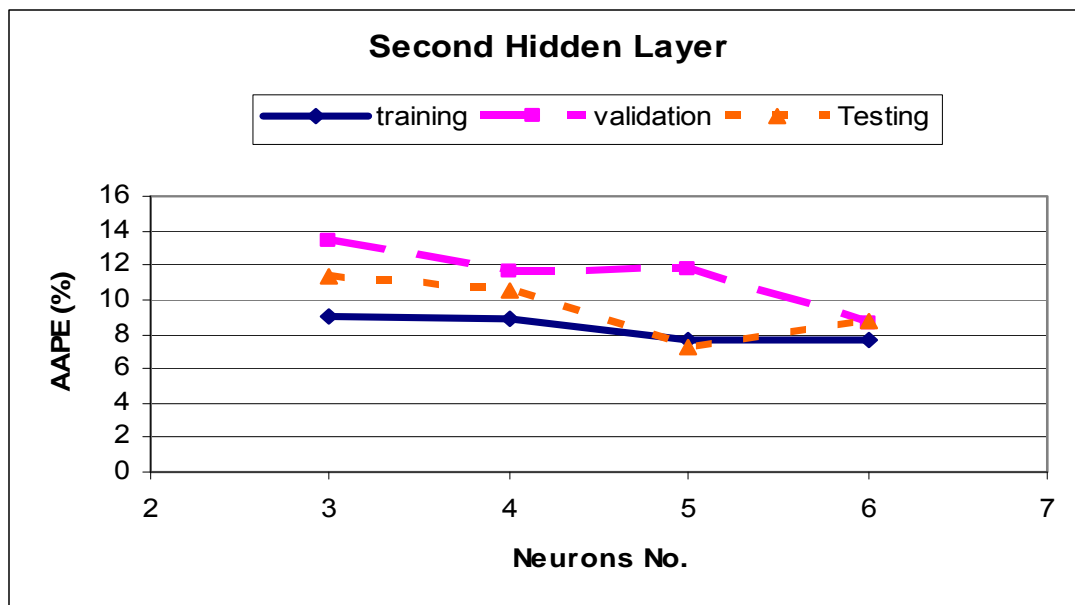


Figure 4.17: Impact of Neurons in Second Hidden Layer on Absolute Error of Flow Rate Prediction

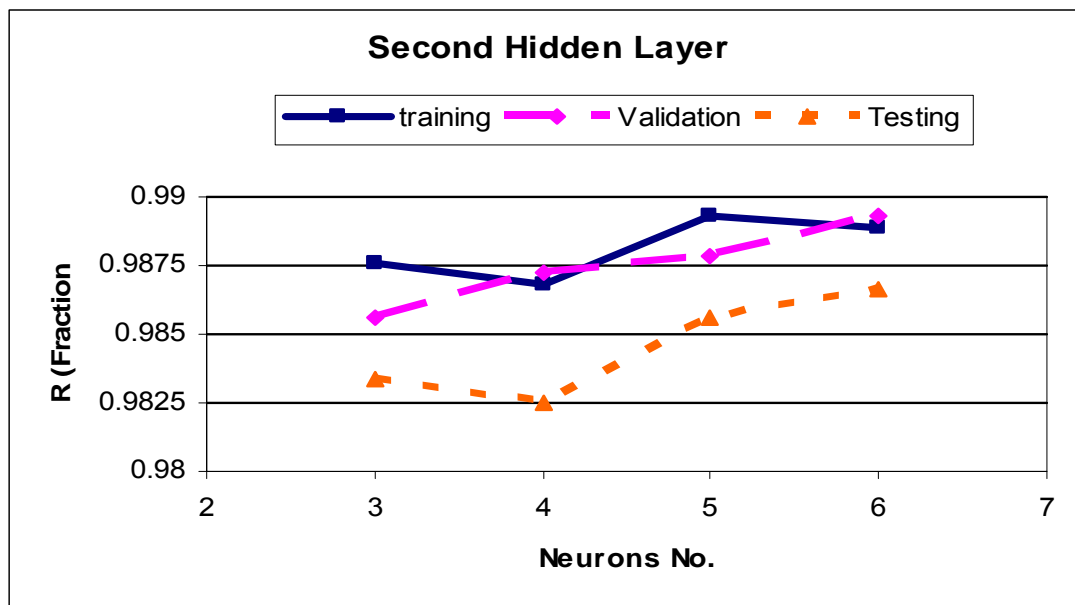


Figure 4.18: Impact of Neurons in Second Hidden Layer on Correlation Coefficient of Flow Rate Prediction



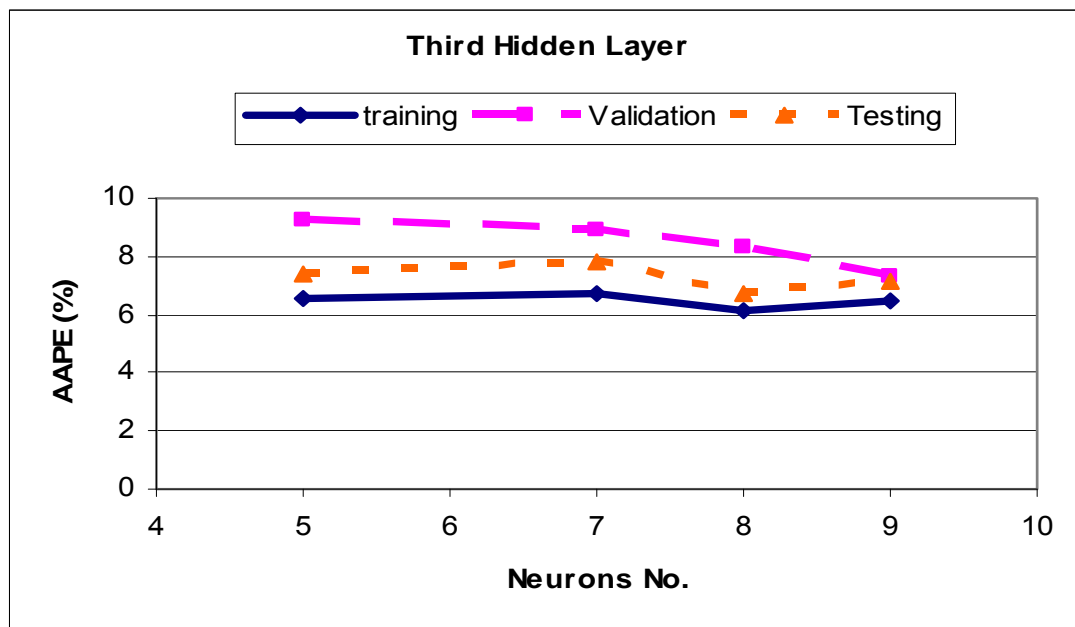


Figure 4.19: Impact of Neurons in Third Hidden Layer on Absolute Error of Flow Rate Prediction

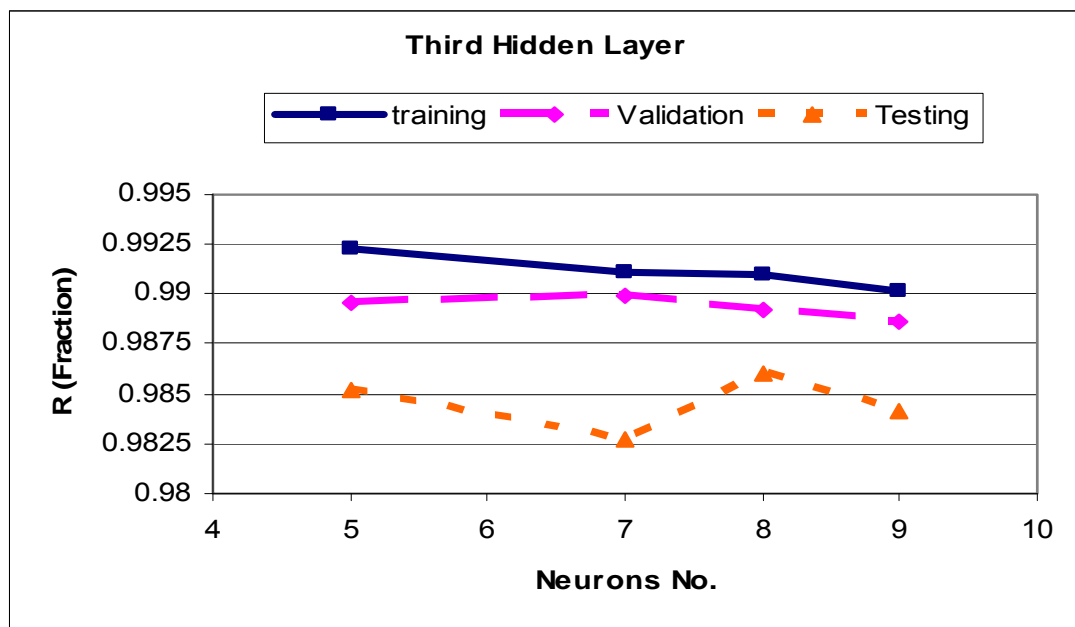


Figure 4.20: Impact of Neurons in Third Hidden Layer on Correlation Coefficient of Flow Rate Prediction

Table 4.1: Impact of Neurons in First Hidden Layer on Absolute Error and Correlation Coefficient of Choke Size Prediction

	Neurons	3	4	5	6	7
Train	AAPE	7.45	6.28	5.72	6.45	6.20
	R	0.98	0.98	0.98	0.98	0.99
Validation	AAPE	7.98	6.71	6.52	7.44	7.40
	R	0.98	0.98	0.98	0.98	0.98
Test	AAPE	7.57	6.48	5.69	7.18	6.94
	R	0.97	0.98	0.98	0.98	0.98

Table 4.2: Impact of Neurons in Second Hidden Layer on Absolute Error and Correlation Coefficient of Choke Size Prediction

	Neurons	7	8	9	10	11
Train	AAPE	4.01	3.65	3.62	3.88	3.73
	R	0.99	0.99	0.99	0.99	0.99
Validation	AAPE	5.06	4.63	4.76	4.93	5.14
	R	0.99	0.99	0.99	0.99	0.99
Test	AAPE	4.24	4.18	3.90	4.36	4.32
	R	0.99	0.99	0.99	0.99	0.99

Table 4.3: Impact of Neurons in Third Hidden Layer on Absolute Error and Correlation Coefficient of Choke Size Prediction

	Neurons	3	4	5	6	7
Train	AAPE	3.14	2.99	3.35	3.30	3.27
	R	0.99	0.99	0.99	0.99	0.99
Validation	AAPE	4.22	4.07	4.22	4.48	4.06
	R	0.99	0.99	0.99	0.99	0.99
Test	AAPE	3.73	3.72	3.70	3.82	3.93
	R	0.99	0.99	0.99	0.99	0.99

Table 4.4: Impact of Neurons in First Hidden Layer on Absolute Error and Correlation Coefficient of Flow Rate Prediction

	Neurons	7	8	9	10
Train	AAPE	13.17	11.06	8.84	9.51
	R	0.98	0.98	0.99	0.99
Validation	AAPE	15.50	12.19	12.86	14.71
	R	0.98	0.98	0.99	0.99
Test	AAPE	15.86	11.08	9.73	10.64
	R	0.98	0.98	0.98	0.98

Table 4.5: Impact of Neurons in Second Hidden Layer on Absolute Error and Correlation Coefficient of Flow Rate Prediction

	Neurons	3	4	5	6
Train	AAPE	9.08	8.92	7.59	7.68
	R	0.99	0.99	0.99	0.99
Validation	AAPE	13.36	11.65	11.81	8.55
	R	0.99	0.99	0.99	0.99
Test	AAPE	11.38	10.56	7.25	8.73
	R	0.98	0.98	0.99	0.99

Table 4.6: Impact of Neurons in Third Hidden Layer on Absolute Error and Correlation Coefficient of Flow Rate Prediction

	Neurons	3	4	5	6
Train	AAPE	6.56	6.70	6.13	6.50
	R	0.99	0.99	0.99	0.99
Validation	AAPE	9.22	8.92	8.34	7.29
	R	0.99	0.99	0.99	0.99
Test	AAPE	7.37	7.83	6.74	7.14
	R	0.99	0.98	0.99	0.98

### 4.3.3 Description of the Trained Neural Network Model

#### 4.3.3.1 Choke Size Prediction

The input and output variable should be normalized before feeding them into the model using the equation below:

$$Z_{i, \text{ normalized}} = [ Z_i - \text{Mean}(Z_i) ] / \text{STD}(Z_i) \quad (4.5)$$

$Z_i$  represent each of the input variables:

$Z(1)$  = wellhead pressure

$Z(2)$  = Oil flow rate

$Z(3)$  = Production gas oil ratio

$Z(4)$  = Relative oil density

$Z(5)$  = Relative gas density

$Z(6)$  = wellhead temperature

And after being processed the output data should be denormalized using the equation below:

$$Dc = Dc_{\text{normalized}} * \text{STD}(Dc) + \text{mean}(Dc) \quad (4.6)$$

The mean and standard deviation values used were as shown in table 4.7.

Table 4.7: The Mean and Standard Deviation Values for Training Data

	$D_c$ (64 <sup>th</sup> in.)	$P_{wh}$ (psig)	$Q_o$ (BPD)	$R_p$ (SCF/STB)	$Y_o$ (Water=1)	$Y_g$ (Air=1)	$T_{wh}$ (°F)
Mean	48.1414	1274.556	5122.284	858.2123	0.8357	0.8817	142.3584
STD	23.2645	1143.296	3981.632	623.505	0.0329	0.1011	33.7064

The values for the weights (w1, w2, w3 and w4) and bias (b1, b2, b3 and b4) are:

w1 =

-1.9419	-0.5612	1.4363	-0.3517	-0.949	0.9603
-1.2995	-1.2703	-0.8865	-1.3262	-2.471	0.3186
1.4497	-2.6423	1.8354	2.5698	0.5332	0.5497
-2.288	5.3731	0.9179	0.7902	1.0239	0.0998
3.5506	-0.6948	-0.2032	-0.9451	1.7412	0.9286

w2 =

-2.6399	1.8851	-2.5129	2.4399	3.4398
-1.8653	1.381	2.5781	-2.3095	-2.7588
2.9392	0.3157	-3.7587	1.6336	3.8108
2.5632	1.3451	-0.5537	0.491	-5.5314
2.519	2.5467	-0.0076	-1.4211	4.5881
-3.2161	2.7756	-0.5342	-3.0236	-1.1922
-0.4524	2.794	3.3226	-2.5232	-1.5543
0.1132	-1.3322	-0.8567	-1.6681	1.1982
0.189	2.6036	-1.5615	-3.5243	5.9235

w3 =

1.3955	-0.1496	0.6101	-1.3179	-0.3187	3.0698	1.3661	0.2917	-2.4817
-2.1829	3.2322	2.7476	1.9736	-2.1263	0.5274	-1.1334	1.4897	-2.0801
-0.2393	-0.0695	2.8986	-0.4629	-2.1236	-2.5099	-0.6332	-1.7498	2.885
0.6507	3.5512	2.2307	-1.0539	1.5081	0.3507	1.1894	-1.4964	-3.9127
-0.1703	-1.6024	-0.5339	-0.3905	-1.5854	-2.2863	0.7464	-1.0708	1.5412

w4 =

-3.6279	3.7168	0.4274	-4.6655	-1.4926
---------	--------	--------	---------	---------

<b>b1 =</b>	<b>b2 =</b>	<b>b3 =</b>	<b>B4 =</b>
0.0171	-5.6727	2.664	2.2711
4.9228	2.7086	-3.4004	
-0.3047	-3.9847	2.643	
4.052	1.4208	-1.388	
3.5972	-2.8585	-2.3528	
	0.7272		
	2.5582		
	5.0035		
	7.5649		

Table 4.8: Summary of Choke Size Neural Network Model

Layer	No. Neurons	Transfer Function
Input	6	-
First Hidden	5	Log sigmoid
Second Hidden	9	Log sigmoid
Third Hidden	5	Log sigmoid
Output	1	Pure line

#### 4.3.3.2 Flow Rate Estimation

The input and output variable should be normalized before feeding them into the model using equation 4.5.

Where  $Z_i$  represent each of the input variables:

$Z(1)$  = Choke Size

$Z(2)$  = wellhead temperature

$Z(3)$  = wellhead pressure

$Z(4)$  = Relative oil density

$Z(5)$  = Relative gas density

$Z(6)$  = Production gas oil ratio

And after being processed the output data should be denormalized using the equation below:

$$Q_o = Q_{o, \text{normalized}} * \text{STD}(Q_o) + \text{mean}(Q_o) \quad (4.7)$$

The mean and standard deviation values used were as shown in table 4.7.

The values for the weights (w1, w2, w3 and w4) and bias (b1, b2, b3 and b4) are:

w1 =

-0.682	0.7381	-0.938	-0.037	-0.456	0.0196
-1.006	-0.179	3.4537	-0.482	-0.439	0.1533
-0.599	3.7118	-0.054	-1.914	-1.433	-1.044
0.5453	0.3413	9.7296	-4.504	-0.39	0.516
3.0235	2.3782	0.5542	1.0623	0.5135	-1.129
0.348	-3.62	2.2901	1.2758	0.6197	-1.174
2.4146	-2.169	-0.486	1.993	-0.719	1.1509
-0.292	-0.312	-2.188	-1.241	0.7102	-0.283
0.0037	-1.624	-0.306	1.1908	-0.916	-0.37

W2 =

0.0633	-1.04	0.514	-1.684	2.8106	1.7108	-1.287	-2.544	-1.156
-0.689	-4.8	-3.39	1.2929	2.6509	6.5715	3.6087	0.4065	1.0722
2.9171	1.1996	0.004	-1.765	-3.428	-0.136	1.306	-0.319	-1.273
-2.285	-0.834	-2.97	0.4852	-0.701	2.9024	2.5576	0.6384	0.048
-1.799	1.9354	1.113	-2.789	1.0323	3.2745	3.3471	2.2257	-0.378

W3 =

4.1789	-3.787	2.4994	3.6117	3.1943
-0.329	2.7748	-4.235	1.6086	-0.926
1.8178	-1.953	0.137	-0.363	-0.396
-2.456	1.8523	1.8819	1.9152	0.7922
-0.502	-3.061	1.2498	2.7839	-6.142
-3.05	1.513	-2.444	-0.838	2.8679
0.676	3.4922	-1.803	-0.356	1.0787
0.0999	0.0142	-1.914	2.6242	-1.159

W4 =

**4.4945   -5.784   -2.232   2.3828   1.9764   1.2183   1.0988   1.5644**

**b1 =**

**7.8912  
6.9047  
7.1877  
2.5123  
-0.508  
-6.016  
1.9662  
5.3028  
6.5918**

**b2 =**

**4.715  
-0.968  
-1.213  
0.6133  
-6.39**

**b3 =**

**-8.701  
7.9333  
-0.999  
-1.103  
0.2869  
3.5502  
0.3193  
-0.088**

**b4 =**

**0.4673**

Table 4.9: Summary of Flow Rate Neural Network Model

Layer	No. Neurons	Transfer Function
Input	6	-
First Hidden	9	Log sigmoid
Second Hidden	5	Log sigmoid
Third Hidden	8	Log sigmoid
Output	1	Pure line



## CHAPTER 5

### RESULTS & DISCUSSION

To show the superiority of the newly developed model over the existing correlations, the collected data were utilized to test the empirical correlations available in the literature.

The newly developed models were compared with the empirical correlations using statistical and graphical analyses in three different ways: firstly by using their correlations with their original coefficients, secondly after recalculating their coefficients using least square multiple linear or nonlinear regression; a thirdly by using the robust regression, which minimizes the effect of outliers by estimating the variance-covariance matrix of the coefficients.

To evaluate some of the empirical correlations, the surface tension and gas compressibility factor were calculated using Abdul-Majeed et al. correlation for the tension and van der Waals Equation of State for the gas compressibility factor.

#### **5.1 Statistical Analysis**

The statistical analysis methods used in the comparison are as follow: Maximum Error, Minimum Error, Average Absolute Percent Error (AAPE), Average Percent Error (APE), Root Mean Square Error (RMSE), Standard Deviation (STD) and the correlation coefficients (R).

The analyses were made for both the choke size prediction and the flow rate estimation. (Tables 5.1 to 5.3 and 5.5 to 5.7)

#### 5.1.1 Correlations in Literature:

For choke size prediction, the lowest AAPE among all the empirical correlations using their original coefficients were found to be for Ros correlation with an AAPE of 8.5%. But after regression Omana correlation was found to have the lowest AAPE among all the correlations of about 7.3% and 7.19% if we utilize the robust fit. (Tables 5.1 to 5.3) (Figures 5.1 and 5.2)

Similarly, for flow rate estimation, the lowest AAPE among all empirical correlations using their original coefficients were found to be for Ros correlation with an AAPE of 18.12%. But after regression Omana correlation was found to have the lowest AAPE among all the correlations of about 14.35% and 13.78% if we utilize the robust fit. (Table 5.4 to 5.6)

Table 5.1: Statistical Accuracy of Choke Size Prediction using Empirical Correlation Original Coefficients

<b>Choke Size Empirical Correlation</b>							
<b>Model</b>	<b>Maximum Error (%)</b>	<b>Minimum Error (%)</b>	<b>AAPE (%)</b>	<b>APEV (%)</b>	<b>RMSE</b>	<b>STD</b>	<b>R</b>
<b>Ashford</b>	68.06	0.27	31.37	31.34	33.13	10.76	0.95
<b>Bizanti &amp; Mansouri</b>	655.20	0.01	60.50	-44.69	82.51	69.37	0.86
<b>Elgibaly &amp; Nashawi</b>	200.34	0.00	20.69	-15.35	28.67	24.22	0.93
<b>Pilehvari</b>	53.02	0.13	27.22	27.09	28.35	8.34	0.97
<b>Secen</b>	99.02	0.01	11.55	9.03	14.12	10.86	0.96
<b>Omana</b>	1242.03	0.13	55.45	28.26	91.97	87.53	0.29
<b>Towailib &amp; Marhoun</b>	146.24	0.00	10.54	0.40	13.81	13.81	0.97
<b>Rumah &amp; Bizanti</b>	63.24	0.01	23.13	22.73	25.65	11.88	0.96
<b>Poettman &amp; Beck</b>	63.46	0.00	29.89	29.79	31.40	9.93	0.95
<b>Attar &amp; Abdul-Majeed</b>	181.79	0.07	25.06	-23.65	31.62	20.99	0.95
<b>Surbey</b>	442.35	0.01	32.06	10.06	41.42	40.18	0.87
<b>Gilbert</b>	147.51	0.00	12.22	-8.56	17.02	14.71	0.95
<b>Achong</b>	129.51	0.00	11.03	4.46	15.10	14.43	0.94
<b>Baxendaell</b>	121.34	0.00	9.48	2.14	12.97	12.79	0.95
<b>Ros</b>	117.55	0.01	8.53	0.43	11.99	11.98	0.96
<b>Osman &amp; Dokla</b>	273.32	1.60	71.74	-71.74	75.39	23.16	0.96

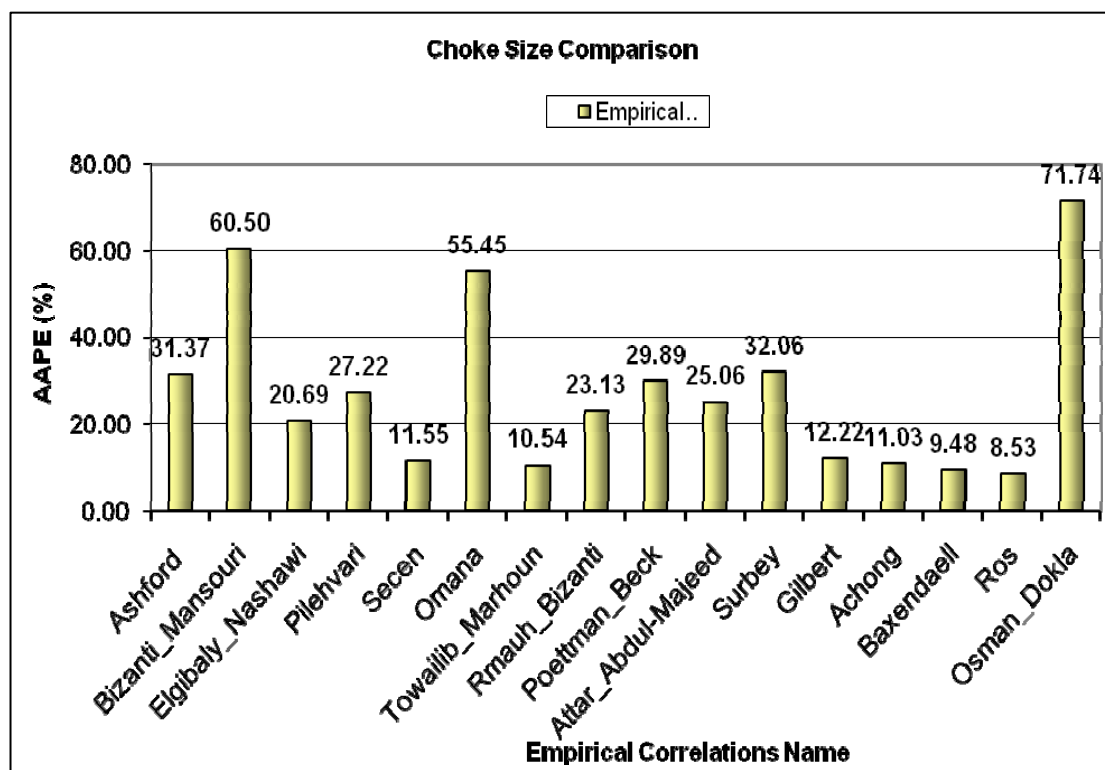


Figure 5.1: Statistical Accuracy of Choke Size Prediction using Empirical Correlation Original Coefficients

Table 5.2: Statistical Accuracy of Choke Size Prediction using Empirical Correlation after Regression

<b>Choke Size Empirical Correlation After Regression</b>							
<b>Model</b>	<b>Maximum Error (%)</b>	<b>Minimum Error (%)</b>	<b>AAPE (%)</b>	<b>APEV (%)</b>	<b>RMSE</b>	<b>STD</b>	<b>R</b>
Ashford	113.09	0.00	7.98	-0.56	10.98	10.97	0.97
Bizanti & Mansouri	94.51	0.00	7.64	-0.50	10.27	10.26	0.97
Elgibaly & Nashawi	93.81	0.00	7.59	-0.49	10.19	10.18	0.97
Pilehvari	93.81	0.00	7.59	-0.49	10.19	10.18	0.97
Secen	94.51	0.00	7.64	-0.50	10.27	10.26	0.97
Omana	95.60	0.00	7.30	-0.48	10.17	10.16	0.97
Towailib & Marhoun	126.93	0.00	8.49	-0.64	11.71	11.70	0.97
Rumah & Bizanti	94.51	0.00	7.64	-0.50	10.27	10.26	0.97
Poettman & Beck	96.93	0.00	7.97	-0.55	11.02	11.01	0.97
Attar & Abdul-Majeed	94.51	0.00	7.64	-0.50	10.27	10.26	0.97
Surbey	93.81	0.00	7.59	-0.49	10.19	10.18	0.97
Gilbert	93.81	0.00	7.59	-0.49	10.19	10.18	0.97
Achong	93.81	0.00	7.59	-0.49	10.19	10.18	0.97
Baxendaell	93.81	0.00	7.59	-0.49	10.19	10.18	0.97
Ros	93.81	0.00	7.59	-0.49	10.19	10.18	0.97
Osman & Dokla	93.81	0.00	7.59	-0.49	10.19	10.18	0.97

Table 5.3: Statistical Accuracy of Choke Size Prediction using Empirical Correlation after Robust fit

<b>Choke Size Empirical Correlation After Robustfit</b>							
<b>Model</b>	<b>Maximum Error (%)</b>	<b>Minimum Error (%)</b>	<b>AAPE (%)</b>	<b>APEV (%)</b>	<b>RMSE</b>	<b>STD</b>	<b>R</b>
Ashford	115.13	0.01	7.98	-1.04	11.21	11.17	0.97
Bizanti & Mansouri	100.54	0.01	7.48	-0.62	10.42	10.40	0.97
Elgibaly & Nashawi	99.88	0.00	7.44	-0.63	10.34	10.32	0.97
Pilehvari	99.88	0.00	7.44	-0.63	10.34	10.32	0.97
Secen	100.54	0.01	7.48	-0.62	10.42	10.40	0.97
Omana	102.81	0.00	7.19	-1.08	10.43	10.37	0.97
Towailib & Marhoun	128.35	0.01	8.34	-0.91	11.79	11.76	0.97
Rumah & Bizanti	100.54	0.01	7.48	-0.62	10.42	10.40	0.97
Poettman & Beck	124.10	0.00	7.91	-1.08	11.47	11.42	0.97
Attar & Abdul-Majeed	100.54	0.01	7.48	-0.62	10.42	10.40	0.97
Surbey	99.88	0.00	7.44	-0.63	10.34	10.32	0.97
Gilbert	99.88	0.00	7.44	-0.63	10.34	10.32	0.97
Achong	99.88	0.00	7.44	-0.63	10.34	10.32	0.97
Baxendaell	99.88	0.00	7.44	-0.63	10.34	10.32	0.97
Ros	99.88	0.00	7.44	-0.63	10.34	10.32	0.97
Osman & Dokla	99.88	0.00	7.44	-0.63	10.34	10.32	0.97

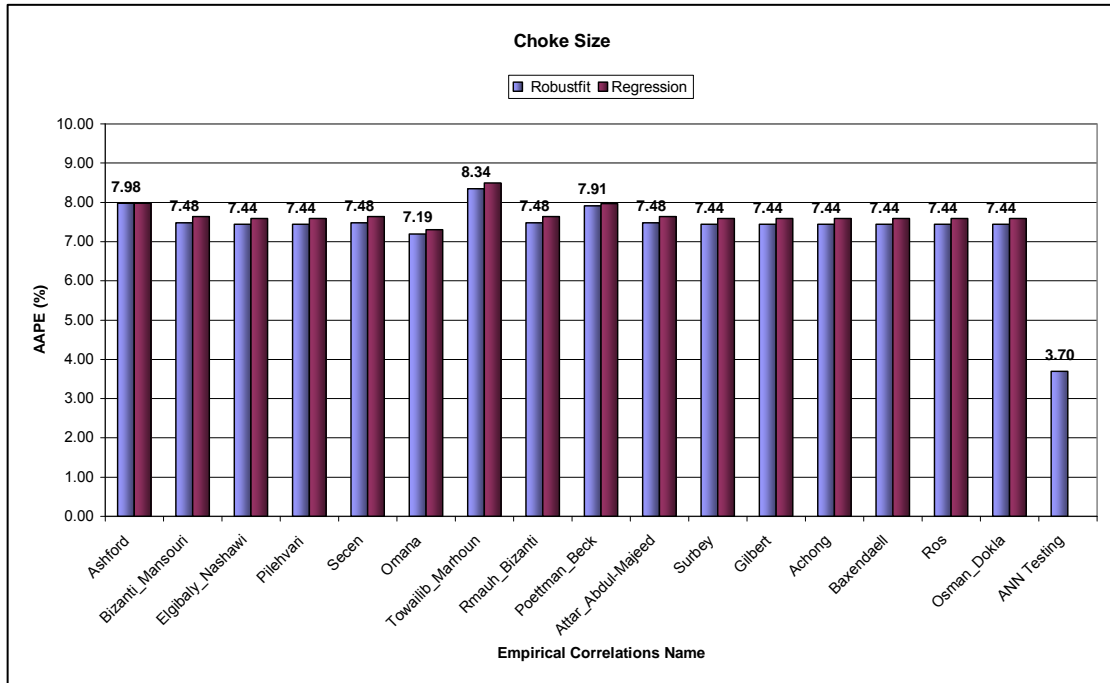


Figure 5.2: Statistical Accuracy of Choke Size Prediction using Empirical Correlation after Regression & Robust fit

Table 5.4: Statistical Accuracy of Flow Rate Estimation using Empirical Correlation Original Coefficients

<i>Flow Rate Estimation Empirical Correlation</i>							
Model	Maximum Error (%)	Minimum Error (%)	AAPE (%)	APEV (%)	RMSE	STD	R
Ashford	881.7	0.7	130.0	-130.0	154.6	83.7	0.93
Bizanti & Mansouri	588.0	0.0	53.9	12.9	68.6	67.4	0.38
Elgibaly & Nashawi	319.27	0.00	25.93	12.81	35.83	33.47	0.75
Pilehvari	388.1	0.0	101.6	-101.4	111.8	47.2	0.93
Secen	334.4	0.0	29.9	-26.1	41.4	32.1	0.90
Omana	4242.2	0.3	412.0	-400.1	723.6	603.0	0.52
Towailib & Marhoun	187.84	0.00	22.72	-6.62	29.53	28.78	0.93
Rumah & Bizanti	484.9	0.1	77.8	-77.3	96.5	57.9	0.91
Poettman & Beck	648.8	0.0	116.2	-116.1	134.8	68.5	0.94
Attar & Abdul-Majeed	112.4	0.1	28.0	25.1	32.0	19.8	0.88
Surbey	698.8	0.0	95.7	-75.7	152.1	132.0	0.47
Gilbert	238.0	0.0	19.5	10.0	26.8	24.9	0.87
Achong	481.7	0.0	25.6	-16.1	43.4	40.3	0.81
Baxendaell	318.0	0.0	20.5	-9.4	31.7	30.3	0.87
Ros	263.0	0.0	18.1	-5.3	27.5	27.0	0.90
Osman & Dokla	91.2	2.7	61.5	61.5	62.2	9.5	0.90

Table 5.5: Statistical Accuracy of Flow Rate Estimation using Empirical Correlation after Regression

<i>Flow Rate Estimation Empirical Correlation after Regression</i>							
Model	Maximum Error (%)	Minimum Error (%)	AAPE (%)	APEV (%)	RMSE	STD	R
Ashford	106.8	0.0	15.6	-2.0	20.1	20.0	0.95
Bizanti & Mansouri	110.9	0.0	15.0	-1.9	19.7	19.6	0.94
Elgibaly & Nashawi	101.0	0.0	14.9	-1.9	19.4	19.3	0.94
Pilehvari	101.0	0.0	14.9	-1.9	19.4	19.3	0.94
Secen	110.9	0.0	15.0	-1.9	19.7	19.6	0.94
Omana	105.0	0.0	14.3	-1.8	18.5	18.4	0.94
Towailib & Marhoun	103.5	0.0	16.0	-2.3	22.0	21.8	0.95
Rumah & Bizanti	110.9	0.0	15.0	-1.9	19.7	19.6	0.94
Poettman & Beck	91.8	0.0	15.7	-2.1	20.2	20.1	0.95
Attar & Abdul-Majeed	110.9	0.0	15.0	-1.9	19.7	19.6	0.94
Surbey	101.0	0.0	14.9	-1.9	19.4	19.3	0.94
Gilbert	101.0	0.0	14.9	-1.9	19.4	19.3	0.94
Achong	101.0	0.0	14.9	-1.9	19.4	19.3	0.94
Baxendaell	101.0	0.0	14.9	-1.9	19.4	19.3	0.94
Ros	101.0	0.0	14.9	-1.9	19.4	19.3	0.94
Osman & Dokla	101.0	0.0	14.9	-1.9	19.4	19.3	0.94

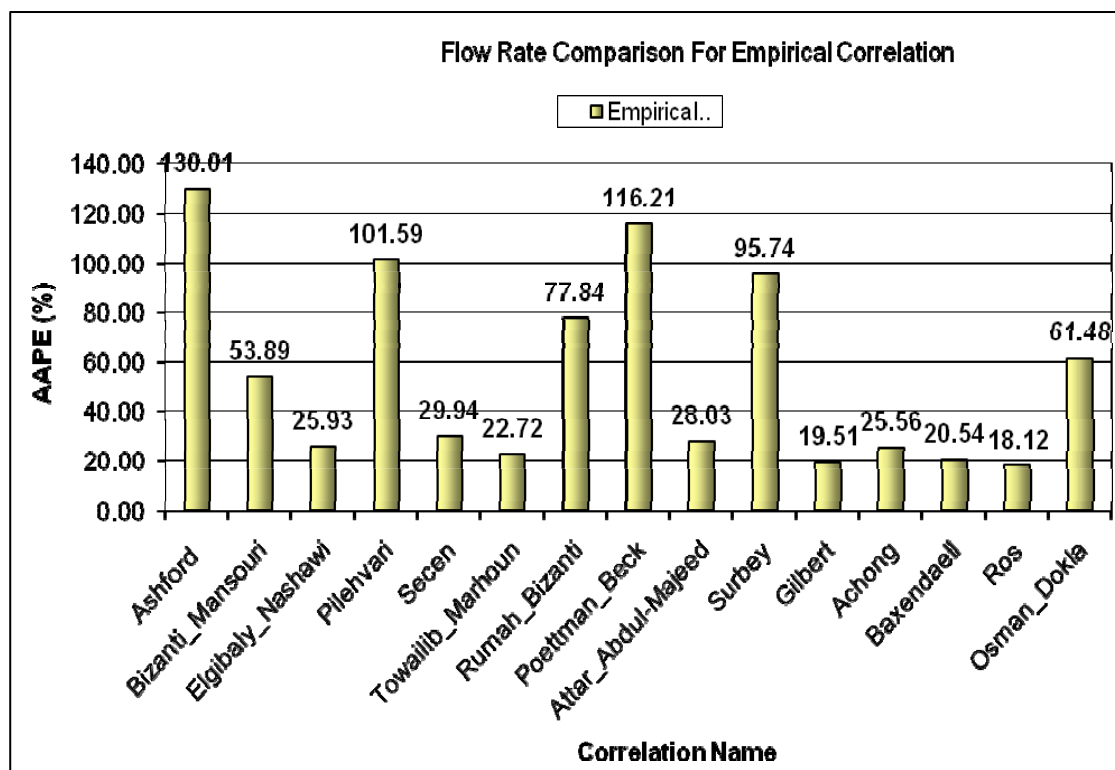


Figure 5.3: Statistical Accuracy of Flow Rate Estimation using Empirical Correlation Original Coefficients

Table 5.6: Statistical Accuracy of Flow Rate Estimation using Empirical Correlation after Robustfit

Model	Maximum Error (%)	Minimum Error (%)	AAPE (%)	APEV (%)	RMSE	STD	R
Ashford	104.27	0.00	15.45	-1.24	19.90	19.86	0.95
Bizanti & Mansouri	116.93	0.00	14.70	-1.33	20.08	20.04	0.94
Elgibaly & Nashawi	118.53	0.00	14.57	-1.26	19.86	19.82	0.94
Pilehvari	118.53	0.00	14.57	-1.26	19.86	19.82	0.94
Secen	116.93	0.00	14.70	-1.33	20.08	20.04	0.94
Omana	97.93	0.00	13.78	-0.25	18.39	18.39	0.94
Towailib & Marhoun	117.54	0.00	15.71	-2.22	22.66	22.55	0.96
Rumah & Bizanti	116.93	0.00	14.70	-1.33	20.08	20.04	0.94
Poettman & Beck	81.33	0.00	15.39	-1.01	19.91	19.89	0.95
Attar & Abdul-Majeed	116.93	0.00	14.70	-1.33	20.08	20.04	0.94
Surbey	118.53	0.00	14.57	-1.26	19.86	19.82	0.94
Gilbert	118.53	0.00	14.57	-1.26	19.86	19.82	0.94
Achong	118.53	0.00	14.57	-1.26	19.86	19.82	0.94
Baxendaell	118.53	0.00	14.57	-1.26	19.86	19.82	0.94
Ros	118.53	0.00	14.57	-1.26	19.86	19.82	0.94
Osman & Dokla	118.53	0.00	14.57	-1.26	19.86	19.82	0.94



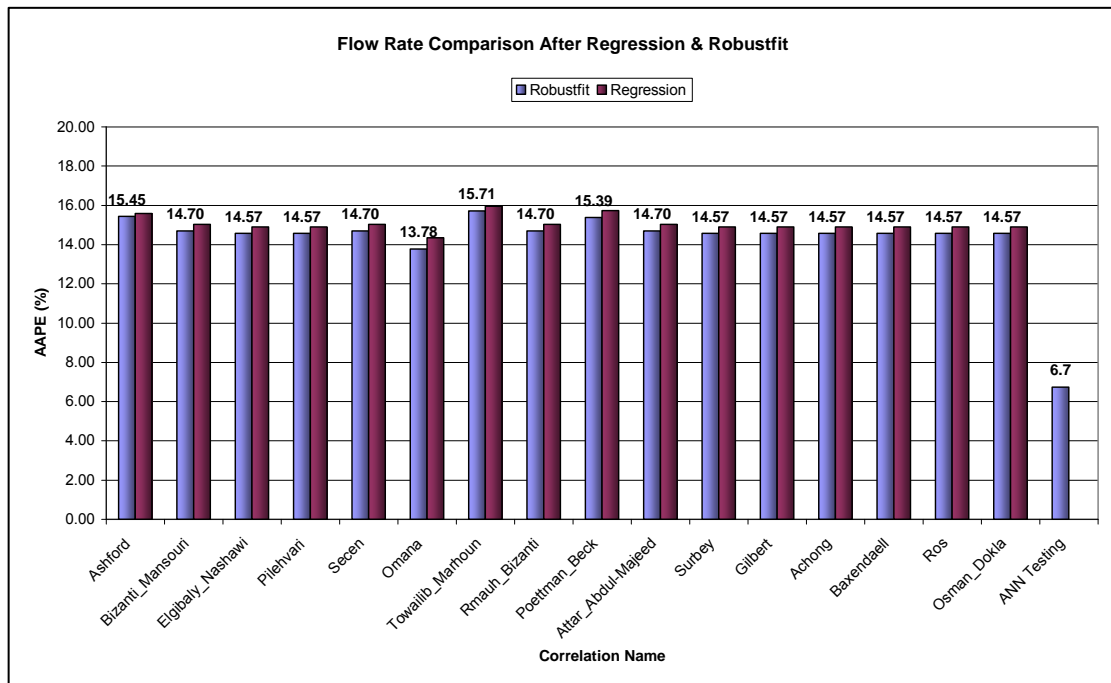


Figure 5.4: Statistical Accuracy of Flow Rate Estimation using Empirical Correlation after Regression & Robust fit

### 5.1.2 Newly Developed ANN Model:

The newly developed model for choke size prediction has provided a superior result compared to the correlations available in the literature with an average absolute percent error (AAPE) of 3.7%, root mean square error (RMSE) of 5.59, standard deviation (STD) of 5.56, correlation coefficients of 0.991 and a maximum error of 37.7%. The new model results are shown in table 5.7.

Similarly, the newly developed model for flow rate estimation has provided a superior result compared to the models available in the literature with an average absolute percent error (AAPE) of 6.7%, root mean square error (RMSE) of 10.5, standard deviation (STD) of 10.5, correlation coefficients (R) of 0.986, average percent error (APE) of 0.4, minimum error of 0 but with a maximum error of 71.7%. The new model result is shown in table 5.8.

Both newly developed models have provided a lower error and narrower variation than the existing correlations.

Table 5.7: Statistical Accuracy of Choke Size Prediction of the Newly Developed Model Using ANN

	Maximum Error (%)	Minimum Error (%)	APE (%)	RMSE	STDE	AAPE (%)	R
<b>Training</b>	37.65	0.00	-0.28	5.20	5.20	3.35	0.993
<b>Validation</b>	29.84	0.01	-0.65	6.23	6.20	4.22	0.990
<b>Testing</b>	34.83	0.01	-0.64	5.59	5.56	3.70	0.991

Table 5.8: Statistical Accuracy of Flow Rate Estimation of the Newly Developed Model Using ANN

	Maximum Error (%)	Minimum Error (%)	APE (%)	RMSE	STDE	AAPE (%)	R
<b>Training</b>	107.2	0.0	-0.7	9.7	9.6	6.1	0.991
<b>Validation</b>	178.1	0.0	-0.1	17.2	17.2	8.3	0.989
<b>Testing</b>	71.7	0.0	0.4	10.5	10.5	6.7	0.986

## **5.2 Graphical Analysis**

The graphical analysis methods used in the comparison are as follow: cross, scatter, histogram and the overlay plots. In addition to that, incremental analyses were also conducted for both the choke size and flow rate.

Cross plot is a common graphical analysis technique and was generated by plotting the measured versus the estimated values over a straight line of  $45^\circ$  drawn between them. The closer the points to this, line the closer the unity between them. Scatter plot is also a common technique used to summarize the relationship between two variables; we have utilized it to discover the trend by plotting the relative errors with the measured values. The histogram is a well known technique and was used in this study to visualize the error after classifying them into ranges.

### **5.2.1 Choke Size**

The newly developed model has shown a very high agreement between the measured and estimated values compared to the existing correlations with a correlations coefficient of 0.991 and a standard deviation of 5.56. The model has also shown a normal distribution with an average error of -0.64. In addition to that, the scatter plot has also shown that there are no relationships between the measured and predicted values (Figure 5.19 to 5.27).

On the other hand, the investigations of the existing empirical correlation have shown much higher errors than the newly developed model even after the regression and robust fit. A summary of the investigation are

shown below. In addition to that, Figures 5.37 to 5.83 shows the cross, scatter, histogram and the overlay plots for all the correlations, using their original coefficients, after regression and after robust fit.

Towailib and Marhoun correlation and Ros correlation has shown almost normal distribution. Whereas, the cross, scatter, histogram and overlay plots have shown the choke size to be under predicted in Ashford, Pilehvari, Secen, Omana, Rumah and Bizanti, Poettman and Beck, Surbey, Achong and Baxendaell correlations using the original coefficients. The histogram shows a shift of the mean of the error towards the positive side of the plots at 31.34 degree for Ashford, 27.09 for Pilehvari, 9.03 for Secen, at 28.26 for Omana, , 22.7 for Rumah and Bizanti, 29.8 for Poettman and Beck, 10.06 for Surbey, 4.46 for Achong and 2.14 for Baxendaell. After regression and robust fit, the predicted values were found to be normally distributed as can be seen in the histogram with an average error after regression of -0.56 for Ashford, -0.5 for Secen, -0.48 for Omana, -0.61 for Towailib and Marhoun for -0.5 for Rumah and Bizanti, -0.55 for Poettman and Beck and -0.5 for Attar and AbdulMajeed; and the average error after the robust fit was as follow: - 1.04 for Ashford, -0.62 for Secen, -1.08 for Omana, -0.91 for Towailib and Marhoun, -0.62 for Rumah and Bizanti, -1.08 for Poettman and Beck and -0.62 for Attar and AbdulMajeed. The scatter plot showed no obvious trend after regression and after robust fit. The cross plot has also shown the values to be reasonably predicted with a correlation coefficients of 0.97 for all of them. Figure 5.5 shows a comparison plot of these values for all the correlations.

For Bizanti and Mansouri, Elgibaly and Nashawi, Attar and Abdul-Majeed, Gilbert and Osman and Dokla correlations using the original

coefficients; the cross, scatter, histogram and overlay plots have shown the choke size to be over predicted. The histogram showed a shift of the mean of the error towards the negative side of the plots at -44.7, -15.35, -23.65, -8.56 and -71.74 respectively. The scatter and cross plot has also shown the over prediction and how it is increasing. After regression, the correlation coefficients for all Gilbert type correlations have increased to 0.97 and the STD was 10.19. The histogram showed a normal distribution of the data with an average error of -0.5, the scatter plot has shown no relationship between the error and the measured values, and the cross plot has also shown the values to be reasonably predicted. After the robust fit, we noticed a similar observation as after the regression with slight improvements in the average absolute relative error to 7.44%.

#### 5.2.2 Flow Rate:

The newly developed model has shown a very high agreement between the measured and estimated values compared to the existing correlations with a correlations coefficient of 0.986 and a standard deviation of 10.5. The model has also shown a normal distribution with an average error of 0.4. In addition to that, the scatter plot has shown that there are no relationships between the measured and predicted values. (Figure 5.28 to 5.35)

On the other hand, the investigations of the existing empirical correlation have shown much higher error than the newly developed model even after regression and robust fit, a summary of the investigation are shown below. In addition to that, Figures 5.84 to 5.131 shows the cross, scatter, histogram and the overlay plots for all the correlations, using their original coefficients, after regression and after robust fit.

For Ashford, Pilehvari, Secen, Omana, Towailib and Marhoun, Rumah and Bizanti, Poettman and Beck, Pilhevari, Surbey, Achong, Baxendll and Ros the histogram showed that these correlations with their original coefficients over estimate the flow rate with the following average percent error: -130, -101, -26, -400, -6.62, -77.25, -116, -75.7, -16, -9.4, and -5.3 respectively. Whereas for Bizanti and Mansouri, Elgibaly and Nashawi, Attar and AbdulMajeed, Gilbert, and Osman and Dokla, the histogram showed the flow rate is under estimated with an average percent error of 12.9, 12.8, 25, 10 and 61.5 respectively. The scatter plot showed that Elgibaly and Nashawi, Bizanti and Mansouri, and Attar and AbdulMajeed has a trend upward indicating an under estimation as the flow rate increases. The plot also showed that Omana has a trend downward indicating an over estimation. On the other hand, the rest of the correlations have shown no trend, but they have shown major difficulties in estimating the flow rate for some points.

After regression and robust fit, the scatter and histogram plot showed that the correlations have a normal distribution but tend to slightly over estimate the flow rate; this is shown clearly in the average percent error that ranged from -1.85 to -2. This average error decreases for most of the correlations after the robust fit to -1.3 except for Omana which has a lower APE of -0.25 and Towailib and Marhoun which has a higher APE of -2.2. The cross plot after regression and robust fit has high correlation coefficients of 0.95 for Ashford, Towailib and Marhoun, and Poettman and Beck and a correlation coefficient of 0.94 for the rest.

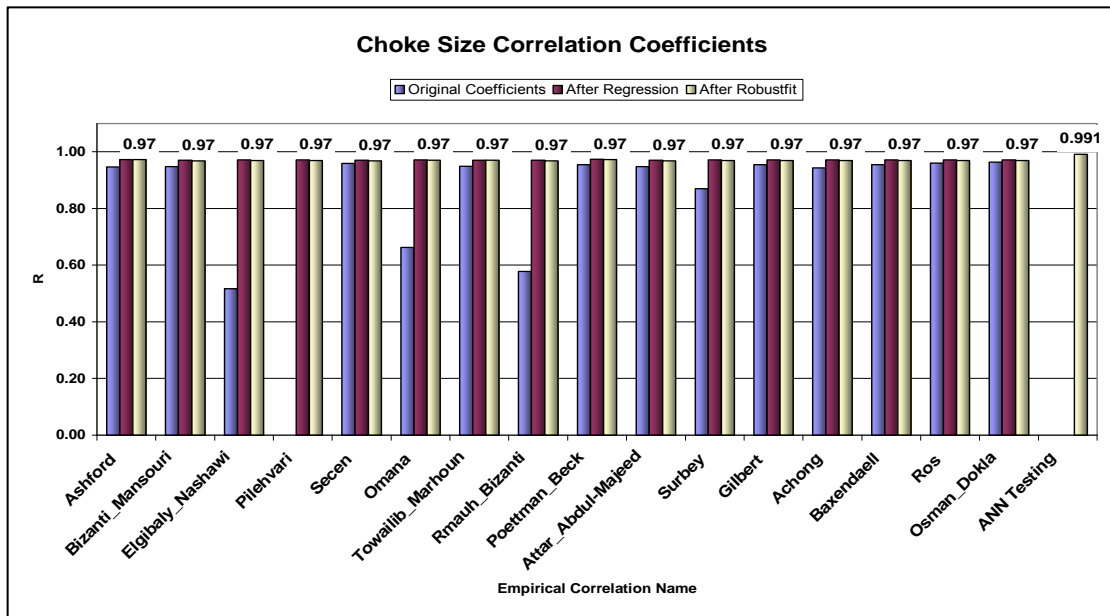


Figure 5.5: Correlation Coefficients of Empirical Correlation for Choke Size Prediction

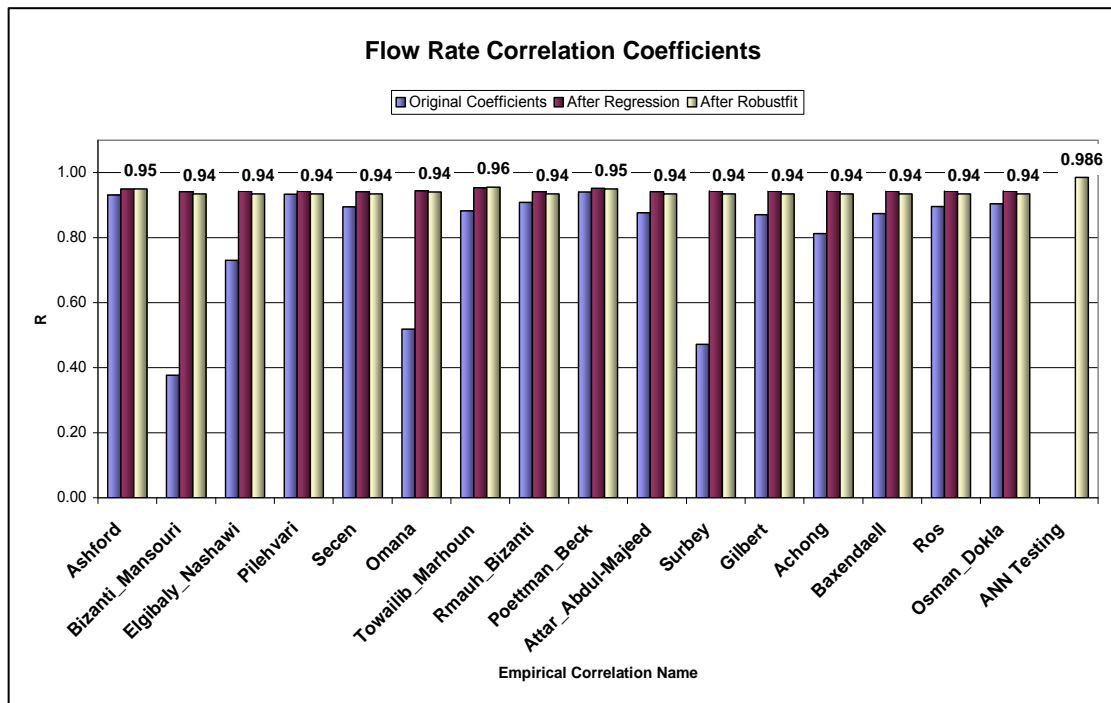


Figure 5.6: Correlation Coefficients of Empirical Correlation for Flow Rate Estimation



## 5.3 Incremental Analysis

### 5.3.1 Choke Size

The data were separated by choke size into ranges. The average absolute percent error and the root mean square error were obtained and plotted for each range of sizes. Figures 5.7 to 5.12 show these plots. Table 5-9 shows the choke size distribution for each range.

In most of the existing empirical correlations the absolute average percent error (AAPE) and the root mean square error (RMSE) were found to be constant over the different ranges of choke sizes except for five correlations namely: Bizanti and Mansouri, Rumah and Bizanti, Osman and Dokla, Attar and AbdulMajeed, and Elgibaly and Nashawi empirical correlations. These correlations the average absolute percent errors were found to be increasing as the choke sizes increase; Bizanti and Mansouri correlation has shown a sharp increase in AAPE as the choke size increases compared to the other correlations. Whereas, in Elgibaly and Nashawi, Attar and AbdulMajeed and Rumah and Bizanti the AAPE were generally decreasing as the choke sizes increase. (Figures 5.7 and 5.8)

After regression the AAPE and RMSE were found to be fluctuating in all the correlations from 6 to 10% and 8 to 14% respectively. Similarly, after robust fit the AAPE and RMSE were found to be fluctuating from 5 to 11% and 8 to 16% respectively. After the regression and robust fit, all Gilbert type correlations were found to follow the same trend and they were found to have lower errors for choke sizes between 12 and 32; but at choke sizes between 32 and 64 all the correlations were found to have more or less the same errors. For larger choke sizes 64 and above,

Ashford, Towailib and Marhoun and Poettmann and Beck correlations were found to be the best. (Figures 5.9 to 5.12)

### 5.3.2 Flow Rate

The data were separated by flow rate into ranges. The average absolute relative error and the root mean square error were obtained and plotted for each range of sizes. Figures 5.13 to 5.18 show these plots. Table 5-10 shows the flow rate distribution for each range.

For the empirical correlations using their original constants, the absolute average percent error (AAPE) and the root mean square error (RMSE) were found to be very high in all ranges, but the best among all was found to be Gilbert type, Attar and AbdulMajeed and Towailib and Marhoun correlations. (Figures 5.13 and 5.14)

After regression, the results have improved dramatically as can be seen in the figures 5.9 to 5.12 and 5.15 to 5.18. No trend was observed for the AAPE and RMSE, and the error was found to be fluctuating from 12 to 19 %. The performance of the different correlations varies in the different flow rate ranges. Omana and Gilbert type correlations were found to be the best for flow rates below 2500 Barrel Per Day (BPD), but for flow rates between 2500 and 5000 BPD Omana correlation is standing alone as the best correlation. For higher flow rates from 5000 to 10000 BPD Towailib and Marhoun is the best among all the others. But as flow rate increases from 10000 to 12500 BPD Poettman and Beck results improve and provide the lowest error. At higher flow rates Ashford correlation were found to have the lowest error. (Figures 5.15 and 5.16)

After the robust fit a similar conclusions were also obtained and the performance of the different correlations were almost the same but at a

lower AAPE for some of the correlations at certain ranges. For example at flow rates below 2500 BPD the AAPE for Omana correlation after regression was 12.7% but after robust fit it dropped to 11.1%. (Figure 5.17 and 5.18)

Table 5.9: Choke Size Ranges Used in Incremental Analysis

Chart Notation	1	2	3	4	5
Choke Size (64 <sup>th</sup> of an Inch)	12-24	24-32	32-64	64-96	96-130

Table 5.10: Flow Rate Ranges Used in Incremental Analysis

Chart Notation	1	2	3	4	5	6
Range (BPD)	250-2500	2500-5000	5000-7500	7500-10000	10000-12500	12500>

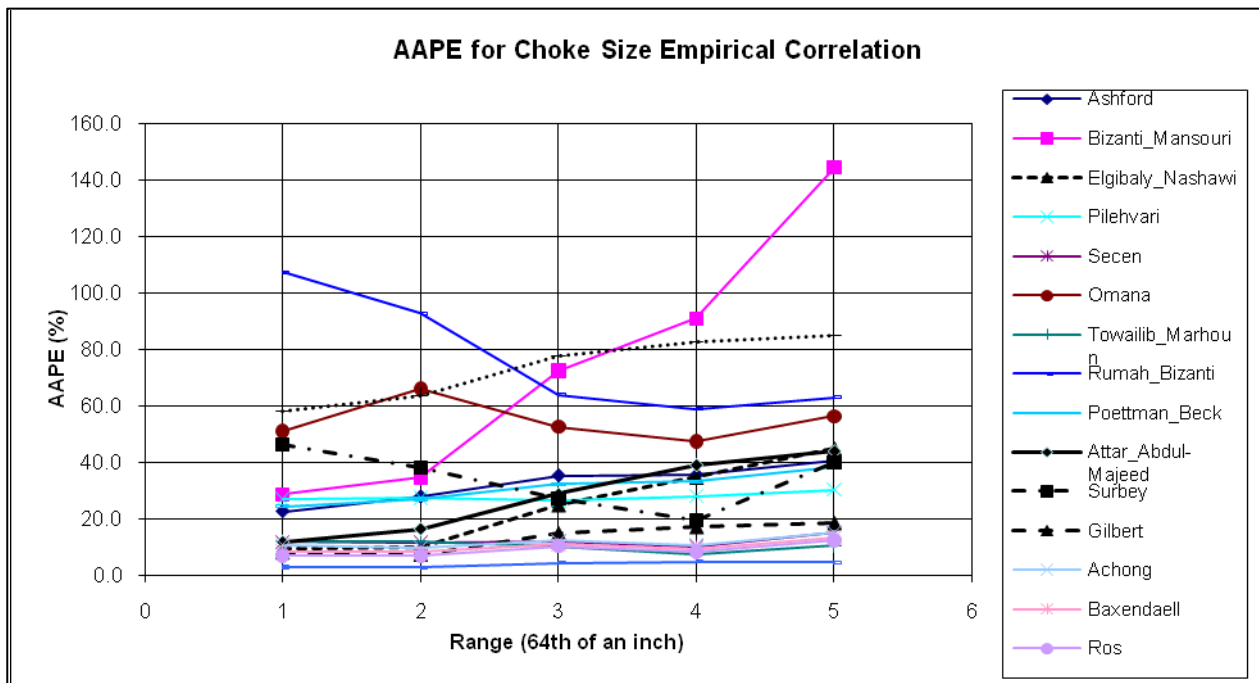


Figure 5.7: Accuracy of Correlation for Choke Size Prediction for Different Flow Rate ranges. (Absolute Average Percent Error)

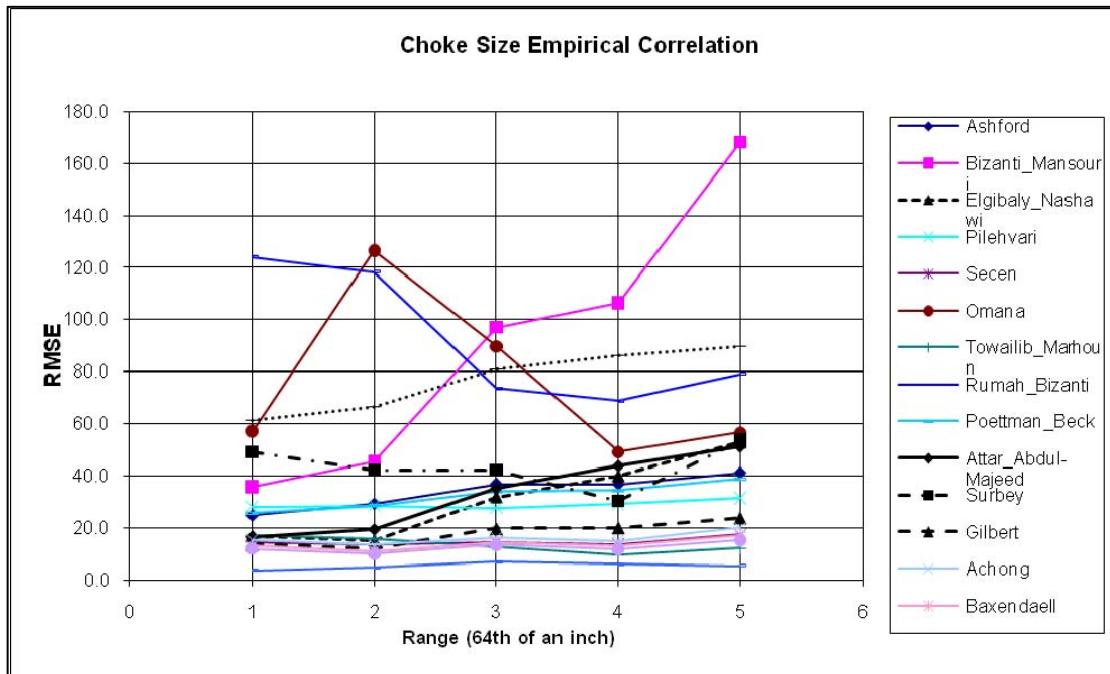


Figure 5.8: Accuracy of Correlation for Choke Size Prediction for Different Flow Rate ranges. (Root Mean Square Error)

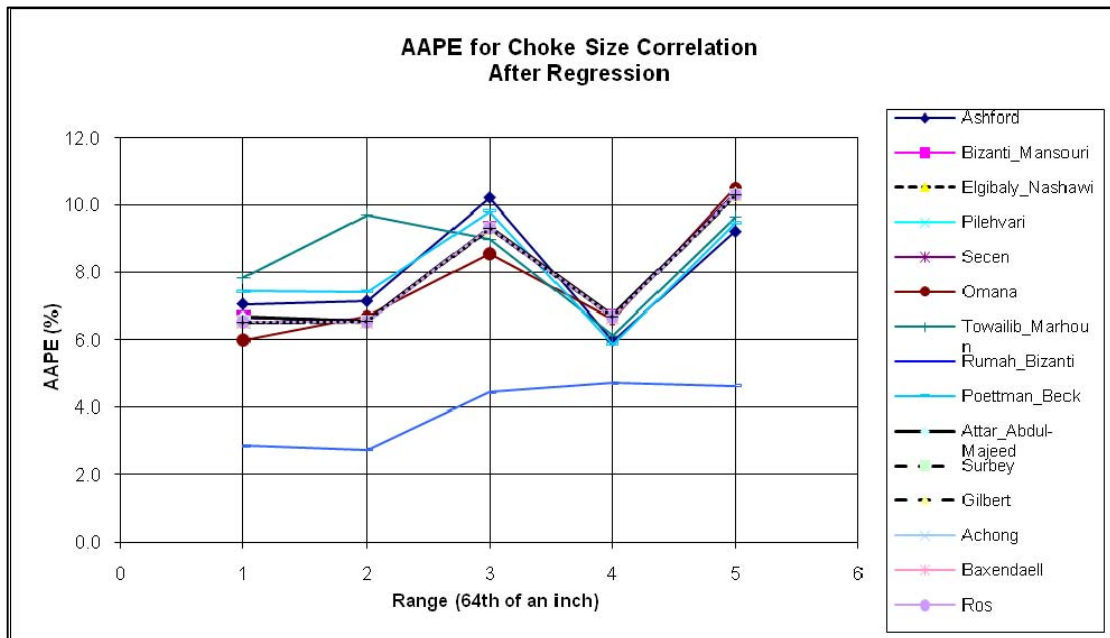


Figure 5.9: Accuracy of Correlation after Regression for Choke Size Prediction for Different Flow Rate ranges. (Absolute Average Percent Error)

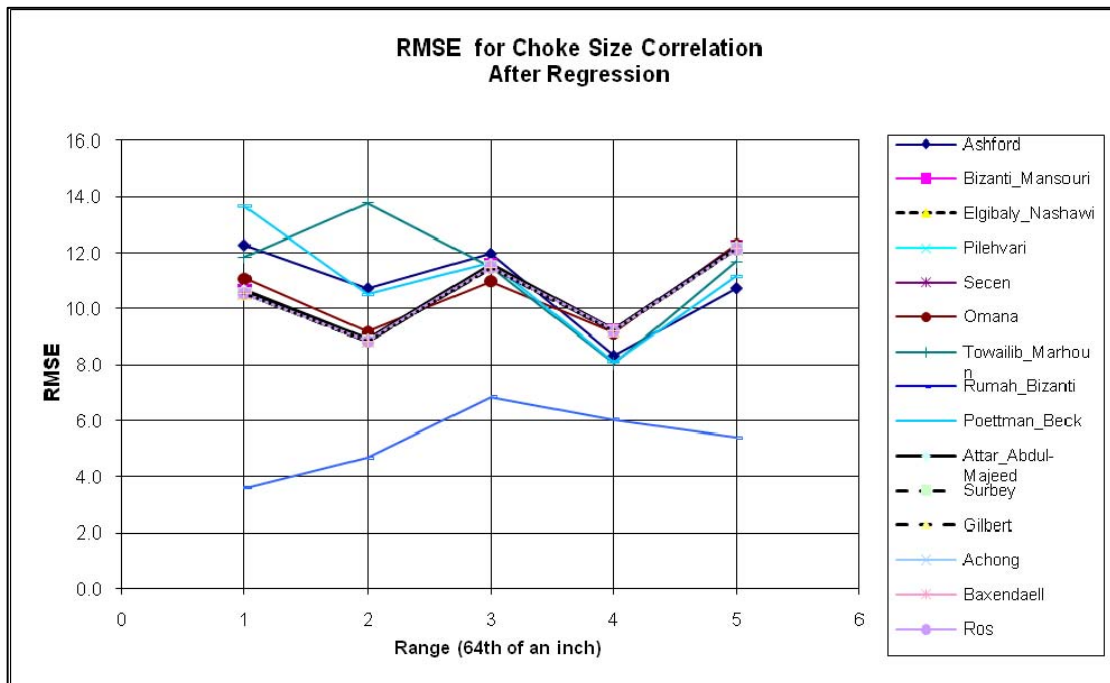


Figure 5.10: Accuracy of Correlation after Regression for Choke Size Prediction for Different Flow Rate ranges. (Root Mean Square Error)

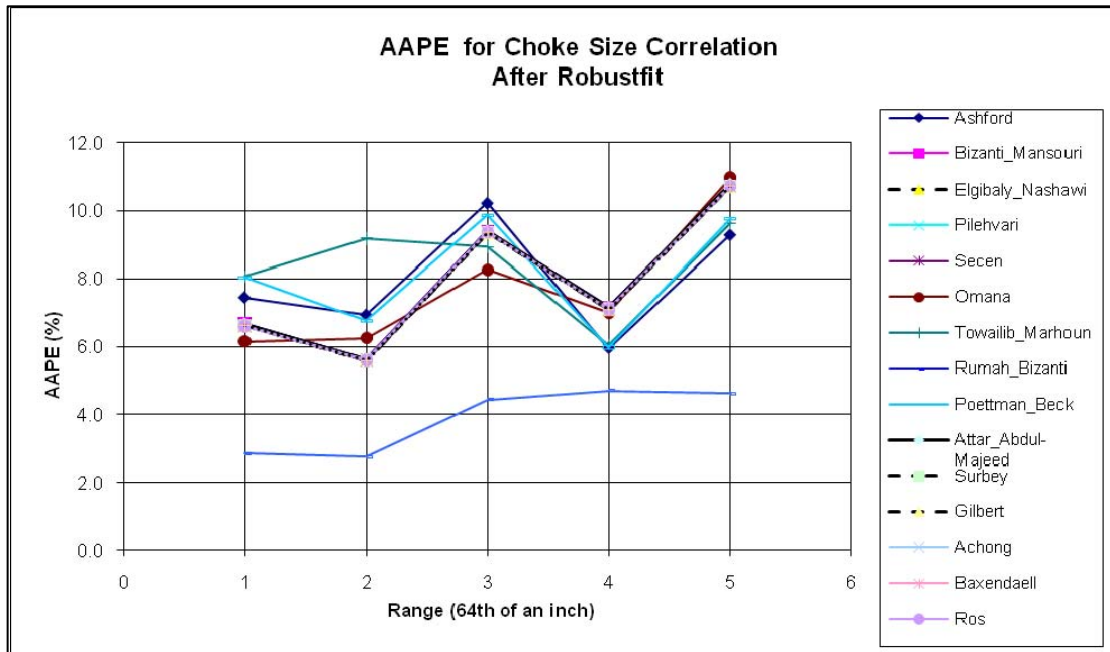


Figure 5.11: Accuracy of Correlation after Robust fit for Choke Size Prediction for Different Flow Rate ranges. (AAPE)



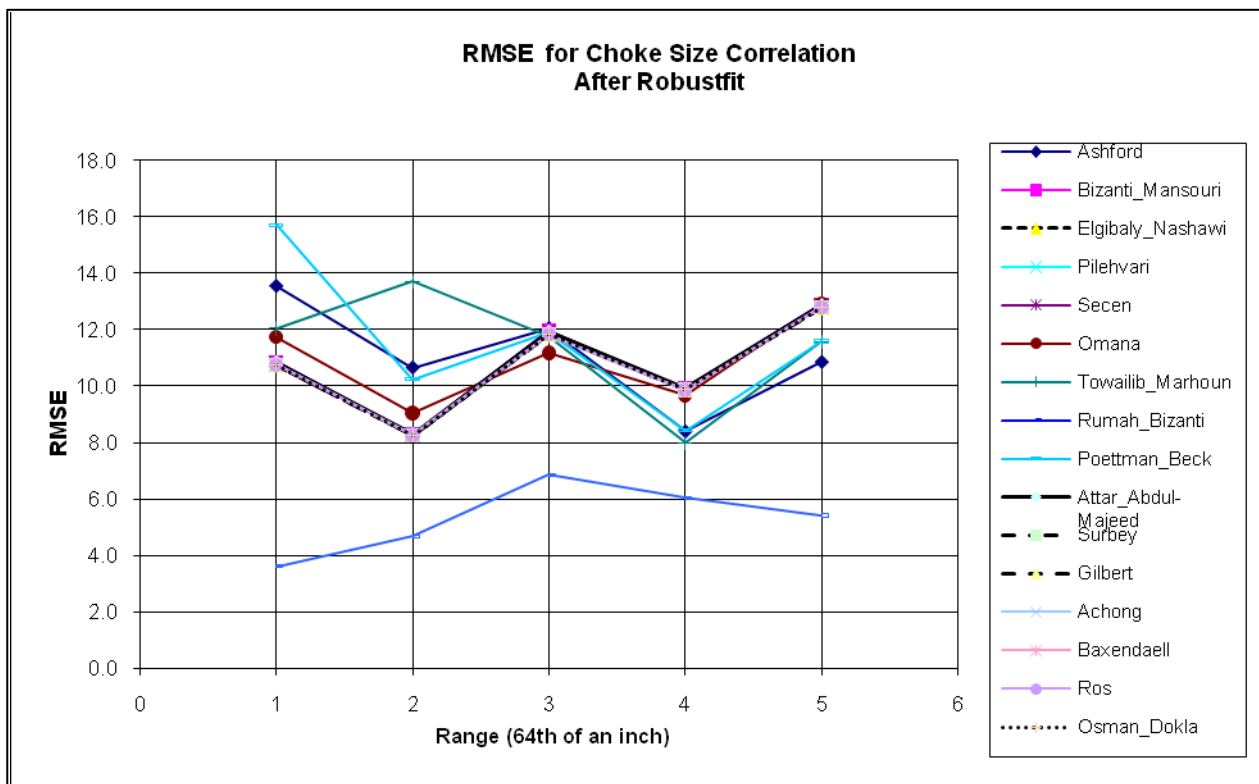


Figure 5.12: Accuracy of Correlation after Robust fit for Choke Size Prediction for Different Flow Rate ranges. (RMSE)

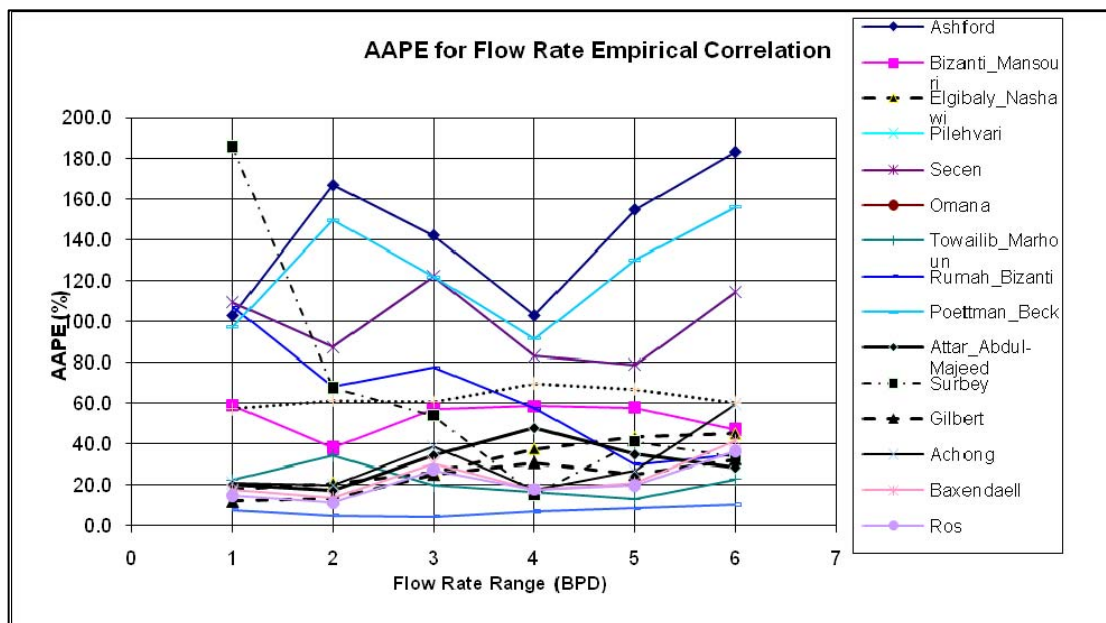


Figure 5.13: Accuracy of Correlation for Flow Rate Estimation for Different Flow Rate ranges. (Absolute Average Percent Error)

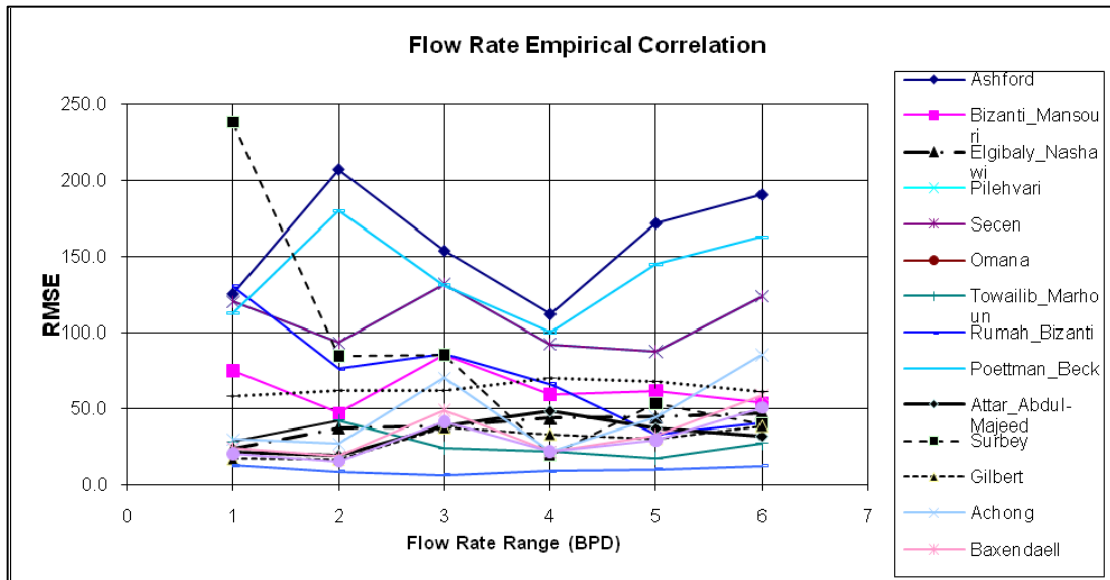


Figure 5.14: Accuracy of Correlation for Flow Rate Estimation for Different Flow Rate ranges. (Root Mean Square Error)

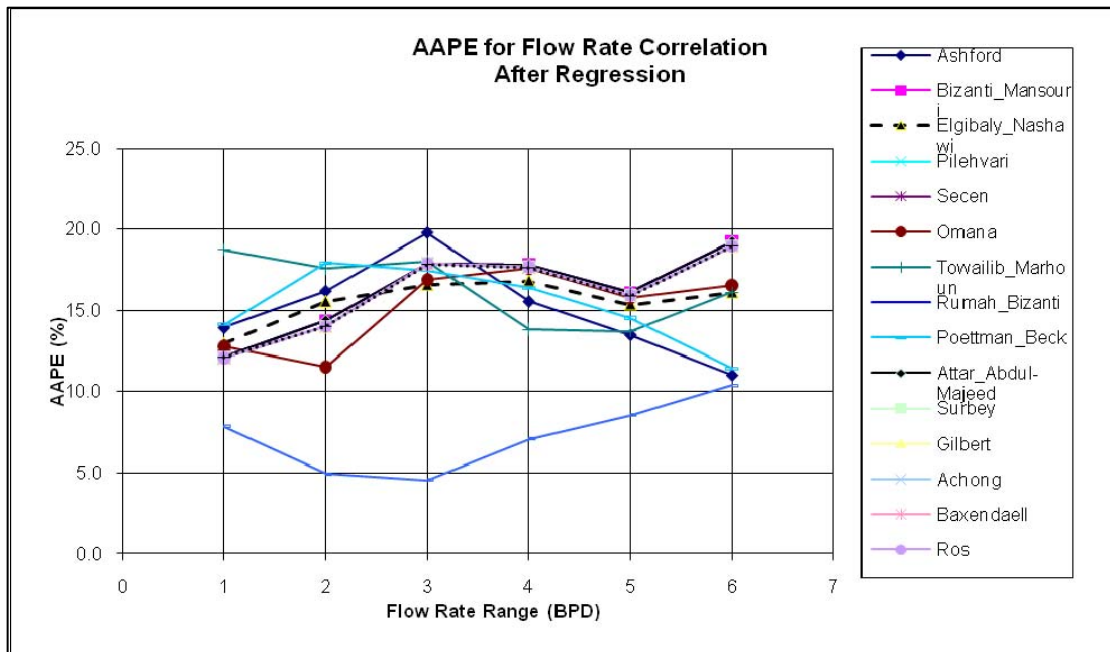


Figure 5.15: Accuracy of Correlation after Regression for Flow Rate Estimation for Different Flow Rate ranges. (Absolute Average Percent Error)

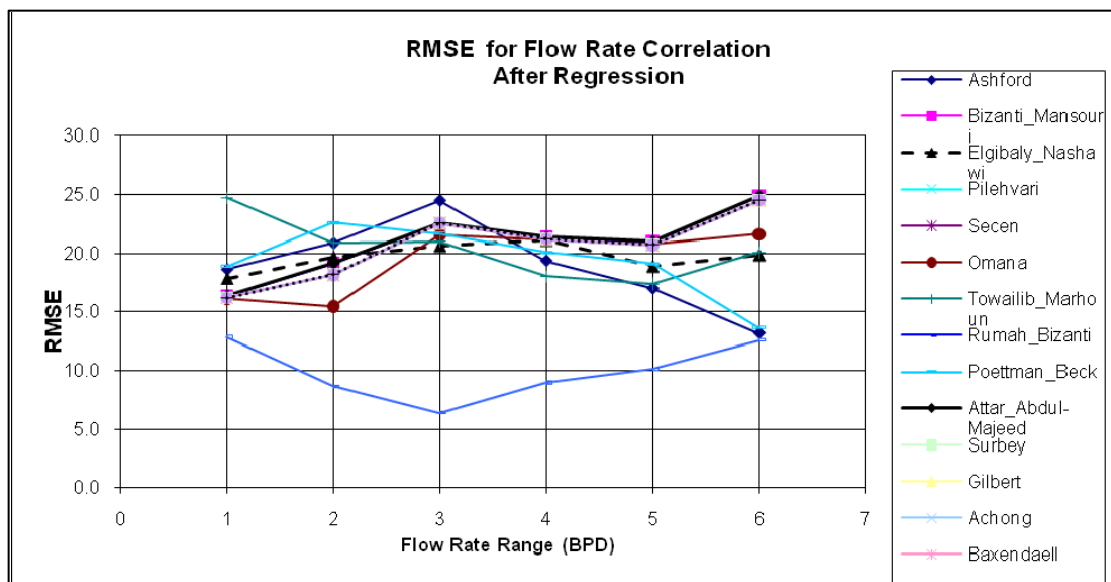


Figure 5.16: Accuracy of Correlation after Regression for Flow Rate Estimation for Different Flow Rate ranges. (Root Mean Square Error)

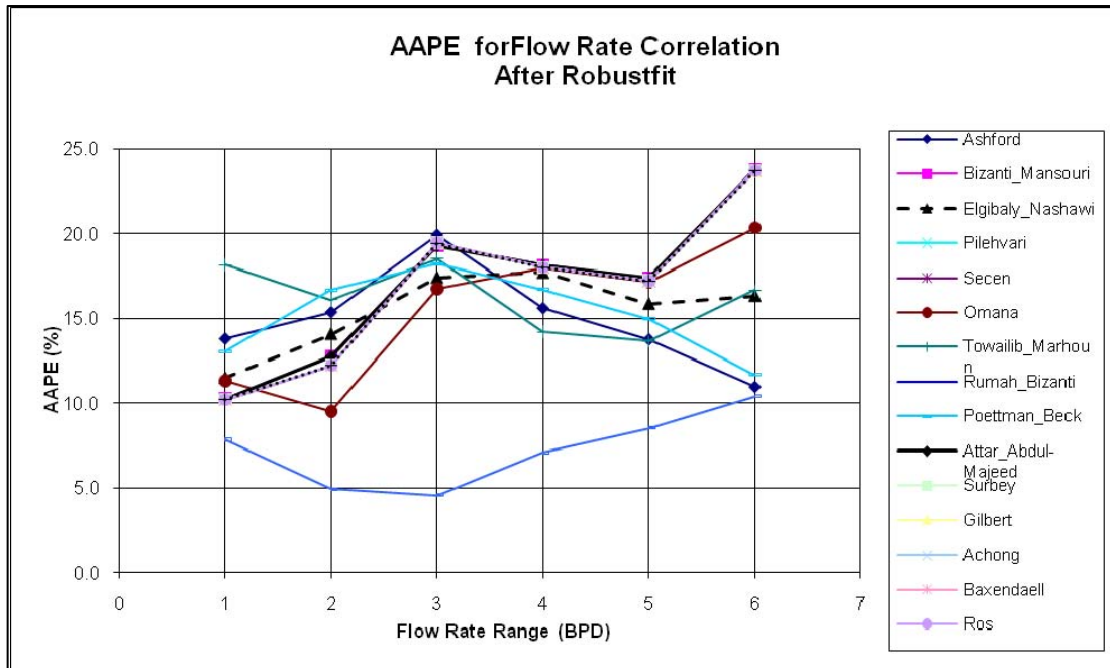


Figure 5.17: Accuracy of Correlation after Robust fit for Flow Rate Estimation for Different Flow Rate ranges. (Absolute Average Percent Error)

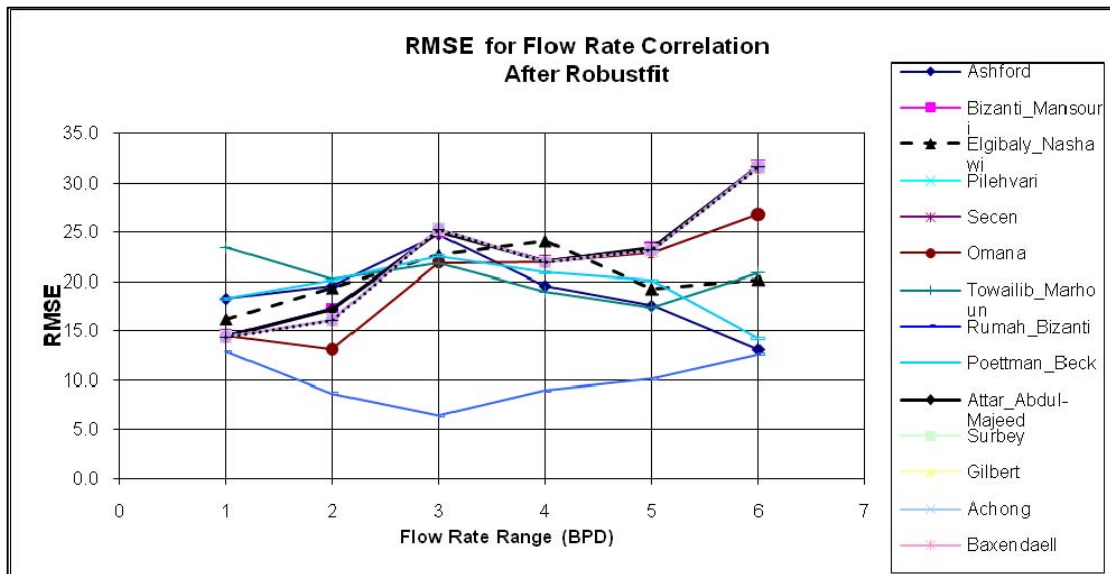


Figure 5.18: Accuracy of Correlation after Robust fit for Flow Rate Estimation for Different Flow Rate ranges. (Root Mean Square Error)

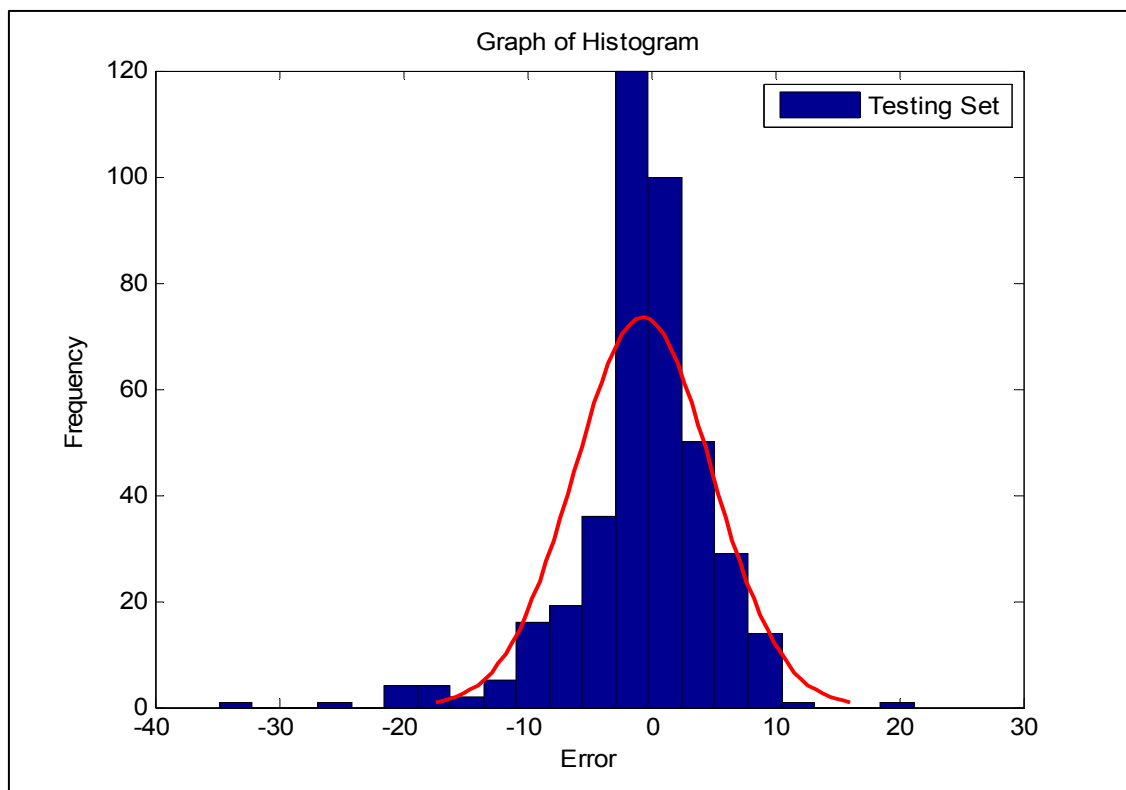


Figure 5.19: Error Distribution Plot of Choke Size Prediction for Testing set (ANN model)



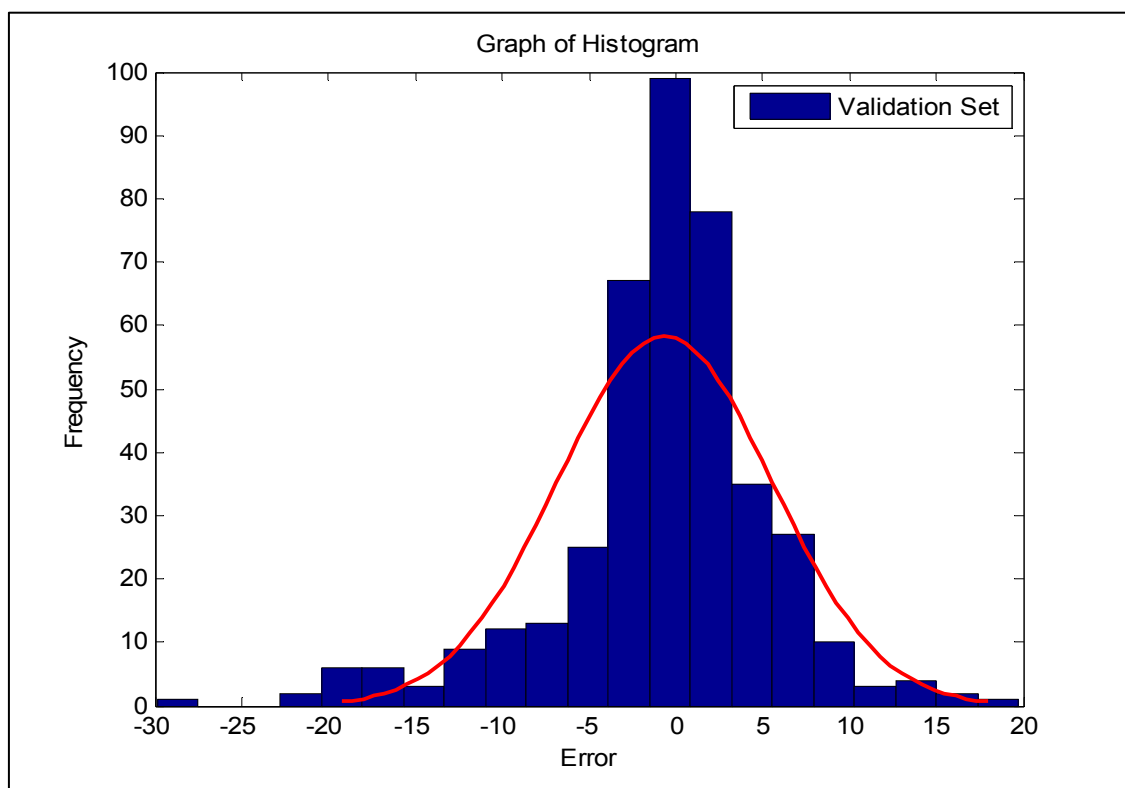


Figure 5.20: Error Distribution Plot of Choke Size Prediction for Validation set (ANN model)

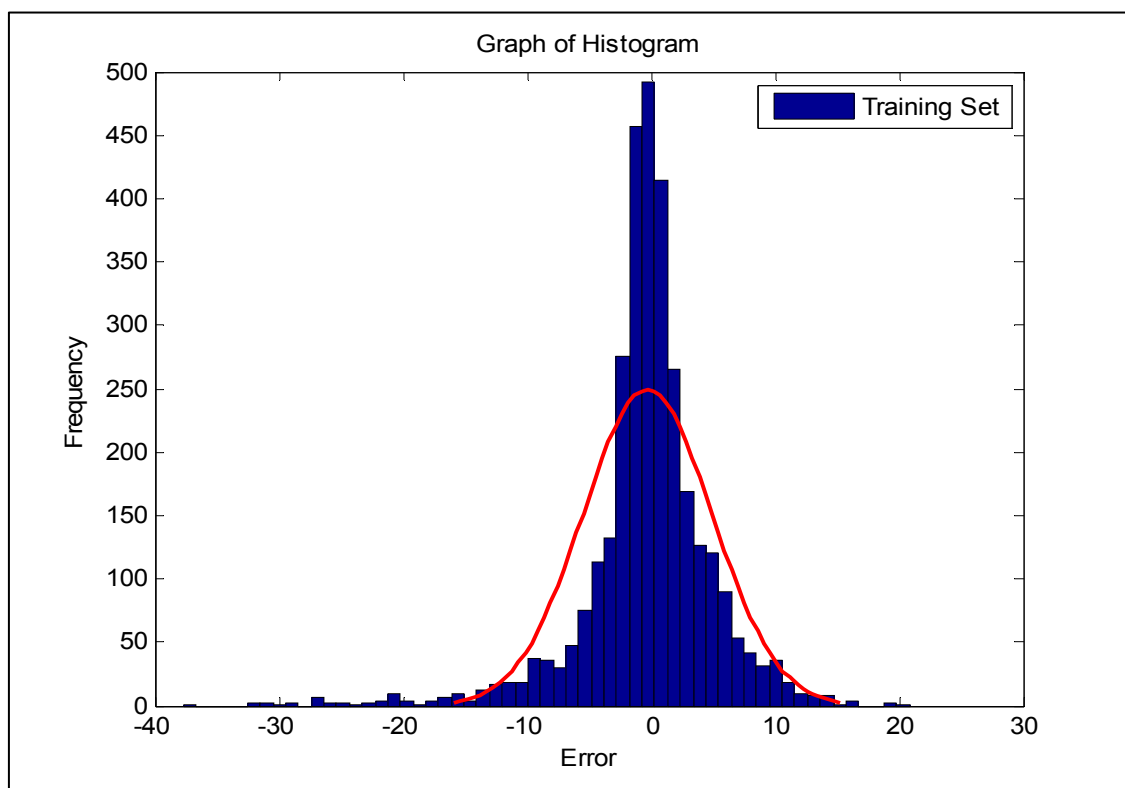


Figure 5.21: Error Distribution Plot of Choke Size Prediction for Training set (ANN model)

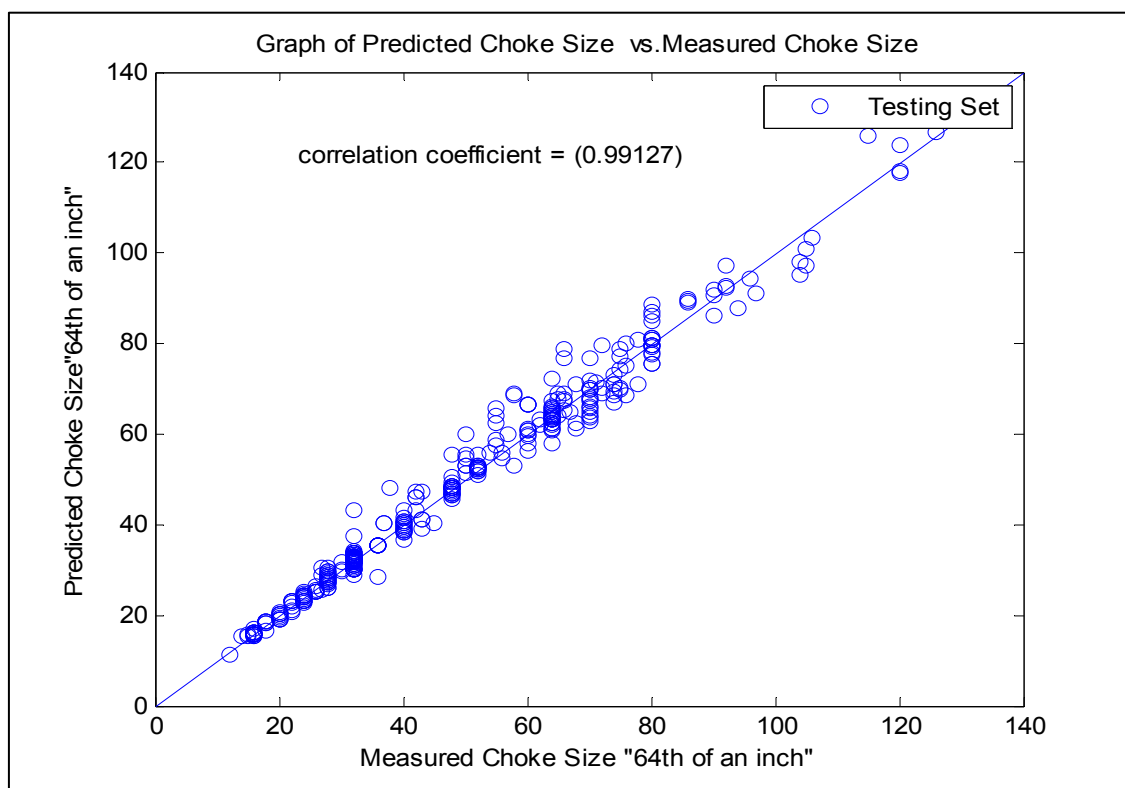


Figure 5.22: Cross Plot of Choke Size Prediction for Testing set (ANN model)

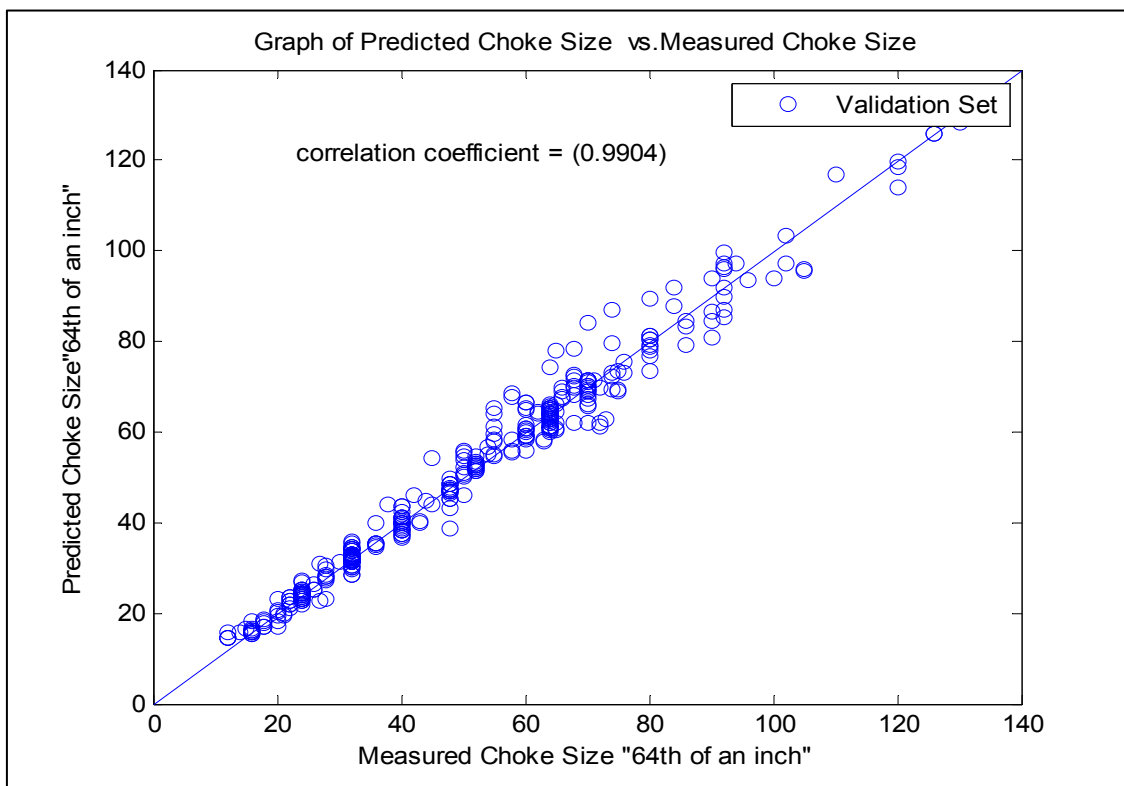


Figure 5.23: Cross Plot of Choke Size Prediction for Validation set (ANN model)

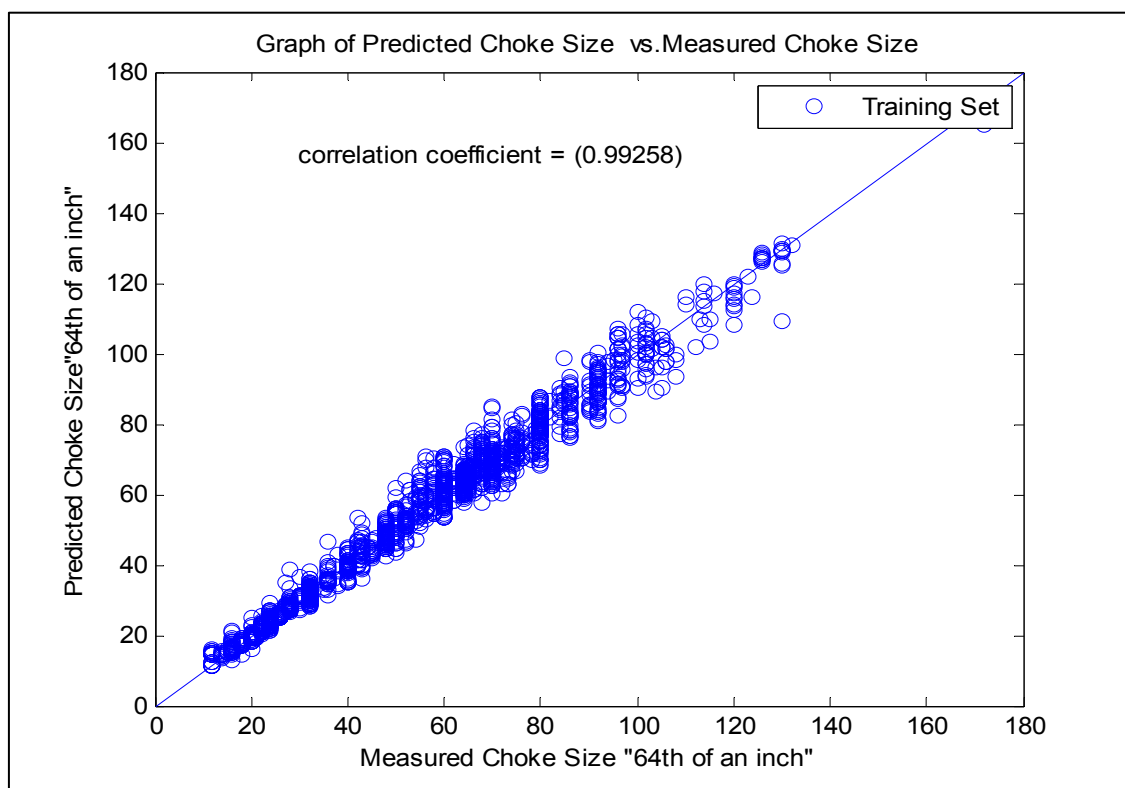


Figure 5.24: Cross Plot of Choke Size Prediction for Training set (ANN model)

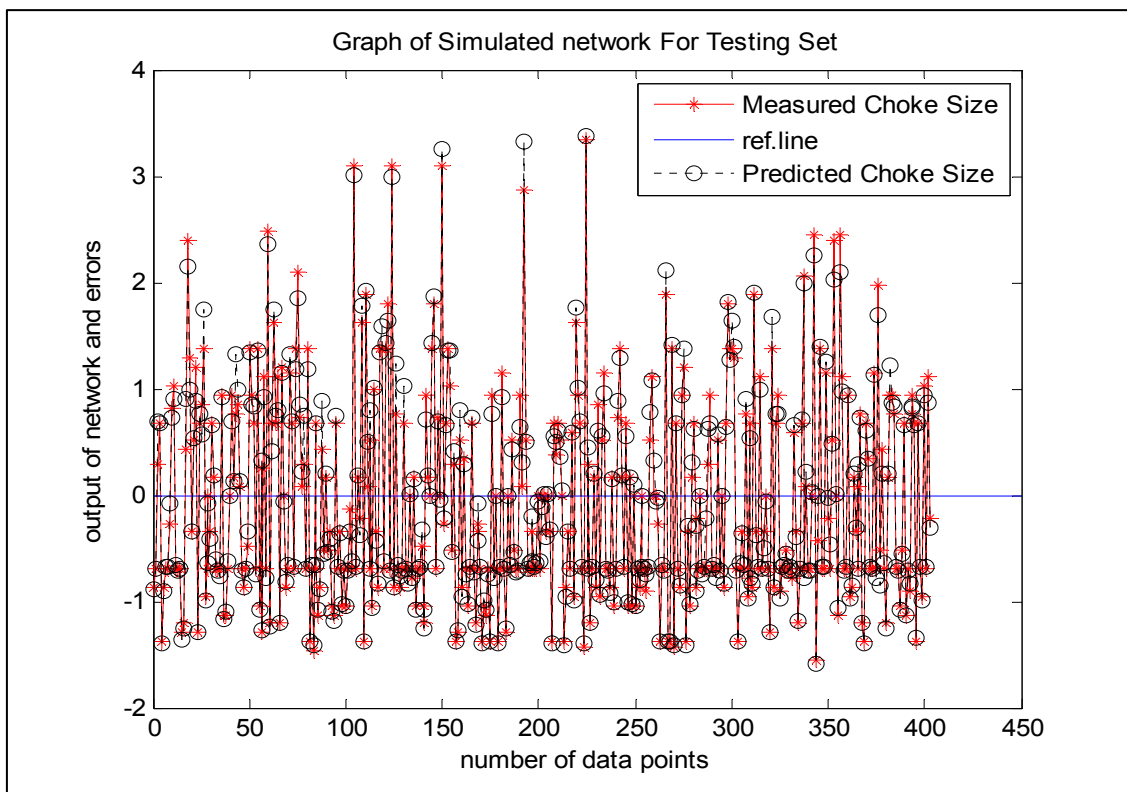


Figure 5.25: Scatter and Overlay Plot of Choke Size Prediction for Testing set (ANN model)

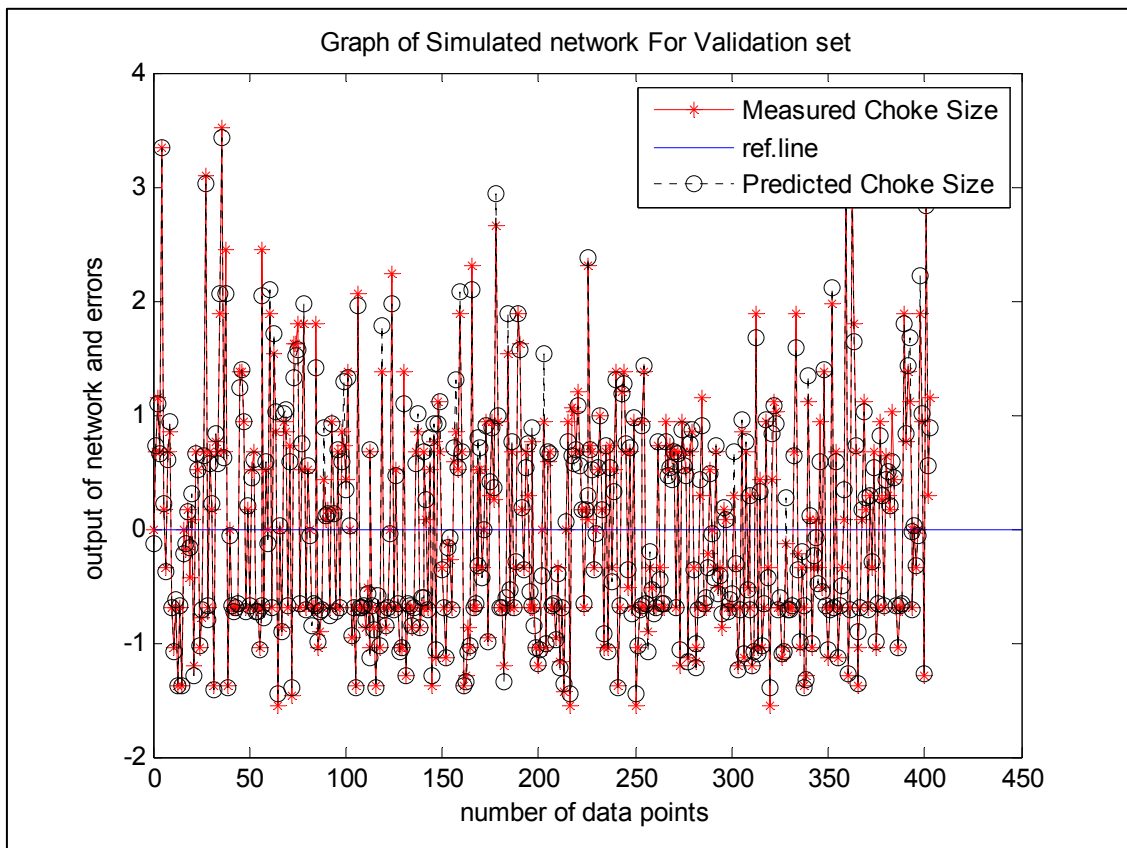


Figure 5.26: Scatter and Overlay Plot of Choke Size Prediction for Validation set (ANN model)

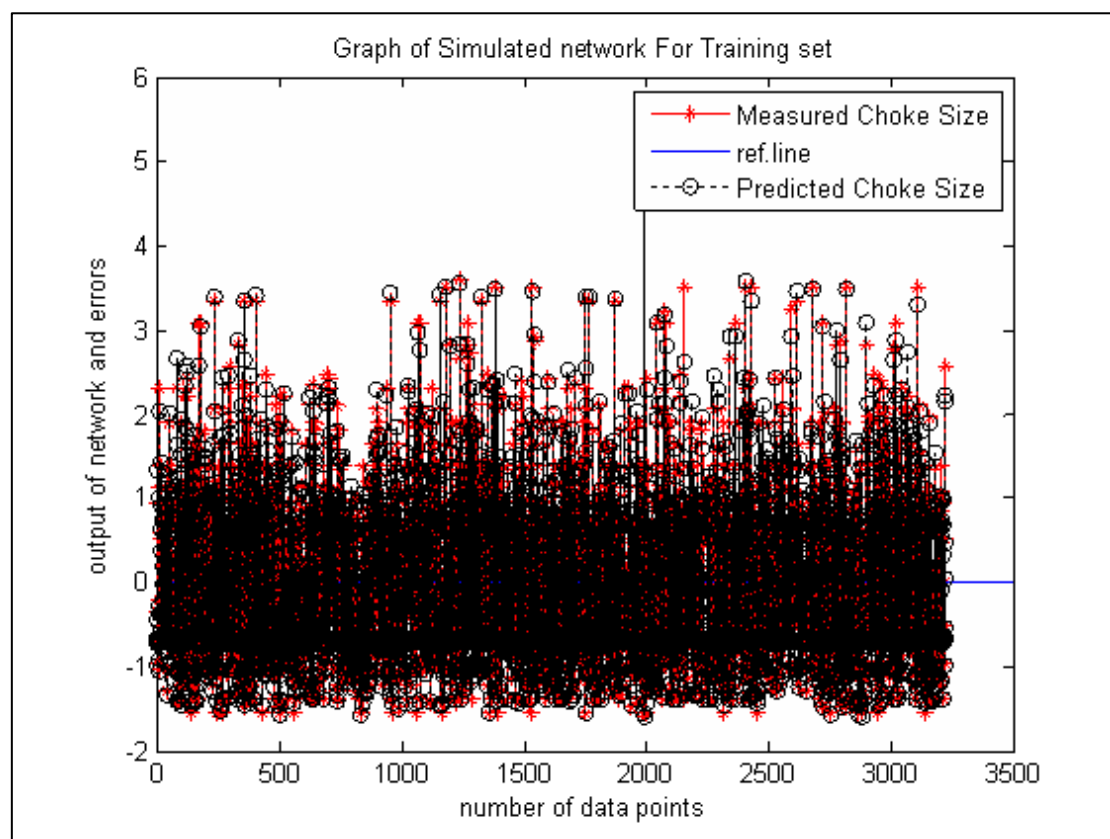


Figure 5.27: Scatter and Overlay Plot of Choke Size Prediction for Training set (ANN model)



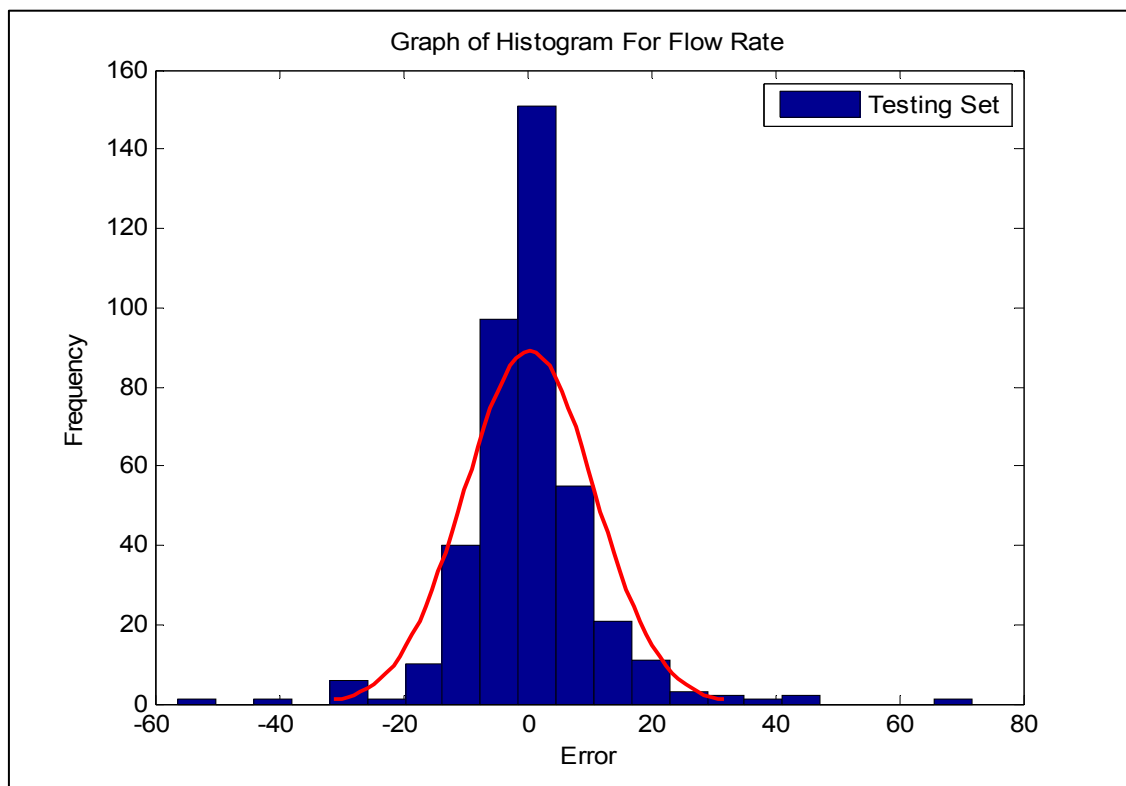


Figure 5.28: Error Distribution Plot of Flow Rate Estimation for Testing set (ANN model)

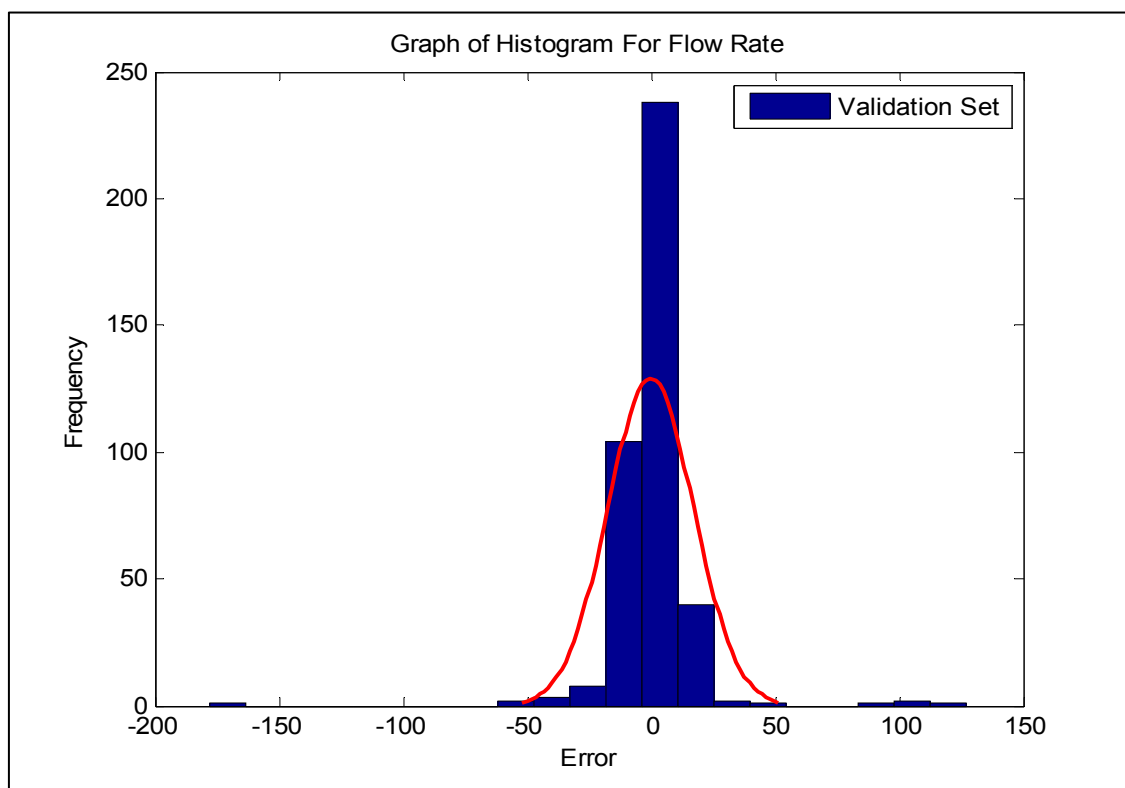


Figure 5.29: Error Distribution Plot of Flow Rate Estimation for Validation set (ANN model)

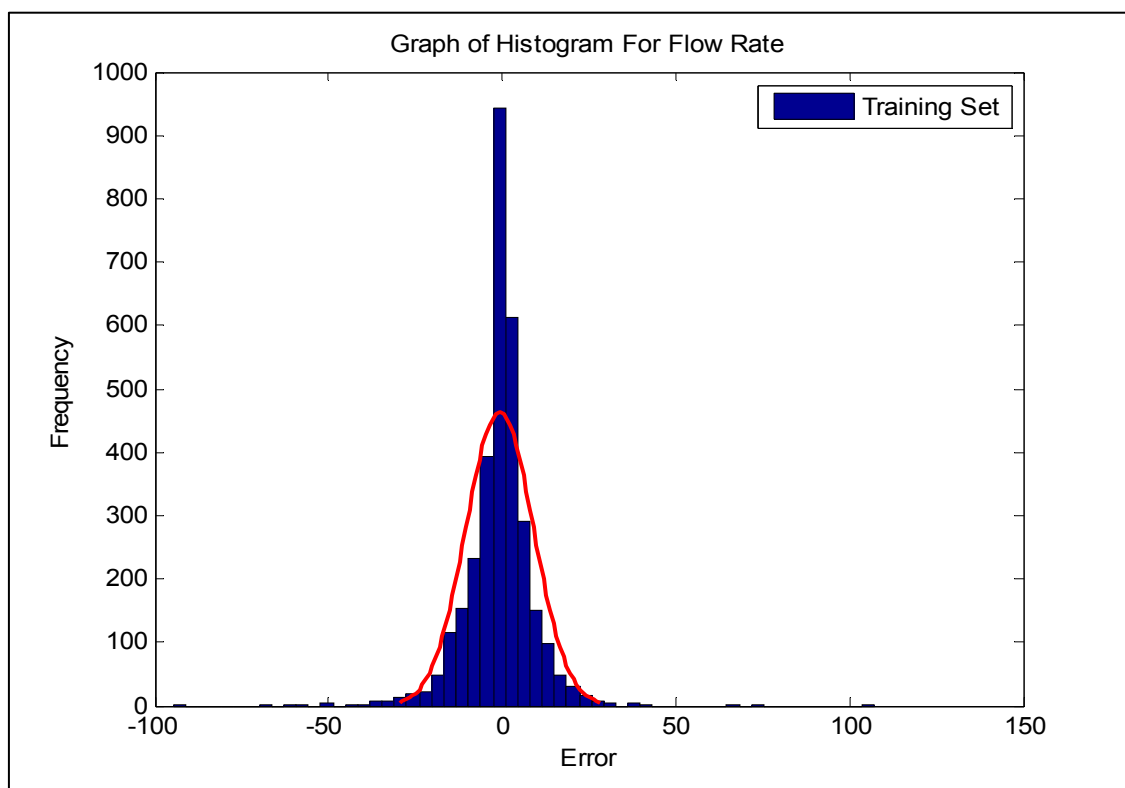


Figure 5.30: Error Distribution Plot of Flow Rate Estimation for Training set (ANN model)

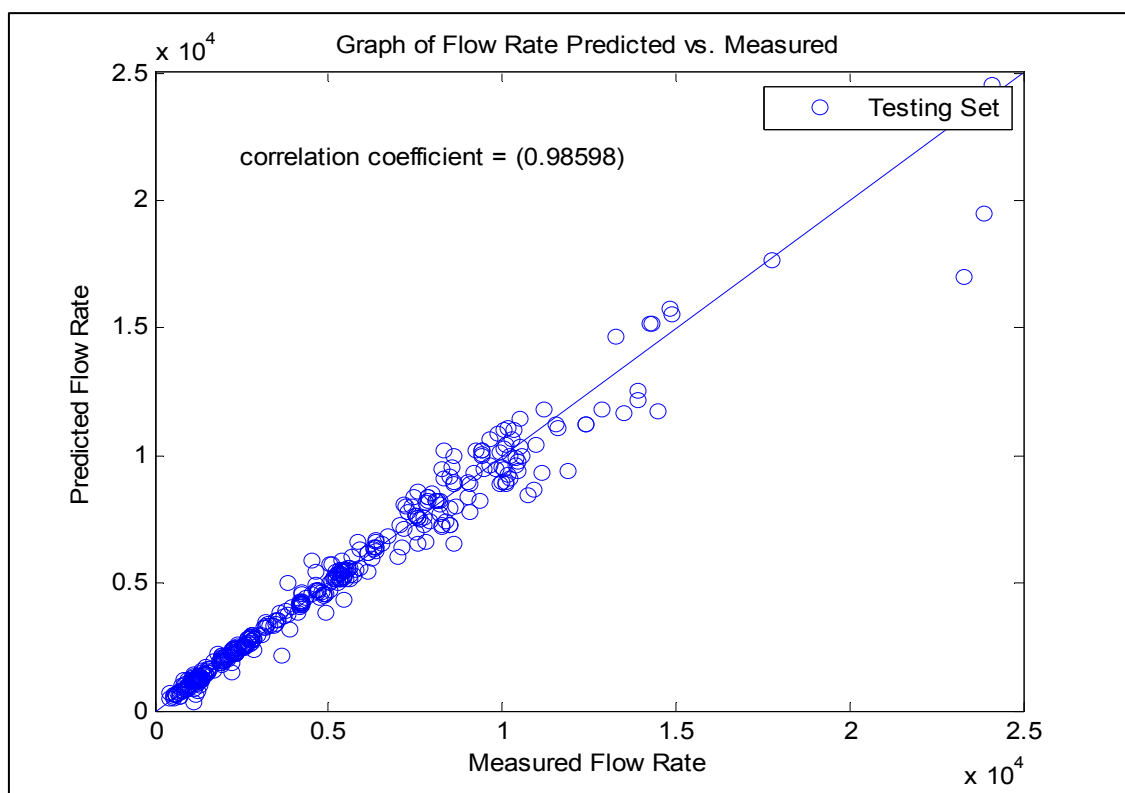


Figure 5.31: Cross Plot of Flow Rate Estimation for Testing set (ANN model)

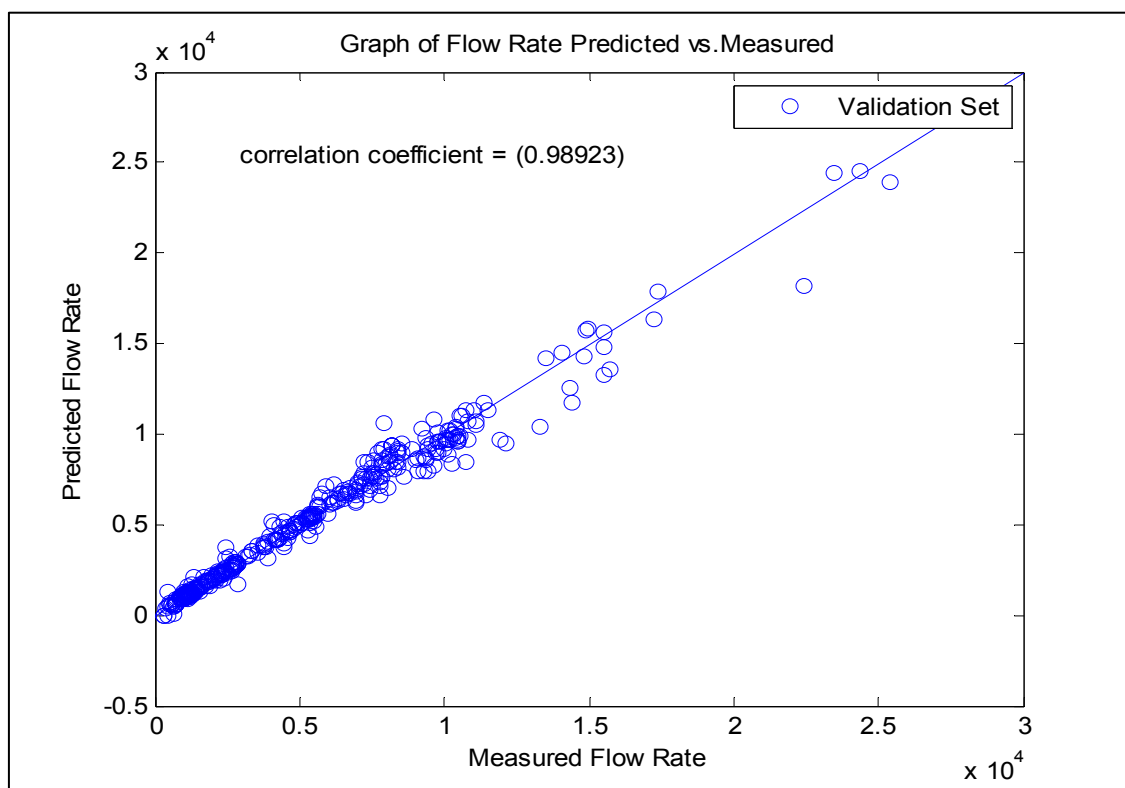


Figure 5.32: Cross Plot of Flow Rate Estimation for Validation set (ANN model)

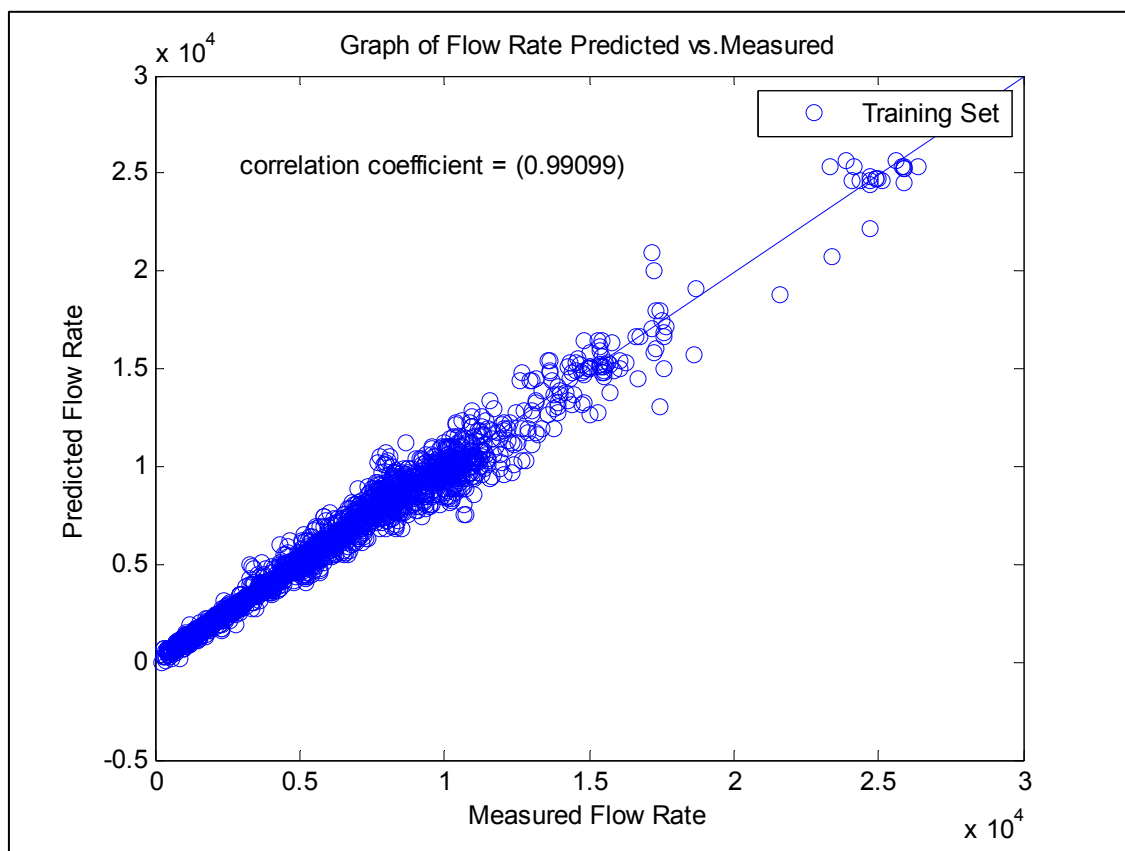


Figure 5.33: Cross Plot of Flow Rate Estimation for Training set (ANN model)

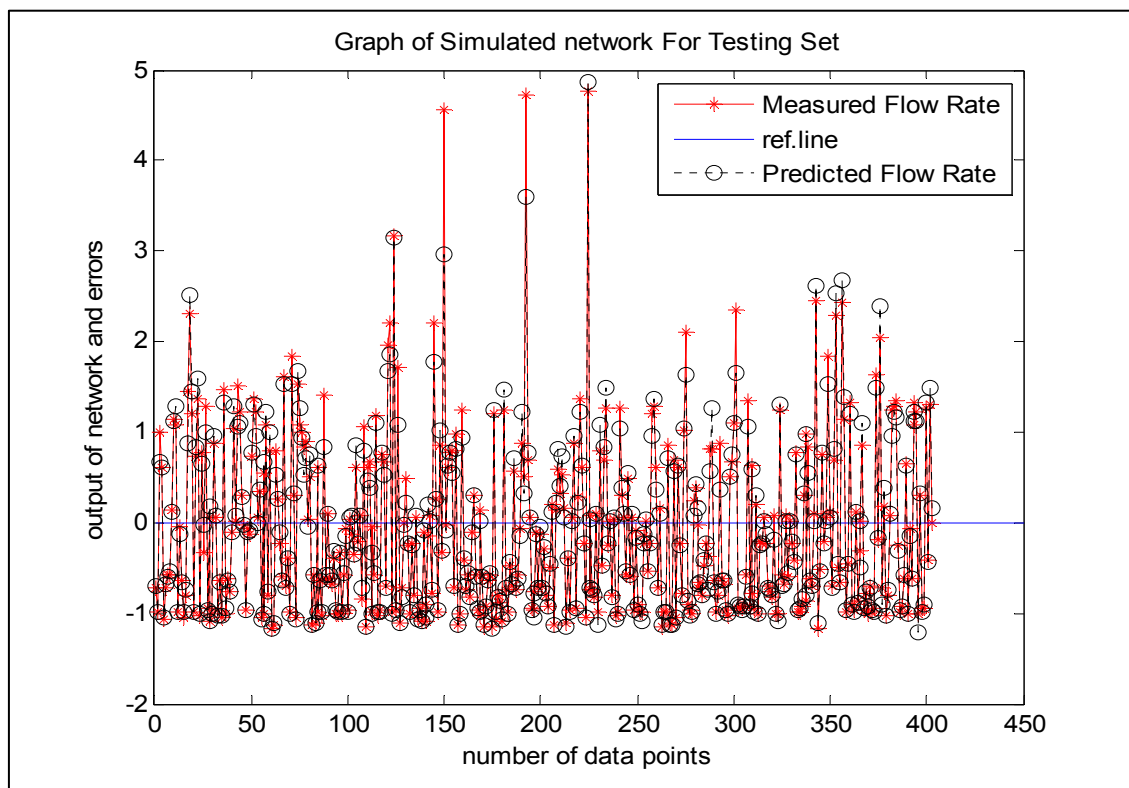


Figure 5.34: Scatter & Overlay Plot of Flow Rate Estimation for Testing set (ANN model)

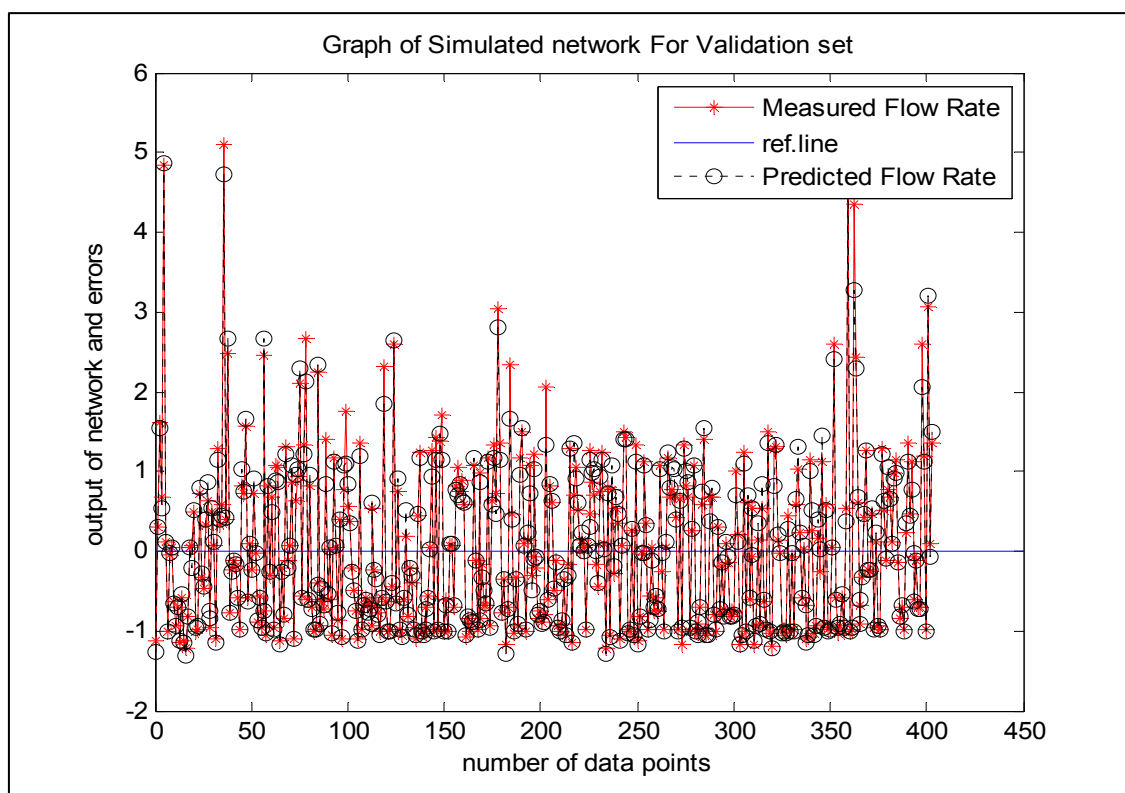


Figure 5.35: Scatter & Overlay Plot of Flow Rate Estimation for Validation set (ANN model)



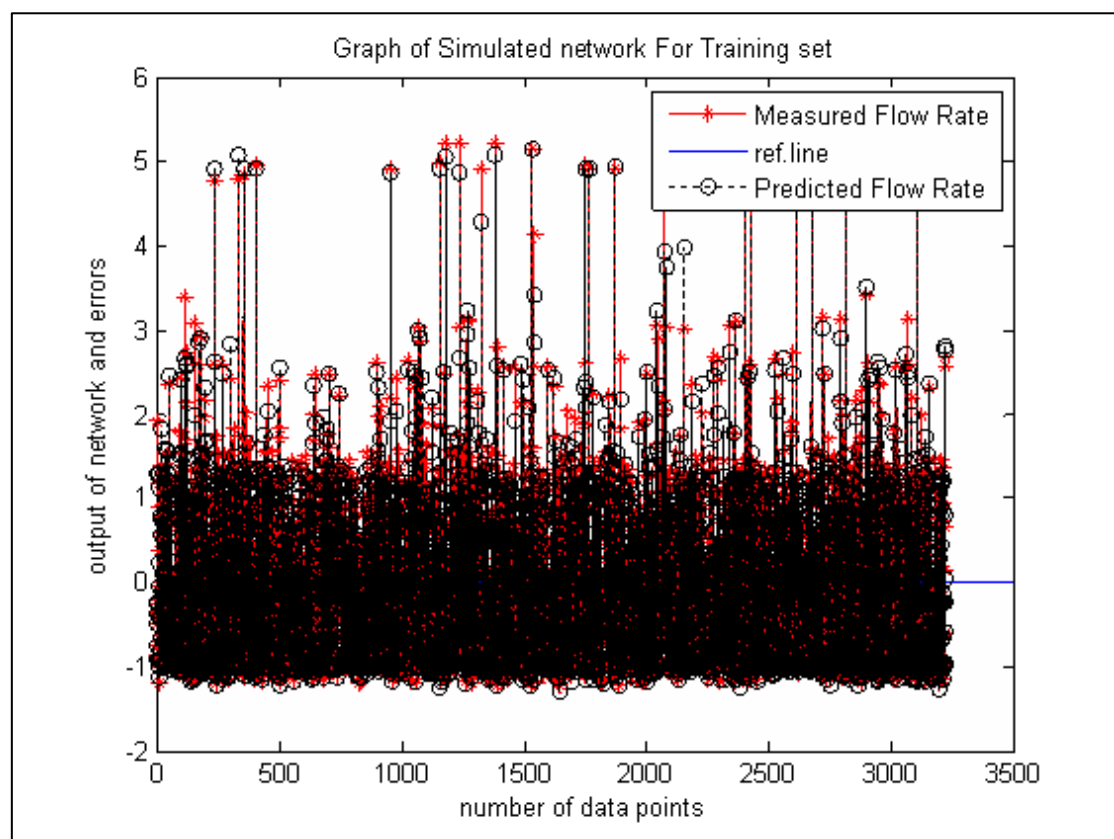


Figure 5.36: Scatter & Overlay Plot of Flow Rate Estimation for Training set (ANN model)

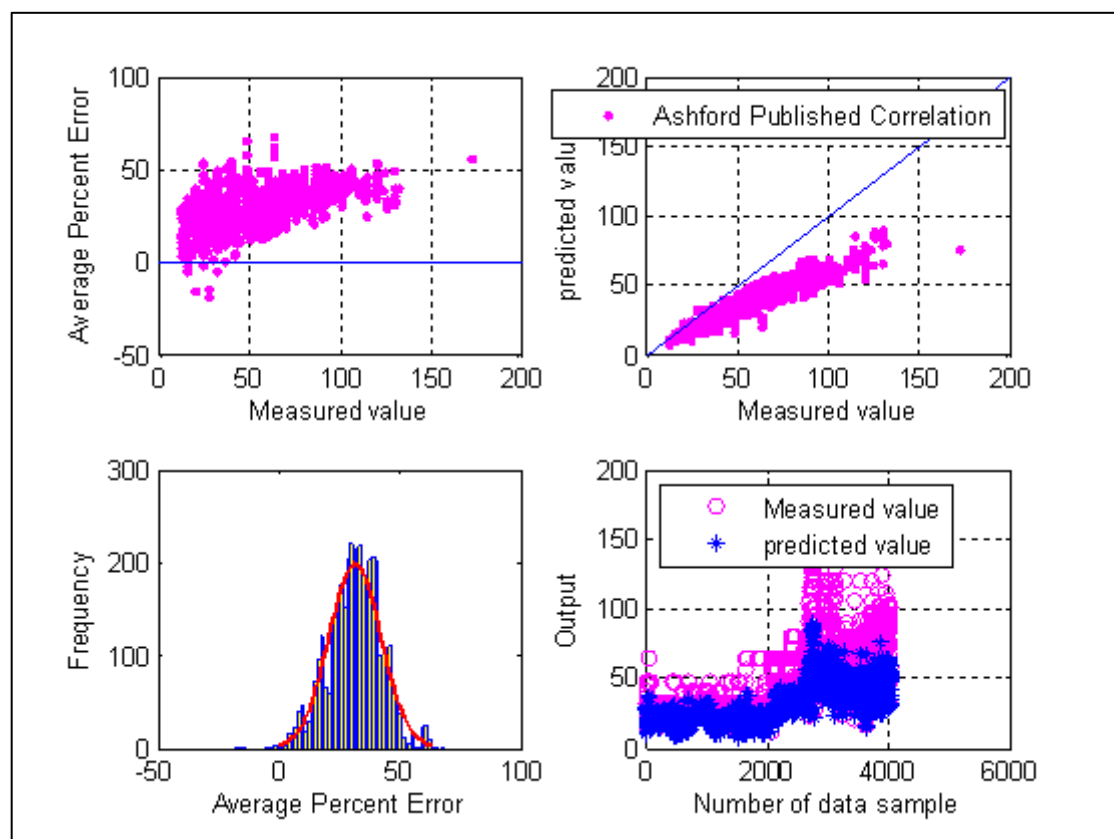


Figure-5.37: Cross, Histogram, Scatter and Overlay plots for Ashford Empirical correlation. (Choke Size Prediction)

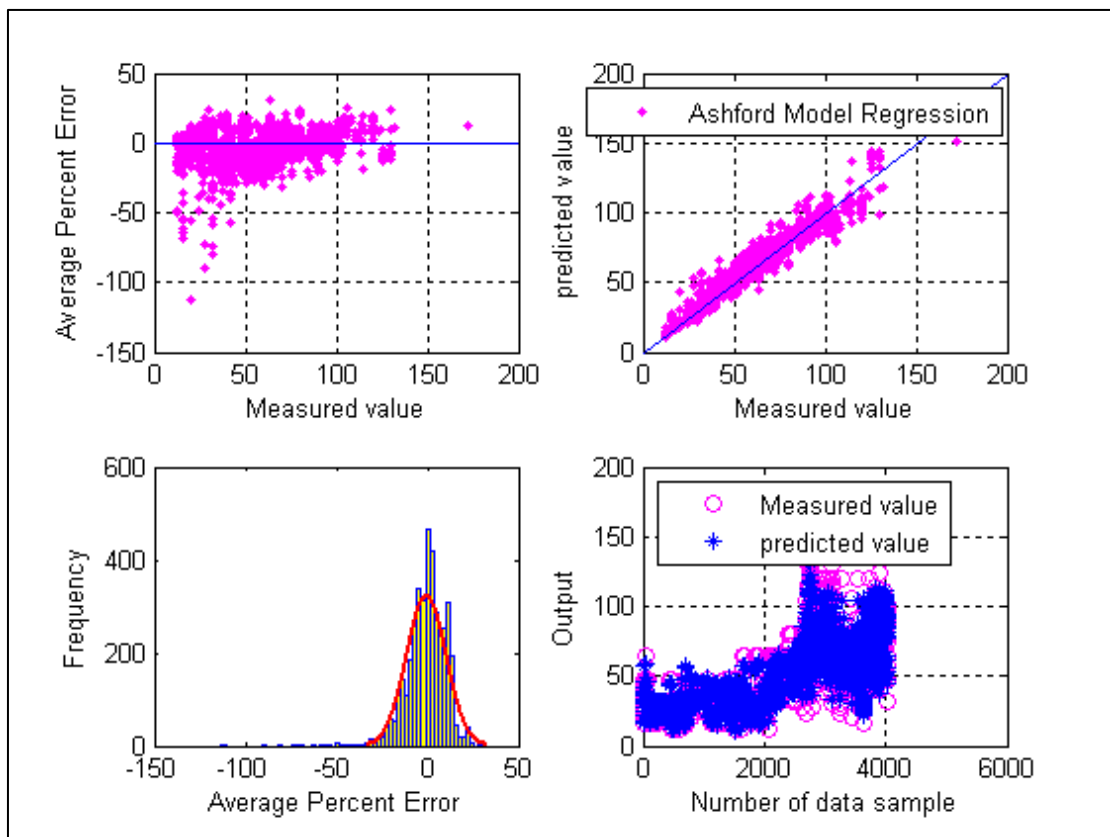


Figure-5.38: Cross, Histogram, Scatter and Overlay plots for Ashford Empirical correlation after regression. (Choke Size Prediction)

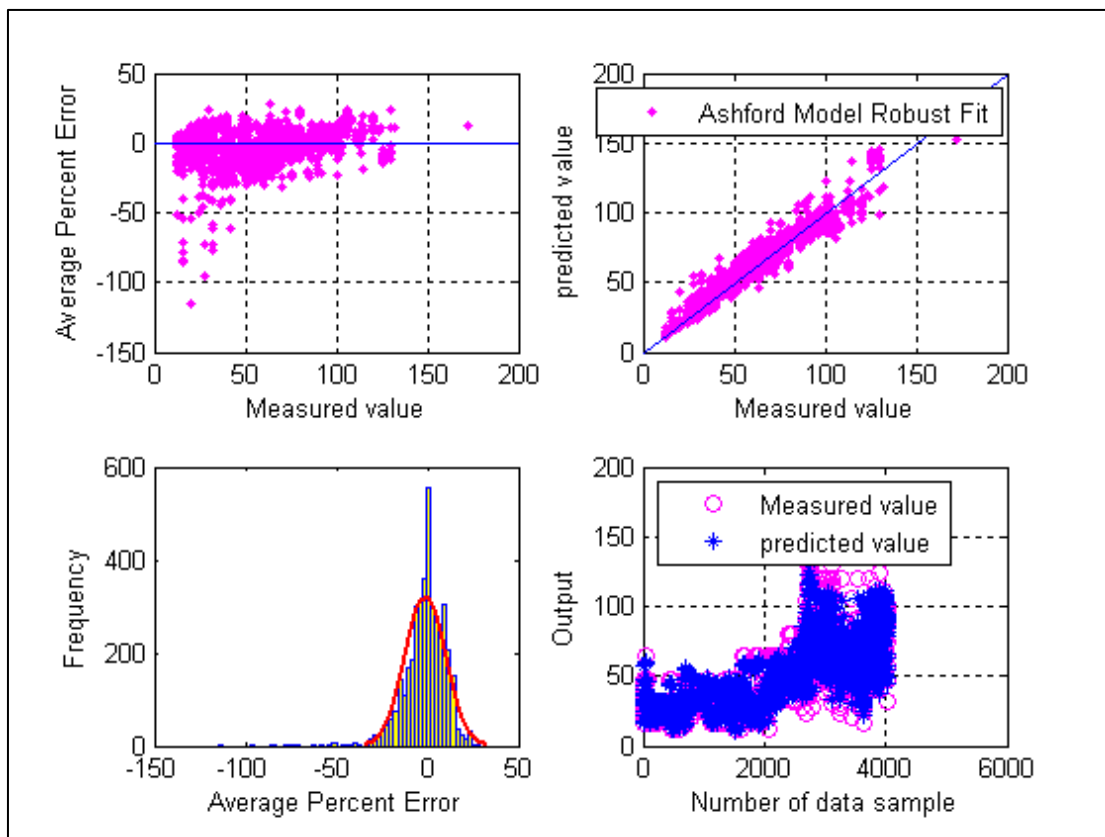


Figure-5.39: Cross, Histogram, Scatter and Overlay plots for Ashford Empirical correlation after robust fit. (Choke Size Prediction)

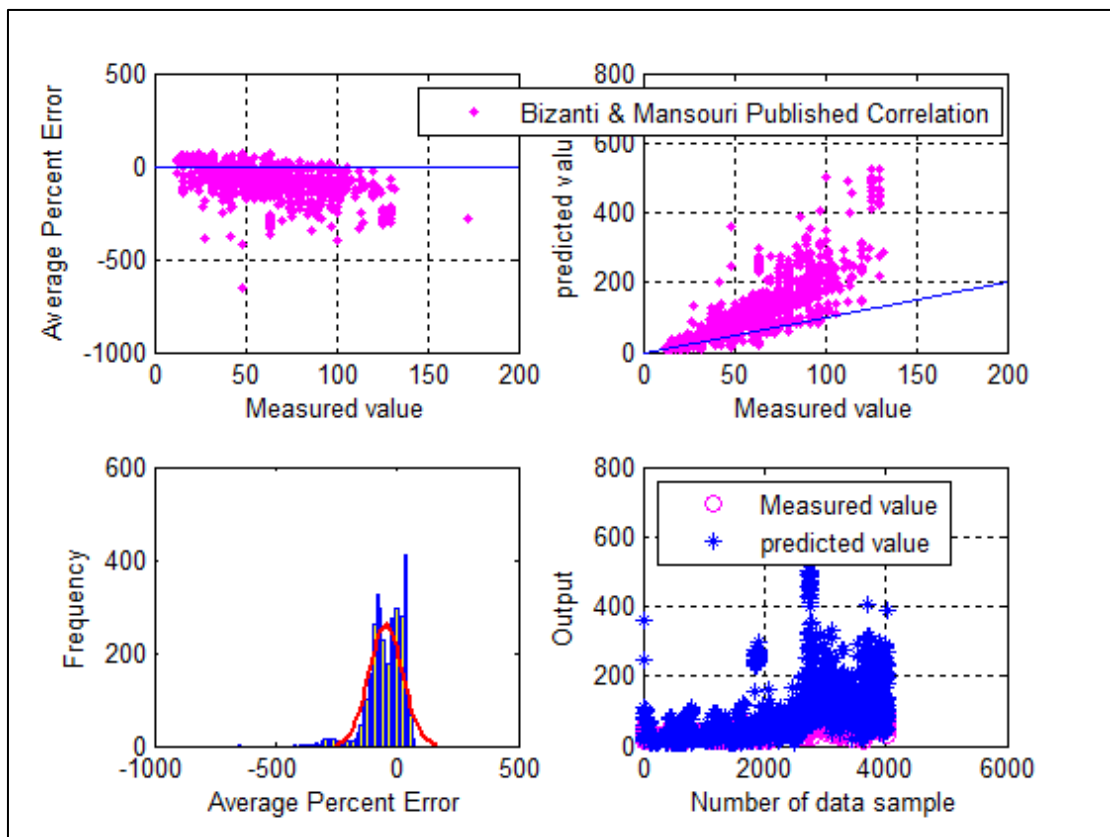


Figure-5.40: Cross, Histogram, Scatter and Overlay plots for Bizanti and Mansouri Empirical correlation. (Choke Size Prediction)

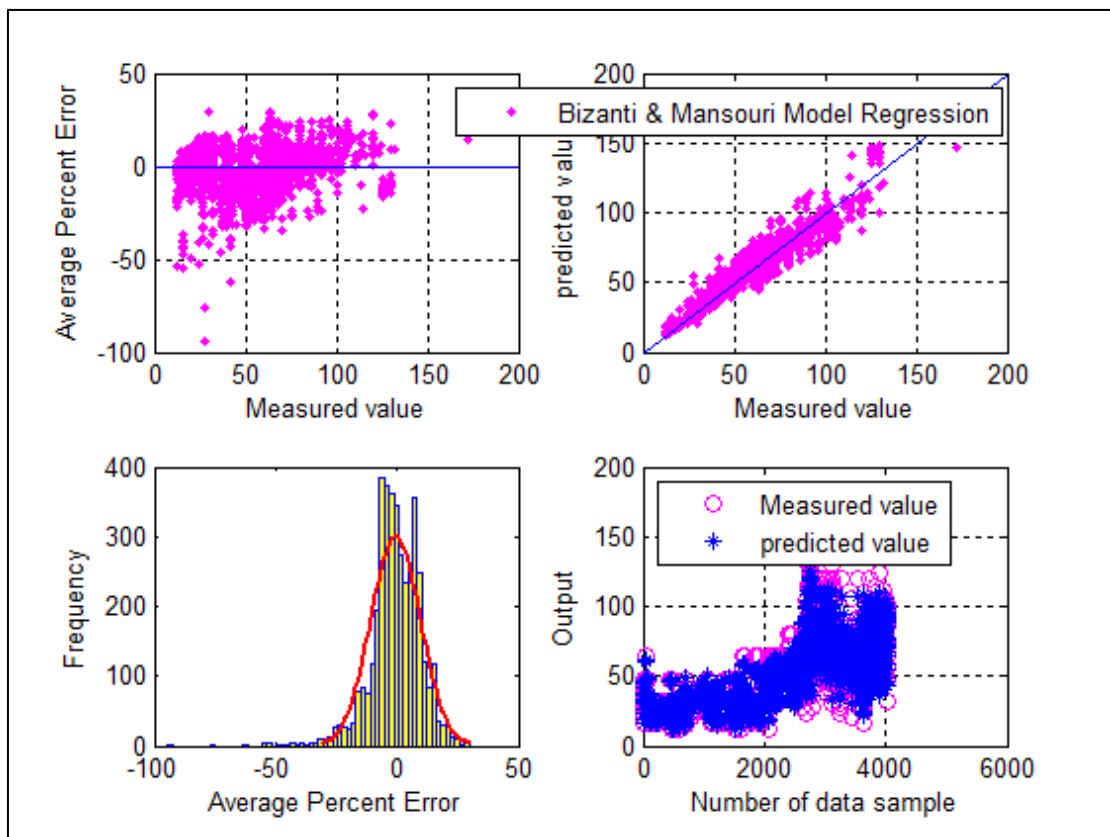


Figure-5.41: Cross, Histogram, Scatter and Overlay plots for Bizanti and Mansouri Empirical correlation after regression. (Choke Size Prediction)

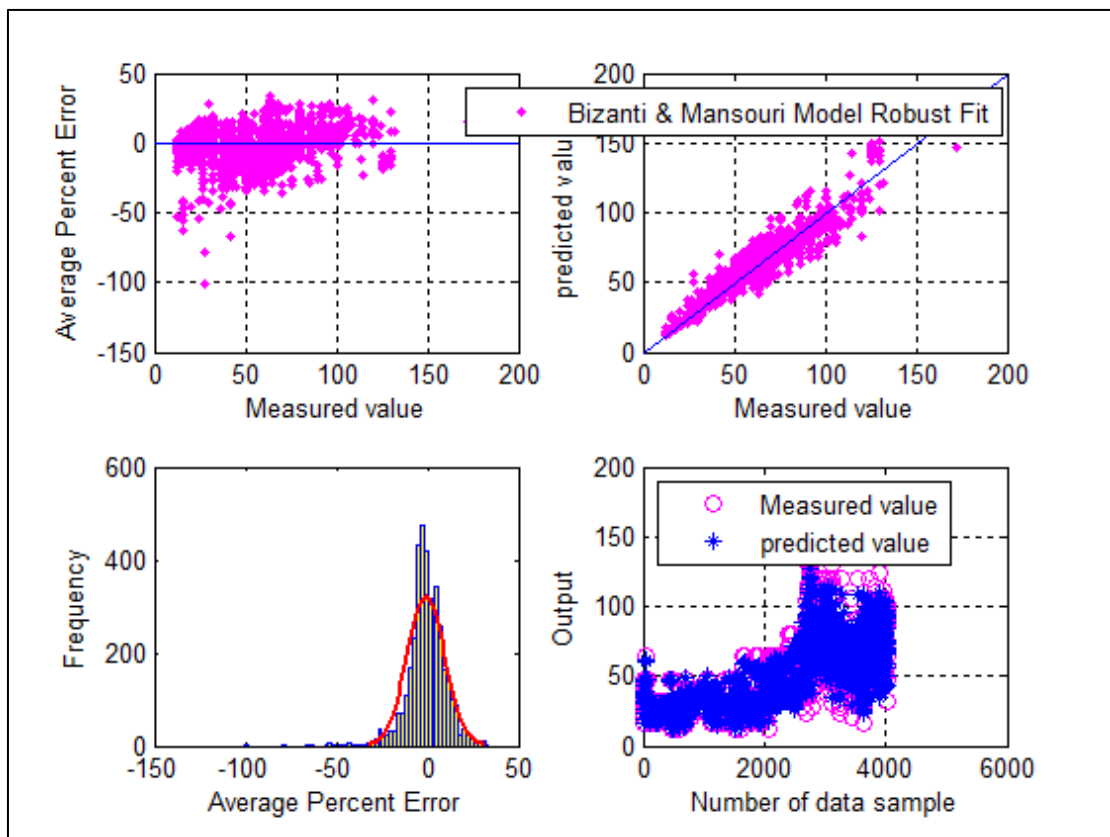


Figure-5.42: Cross, Histogram, Scatter and Overlay plots for Bizanti and Mansouri Empirical correlation after robust fit. (Choke Size Prediction)

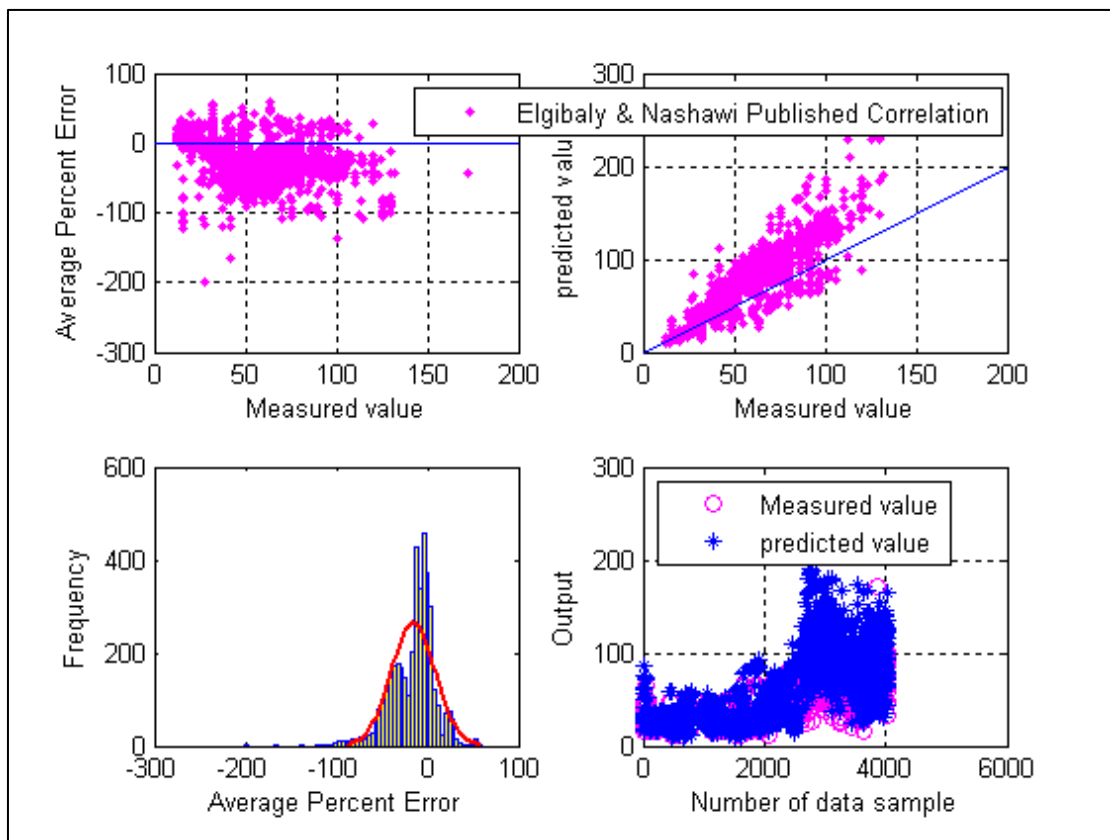


Figure-5.43: Cross, Histogram, Scatter and Overlay plots for Elgibaly and Nashawi Empirical correlation. (Choke Size Prediction)



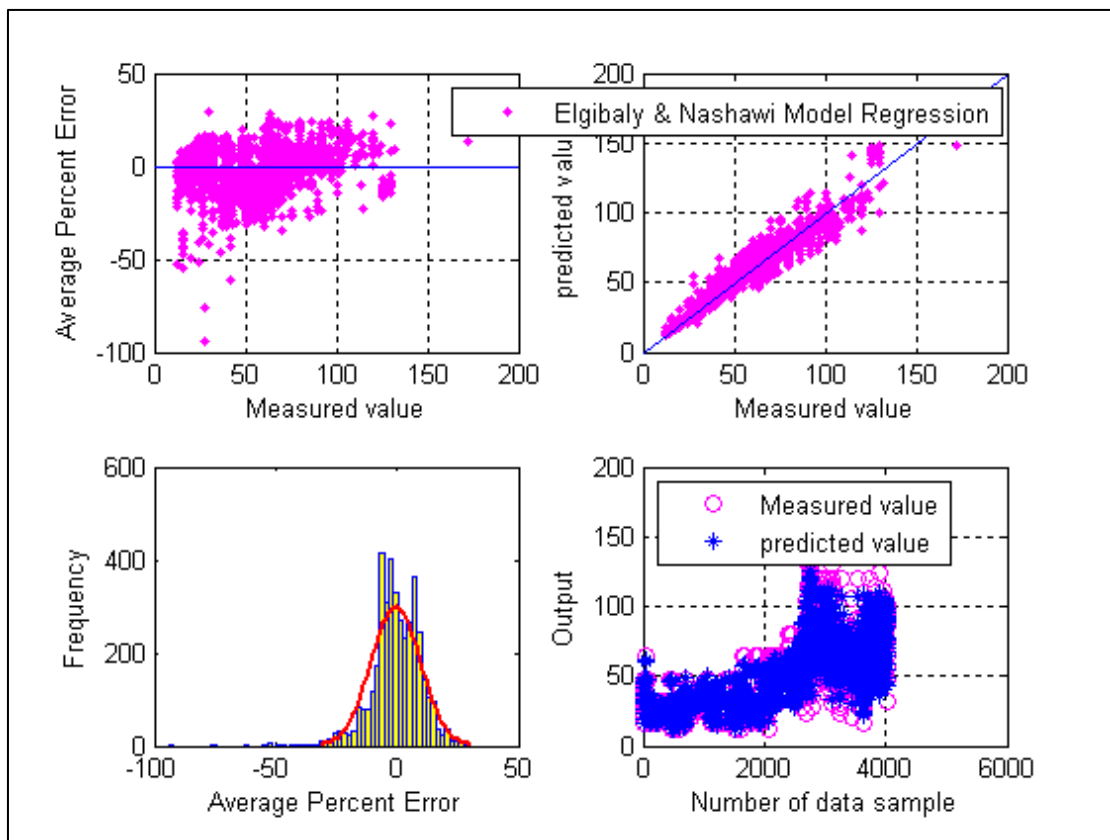


Figure-5.44: Cross, Histogram, Scatter and Overlay plots for Elgibaly and Nashawi Empirical correlation after regression. (Choke Size Prediction)

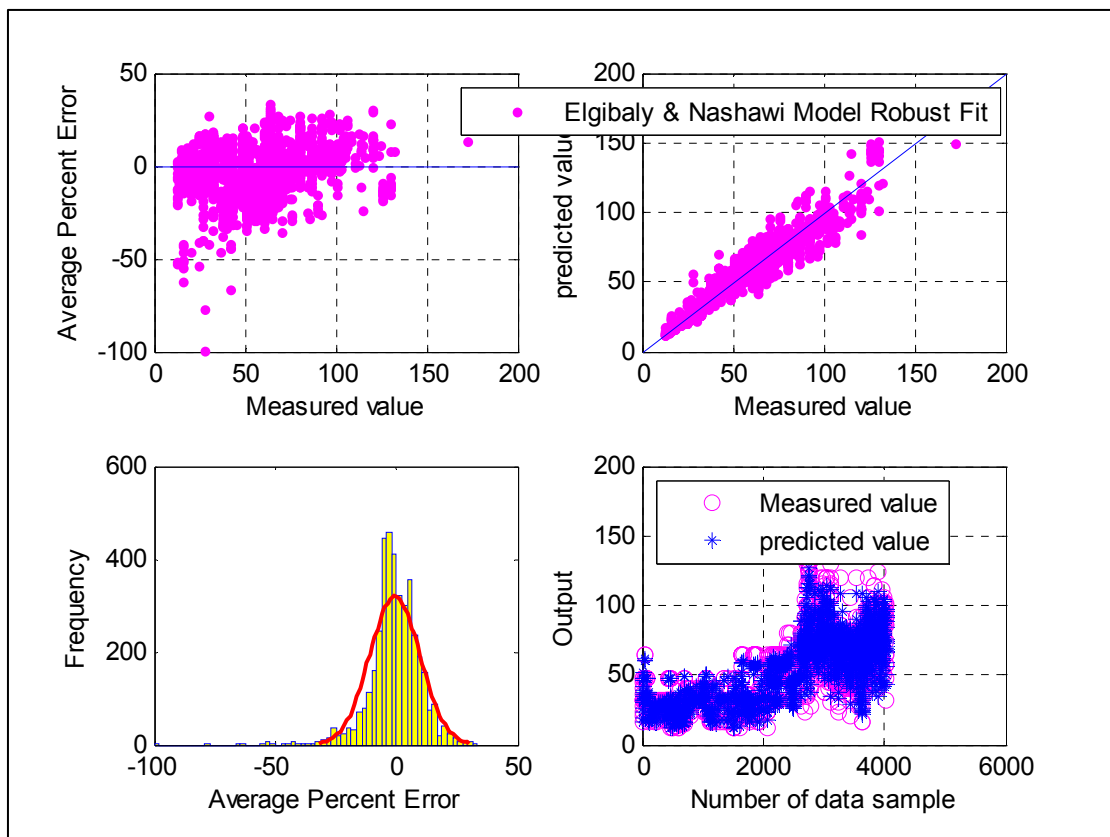


Figure-5.45: Cross, Histogram, Scatter and Overlay plots for Elgibaly and Nashawi Empirical correlation after robust fit. (Choke Size Prediction)

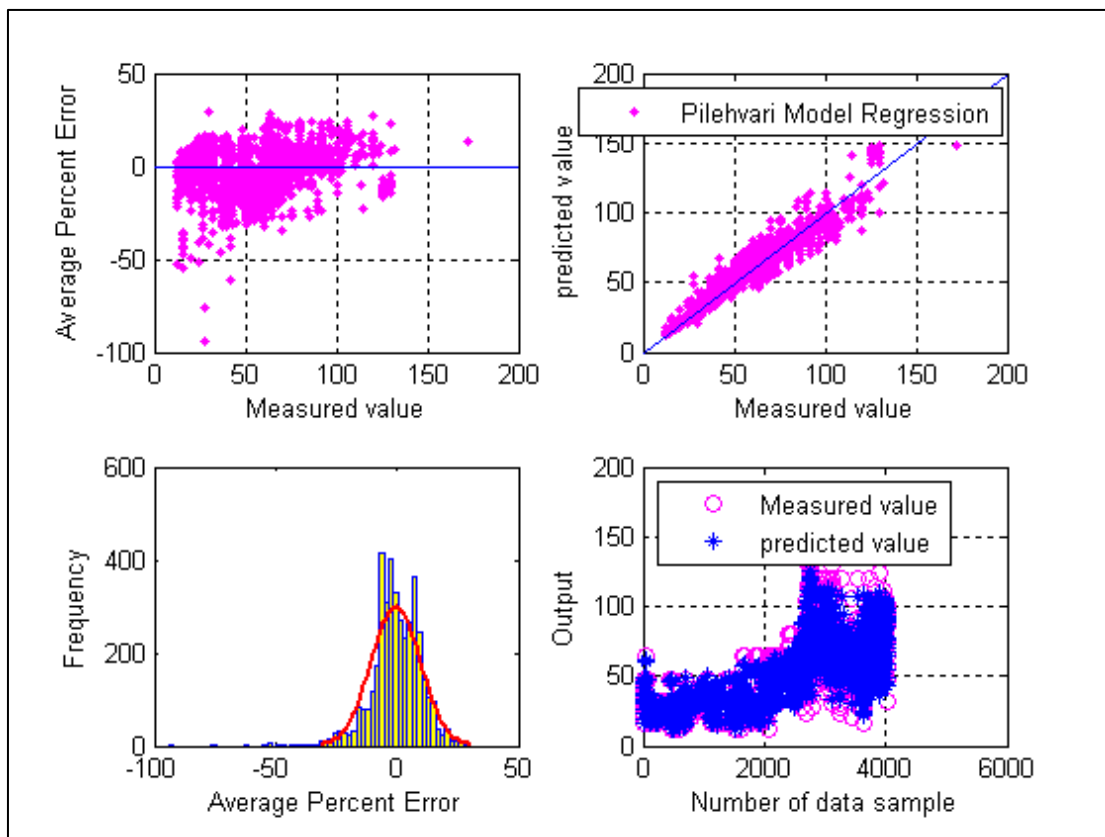


Figure-5.46: Cross, Histogram, Scatter and Overlay plots for Pilehvari Empirical correlation after regression. (Choke Size Prediction)

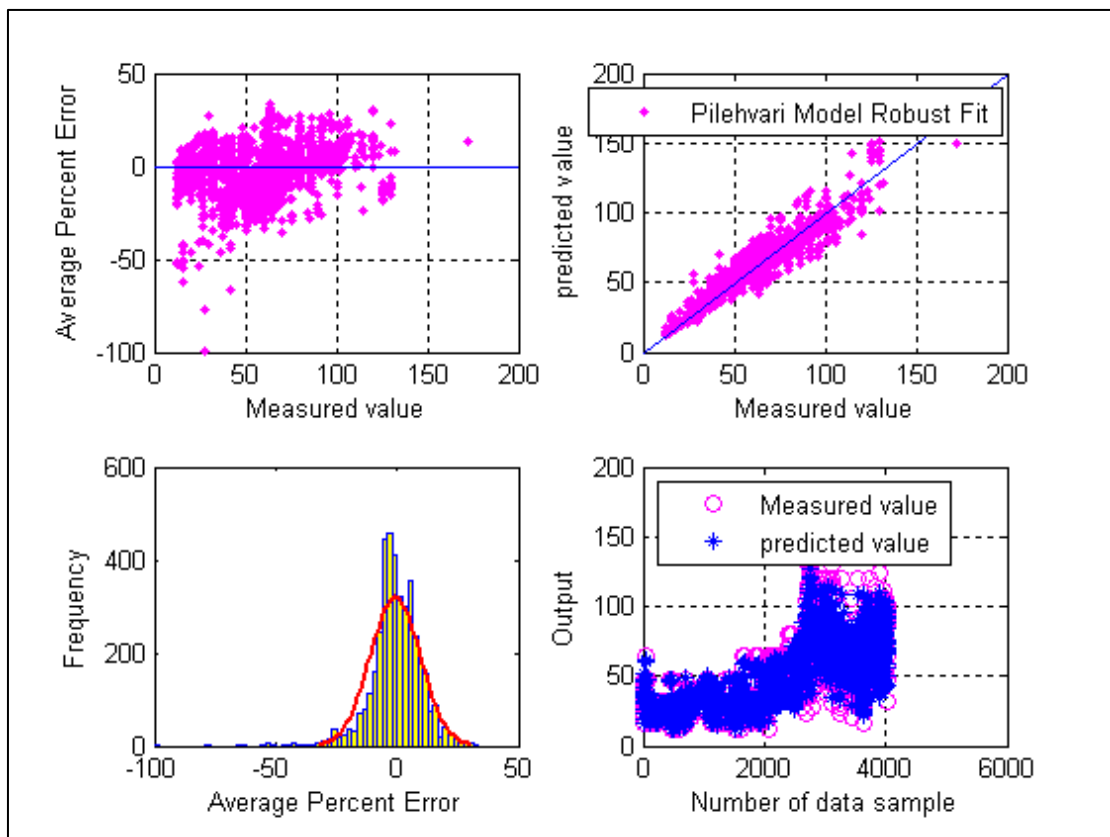


Figure-5.47: Cross, Histogram, Scatter and Overlay plots for Pilehvari Empirical correlation after robust fit. (Choke Size Prediction)

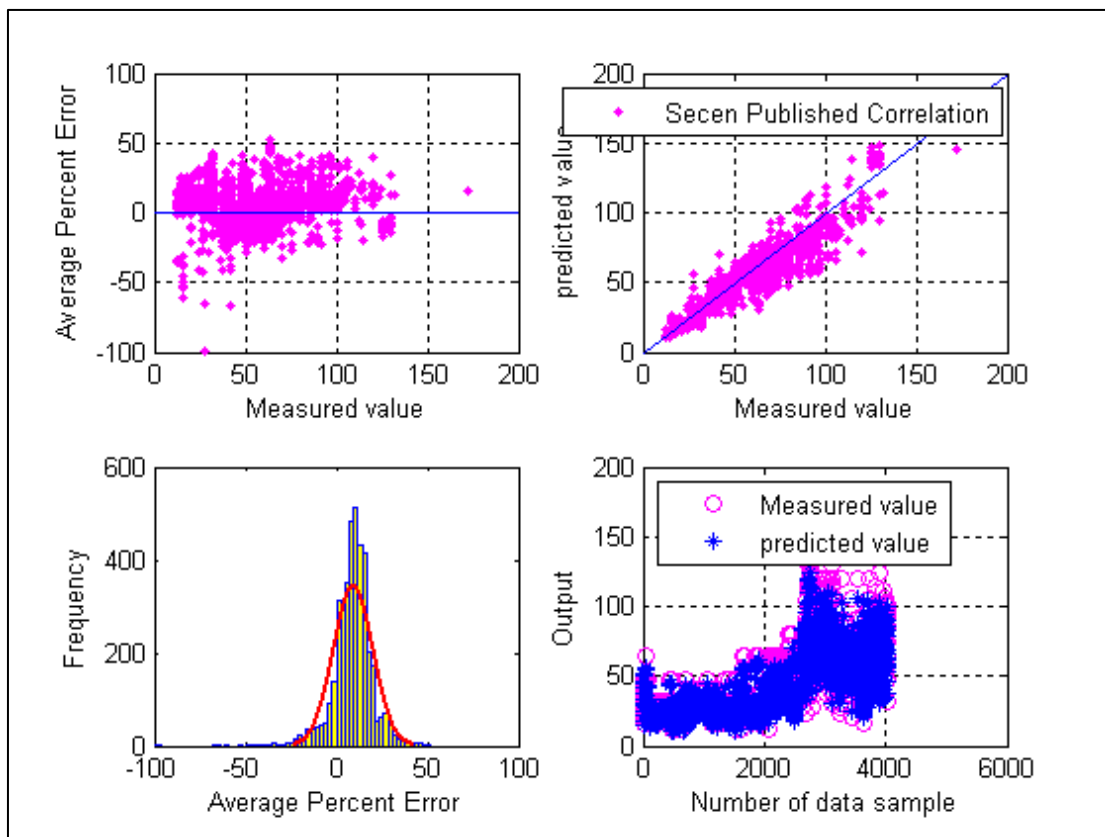


Figure-5.48: Cross, Histogram, Scatter and Overlay plots for Secen Empirical correlation. (Choke Size Prediction)

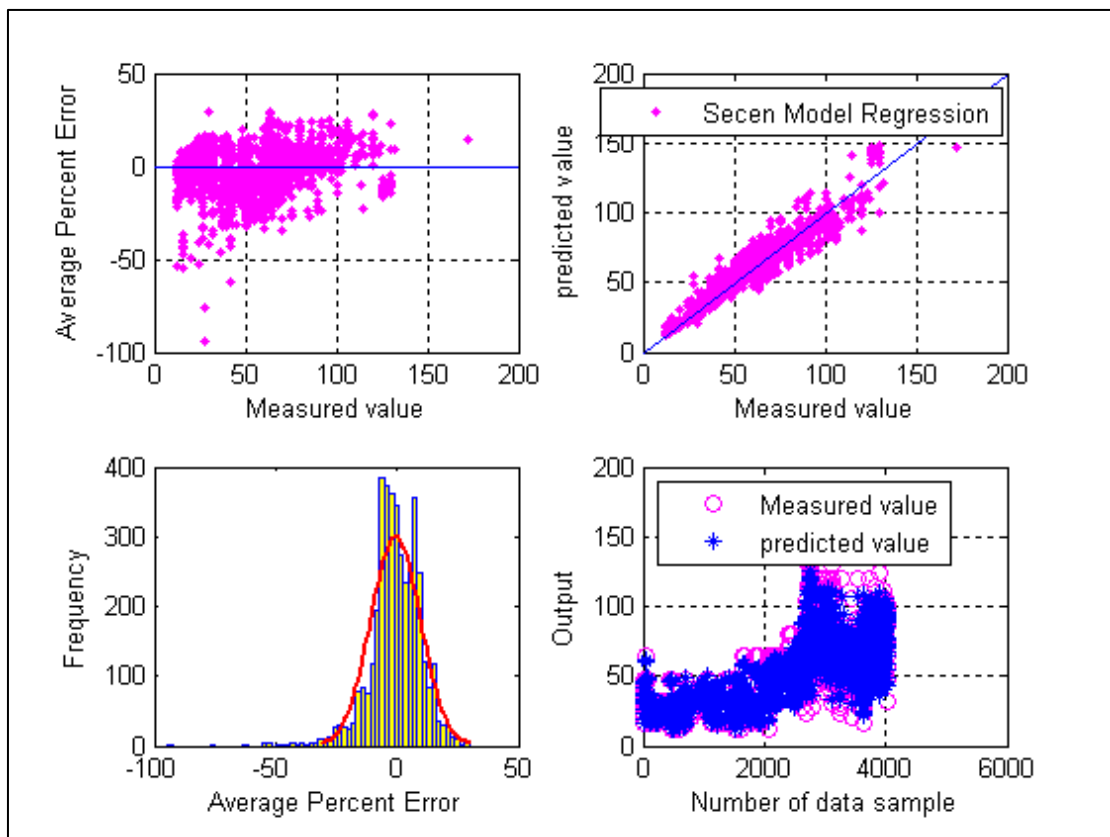


Figure-5.49: Cross, Histogram, Scatter and Overlay plots for Secen Empirical correlation after regression. (Choke Size Prediction)

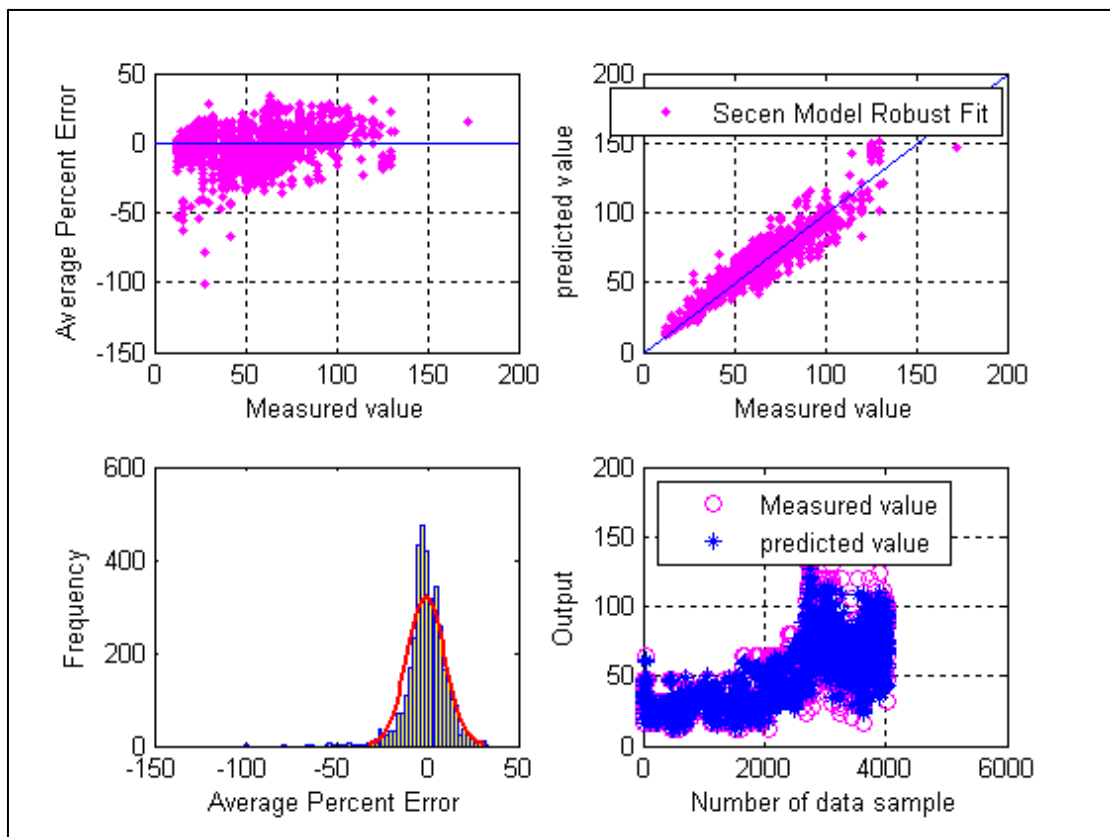


Figure-5.50: Cross, Histogram, Scatter and Overlay plots for Secen Empirical correlation after robust fit. (Choke Size Prediction)

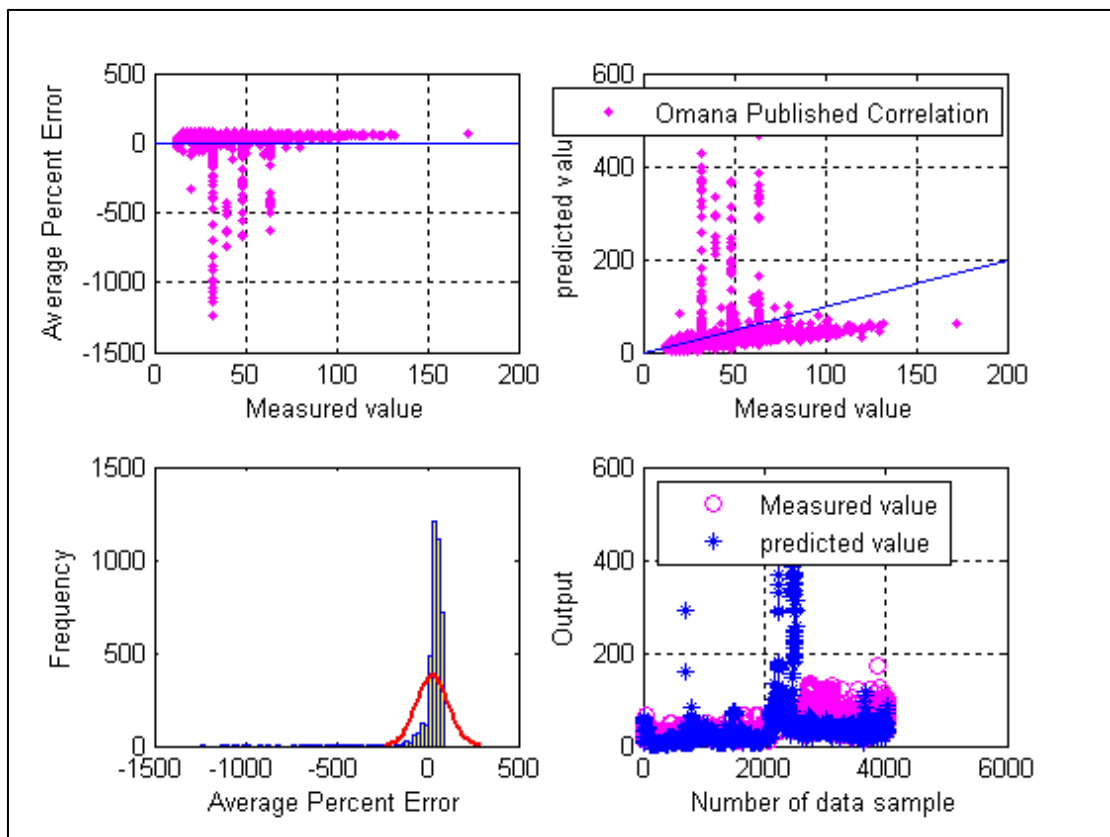


Figure-5.51: Cross, Histogram, Scatter and Overlay plots for Omana Empirical correlation. (Choke Size Prediction)



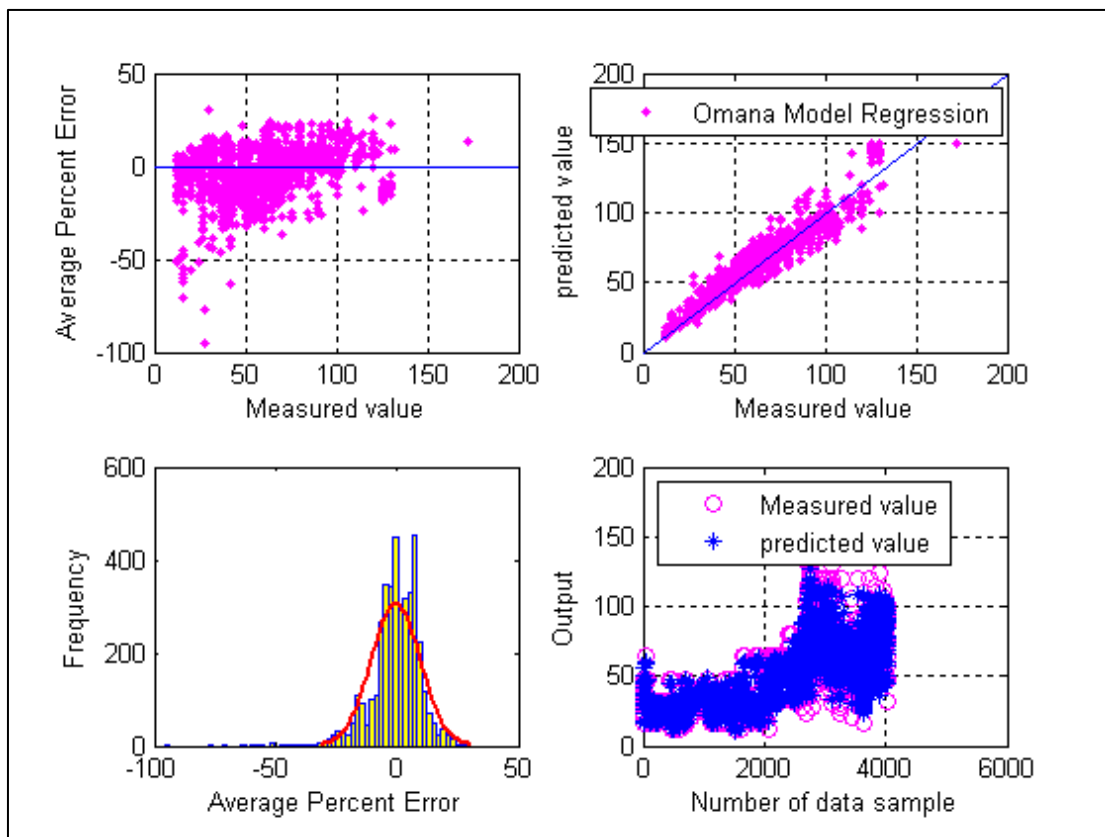


Figure-5.52: Cross, Histogram, Scatter and Overlay plots for Omana Empirical correlation after regression. (Choke Size Prediction)

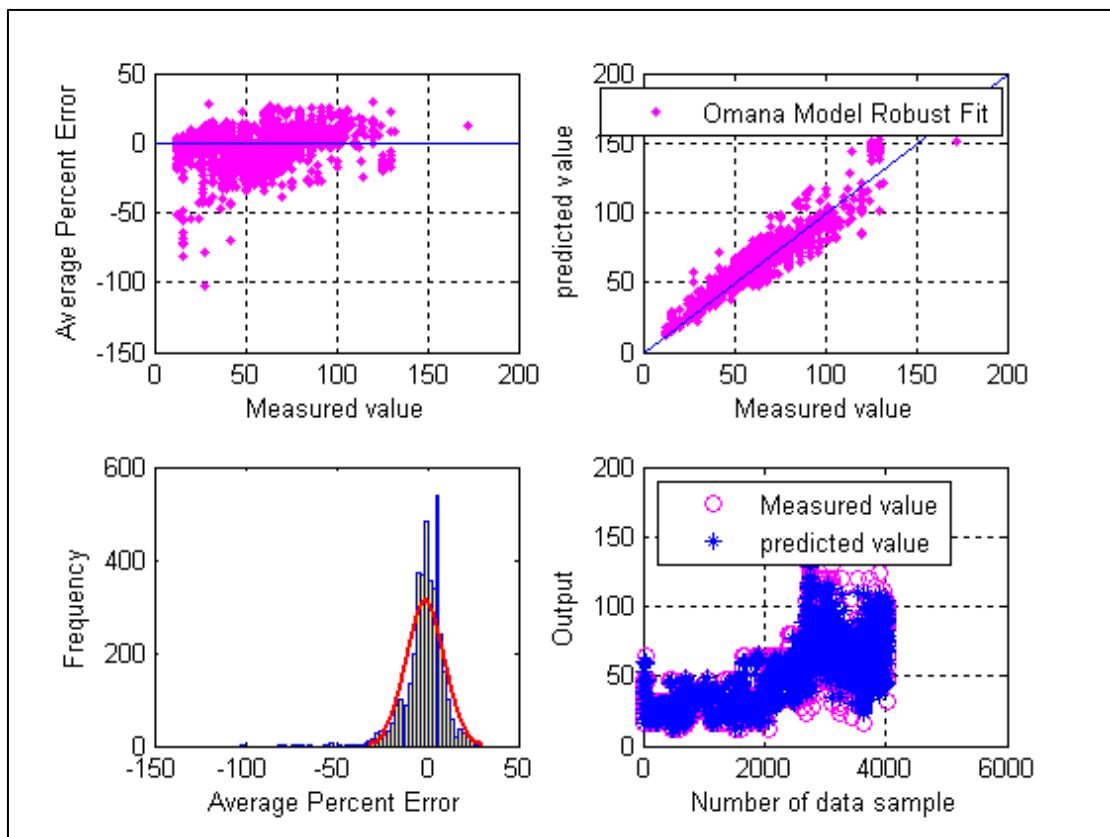


Figure-5.53: Cross, Histogram, Scatter and Overlay plots for Omana Empirical correlation after robust fit. (Choke Size Prediction)

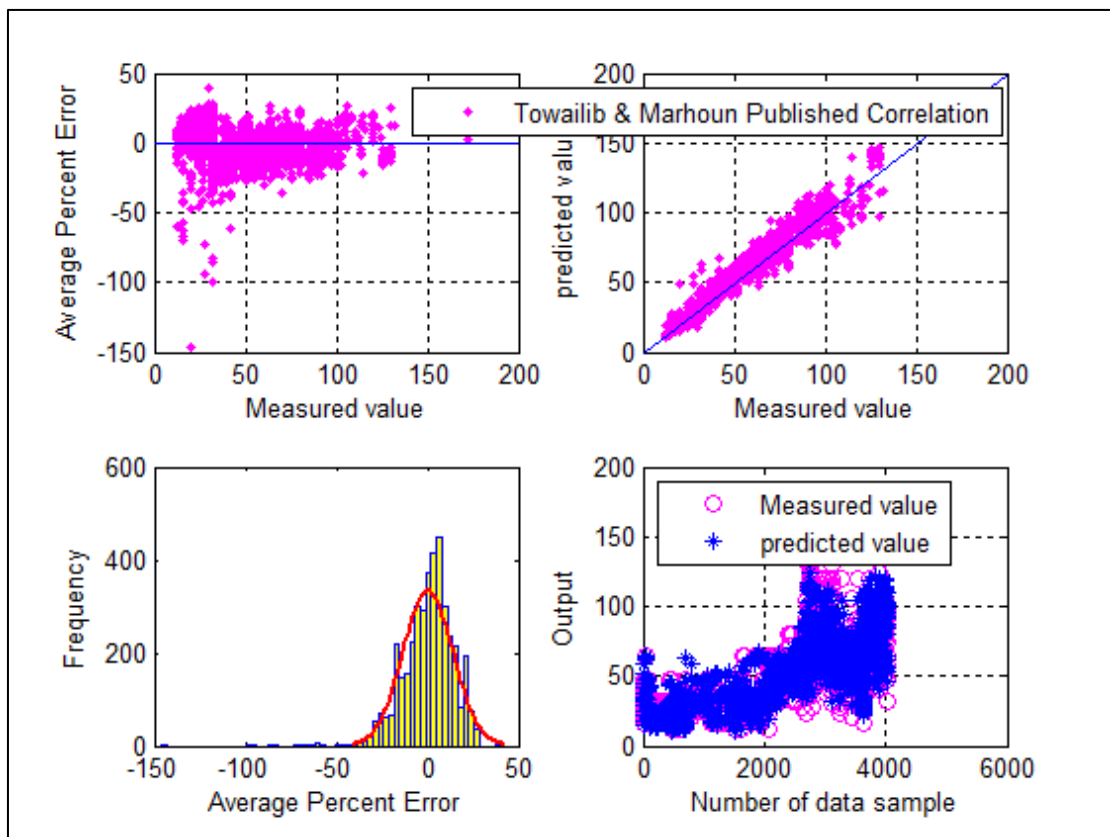


Figure-5.54: Cross, Histogram, Scatter and Overlay plots for Towailib and Marhoun Empirical correlation. (Choke Size Prediction)

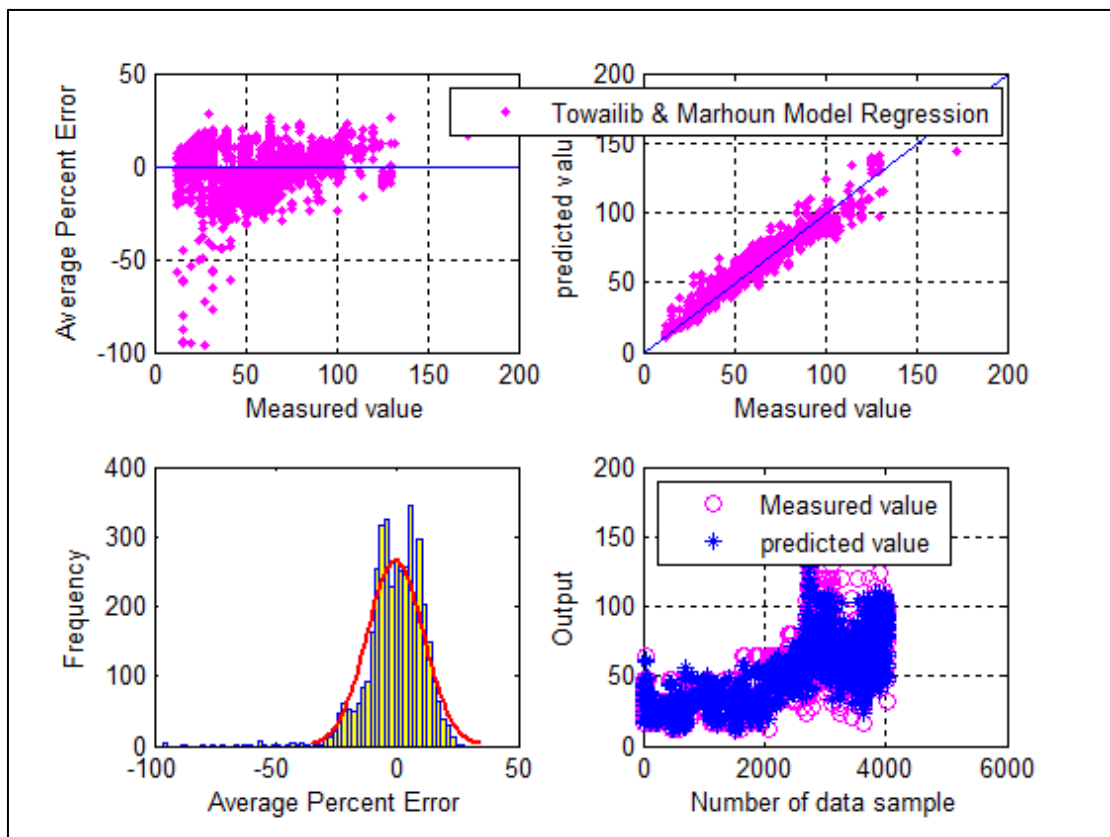


Figure-5.55: Cross, Histogram, Scatter and Overlay plots for Towailib and Marhoun Empirical correlation after regression. (Choke Size Prediction)

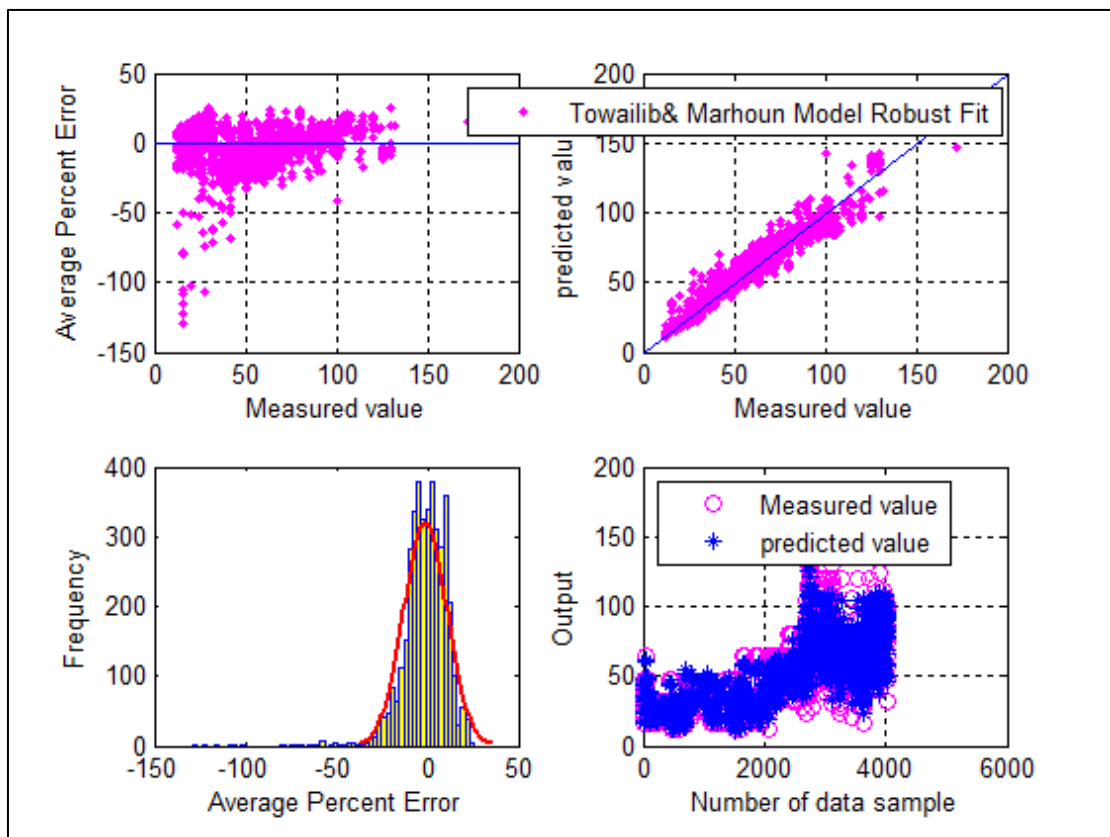


Figure-5.56: Cross, Histogram, Scatter and Overlay plots for Towailib and Marhoun Empirical correlation after robust fit. (Choke Size Prediction)

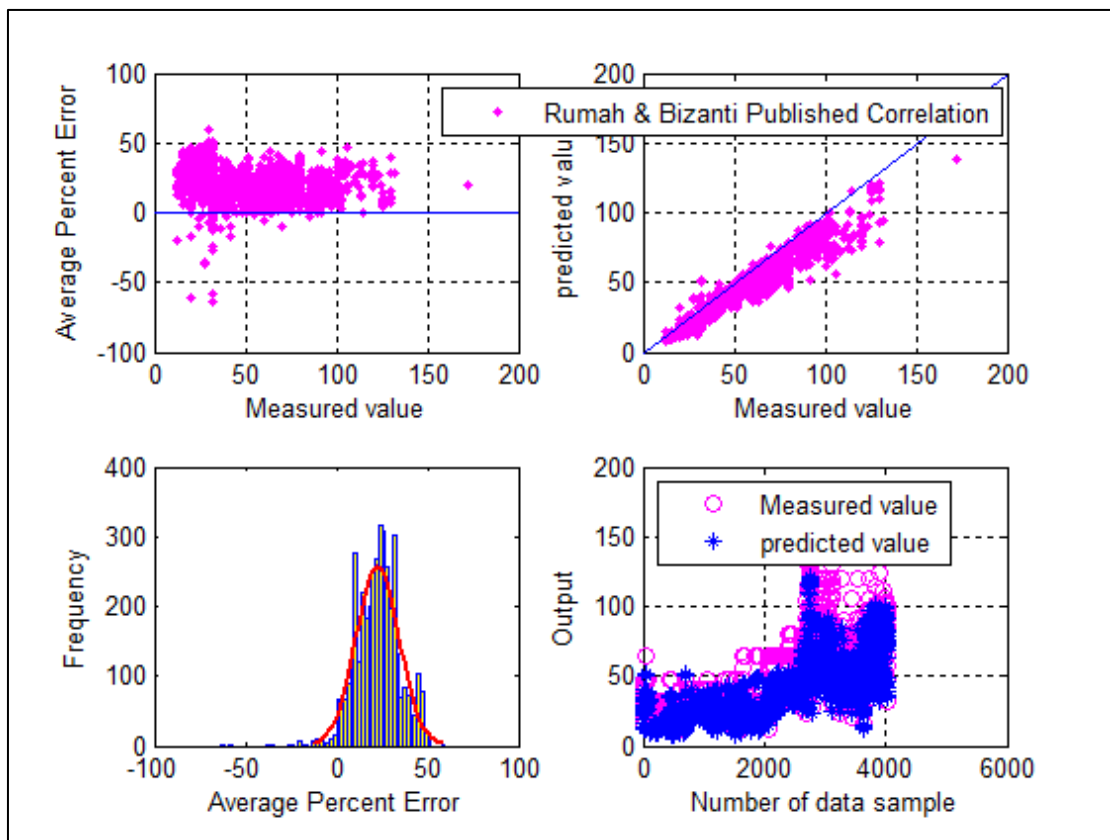


Figure-5.57: Cross, Histogram, Scatter and Overlay plots for Rumah and Bizanti Empirical correlation. (Choke Size Prediction)

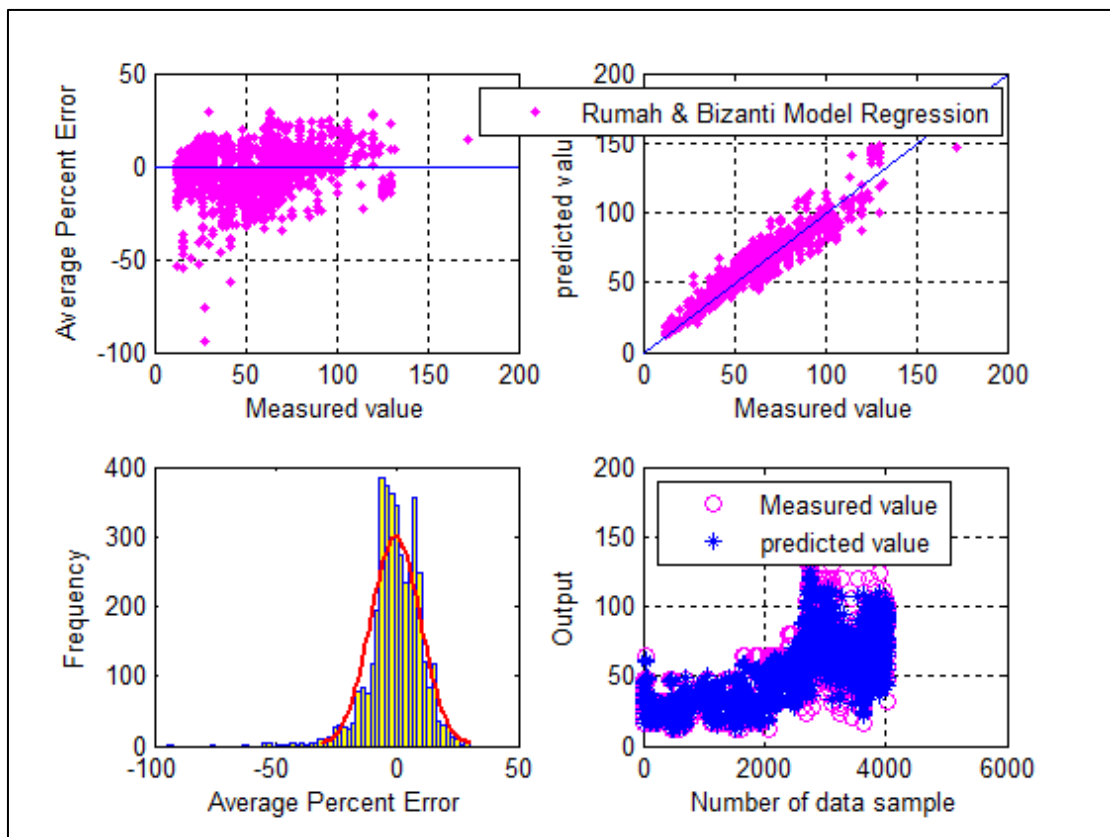


Figure-5.58: Cross, Histogram, Scatter and Overlay plots for Rumah and Bizanti Empirical correlation after regression. (Choke Size Prediction)

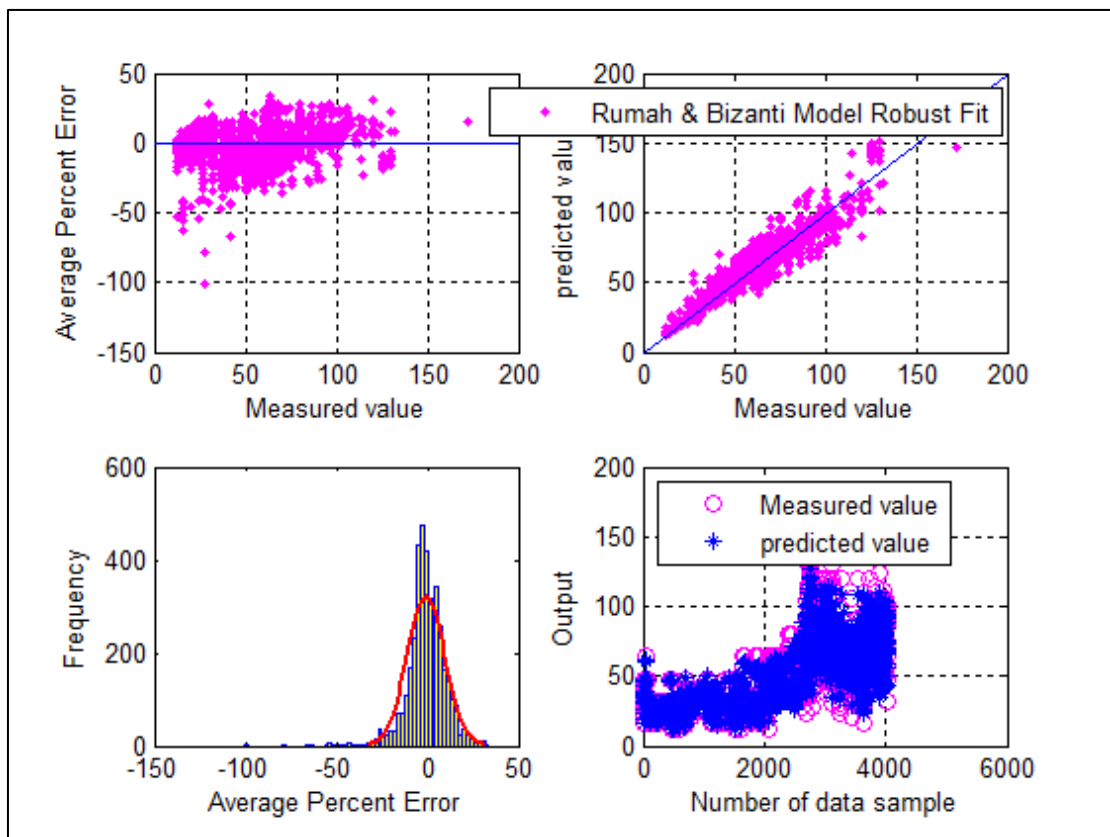


Figure-5.59: Cross, Histogram, Scatter and Overlay plots for Rumah and Bizanti Empirical correlation after robust fit. (Choke Size Prediction)



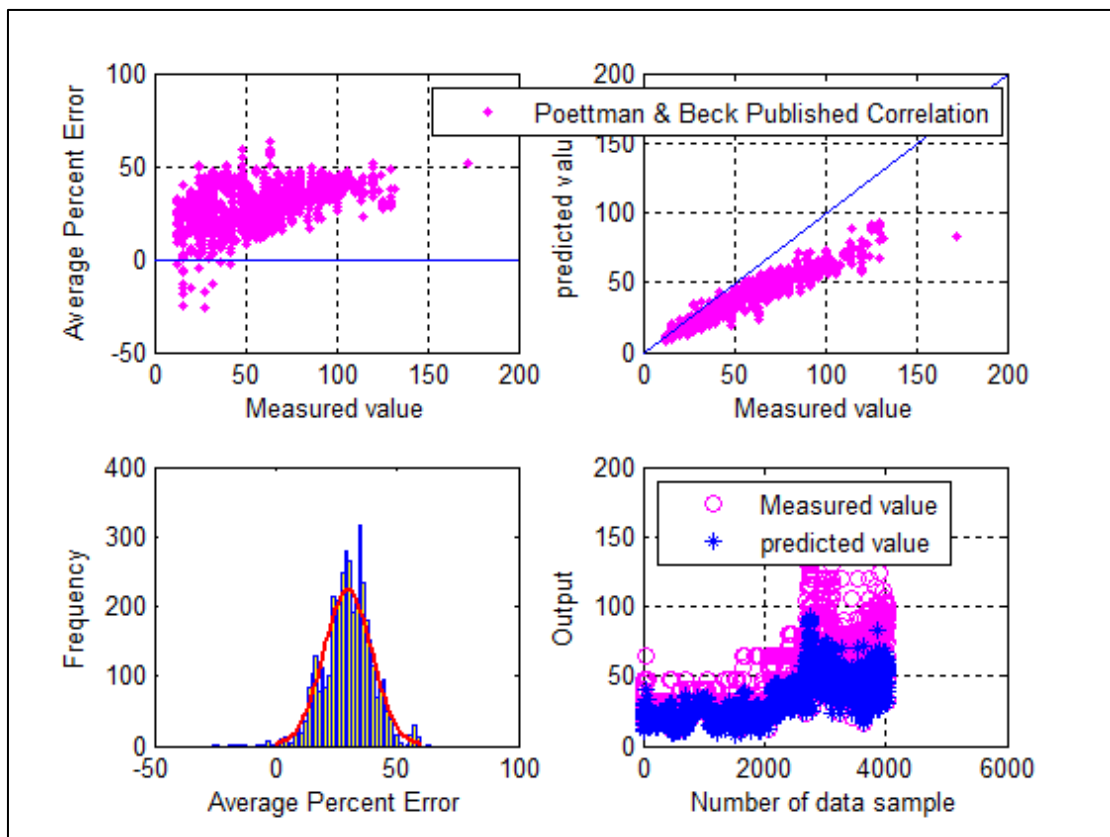


Figure-5.60: Cross, Histogram, Scatter and Overlay plots for Poettman and Beck Empirical correlation. (Choke Size Prediction)

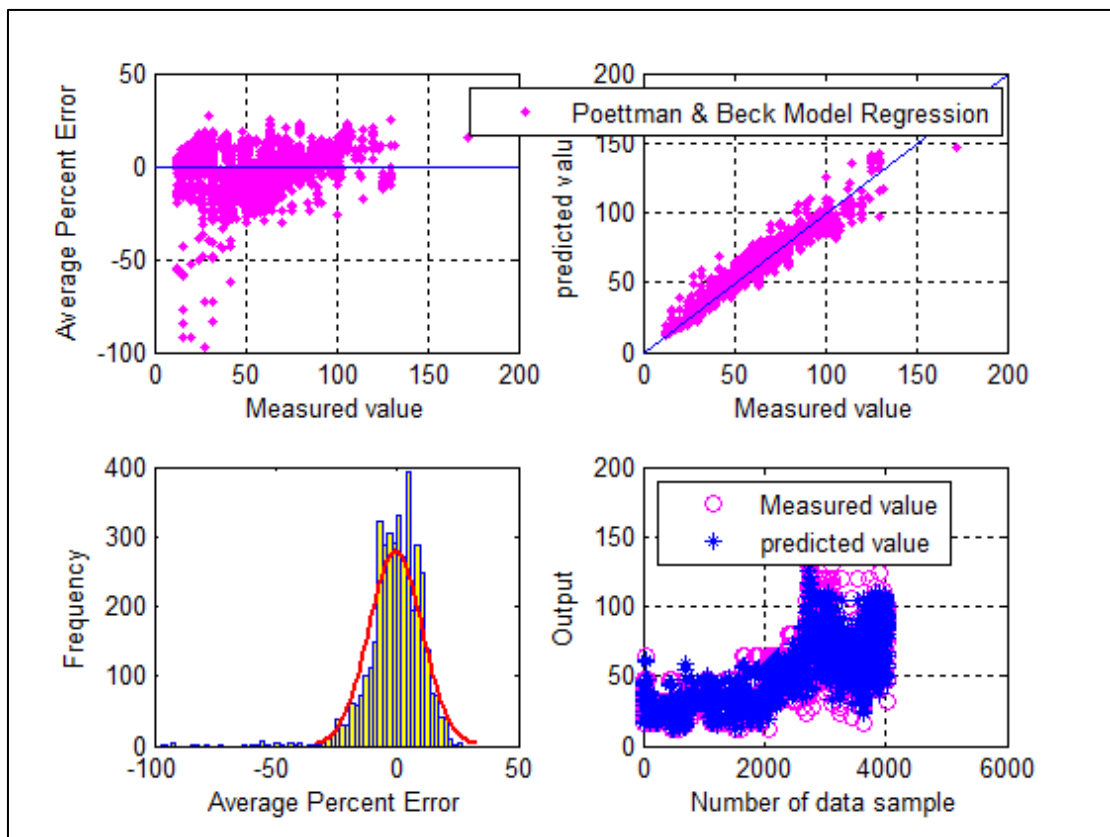


Figure-5.61: Cross, Histogram, Scatter and Overlay plots for Poettman and Beck Empirical correlation after regression. (Choke Size Prediction)

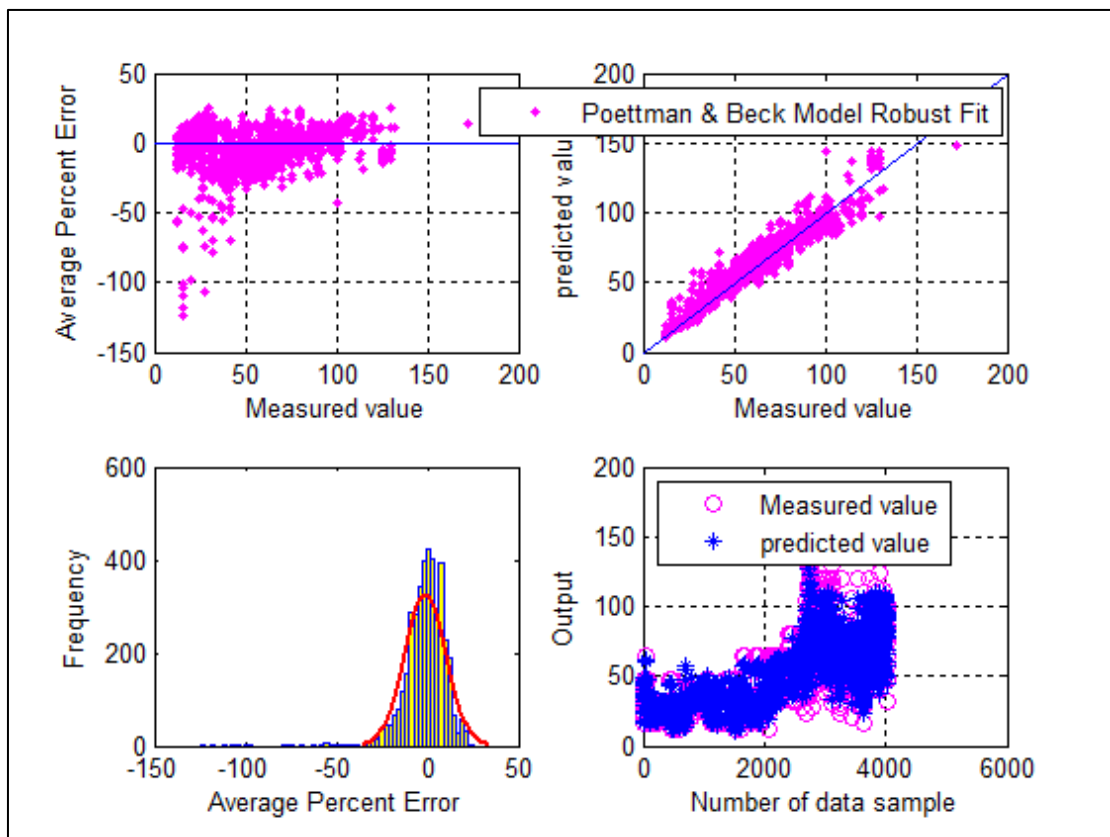


Figure-5.62: Cross, Histogram, Scatter and Overlay plots for Poettman and Beck Empirical correlation after robust fit. (Choke Size Prediction)

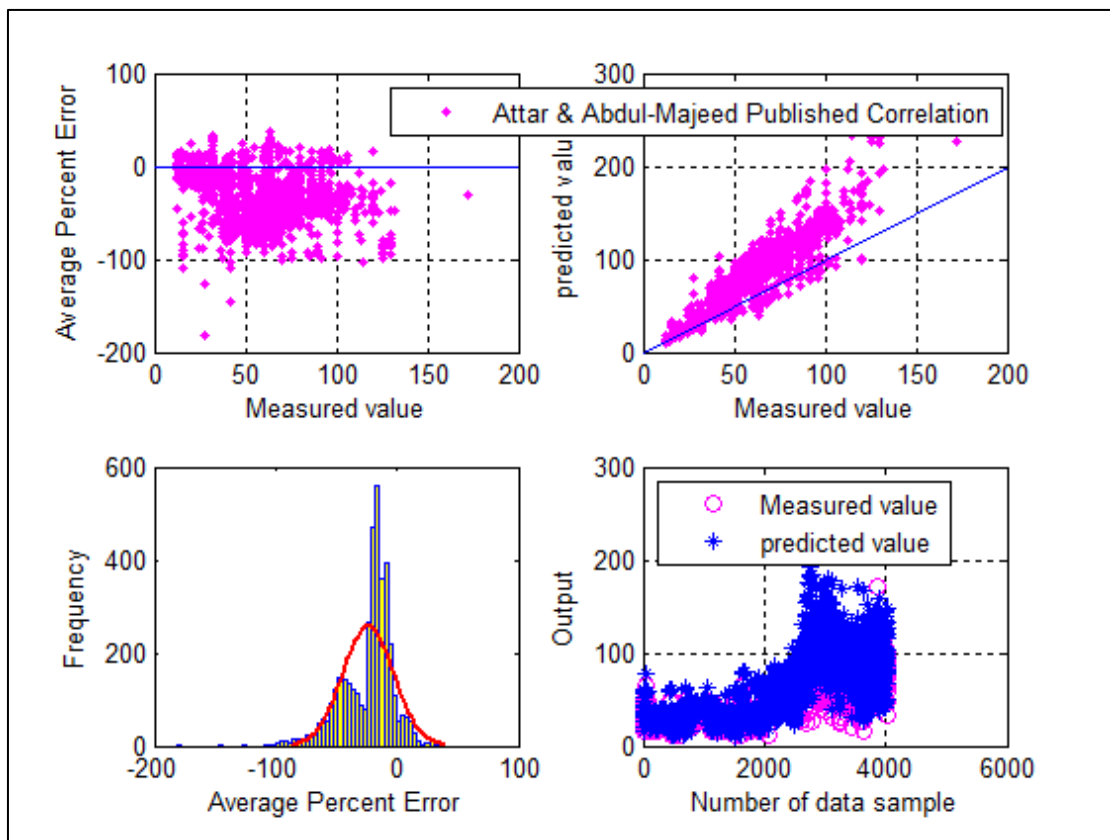


Figure-5.63: Cross, Histogram, Scatter and Overlay plots for Attar and Abdul-Majeed Empirical correlation. (Choke Size Prediction)

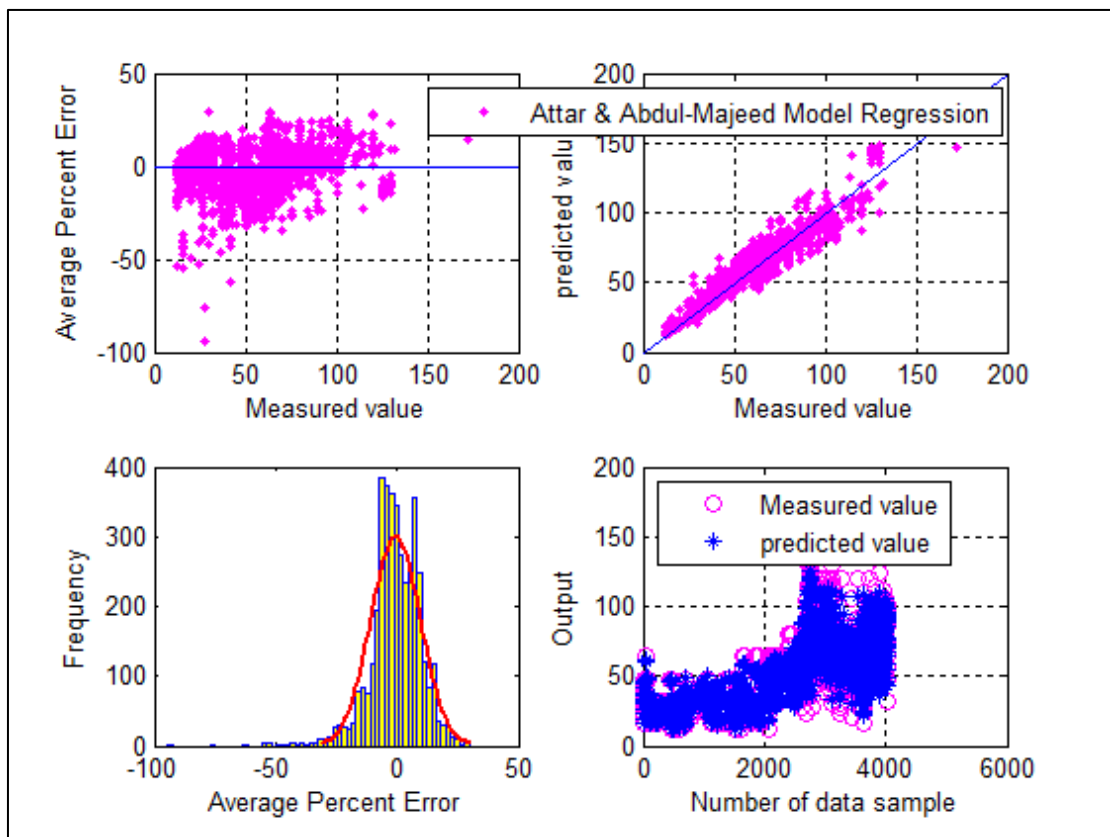


Figure-5.64: Cross, Histogram, Scatter and Overlay plots for Attar and Abdul-Majeed Empirical correlation after regression. (Choke Size Prediction)

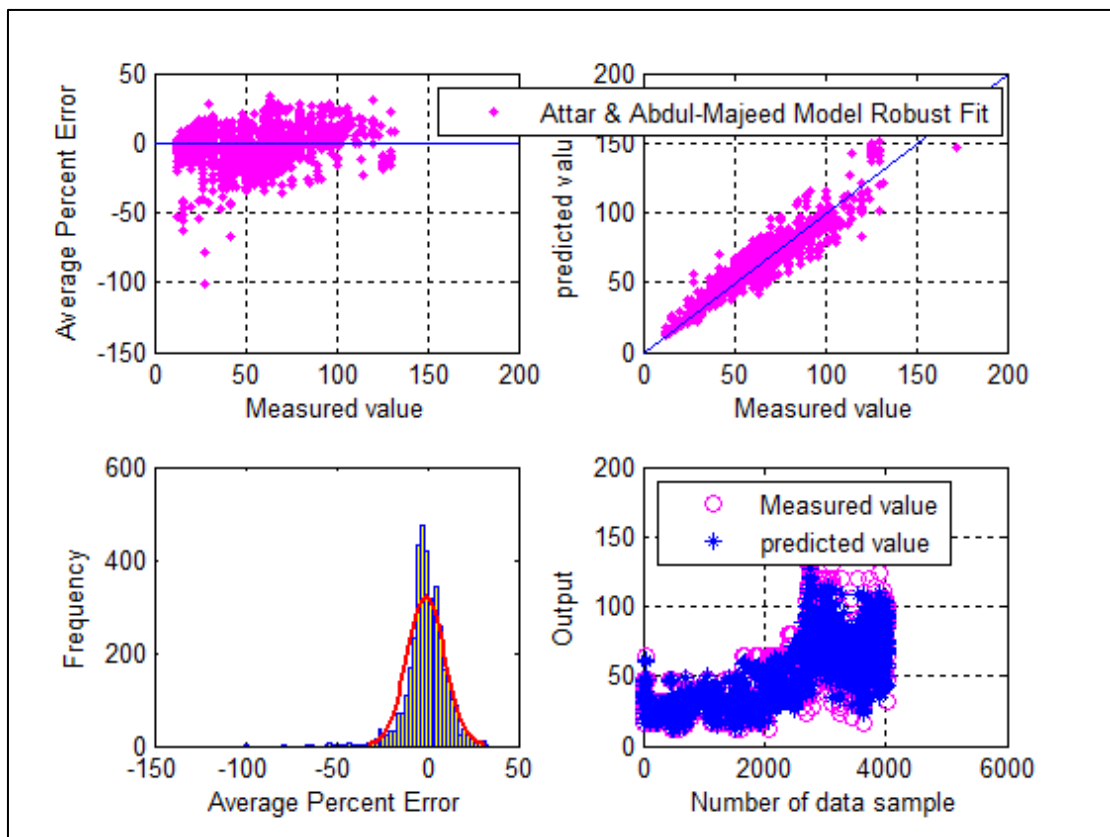


Figure-5.65: Cross, Histogram, Scatter and Overlay plots for Attar and Abdul-Majeed Empirical correlation after robust fit. (Choke Size Prediction)

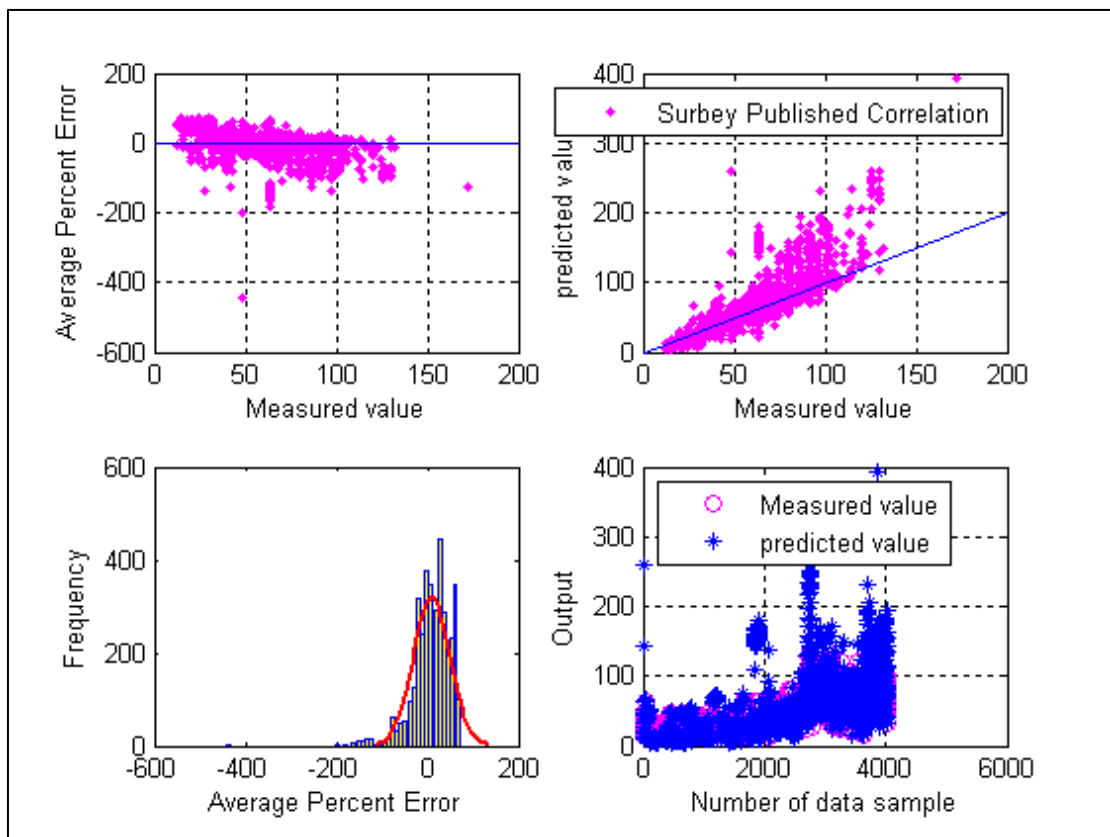


Figure-5.66: Cross, Histogram, Scatter and Overlay plots for Surbey Empirical correlation. (Choke Size Prediction)

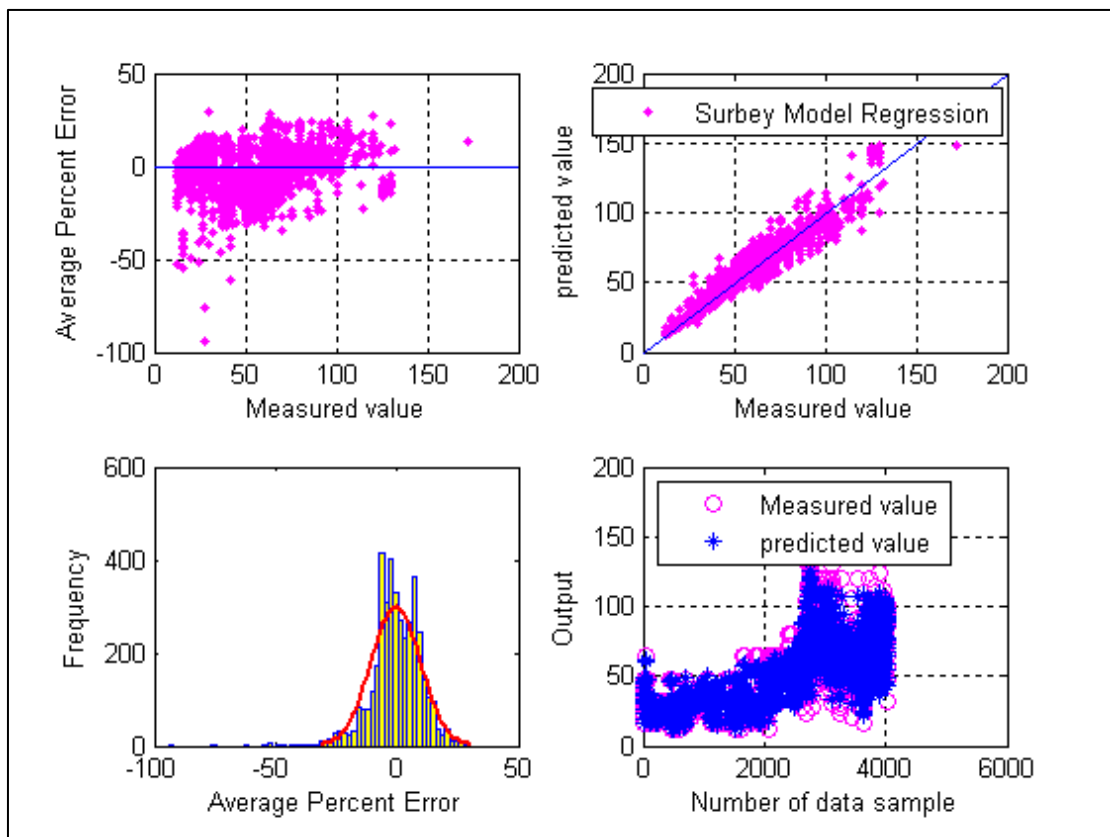


Figure-5.67: Cross, Histogram, Scatter and Overlay plots for Surbey Empirical correlation after regression. (Choke Size Prediction)



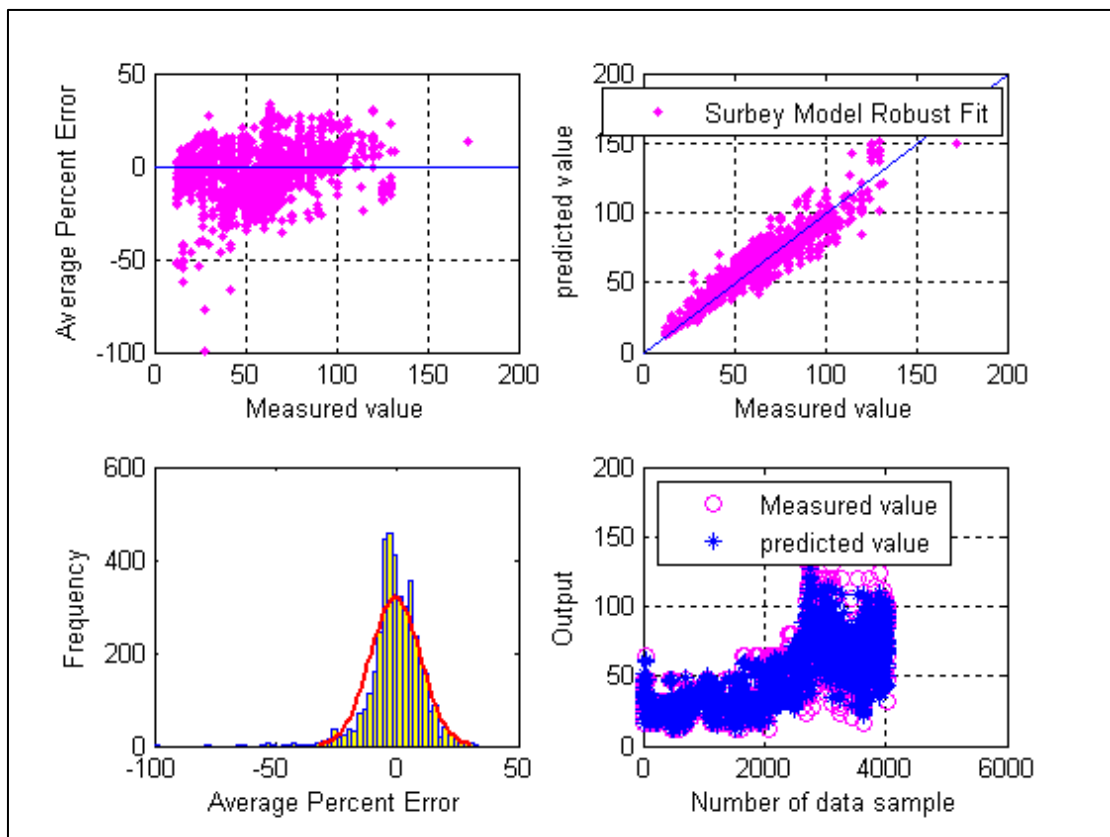


Figure-5.68: Cross, Histogram, Scatter and Overlay plots for Surbey Empirical correlation after robust fit. (Choke Size Prediction)

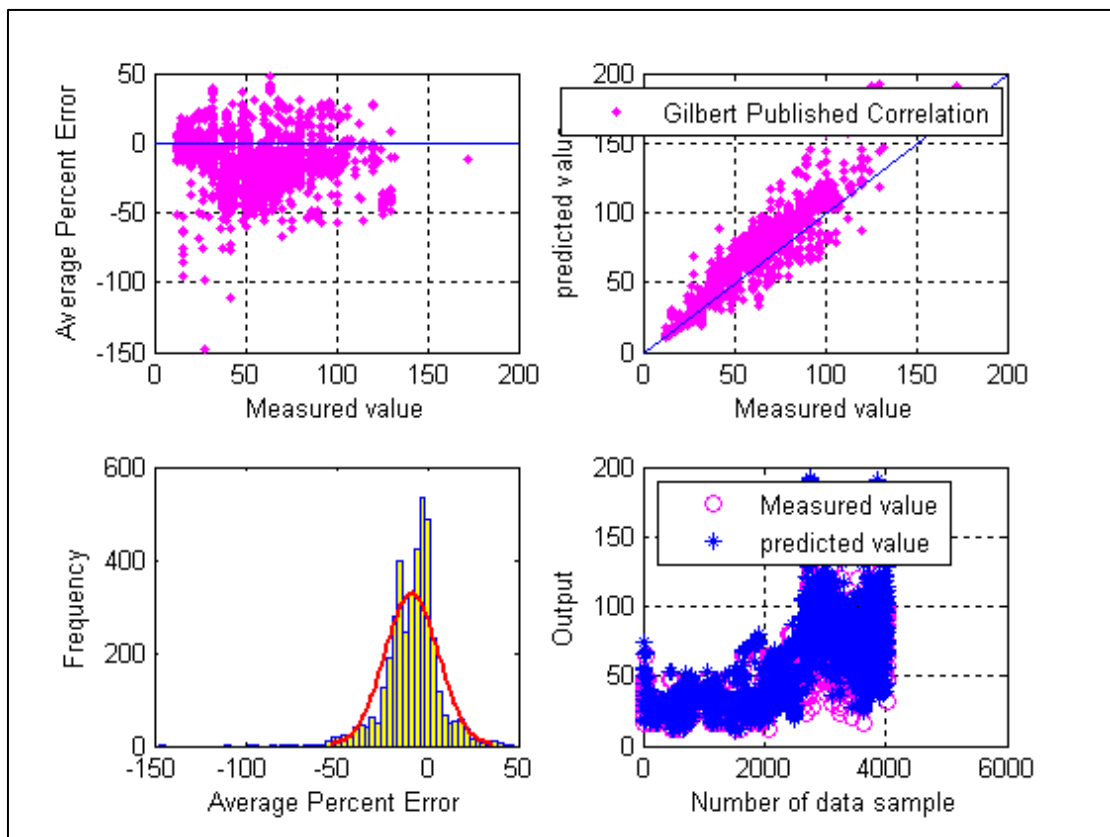


Figure-5.69: Cross, Histogram, Scatter and Overlay plots for Gilbert Empirical correlation. (Choke Size Prediction)

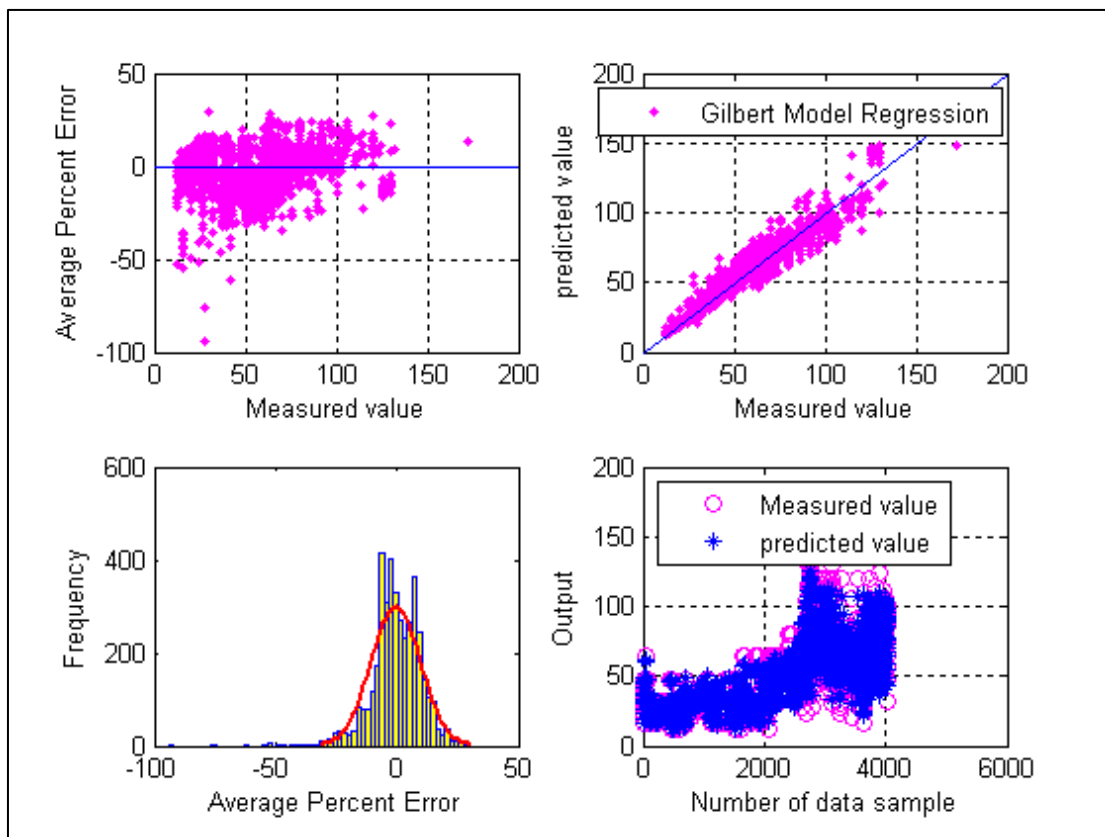


Figure-5.70: Cross, Histogram, Scatter and Overlay plots for Gilbert Empirical correlation after regression. (Choke Size Prediction)

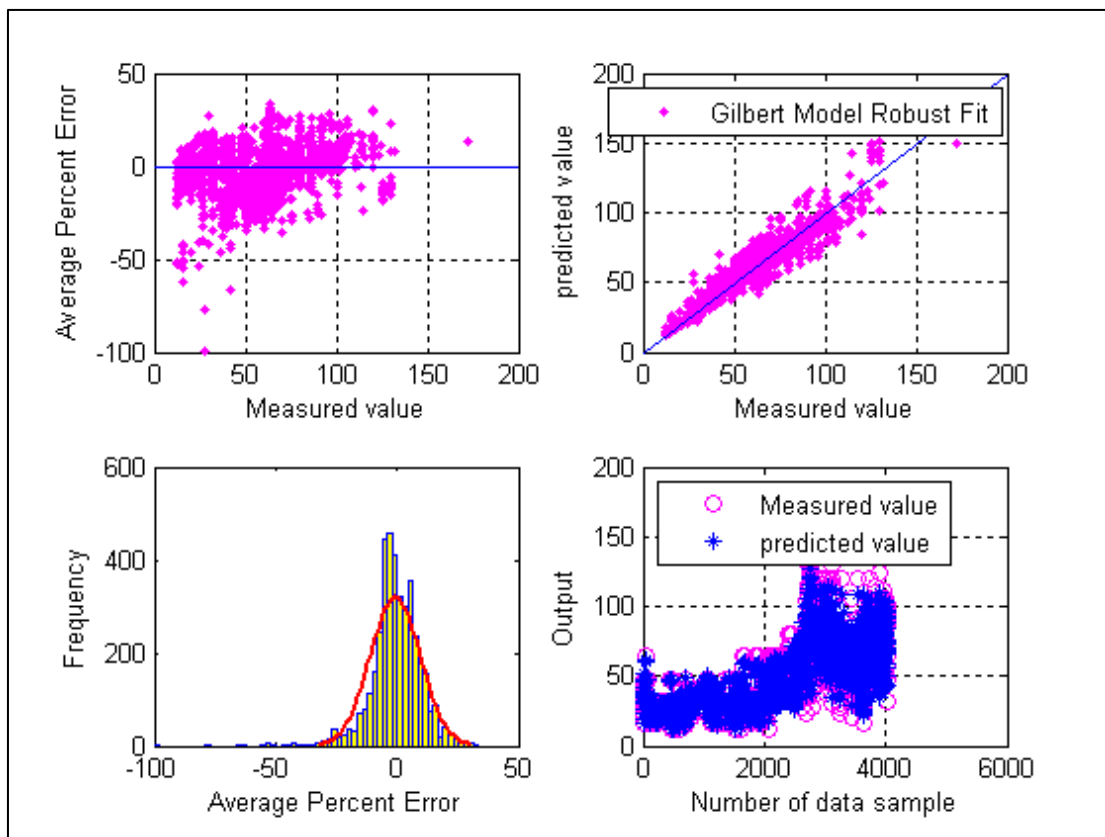


Figure-5.71: Cross, Histogram, Scatter and Overlay plots for Gilbert Empirical correlation after robust fit. (Choke Size Prediction)

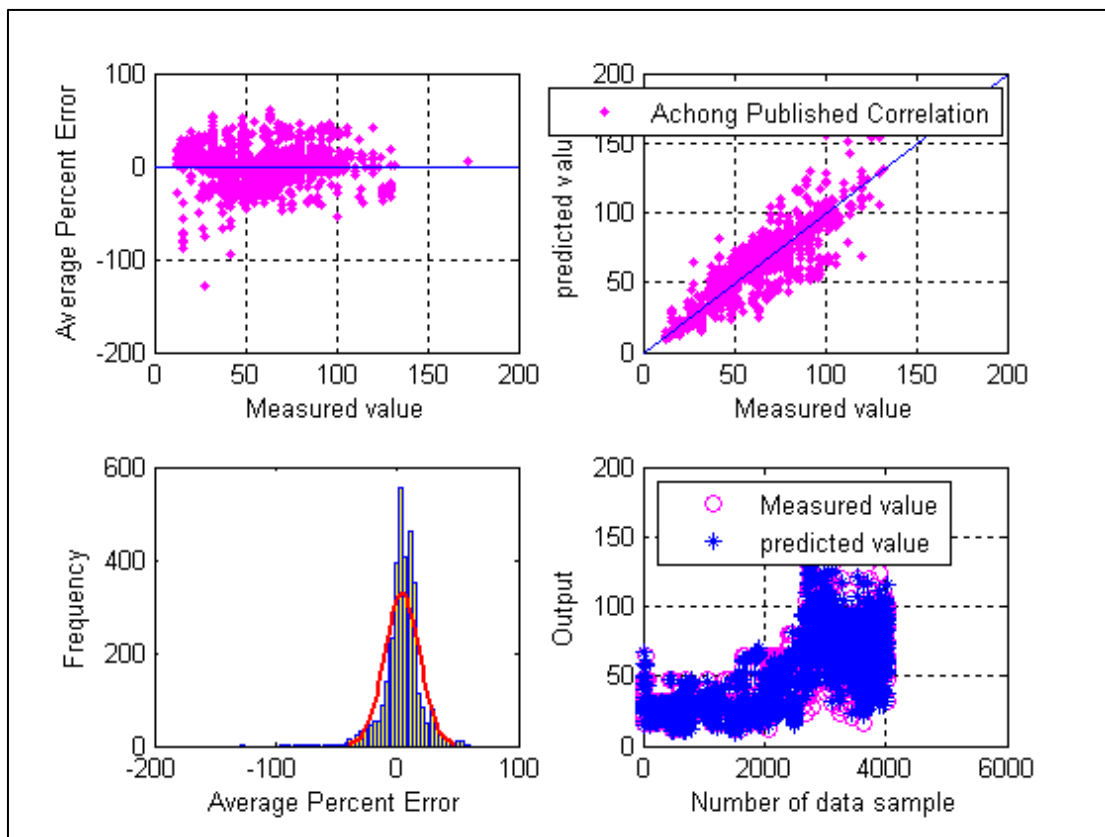


Figure-5.72: Cross, Histogram, Scatter and Overlay plots for Achong Empirical correlation. (Choke Size Prediction)

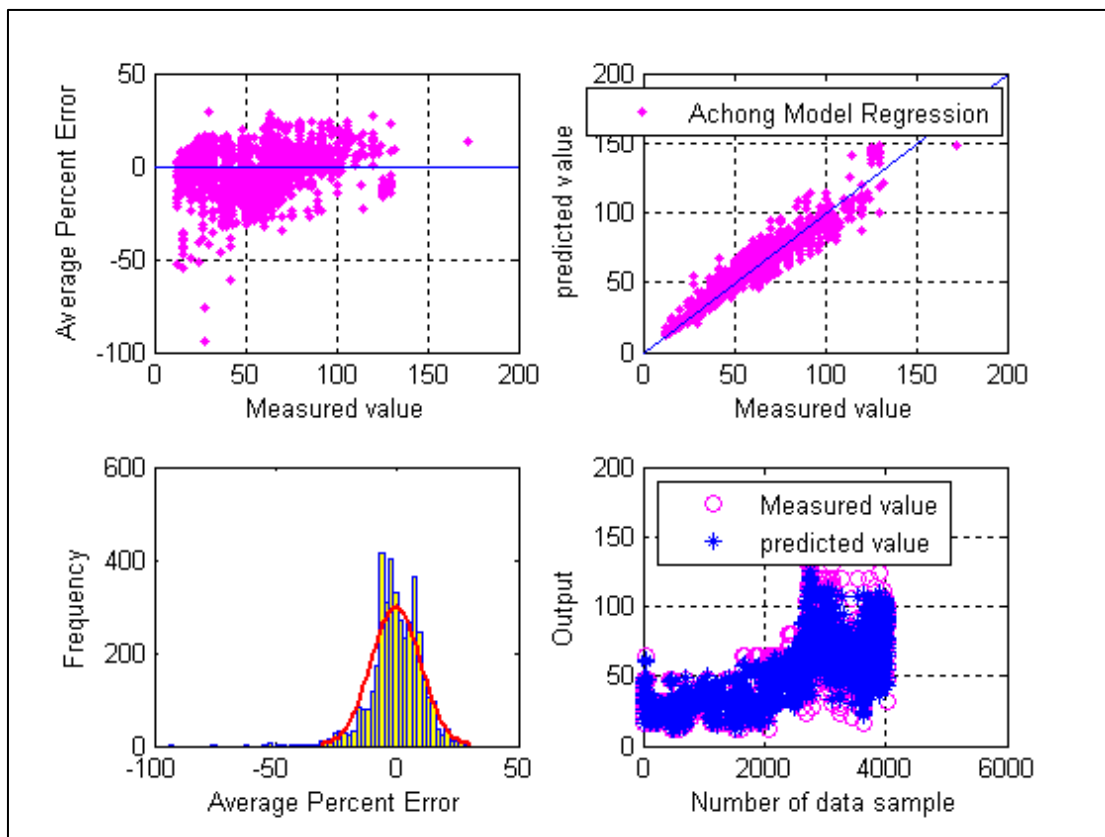


Figure-5.73: Cross, Histogram, Scatter and Overlay plots for Achong Empirical correlation after regression. (Choke Size Prediction)

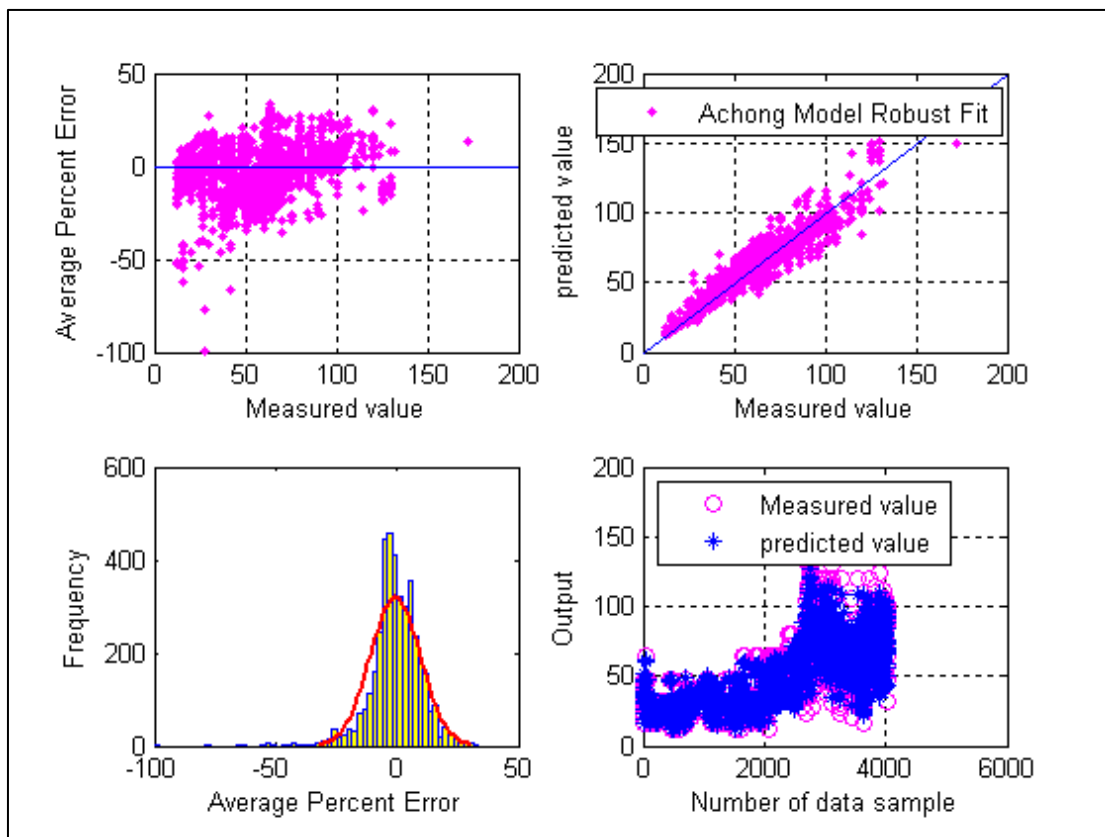


Figure-5.74: Cross, Histogram, Scatter and Overlay plots for Achong Empirical correlation after robust fit. (Choke Size Prediction)

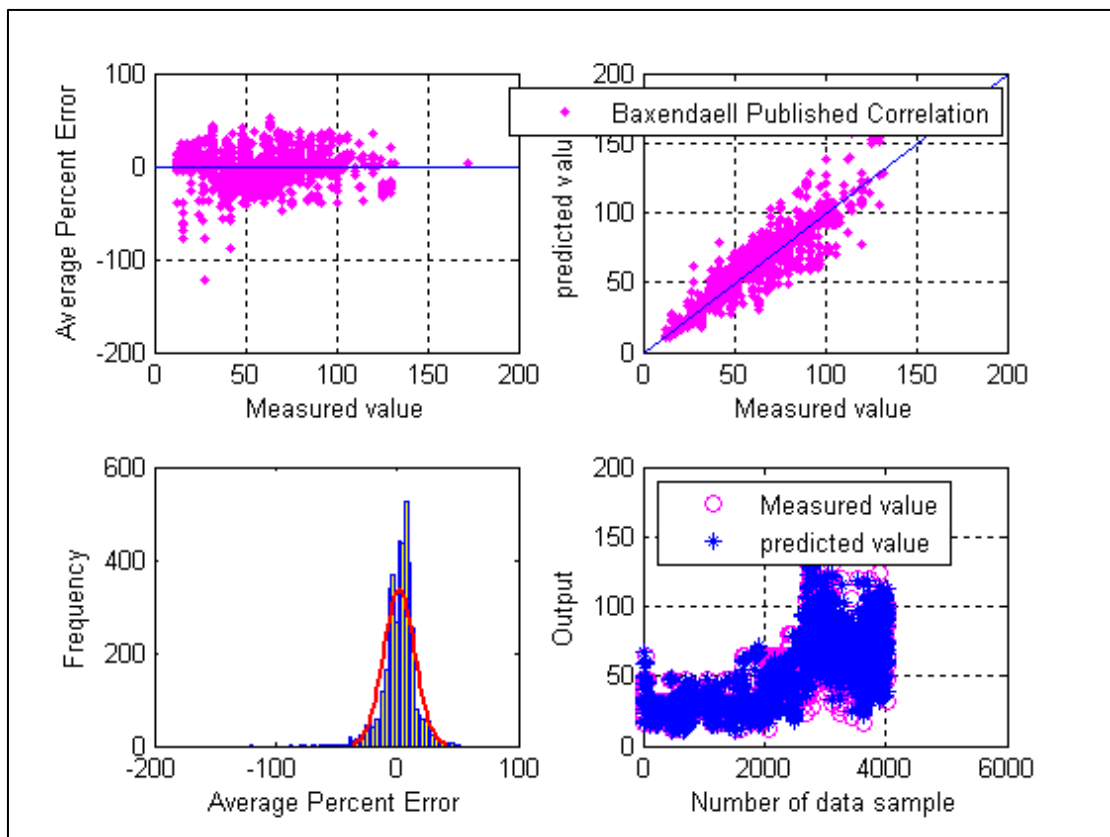


Figure-5.75: Cross, Histogram, Scatter and Overlay plots for Baxendaell Empirical correlation. (Choke Size Prediction)



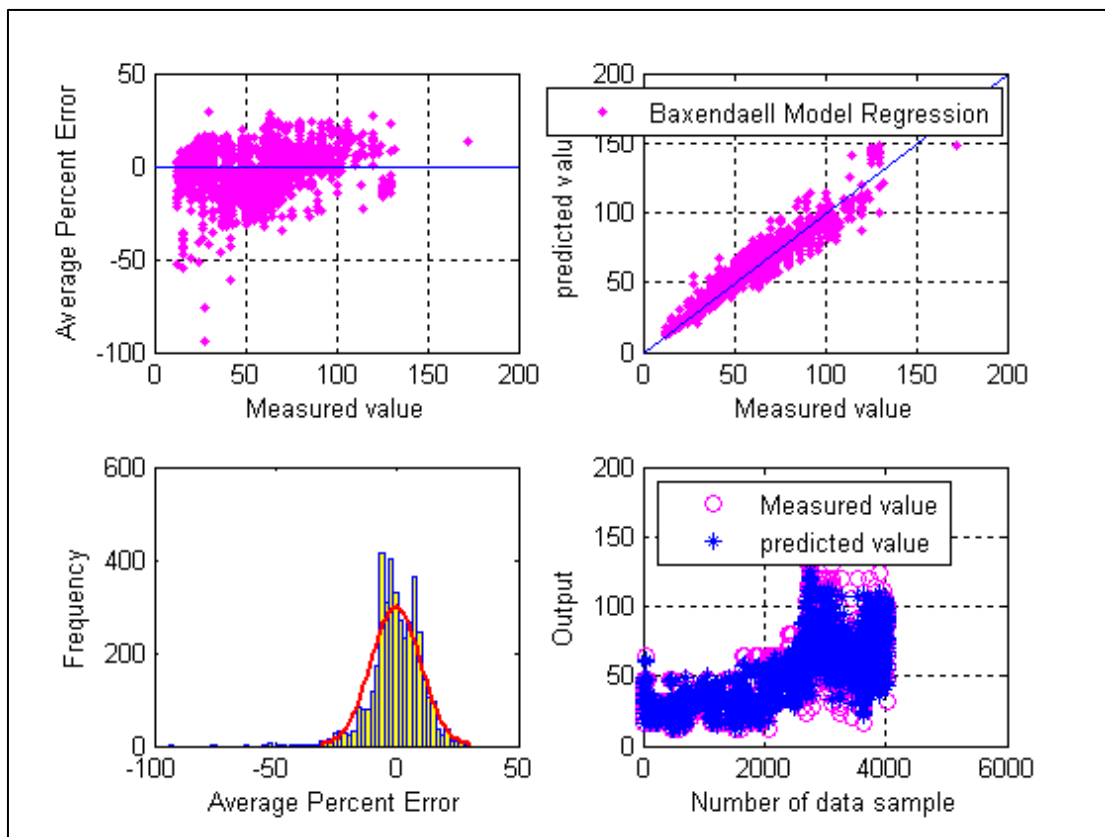


Figure-5.76: Cross, Histogram, Scatter and Overlay plots for Baxendaell Empirical correlation after regression. (Choke Size Prediction)

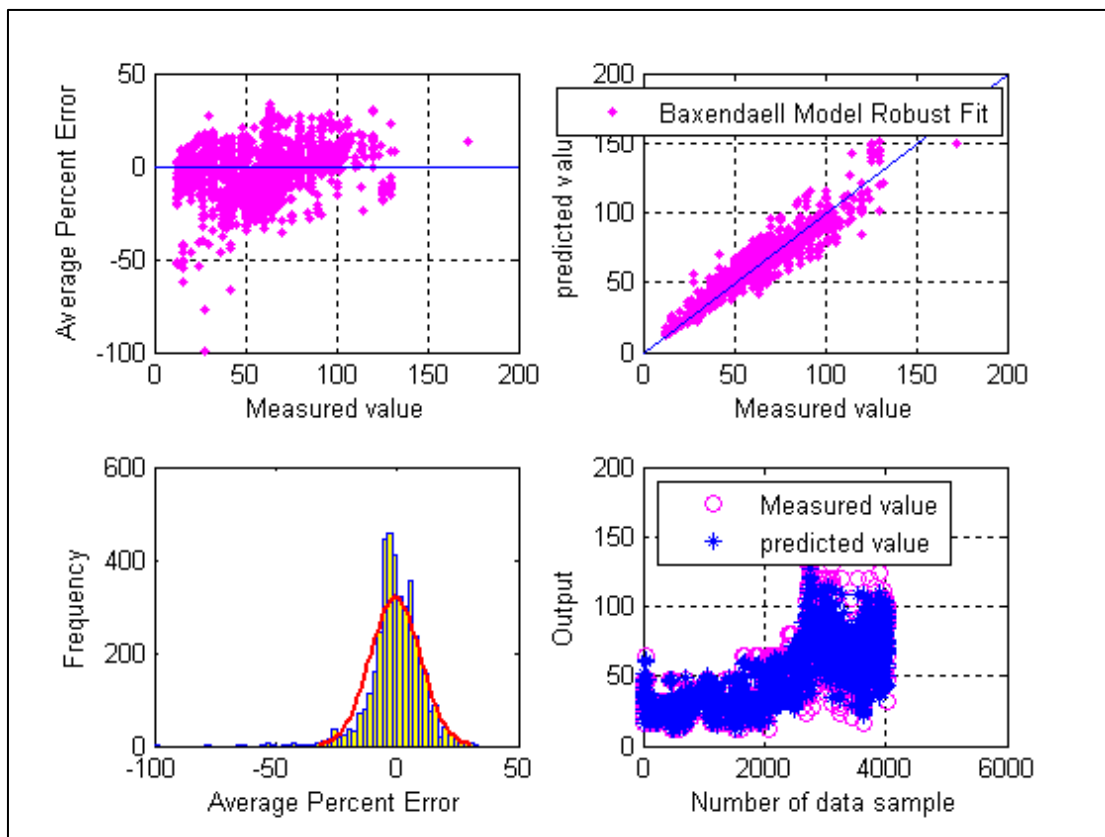


Figure-5.77: Cross, Histogram, Scatter and Overlay plots for Baxendaell Empirical correlation after robust fit. (Choke Size Prediction)

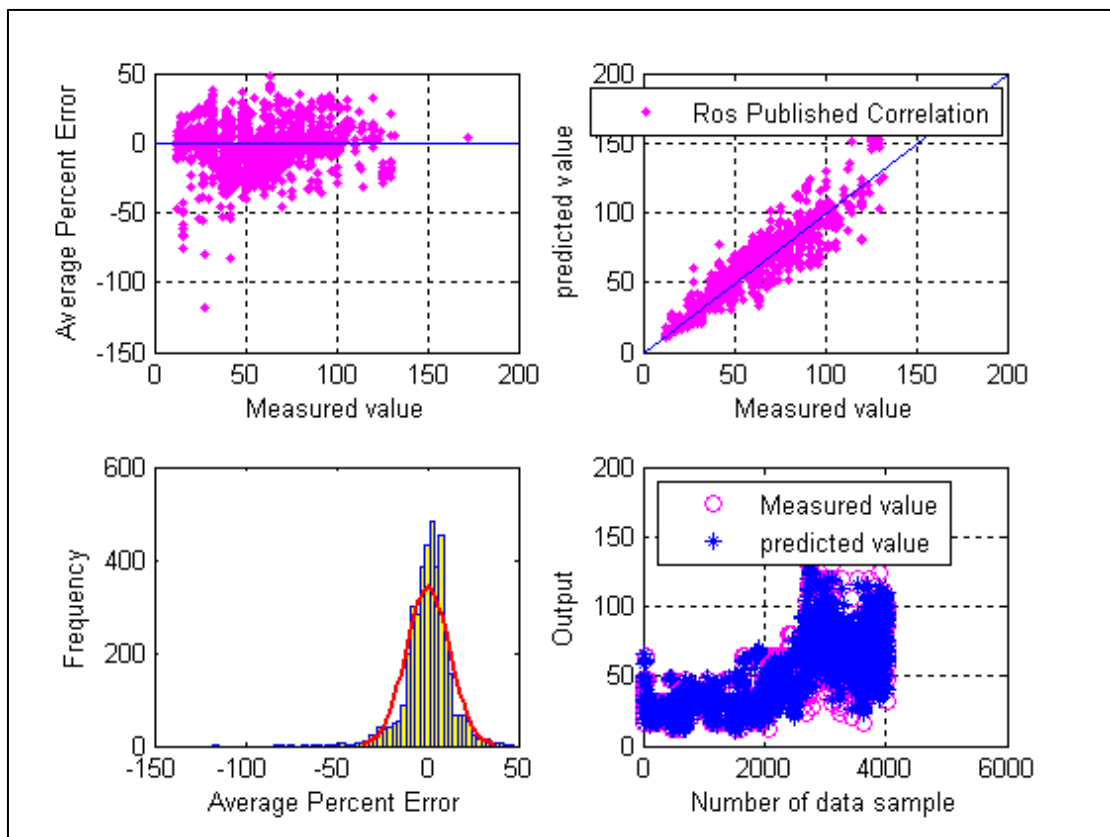


Figure-5.78: Cross, Histogram, Scatter and Overlay plots for Ros Empirical correlation. (Choke Size Prediction)

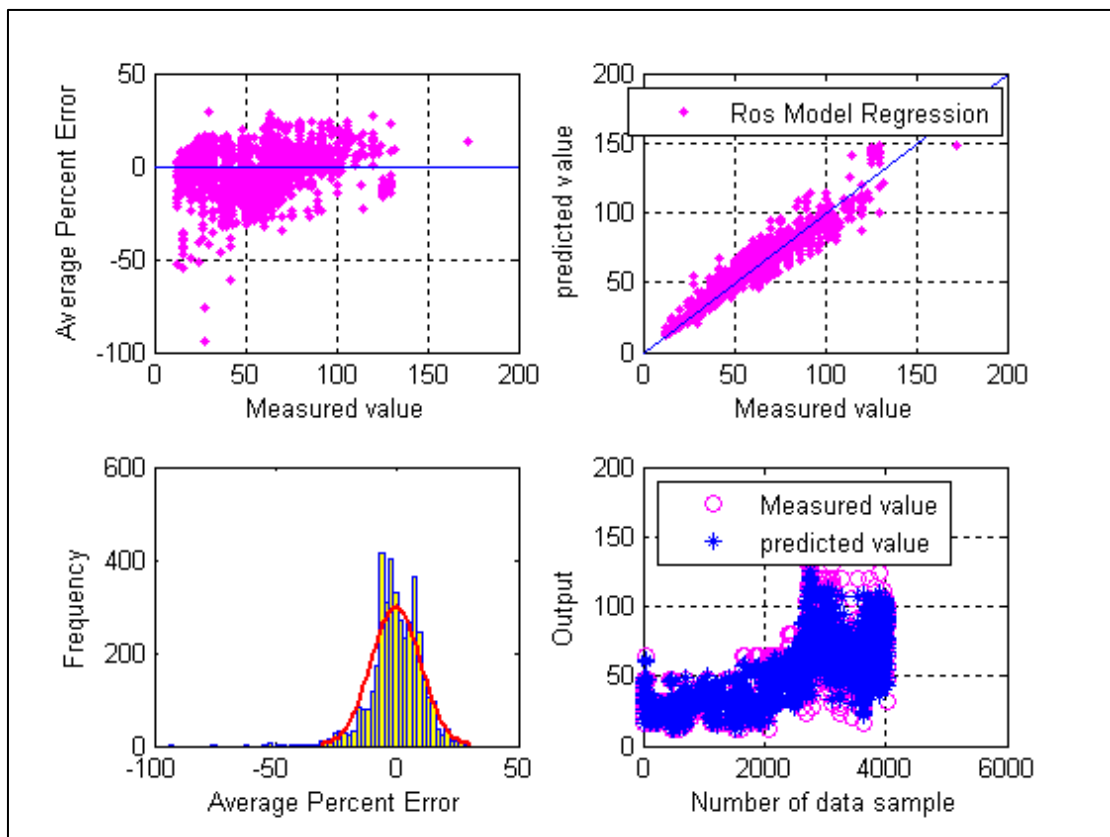


Figure-5.79: Cross, Histogram, Scatter and Overlay plots for Ros Empirical correlation after regression. (Choke Size Prediction)

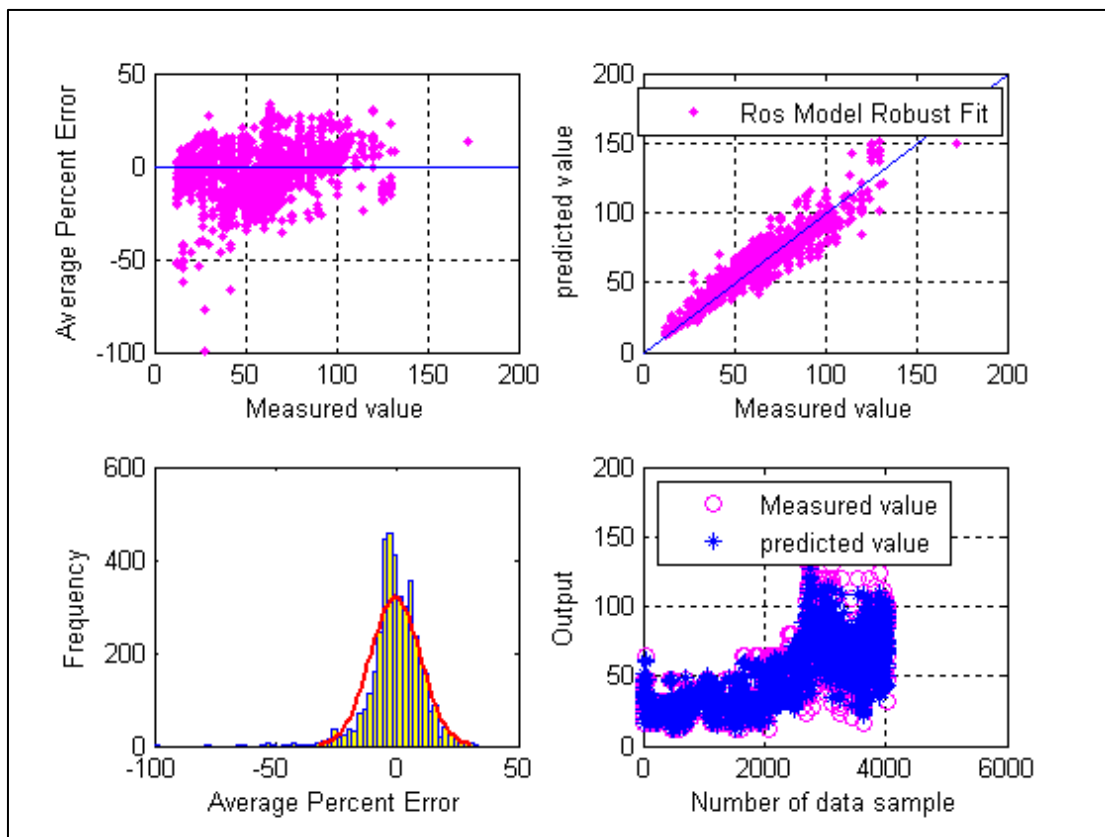


Figure-5.80: Cross, Histogram, Scatter and Overlay plots for Ros Empirical correlation after robust fit. (Choke Size Prediction)

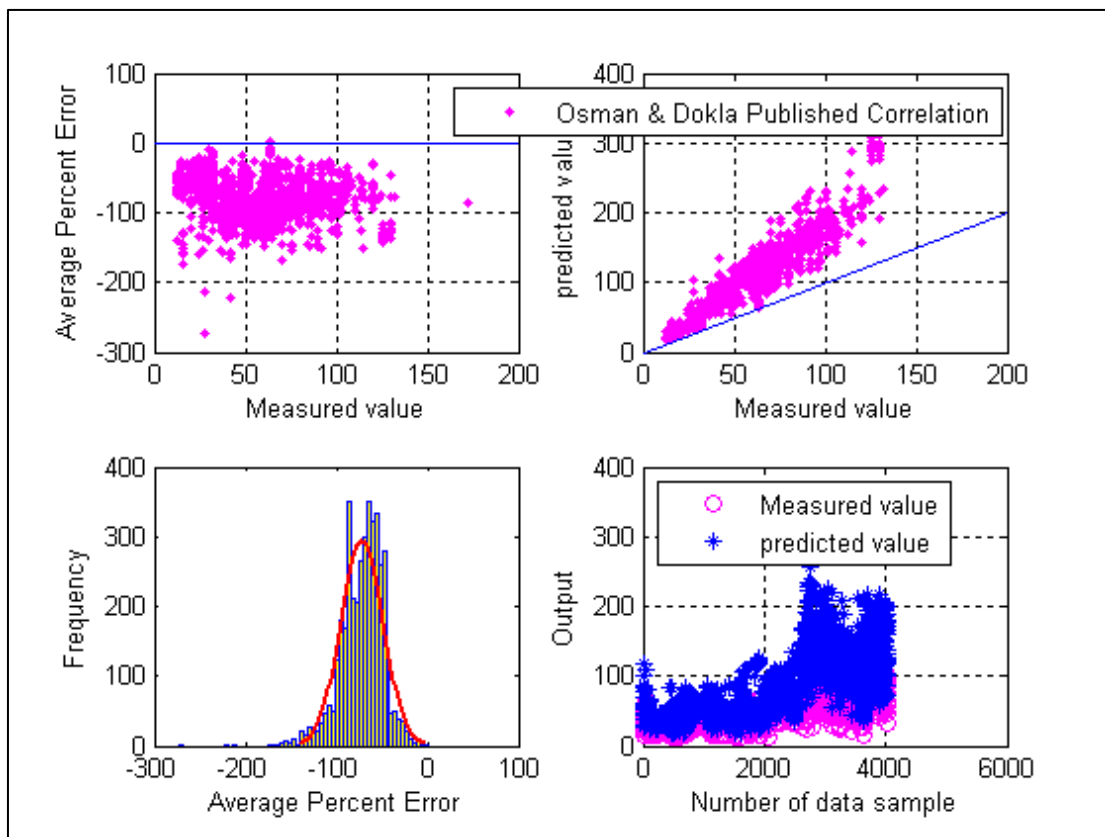


Figure-5.81: Cross, Histogram, Scatter and Overlay plots for Osman and Dokla Empirical correlation. (Choke Size Prediction)

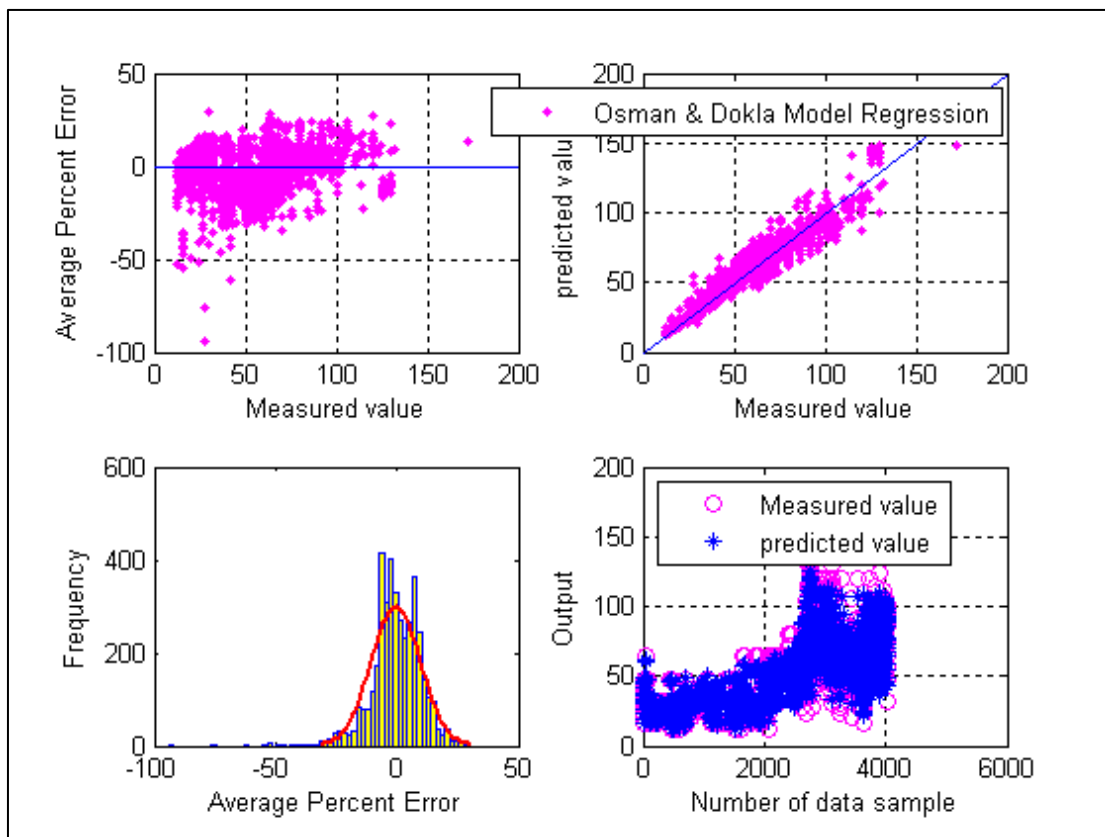


Figure-5.82: Cross, Histogram, Scatter and Overlay plots for Osman and Dokla Empirical correlation after regression. (Choke Size Prediction)

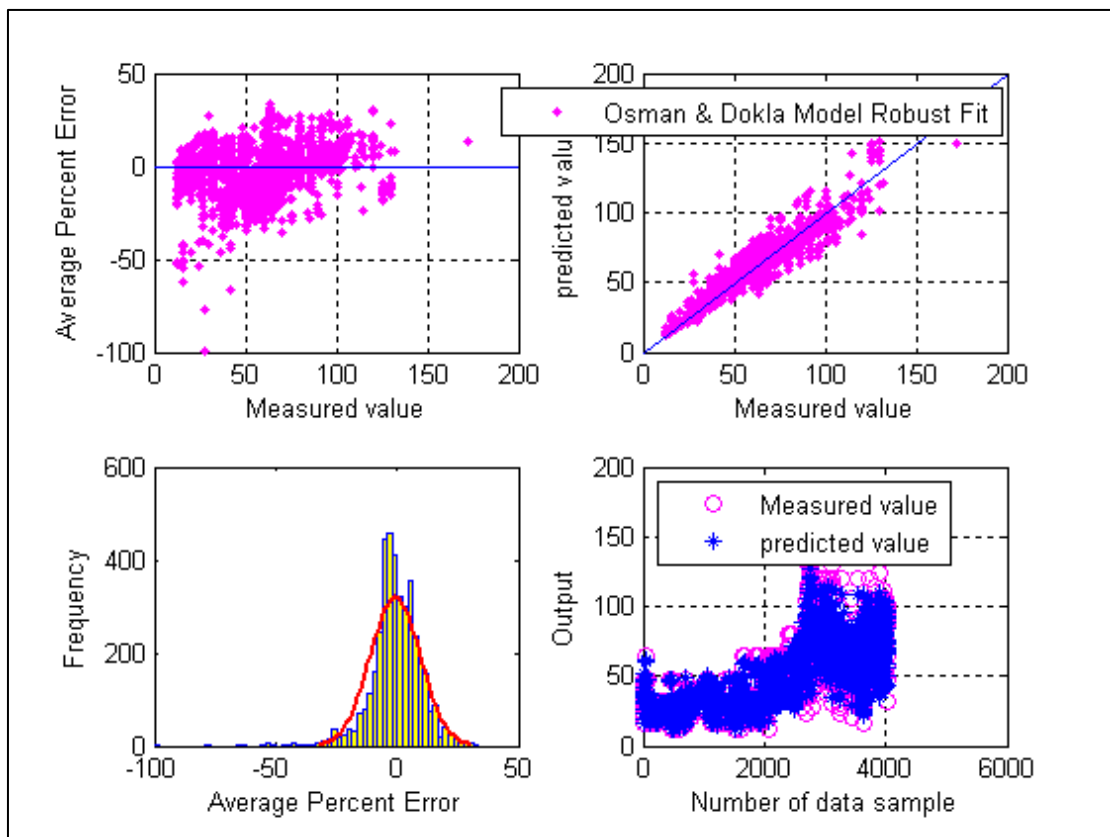


Figure-5.83: Cross, Histogram, Scatter and Overlay plots for Osman and Dokla Empirical correlation after robust fit. (Choke Size Prediction)



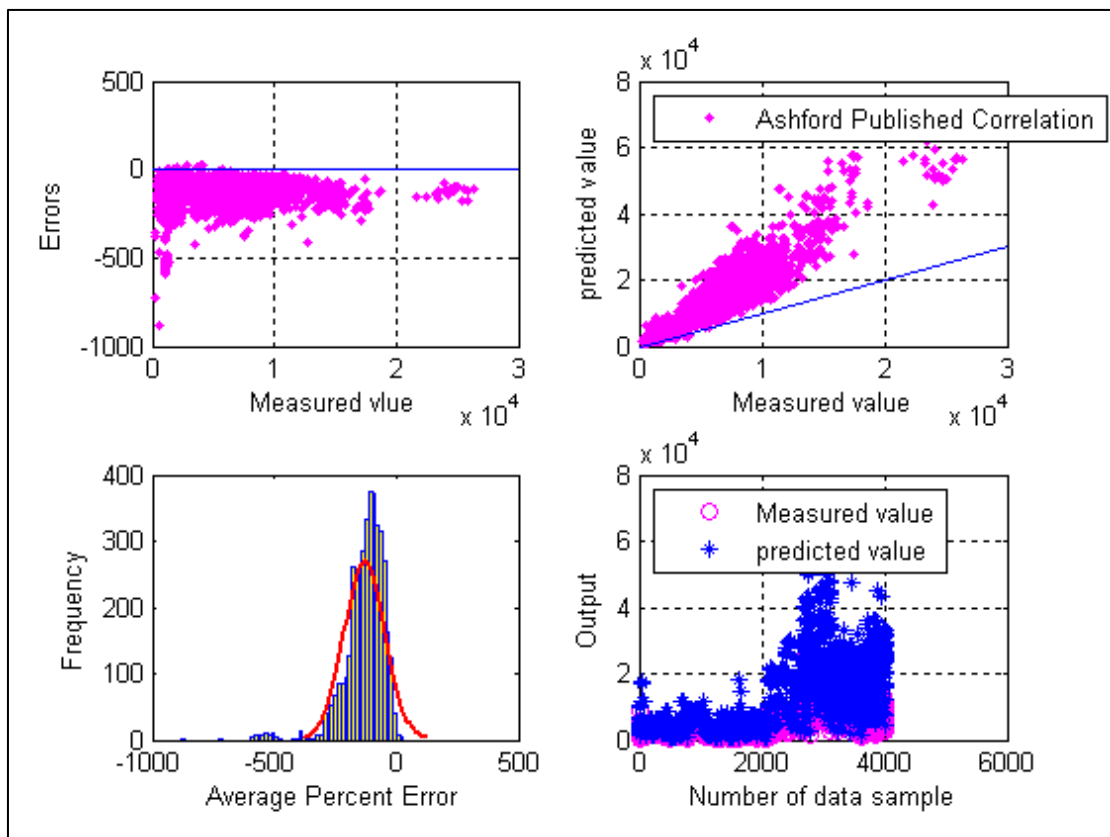


Figure-5.84: Cross, Histogram, Scatter and Overlay plots for Ashford Empirical correlation. (Flow Rate Estimation)

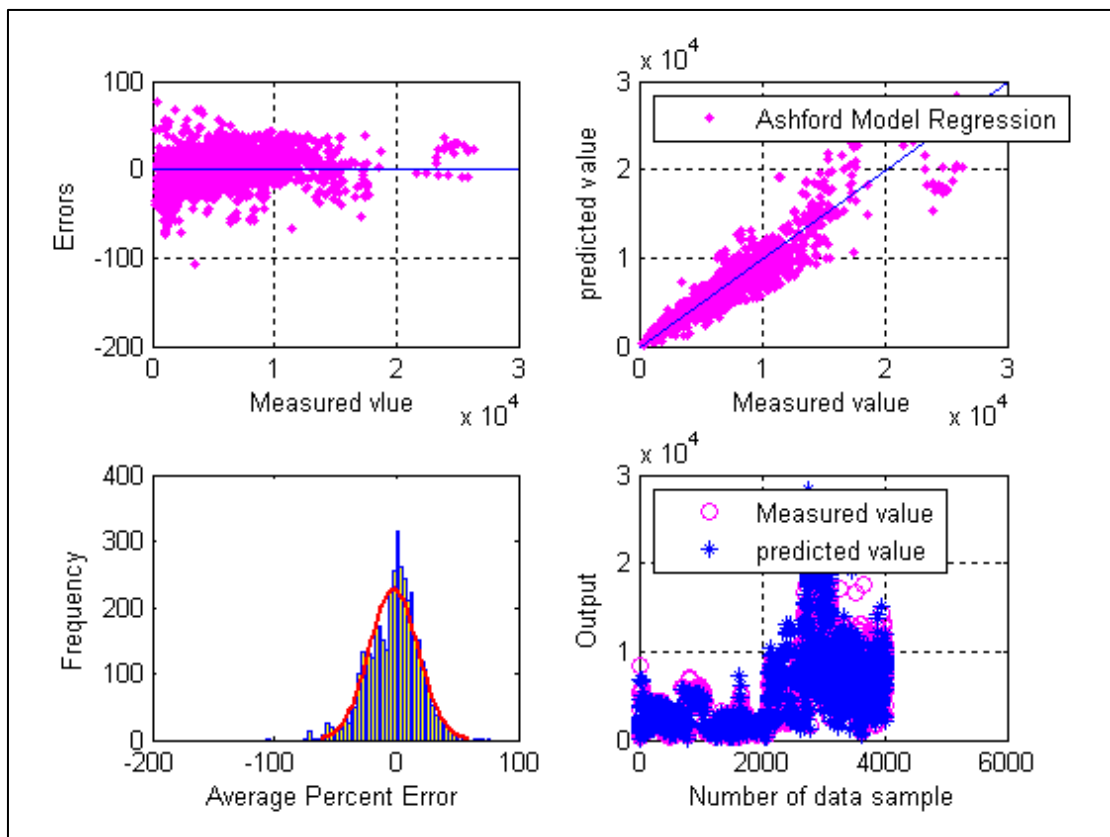


Figure-5.85: Cross, Histogram, Scatter and Overlay plots for Ashford Empirical correlation after regression. (Flow Rate Estimation)

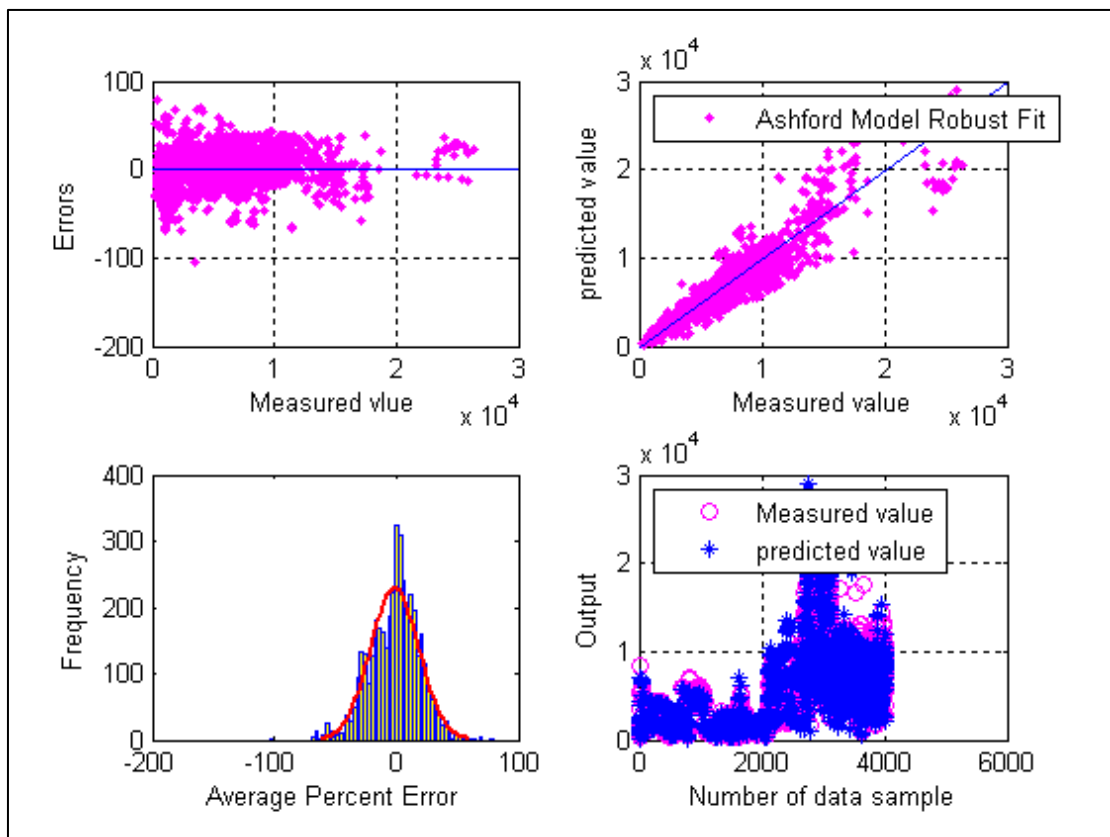


Figure-5.86: Cross, Histogram, Scatter and Overlay plots for Ashford Empirical correlation after robust fit. (Flow Rate Estimation)

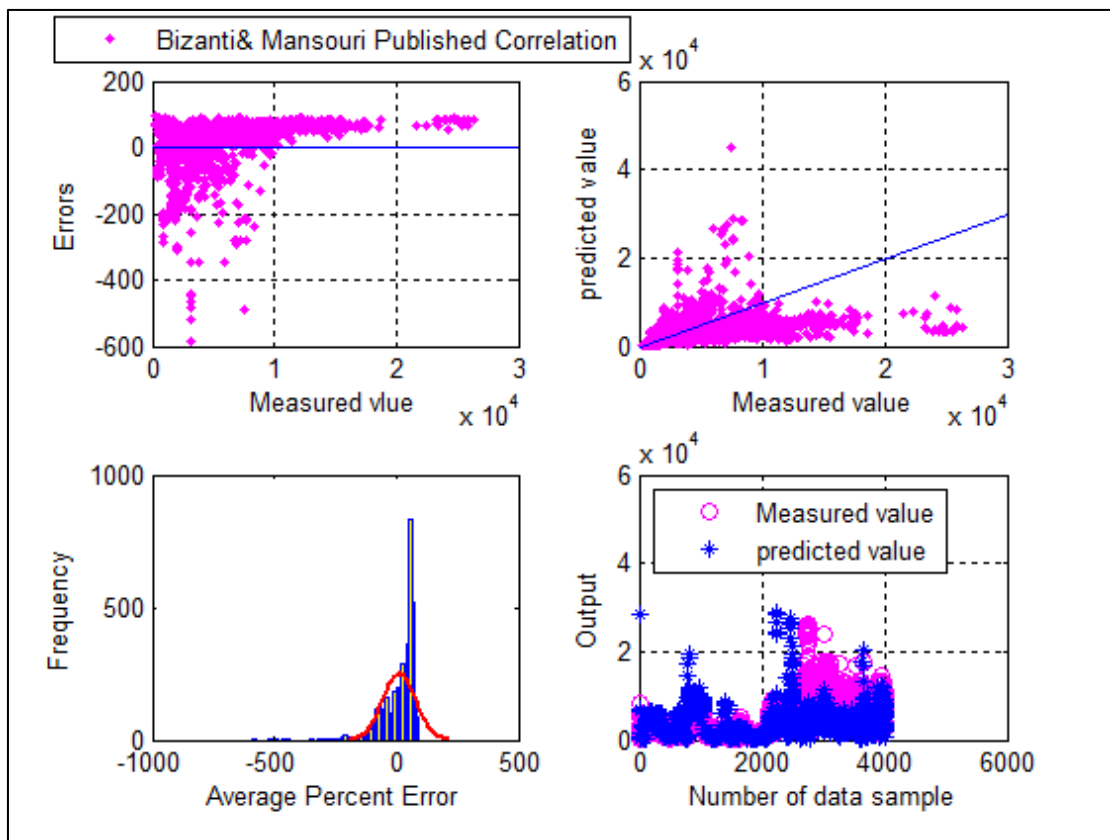


Figure-5.87: Cross, Histogram, Scatter and Overlay plots for Bizanti and Mansouri Empirical correlation. (Flow Rate Estimation)

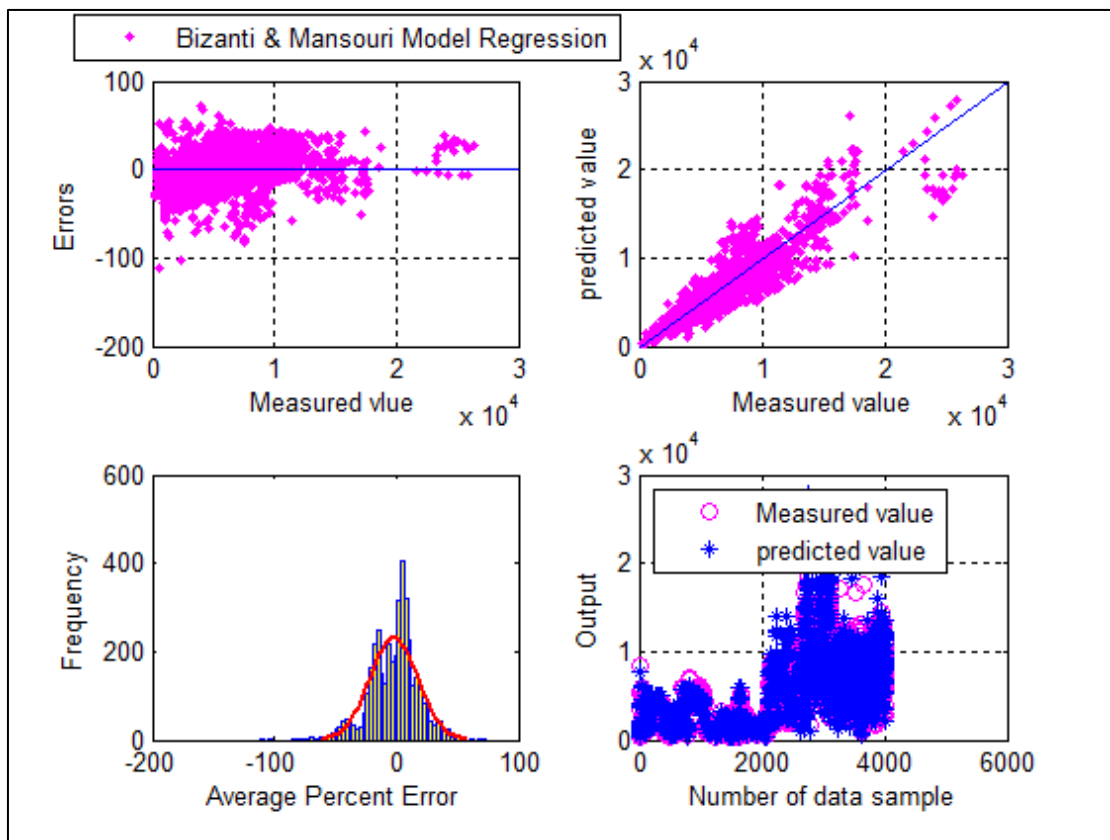


Figure-5.88: Cross, Histogram, Scatter and Overlay plots for Bizanti and Mansouri Empirical correlation after regression. (Flow Rate Estimation)

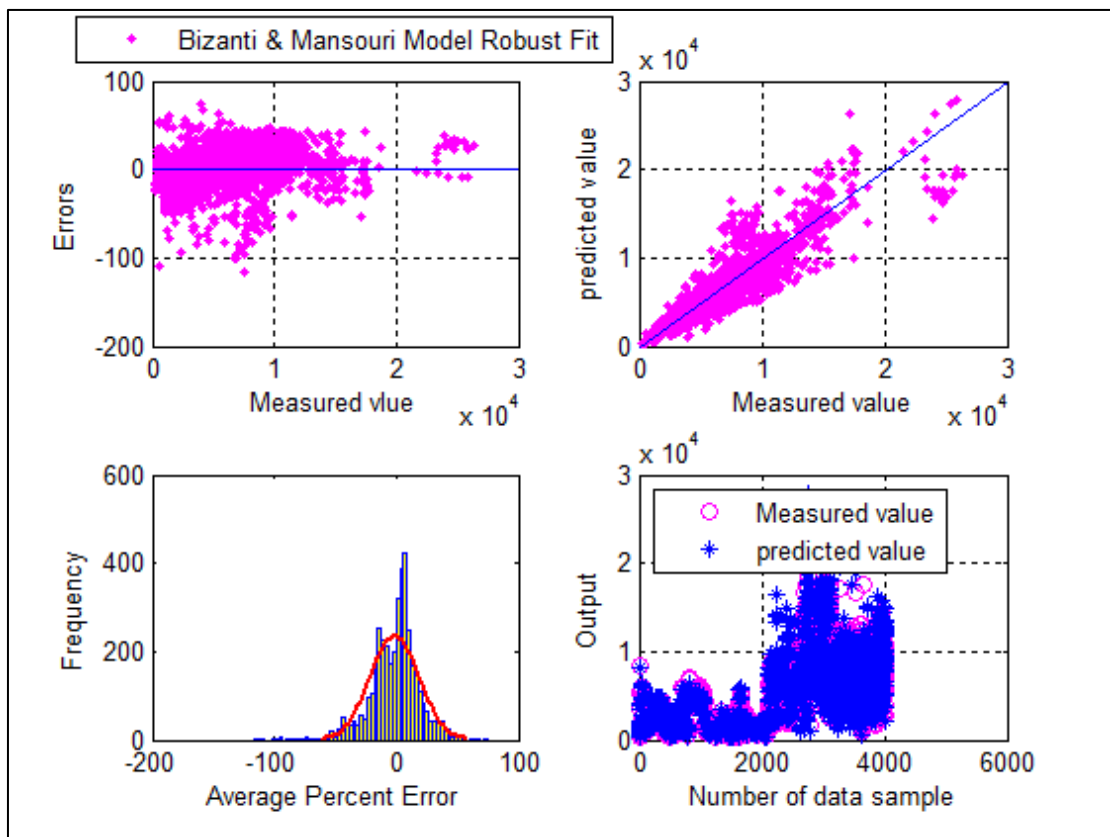


Figure-5.89: Cross, Histogram, Scatter and Overlay plots for Bizanti and Mansouri Empirical correlation after robust fit. (Flow Rate Estimation)

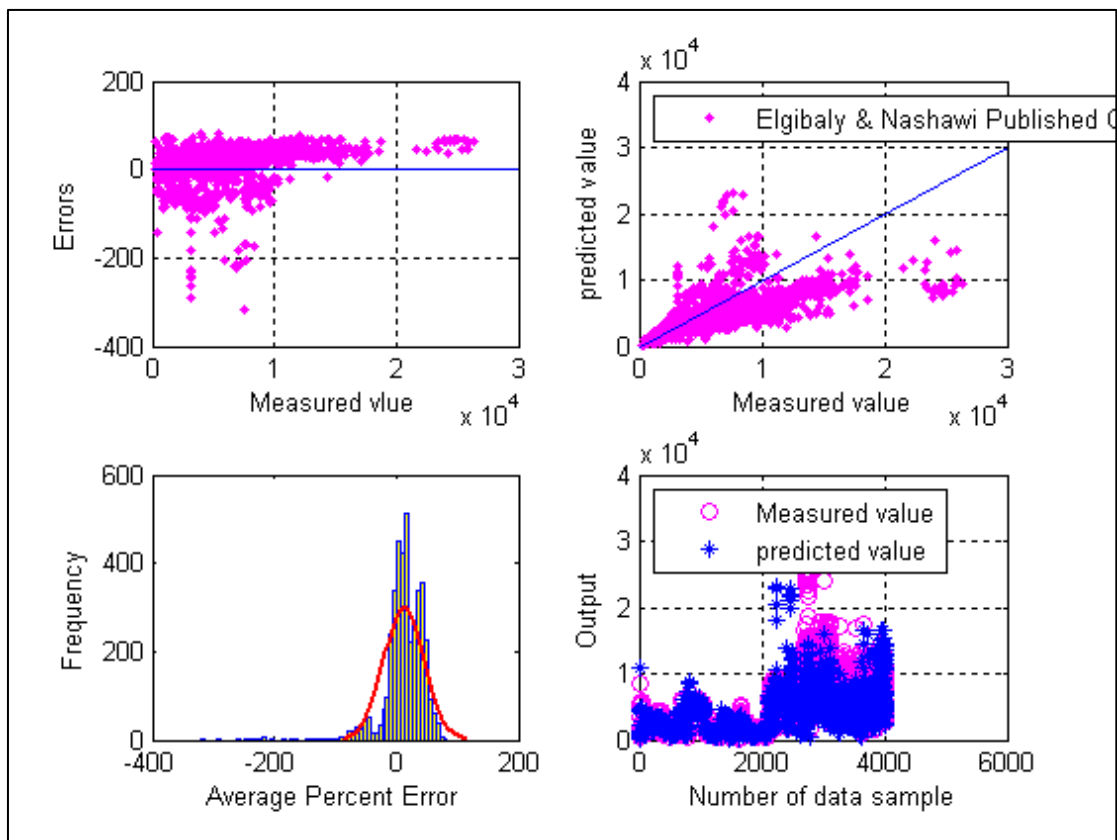


Figure-5.90: Cross, Histogram, Scatter and Overlay plots for Elgibaly and Nashawi Empirical correlation. (Flow Rate Estimation)

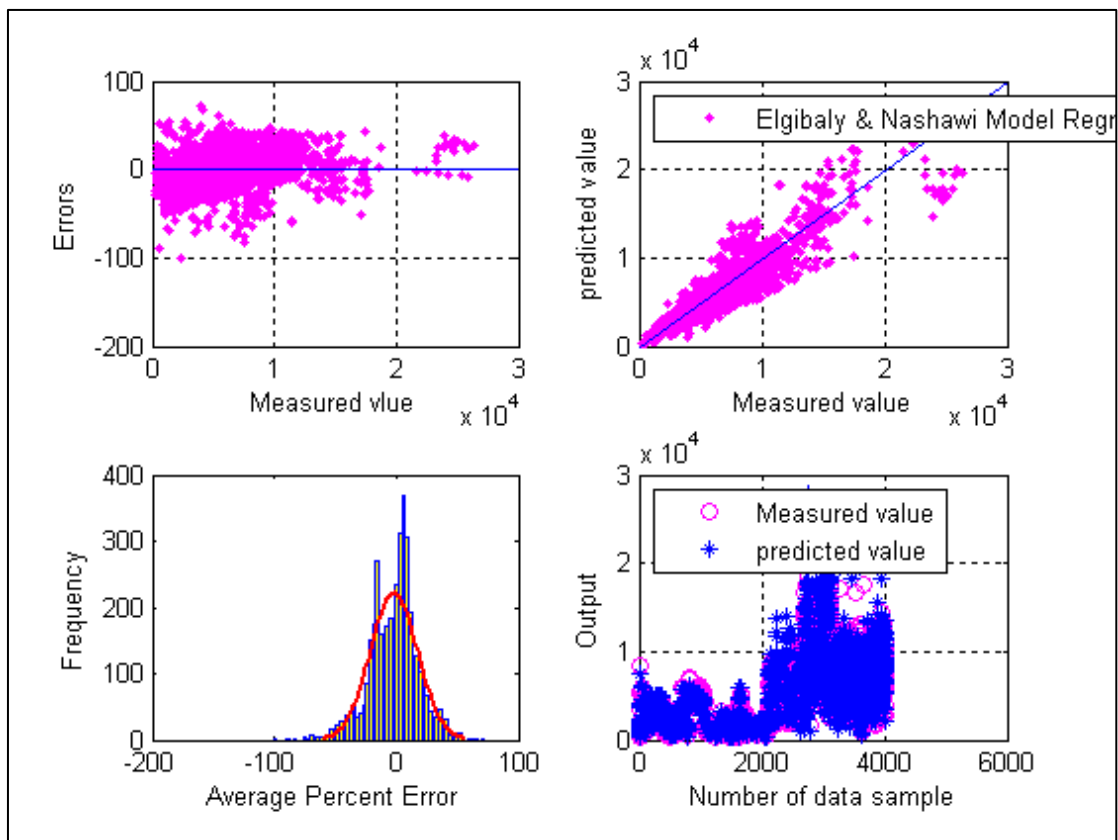


Figure-5.91: Cross, Histogram, Scatter and Overlay plots for Elgibaly and Nashawi Empirical correlation after regression. (Flow Rate Estimation)



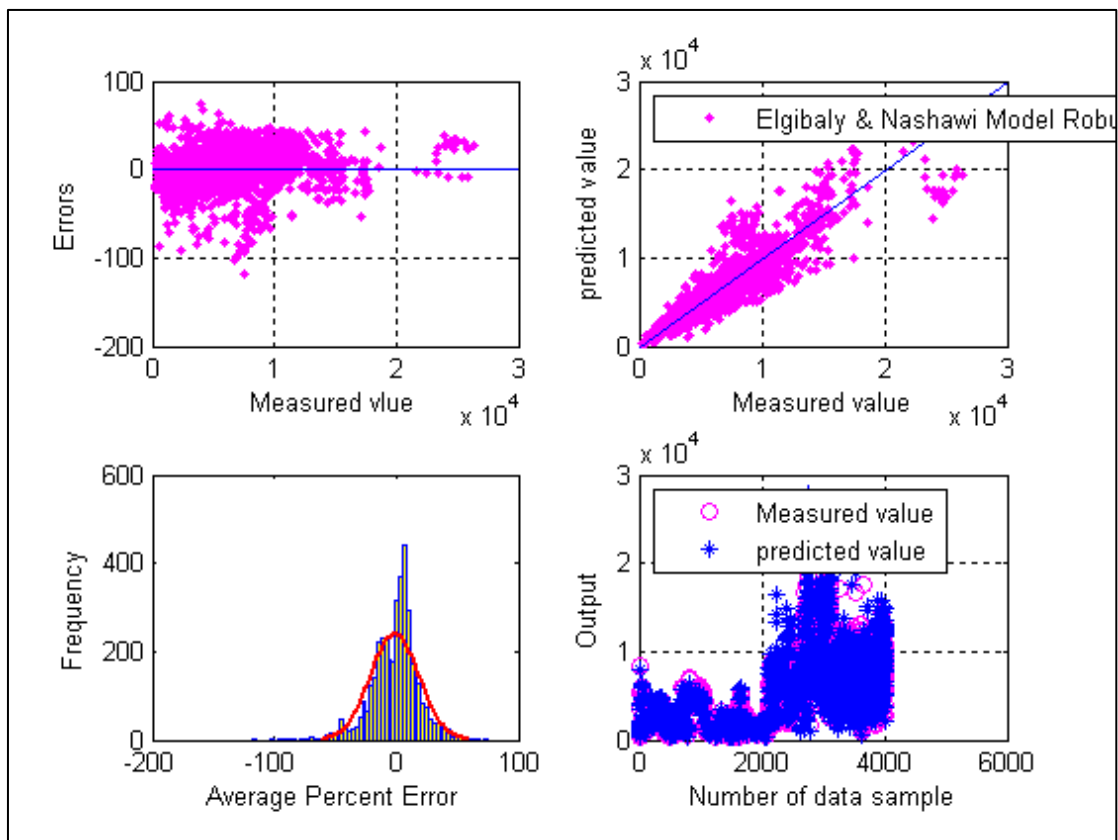


Figure-5.92: Cross, Histogram, Scatter and Overlay plots for Elgibaly and Nashawi Empirical correlation after robust fit. (Flow Rate Estimation)

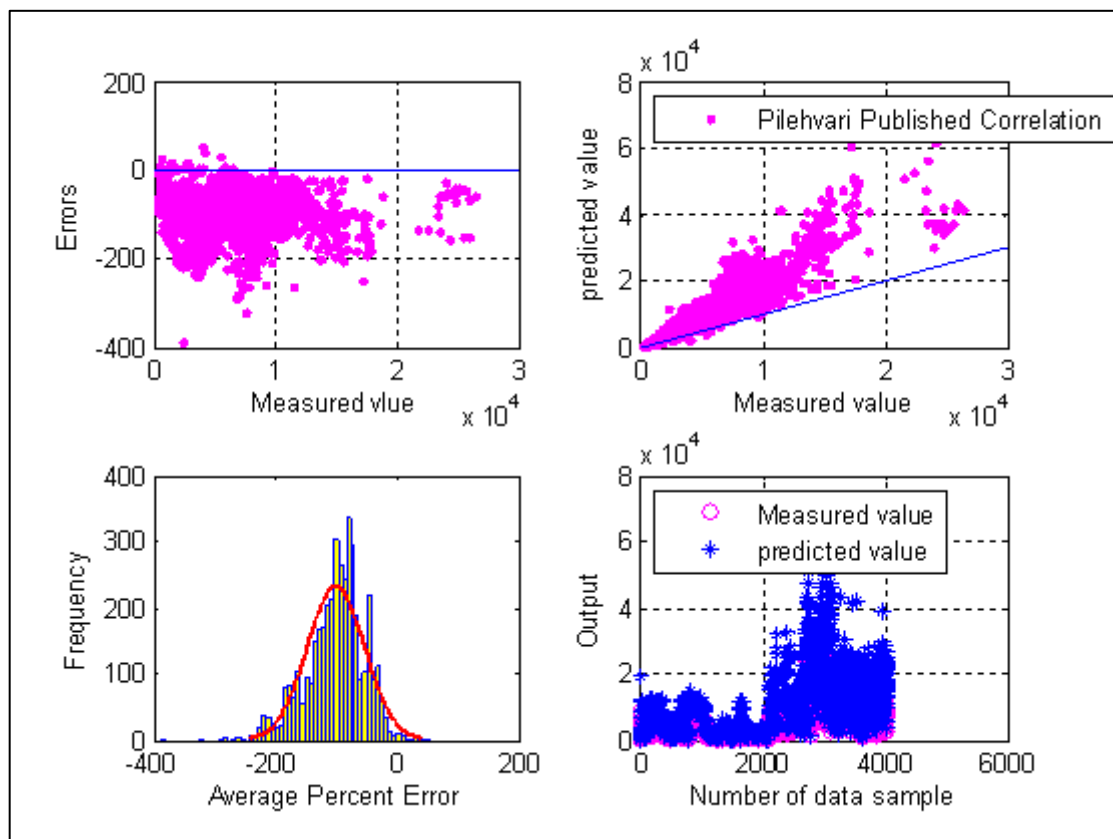


Figure-5.93: Cross, Histogram, Scatter and Overlay plots for Pilehvari Empirical correlation. (Flow Rate Estimation)

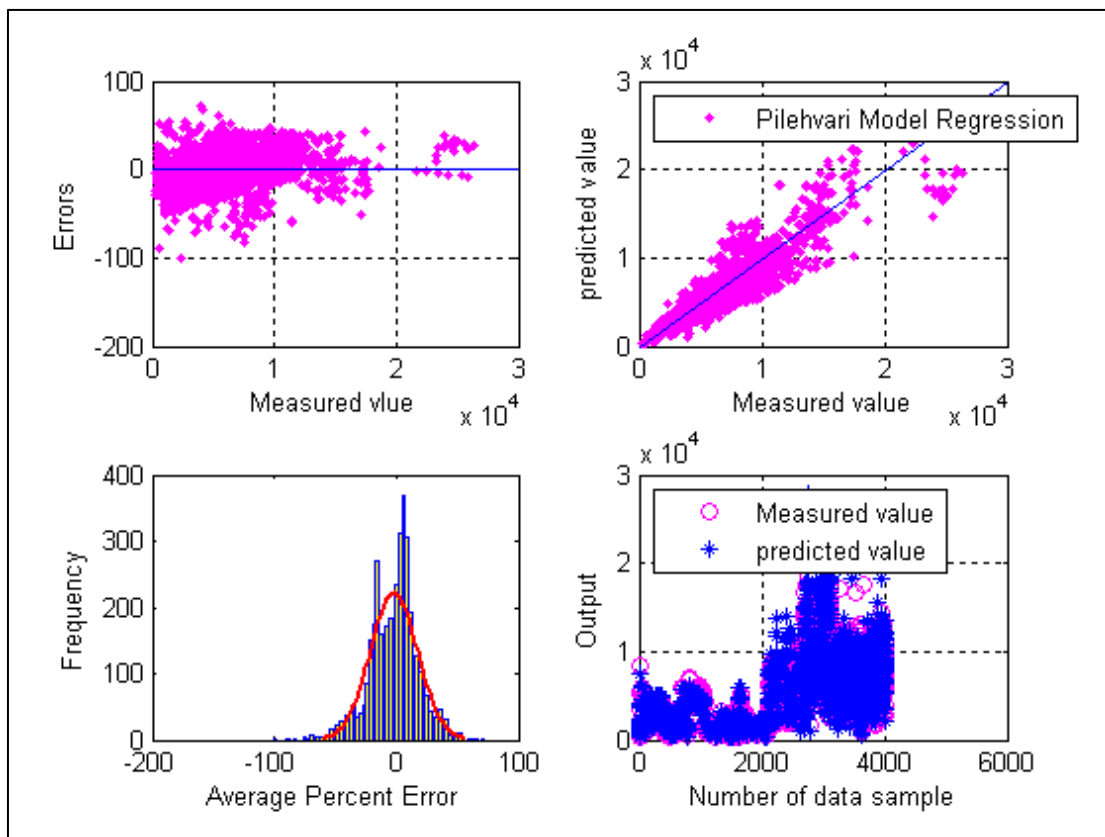


Figure-5.94: Cross, Histogram, Scatter and Overlay plots for Pilehvari Empirical correlation after regression (Flow Rate Estimation)

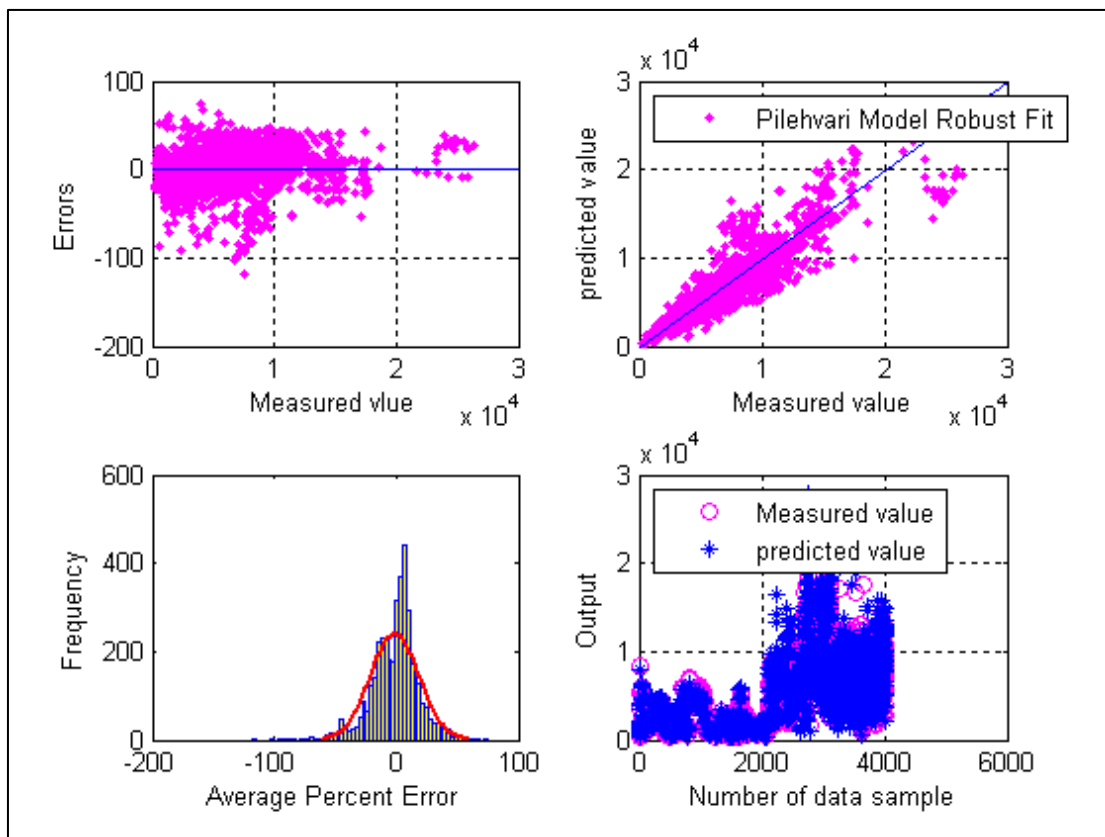


Figure-5.95: Cross, Histogram, Scatter and Overlay plots for Pilehvari Empirical correlation after robust fit. (Flow Rate Estimation)

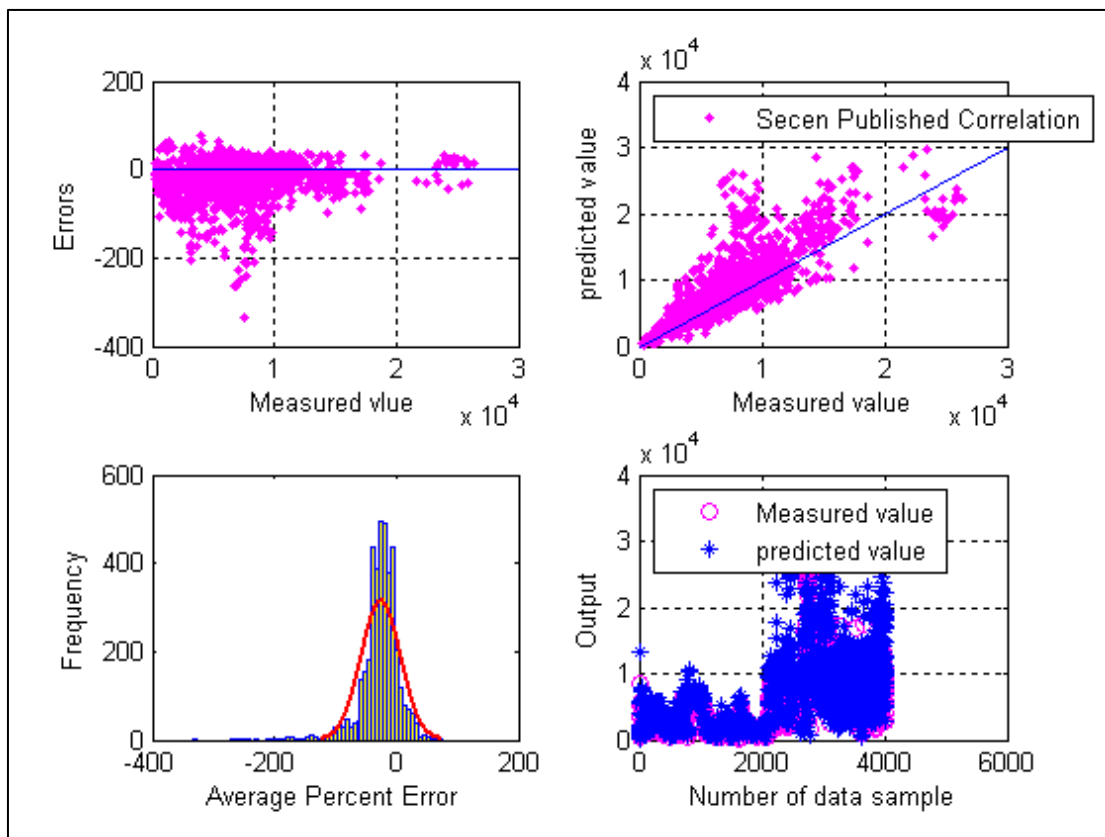


Figure-5.96: Cross, Histogram, Scatter and Overlay plots for Secen Empirical correlation. (Flow Rate Estimation)

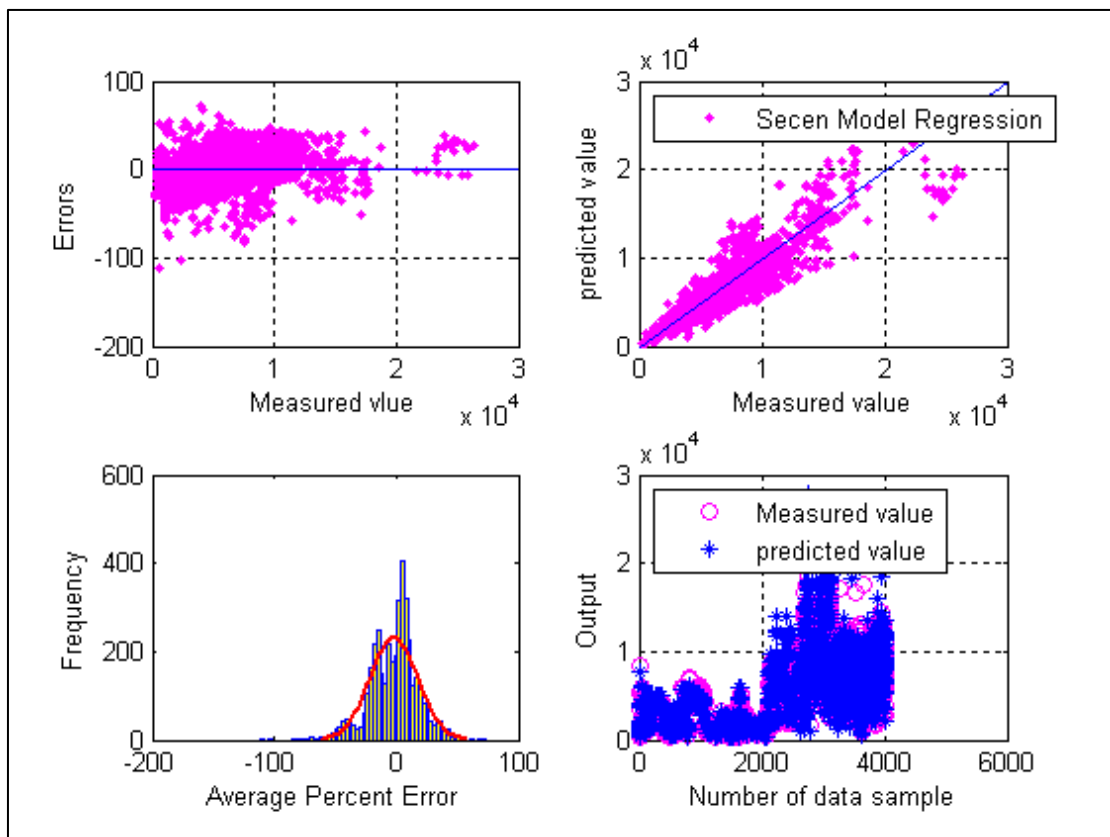


Figure-5.97: Cross, Histogram, Scatter and Overlay plots for Secen Empirical correlation after regression. (Flow Rate Estimation)

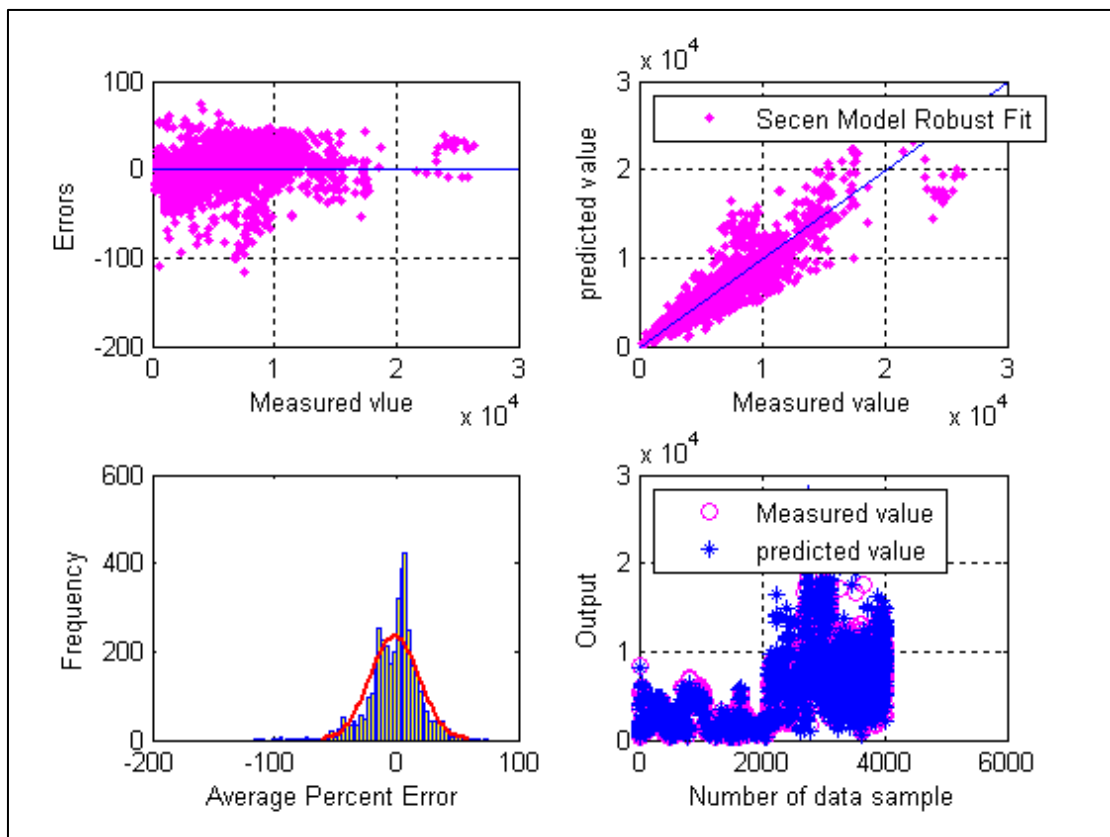


Figure-5.98: Cross, Histogram, Scatter and Overlay plots for Secen Empirical correlation after robust fit. (Flow Rate Estimation)

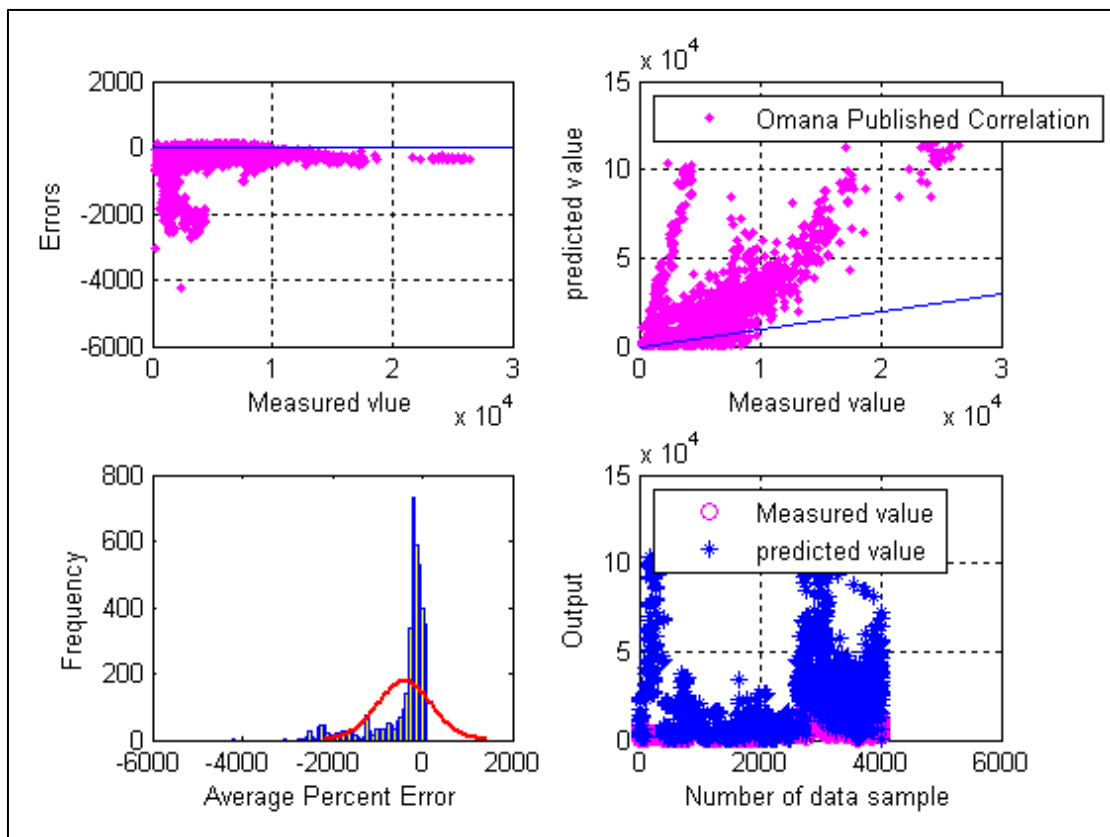


Figure-5.99: Cross, Histogram, Scatter and Overlay plots for Omana Empirical correlation. (Flow Rate Estimation)



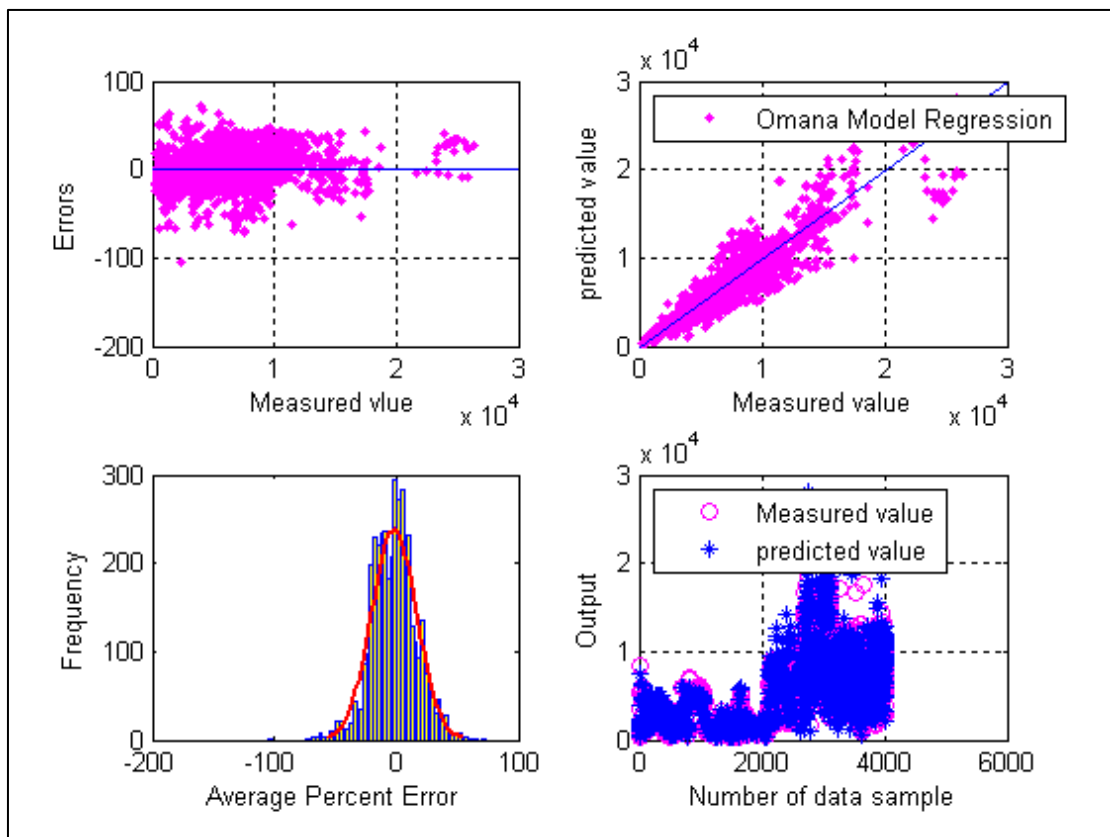


Figure-5.100: Cross, Histogram, Scatter and Overlay plots for Omana Empirical correlation after regression. (Flow Rate Estimation)

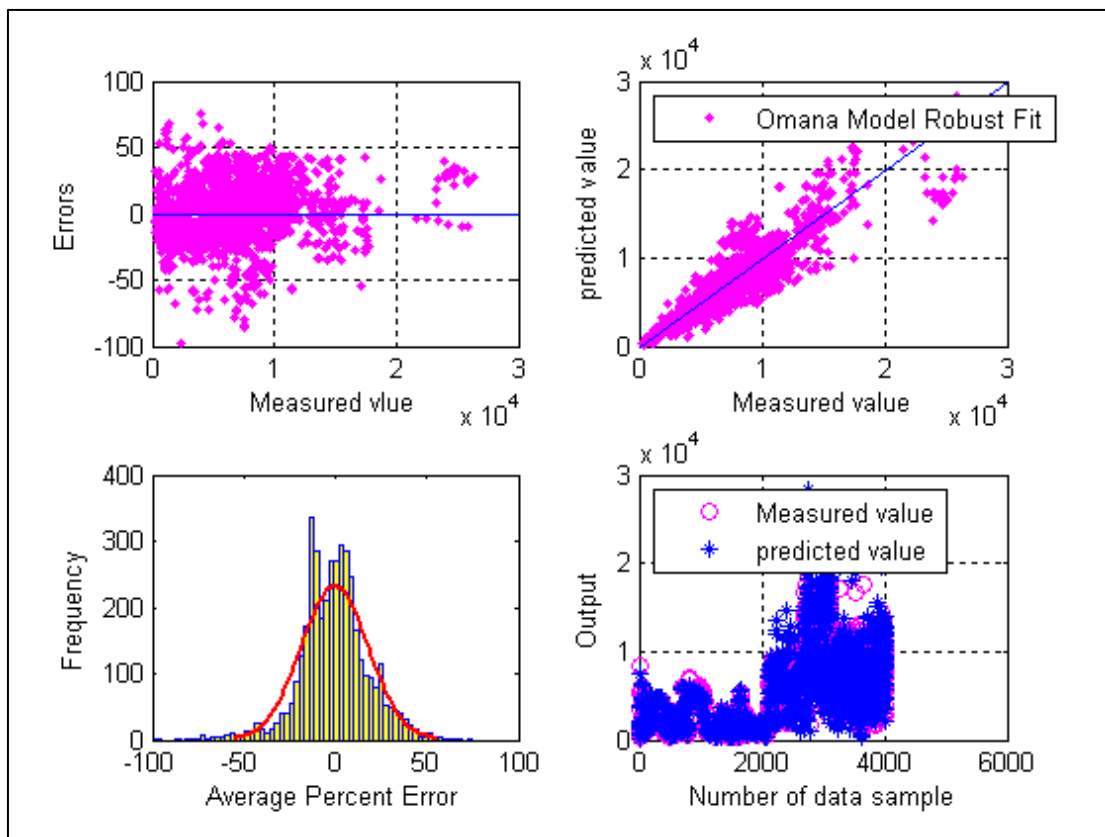


Figure-5.101: Cross, Histogram, Scatter and Overlay plots for Omana Empirical correlation after robust fit. (Flow Rate Estimation)

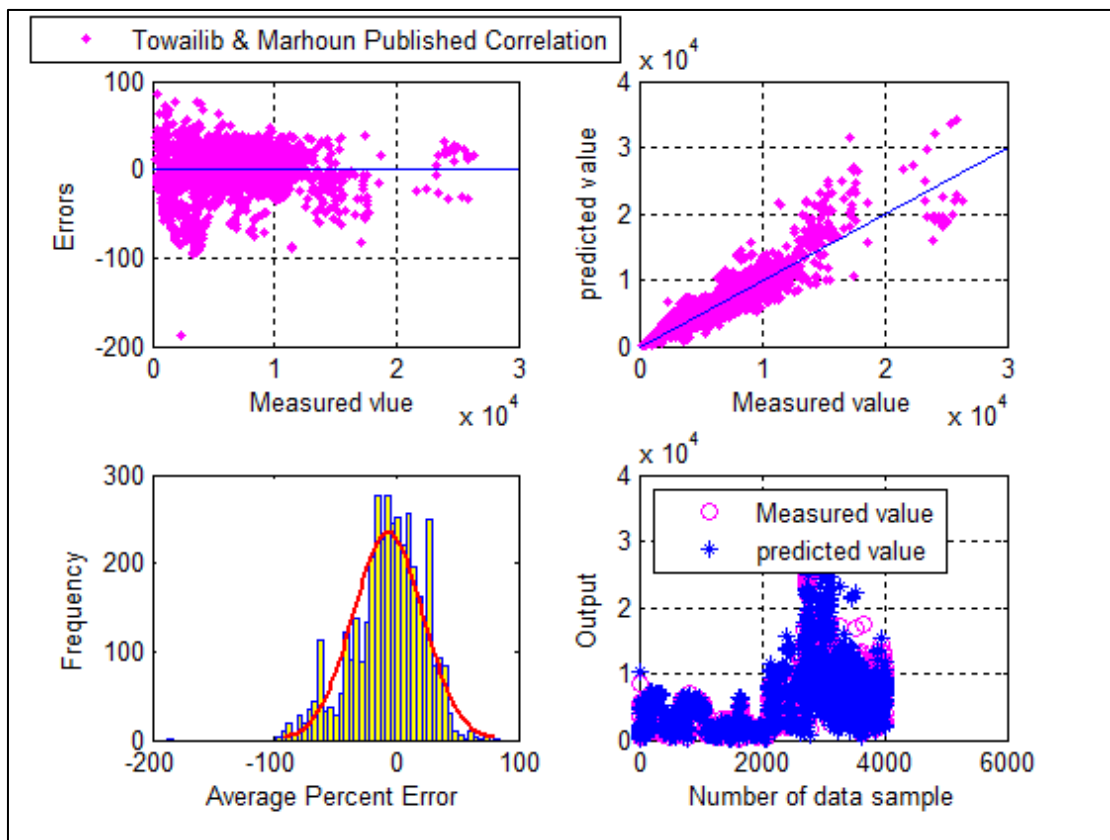


Figure-5.102: Cross, Histogram, Scatter and Overlay plots for Towailib and Marhoun Empirical correlation. (Flow Rate Estimation)

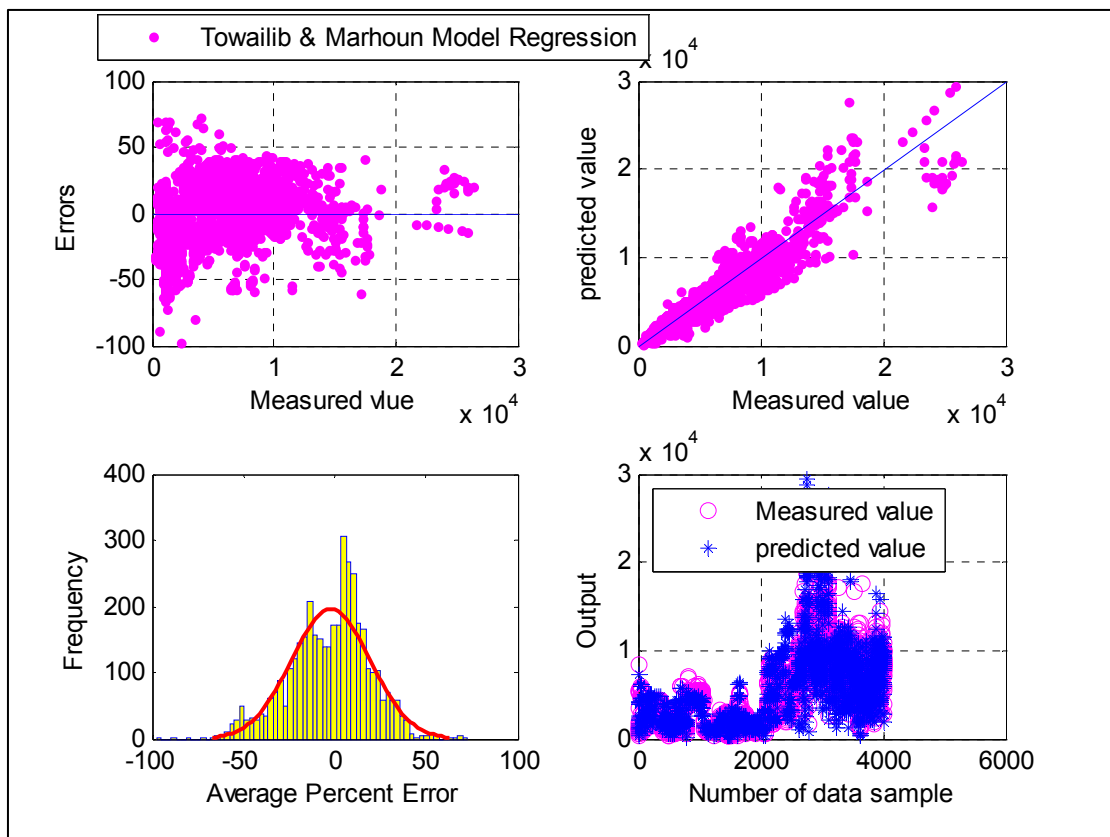


Figure-5.103: Cross, Histogram, Scatter and Overlay plots for Towailib and Marhoun Empirical correlation after regression. (Flow Rate Estimation)

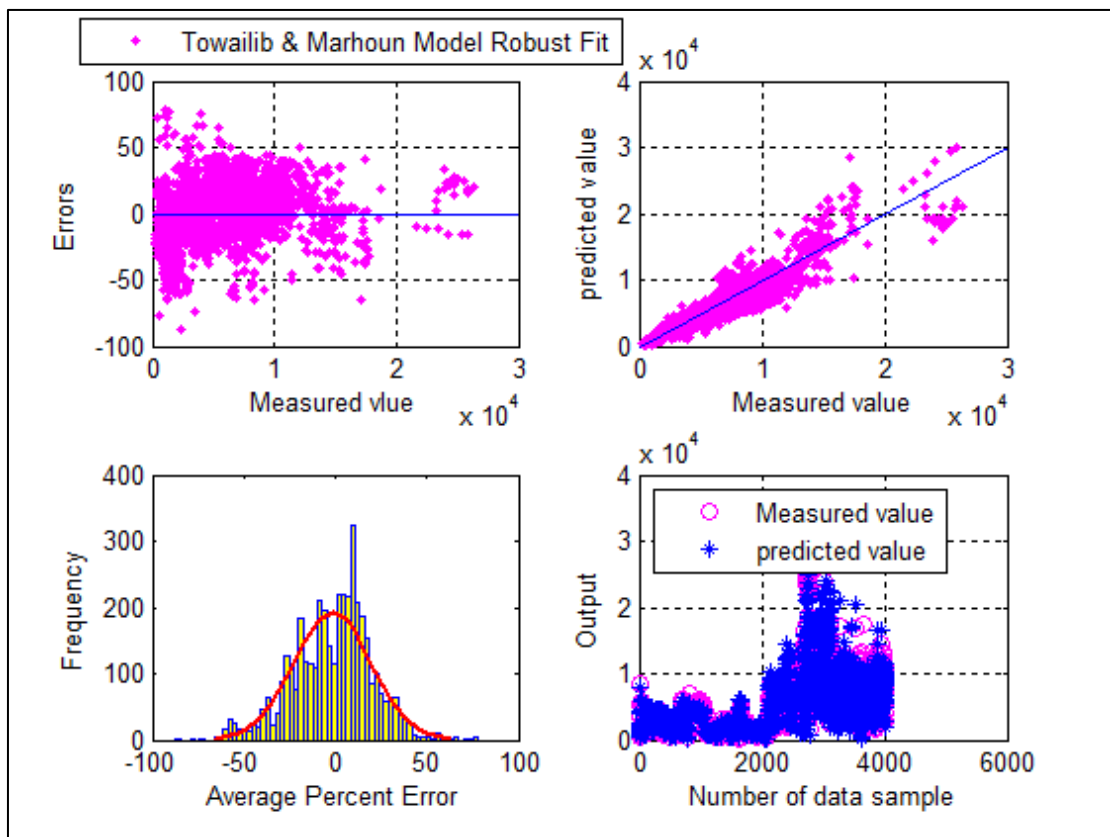


Figure-5.104: Cross, Histogram, Scatter and Overlay plots for Towailib and Marhoun Empirical correlation after robust fit. (Flow Rate Estimation)

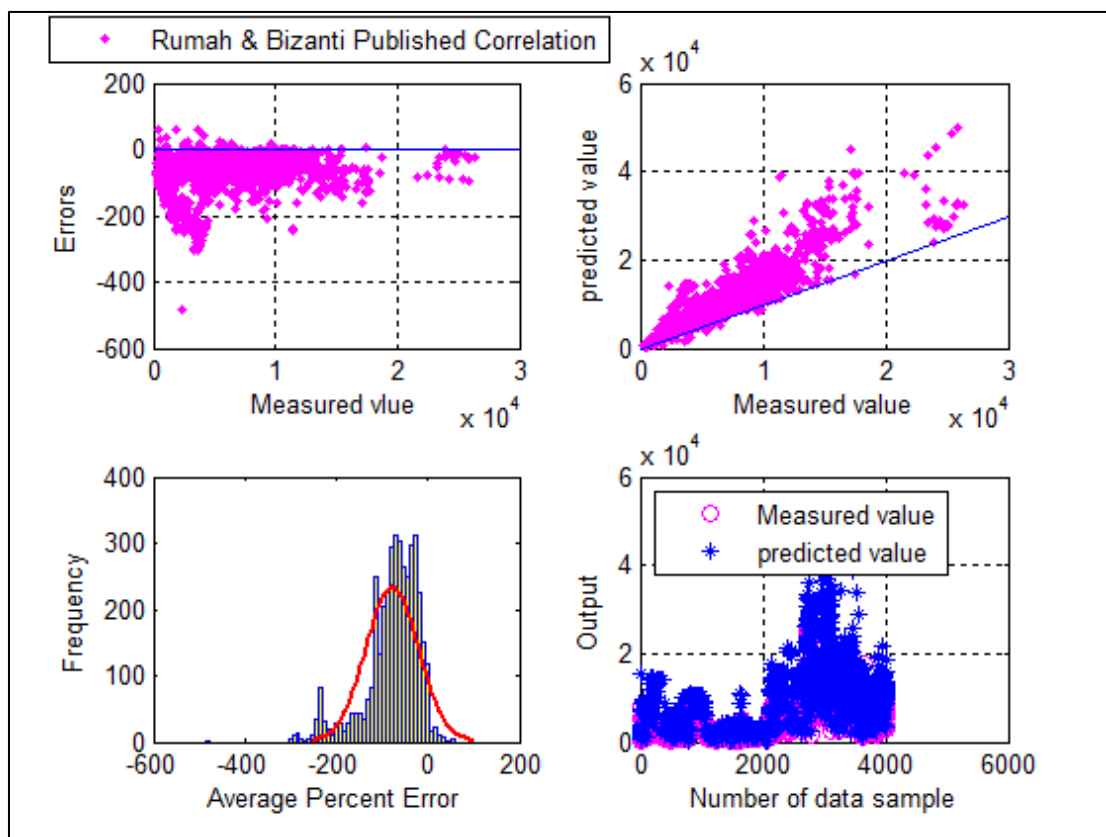


Figure-5.105: Cross, Histogram, Scatter and Overlay plots for Rumah and Bizanti Empirical correlation. (Flow Rate Estimation)

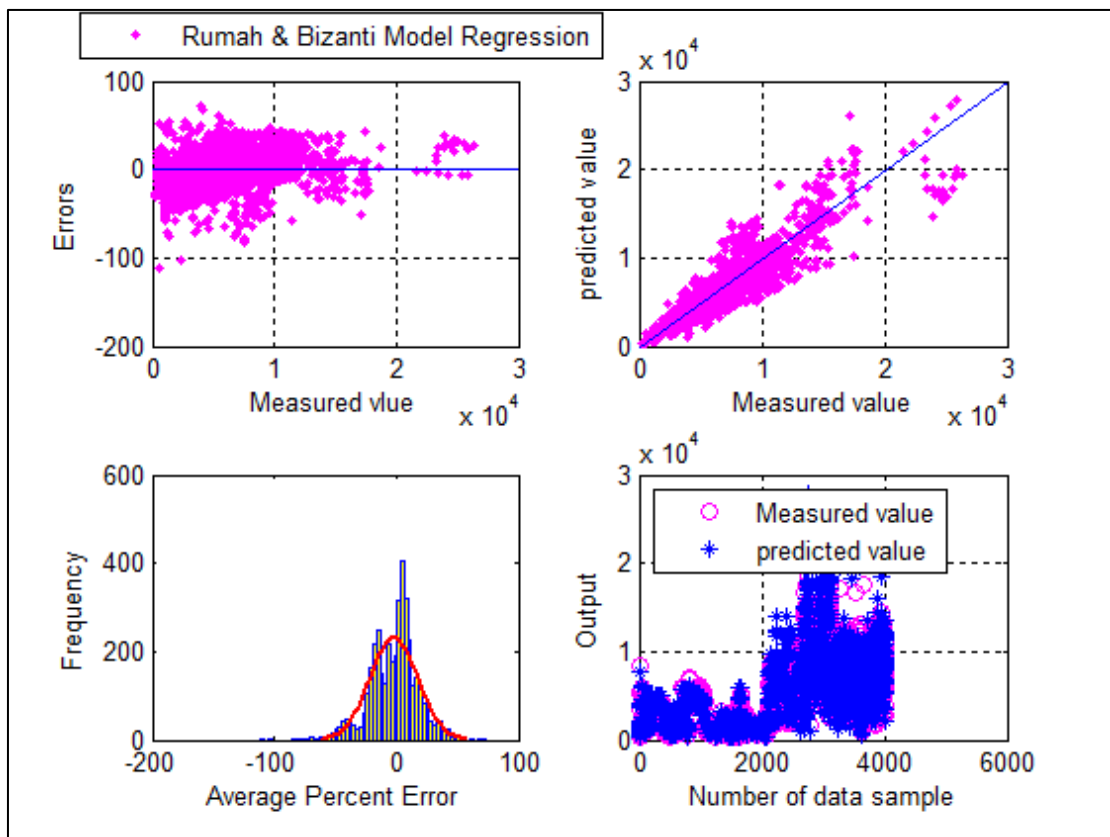


Figure-5.106: Cross, Histogram, Scatter and Overlay plots for Rumah and Bizanti Empirical correlation after regression. (Flow Rate Estimation)

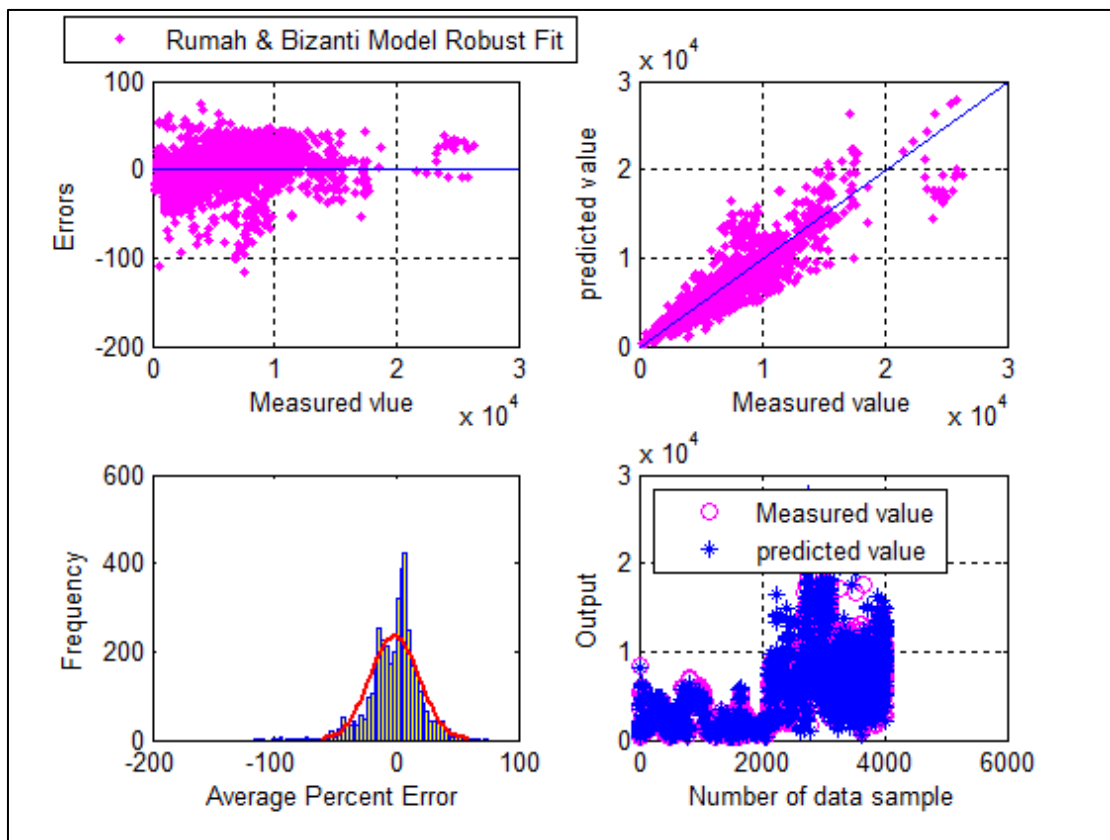


Figure-5.107: Cross, Histogram, Scatter and Overlay plots for Rumah and Bizanti Empirical correlation after robust fit. (Flow Rate Estimation)



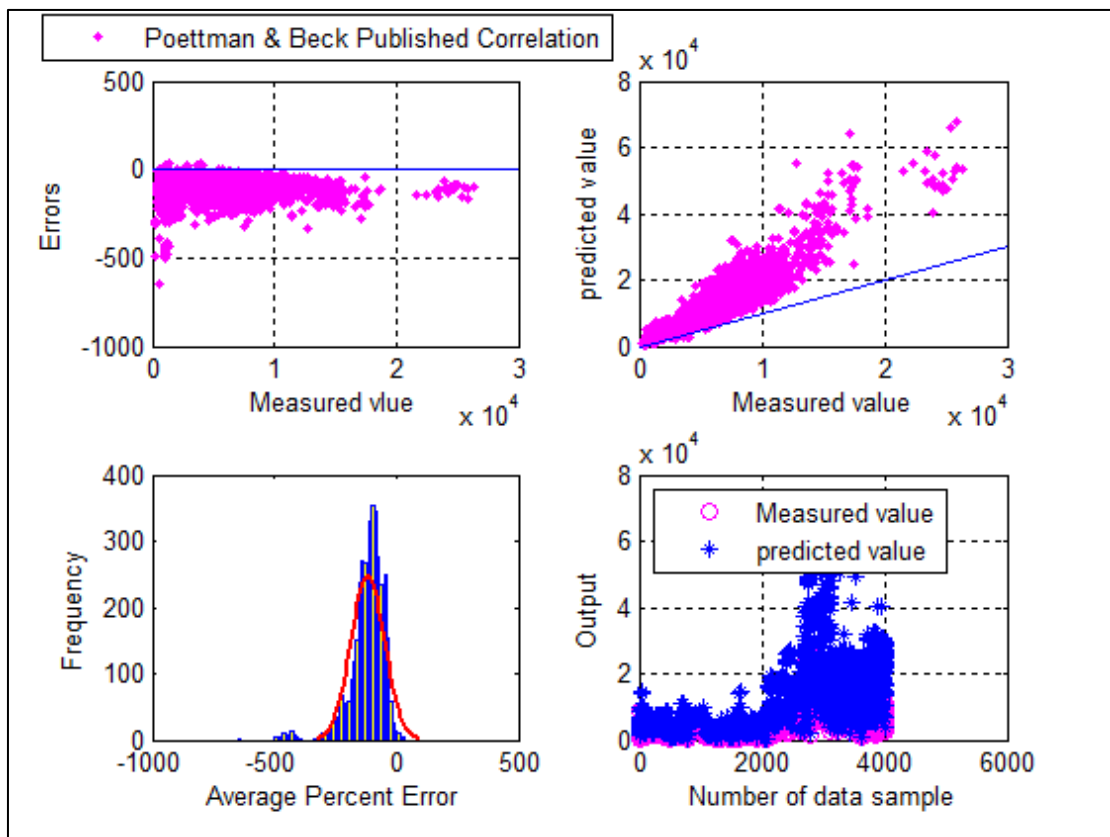


Figure-5.108: Cross, Histogram, Scatter and Overlay plots for Poettman and Beck Empirical correlation. (Flow Rate Estimation)

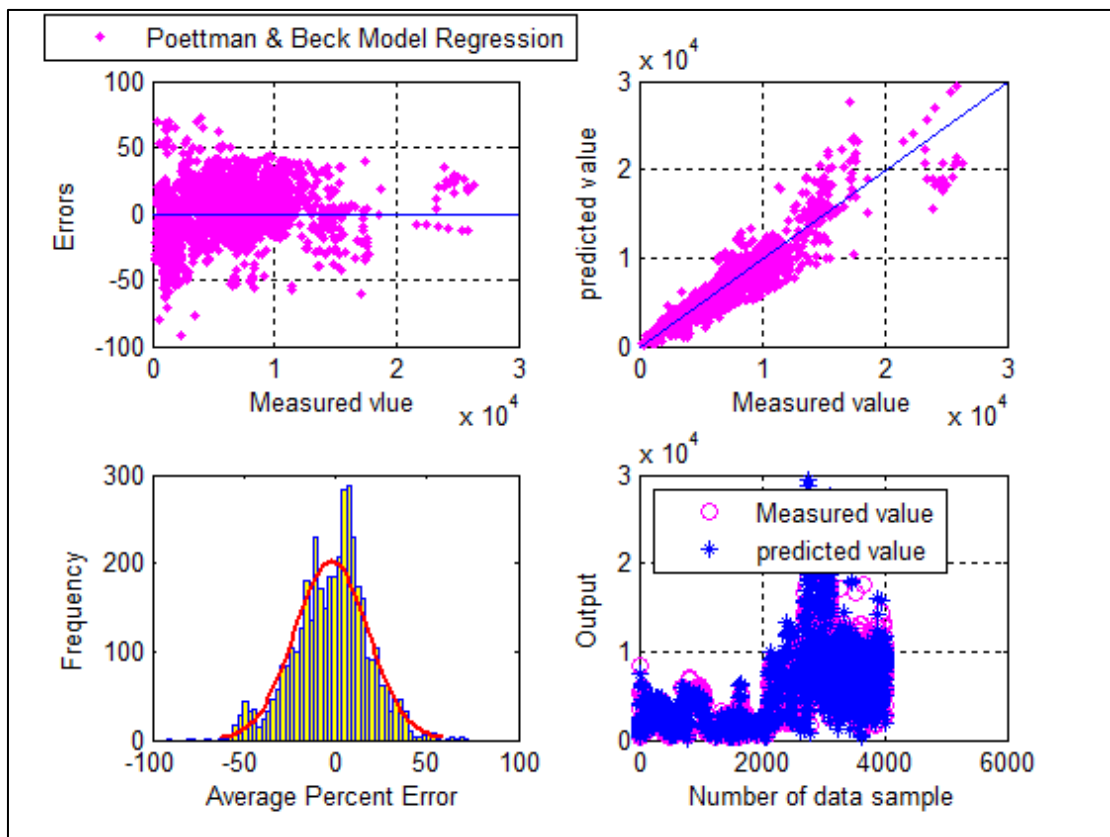


Figure-5.109: Cross, Histogram, Scatter and Overlay plots for Poettman and Beck Empirical correlation after regression. (Flow Rate Estimation)

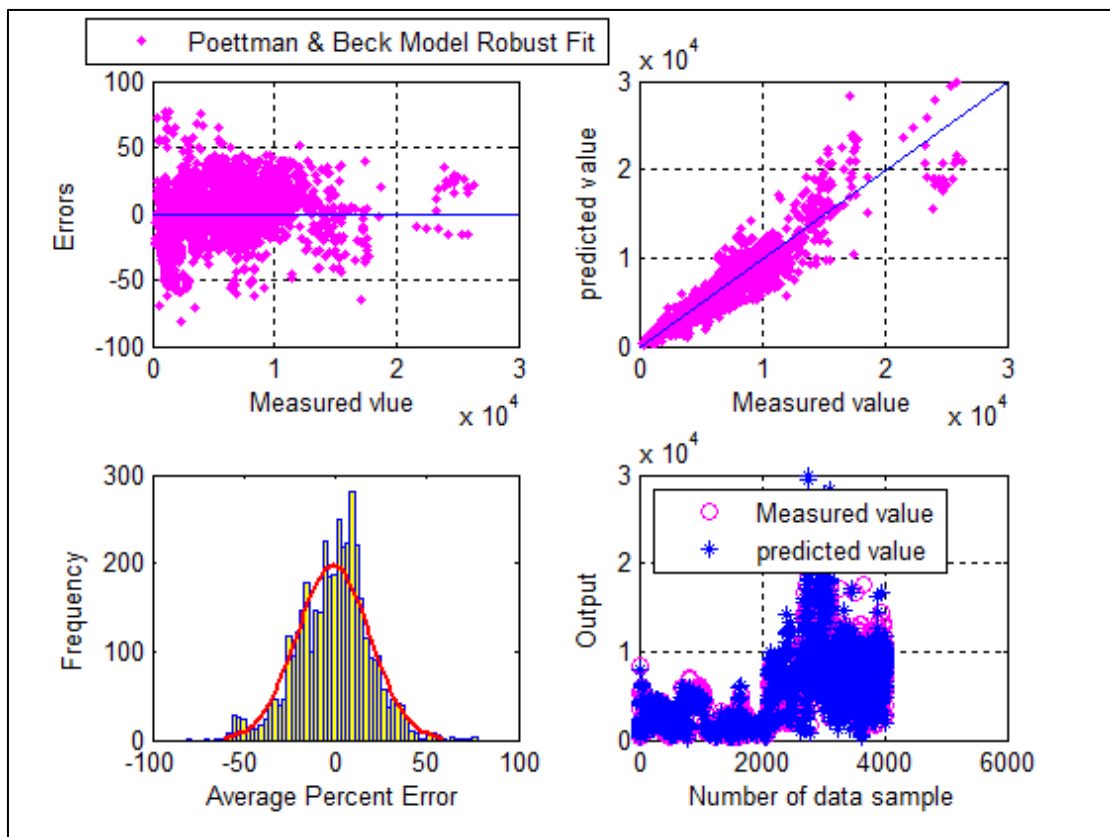


Figure-5.110: Cross, Histogram, Scatter and Overlay plots for Poettman and Beck Empirical correlation after robust fit. (Flow Rate Estimation)

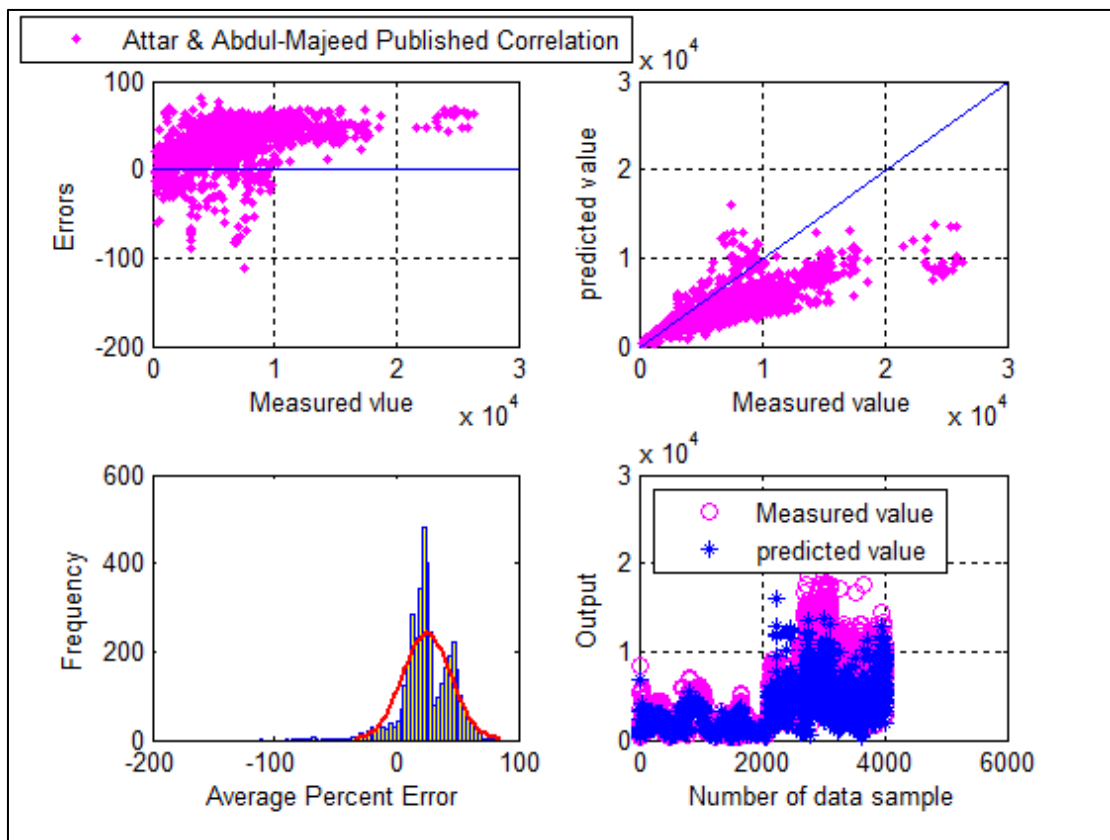


Figure-5.111: Cross, Histogram, Scatter and Overlay plots for Attar and Abdul-Majeed Empirical correlation. (Flow Rate Estimation)

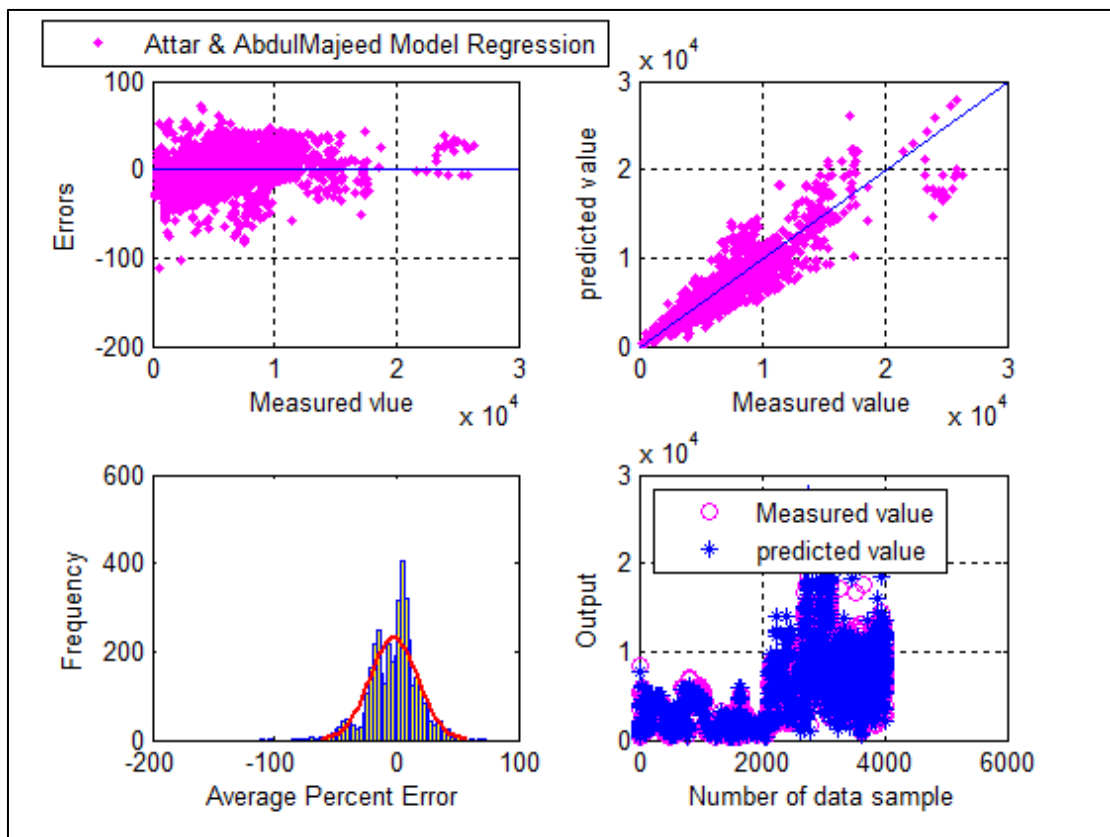


Figure-5.112: Cross, Histogram, Scatter and Overlay plots for Attar and Abdul-Majeed Empirical correlation after regression. (Flow Rate Estimation)

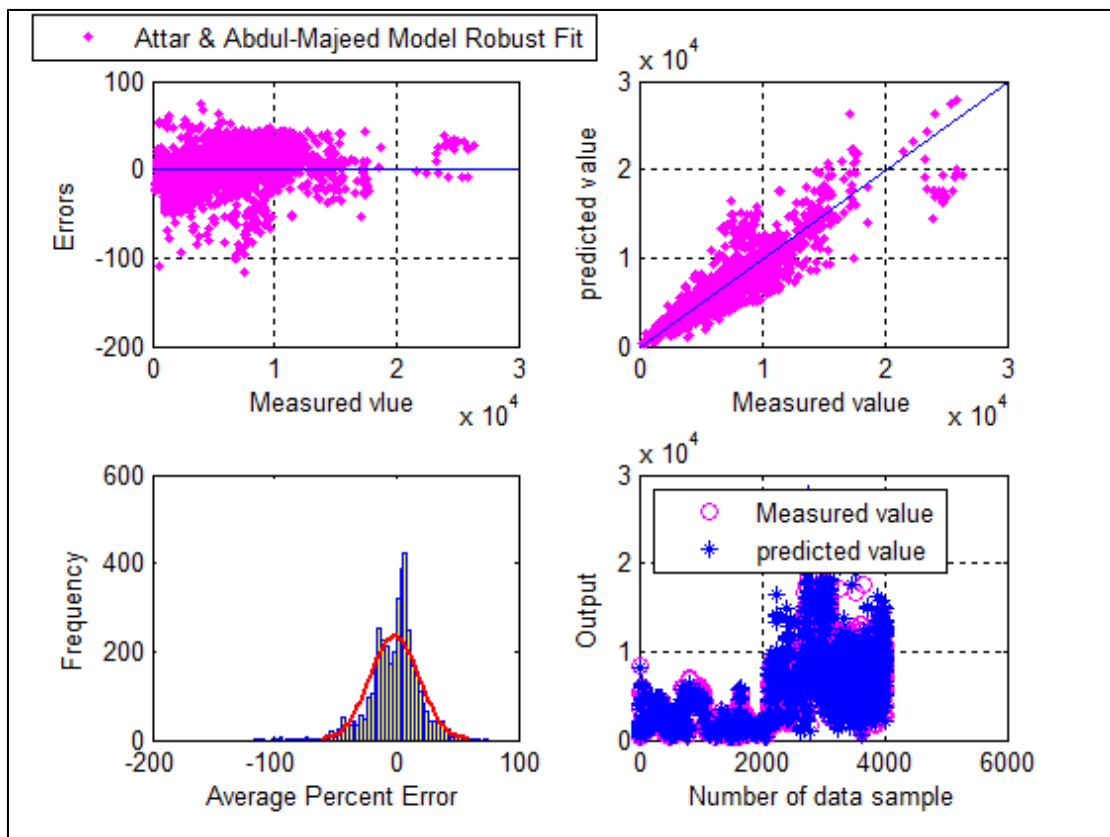


Figure-5.113: Cross, Histogram, Scatter and Overlay plots for Attar and Abdul-Majeed Empirical correlation after robust fit. (Flow Rate Estimation)

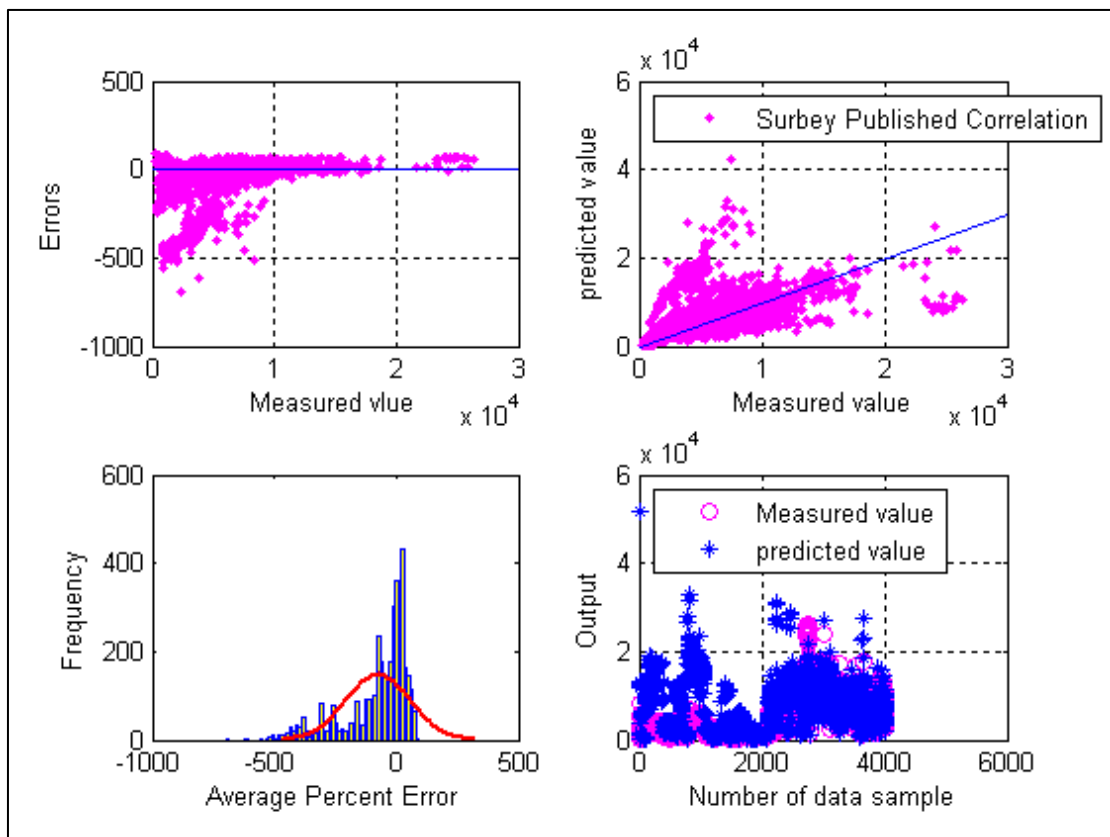


Figure-5.114: Cross, Histogram, Scatter and Overlay plots for Surbey Empirical correlation. (Flow Rate Estimation)

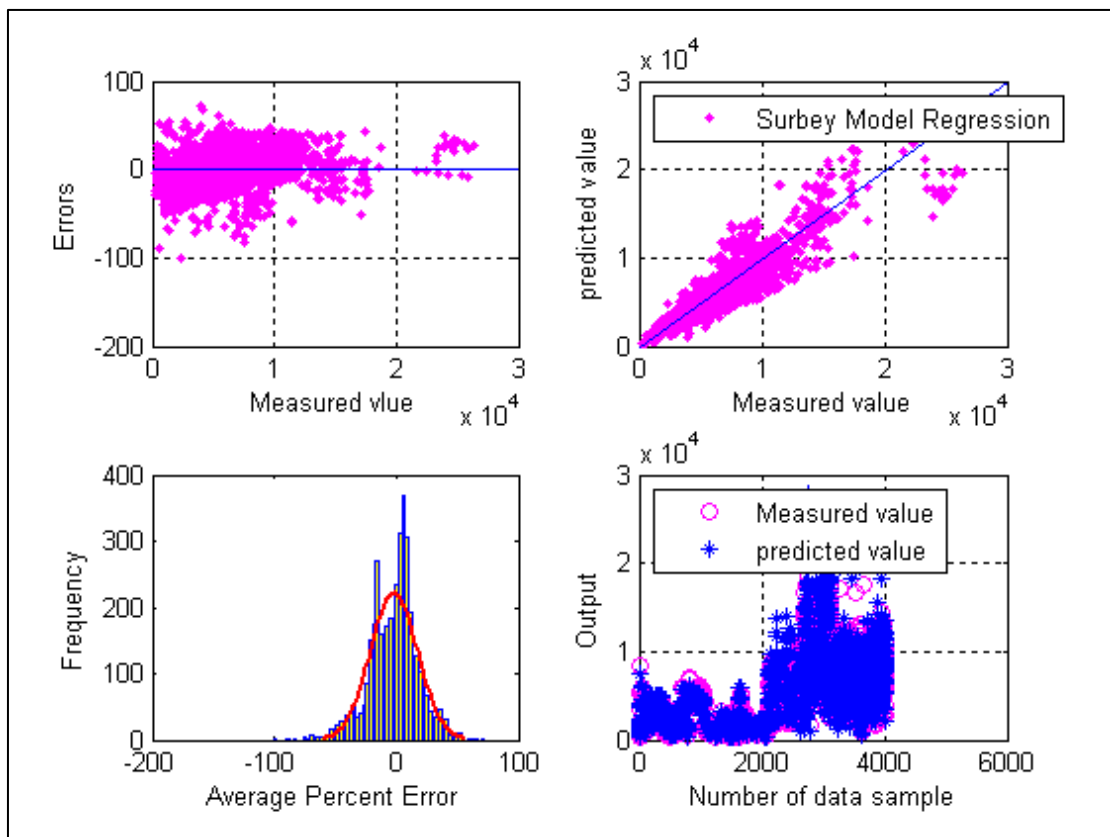


Figure-5.115: Cross, Histogram, Scatter and Overlay plots for Surbey Empirical correlation after regression. (Flow Rate Estimation)



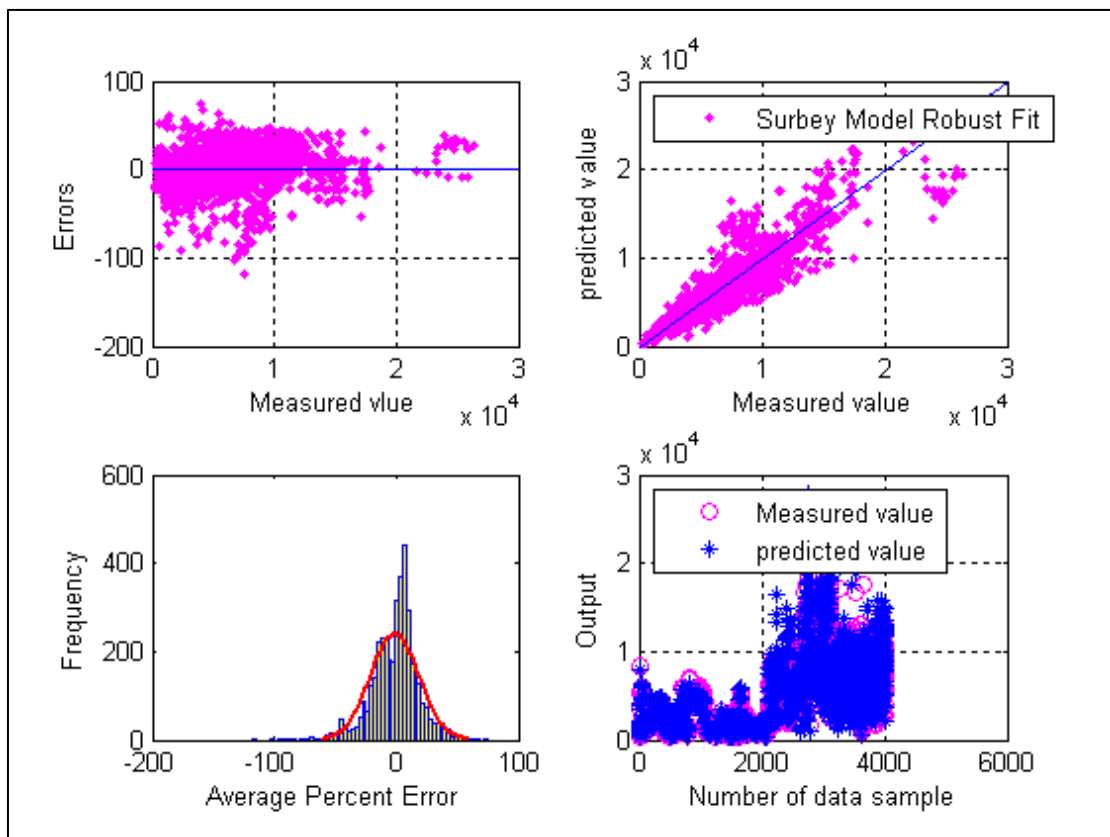


Figure-5.116: Cross, Histogram, Scatter and Overlay plots for Surbey Empirical correlation after robust fit. (Flow Rate Estimation)

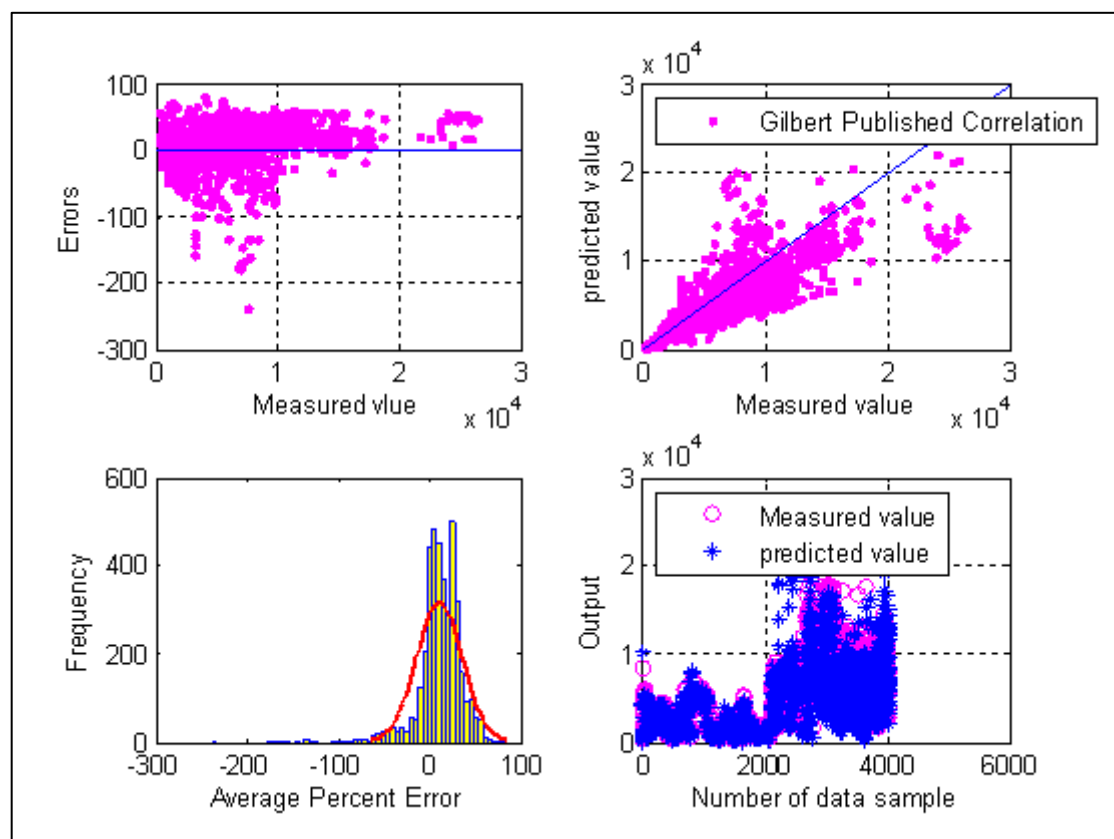


Figure-5.117: Cross, Histogram, Scatter and Overlay plots for Gilbert Empirical correlation. (Flow Rate Estimation)

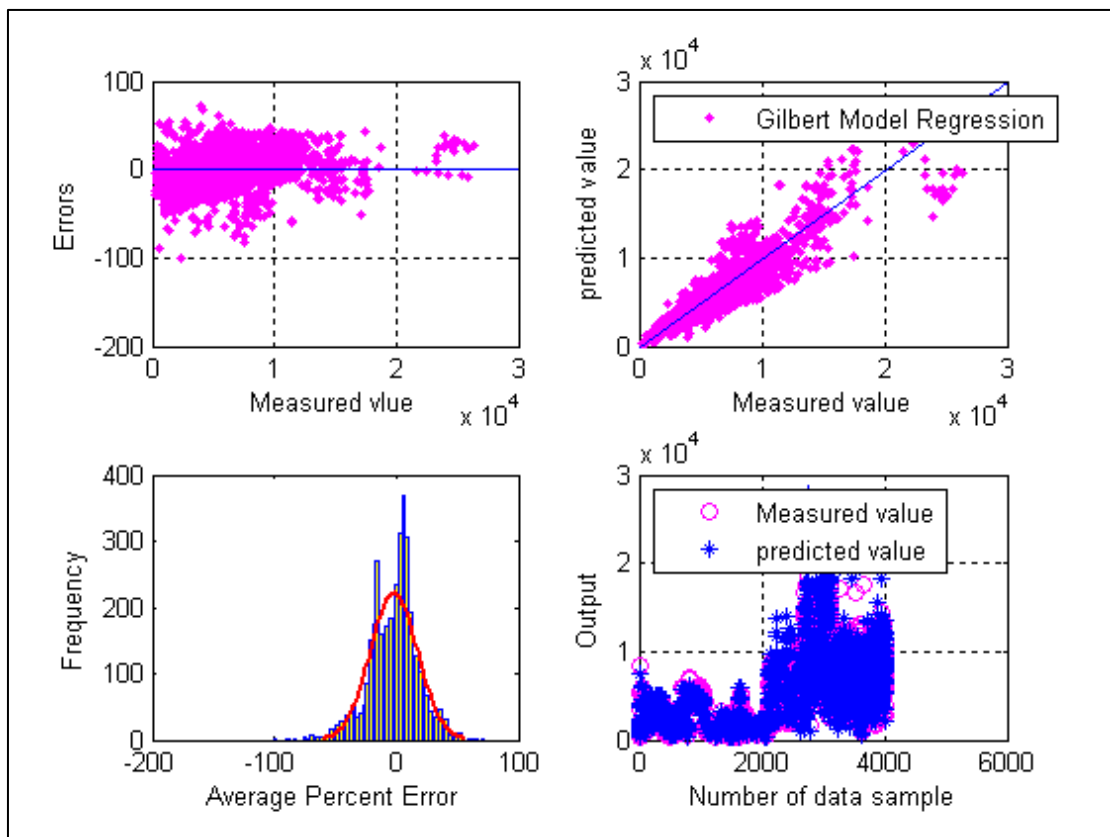


Figure-5.118: Cross, Histogram, Scatter and Overlay plots for Gilbert Empirical correlation after regression. (Flow Rate Estimation)

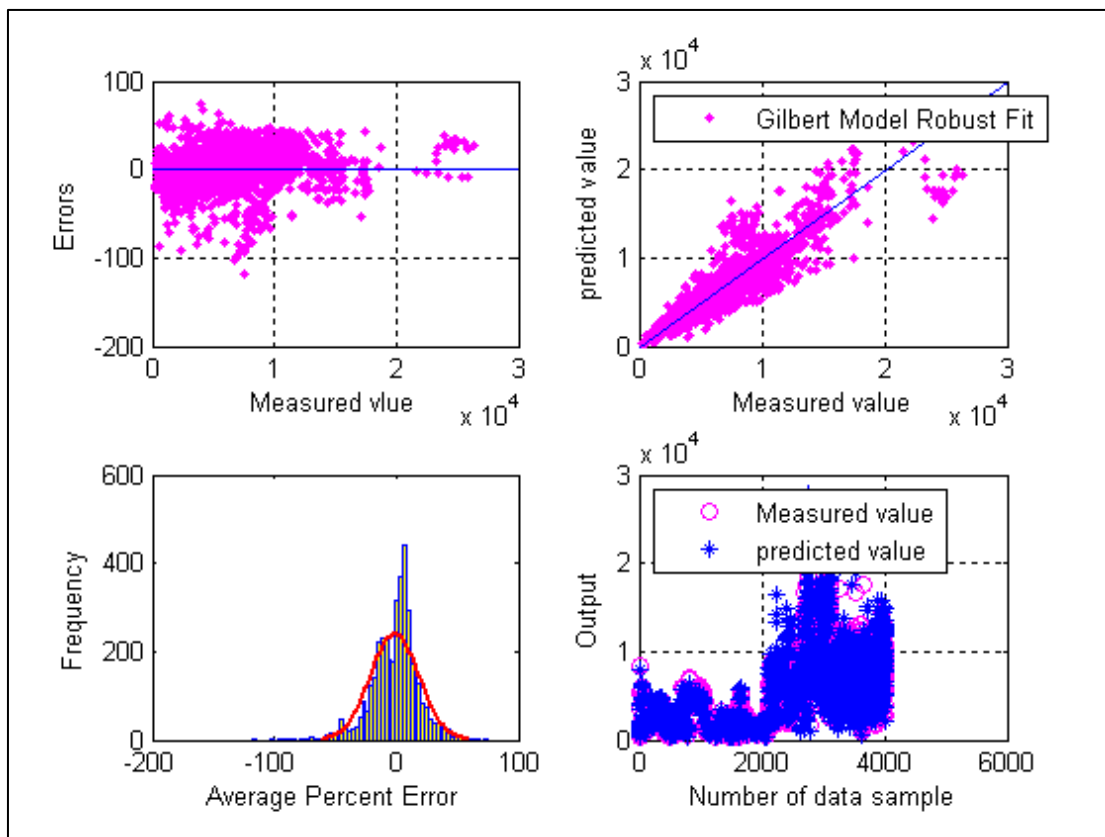


Figure-5.119: Cross, Histogram, Scatter and Overlay plots for Gilbert Empirical correlation after robust fit. (Flow Rate Estimation)

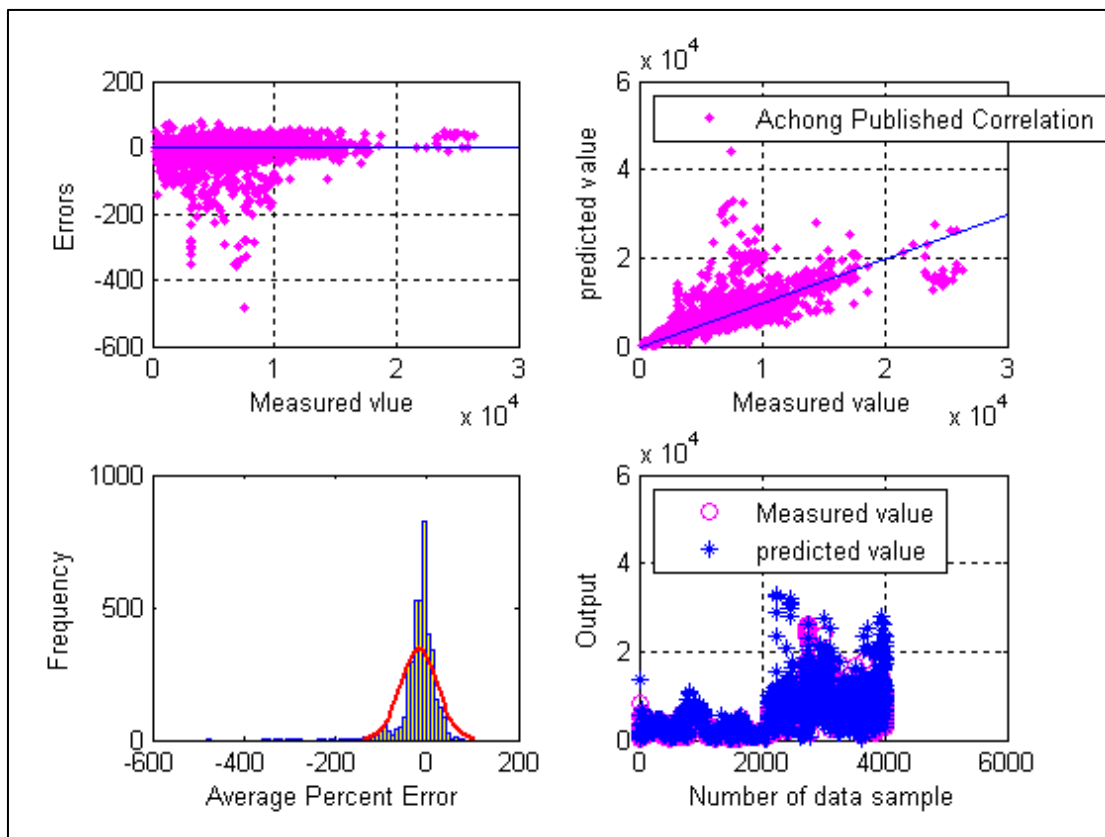


Figure-5.120: Cross, Histogram, Scatter and Overlay plots for Achong Empirical correlation. (Flow Rate Estimation)

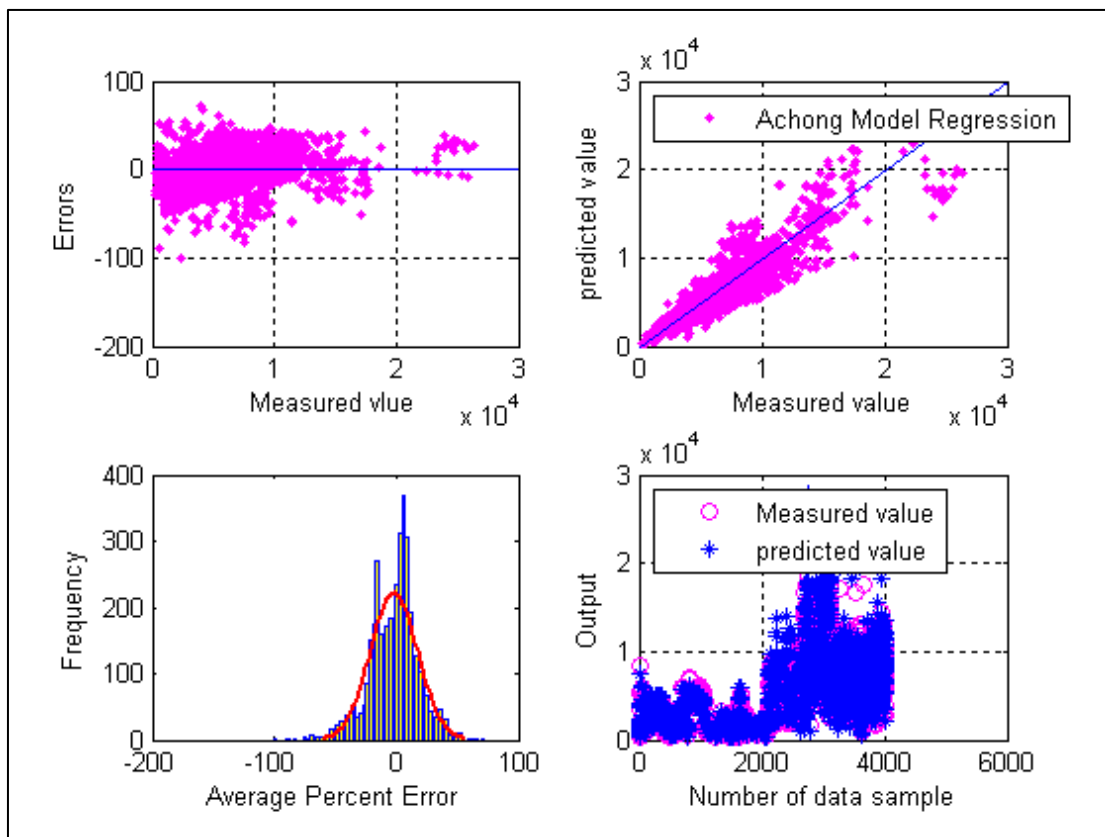


Figure-5.121: Cross, Histogram, Scatter and Overlay plots for Achong Empirical correlation after regression. (Flow Rate Estimation)

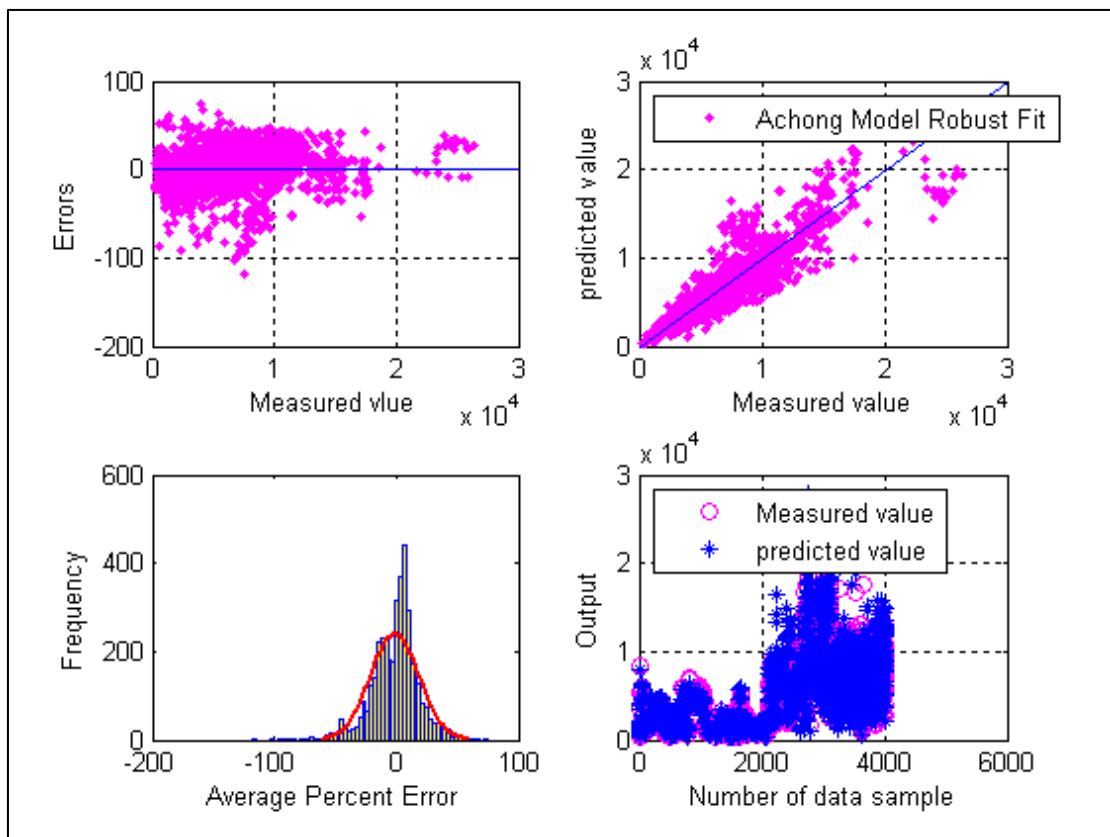


Figure-5.122: Cross, Histogram, Scatter and Overlay plots for Achong Empirical correlation after robust fit. (Flow Rate Estimation)

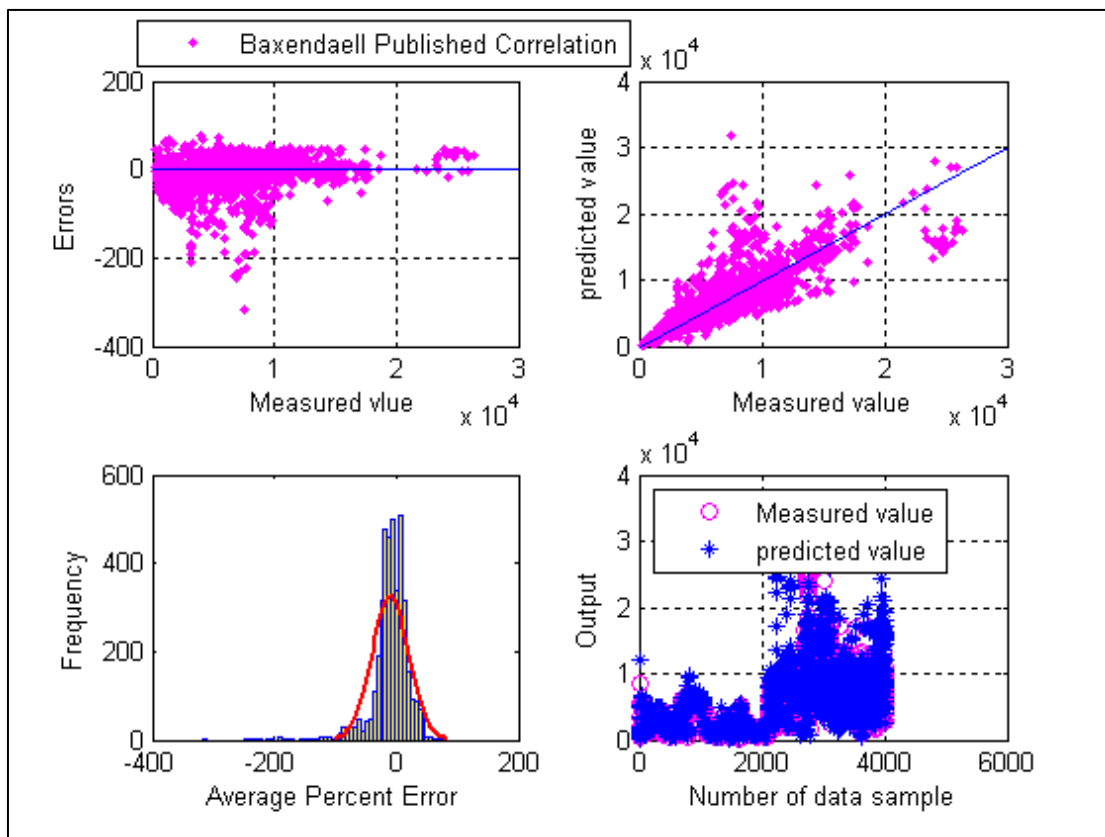


Figure-5.123: Cross, Histogram, Scatter and Overlay plots for Baxendaell Empirical correlation. (Flow Rate Estimation)



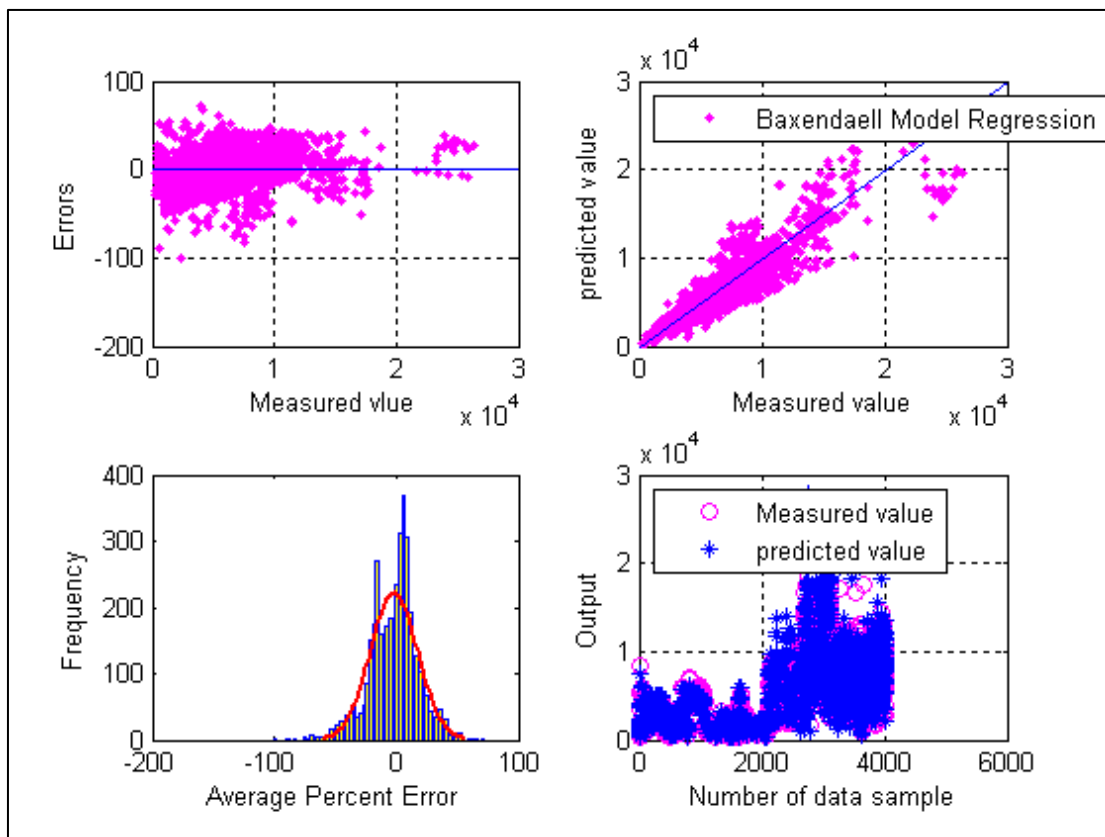


Figure-5.124: Cross, Histogram, Scatter and Overlay plots for Baxendaell Empirical correlation after regression. (Flow Rate Estimation)

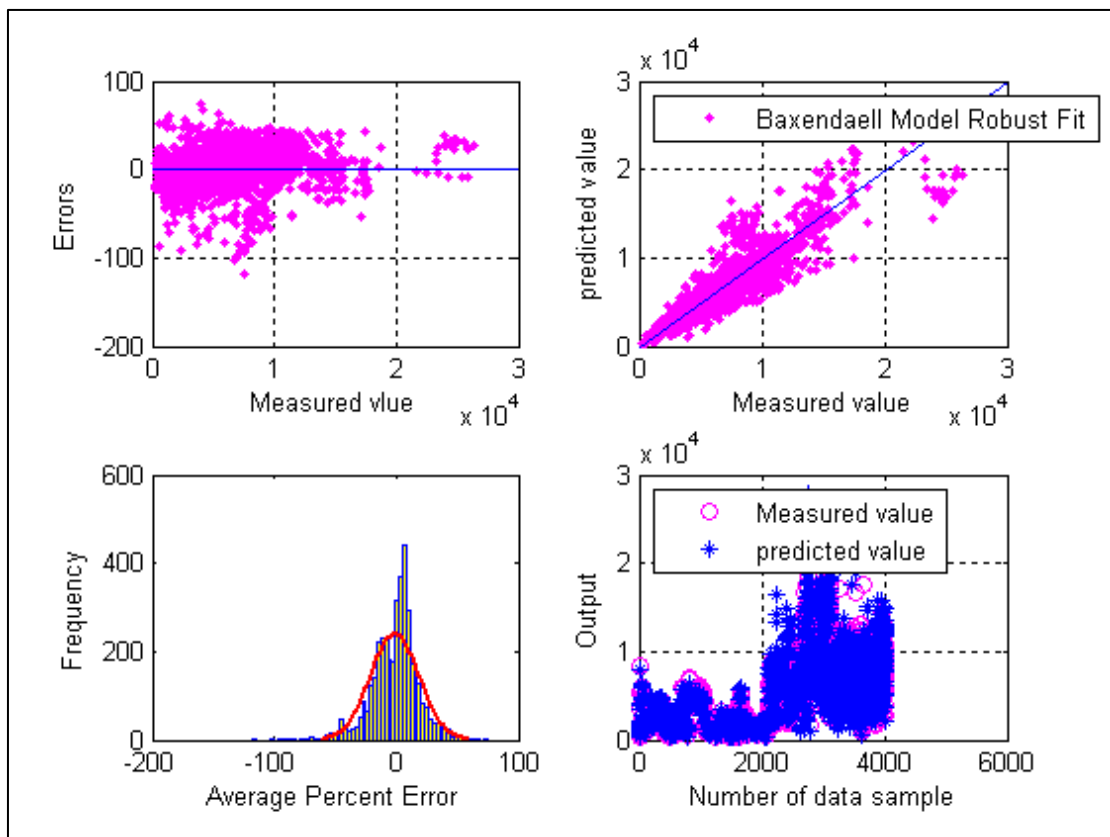


Figure-5.125: Cross, Histogram, Scatter and Overlay plots for Baxendaell Empirical correlation after robust fit. (Flow Rate Estimation)

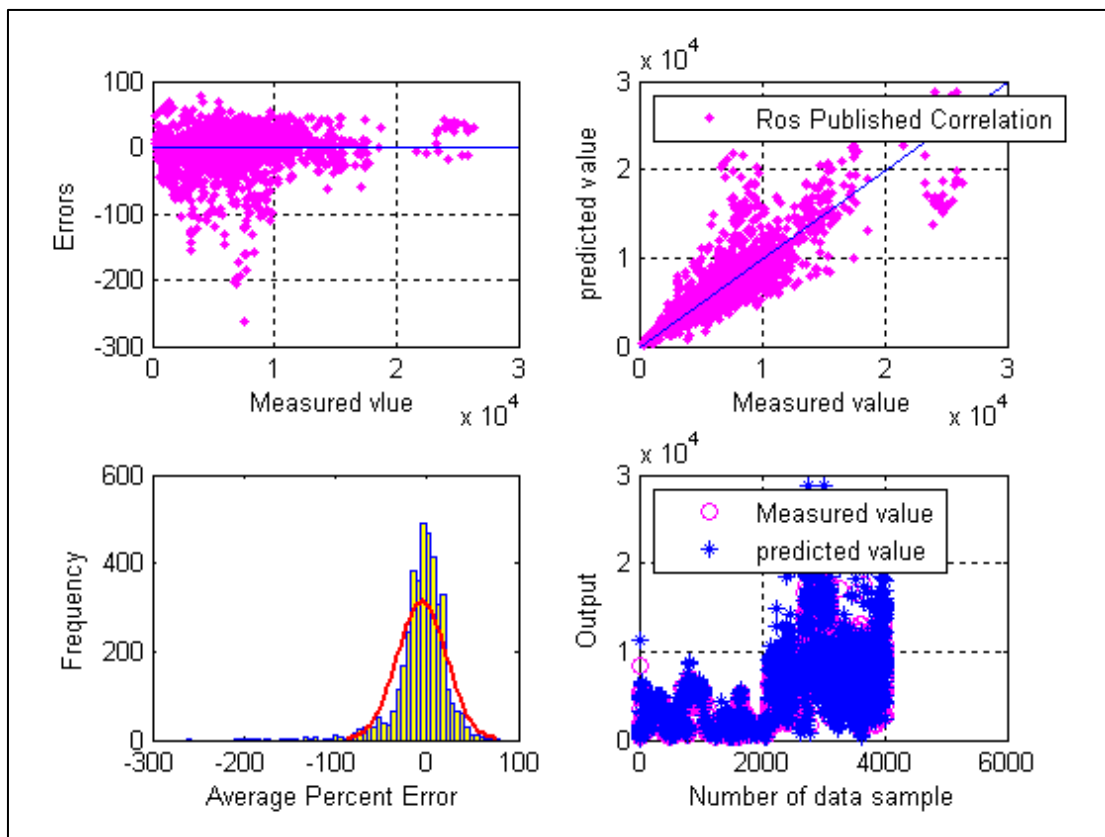


Figure-5.126: Cross, Histogram, Scatter and Overlay plots for Ros Empirical correlation. (Flow Rate Estimation)

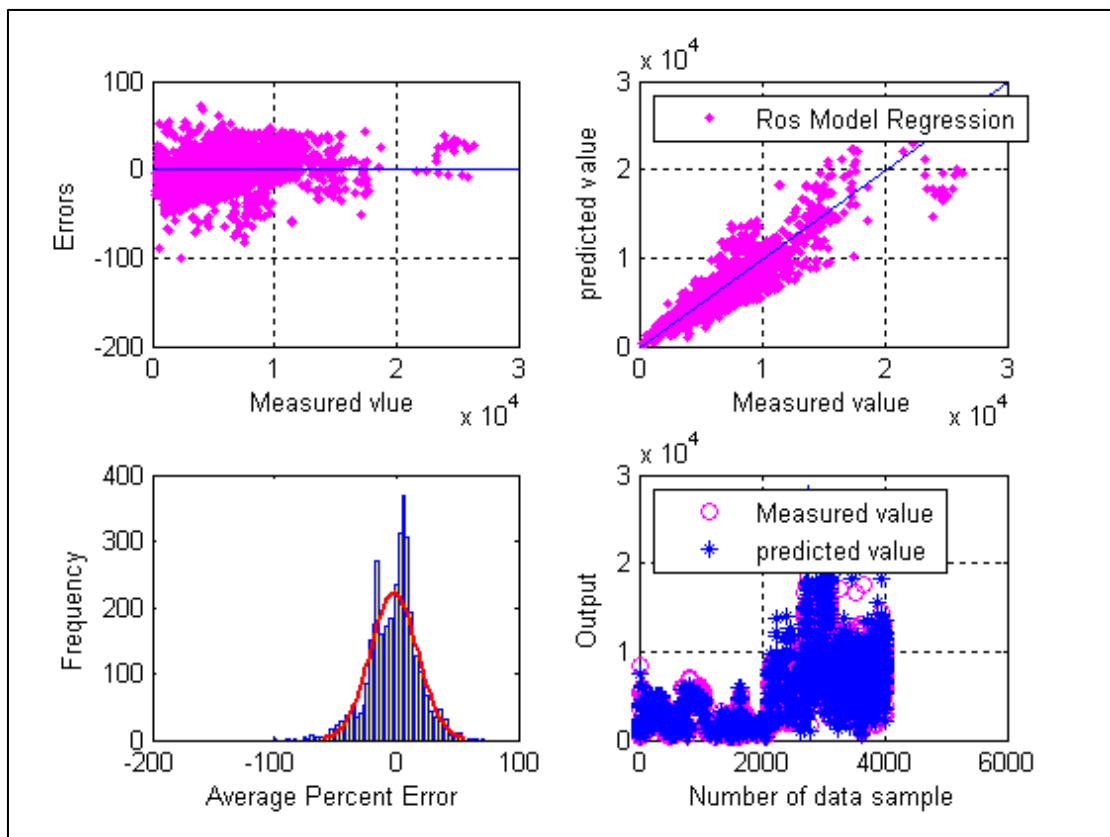


Figure-5.127: Cross, Histogram, Scatter and Overlay plots for Ros Empirical correlation after regression. (Flow Rate Estimation)

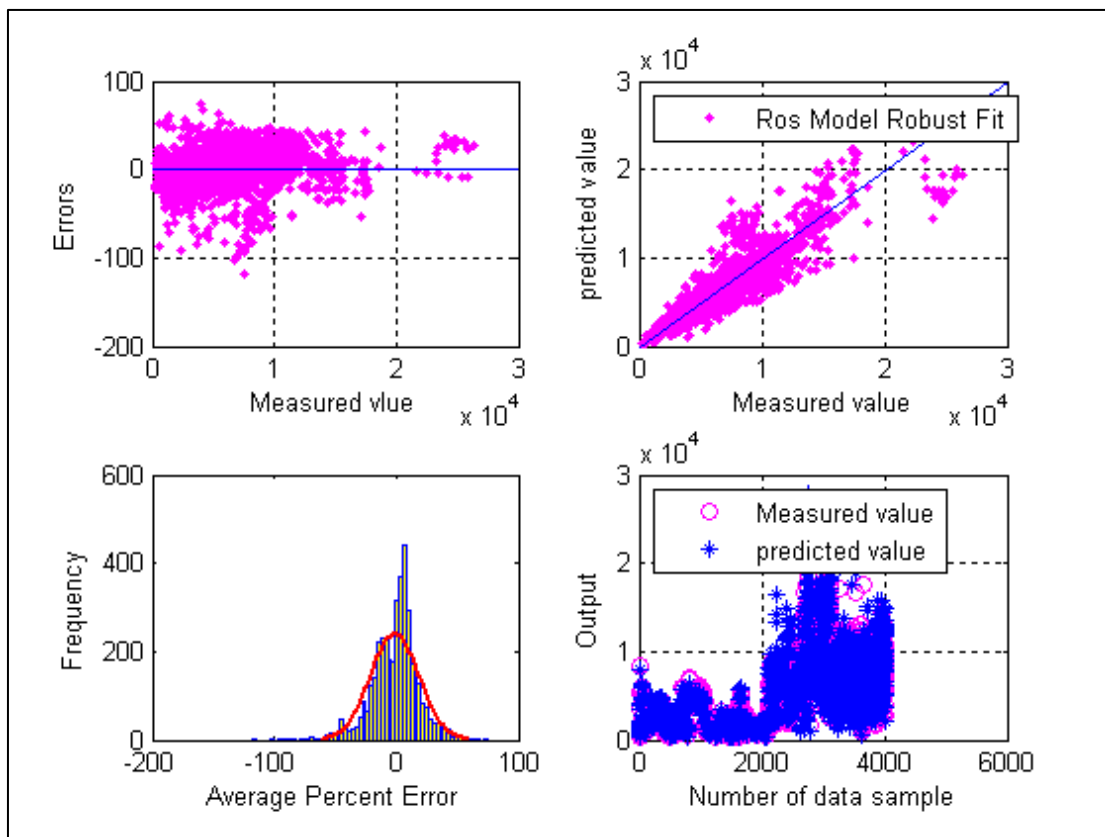


Figure-5.128: Cross, Histogram, Scatter and Overlay plots for Ros Empirical correlation after robust fit. (Flow Rate Estimation)

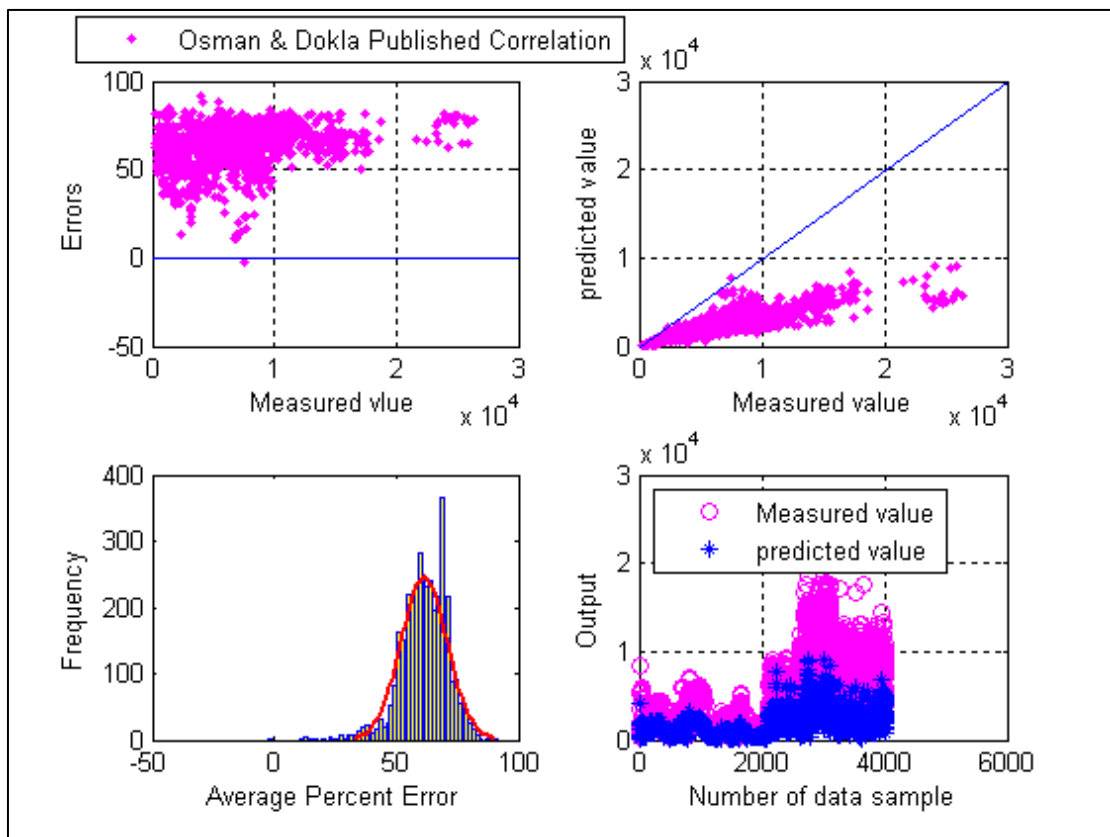


Figure-5.129: Cross, Histogram, Scatter and Overlay plots for Osman and Dokla Empirical correlation. (Flow Rate Estimation)

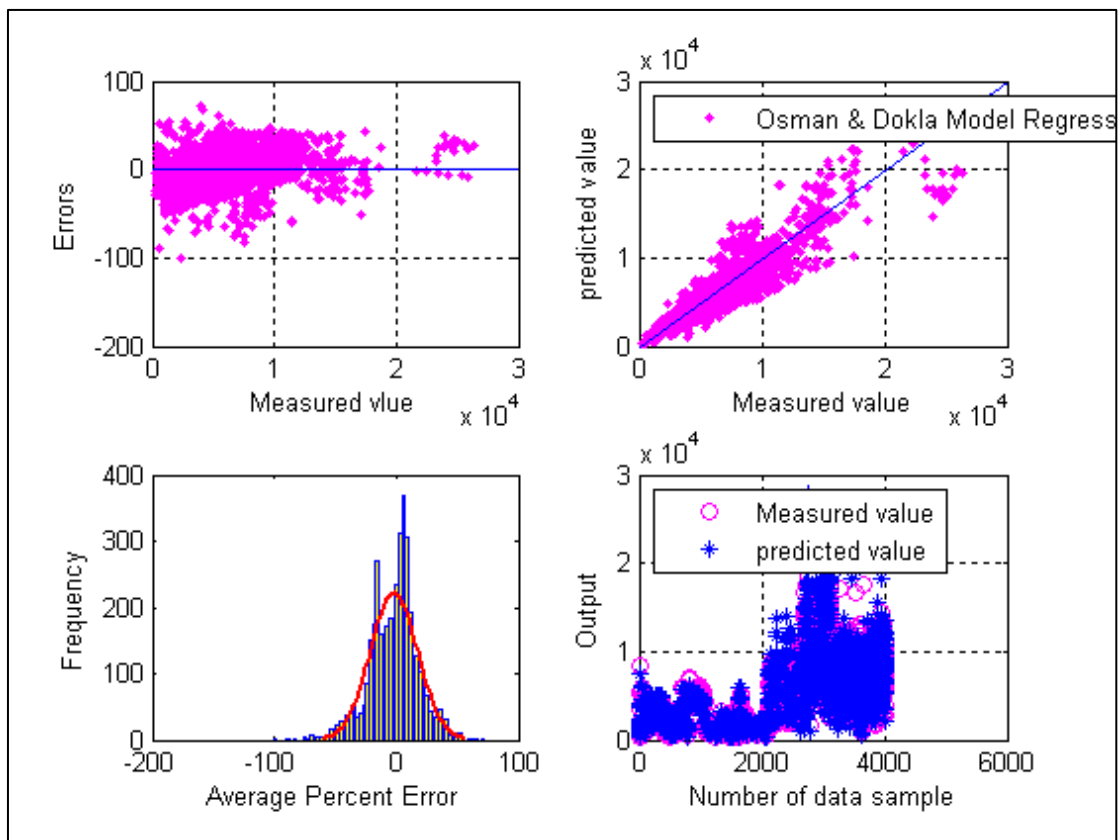


Figure-5.130: Cross, Histogram, Scatter and Overlay plots for Osman and Dokla Empirical correlation after regression. (Flow Rate Estimation)

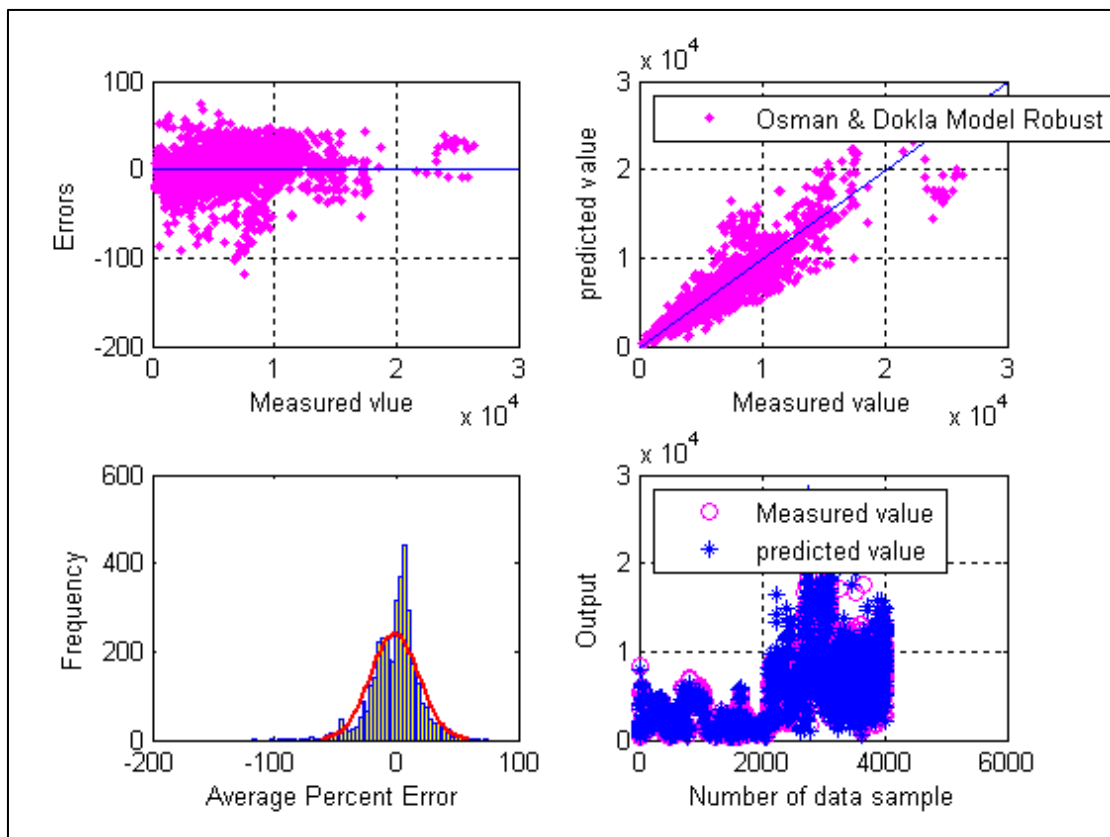


Figure-5.131: Cross, Histogram, Scatter and Overlay plots for Osman and Dokla Empirical correlation after robust fit. (Flow Rate Estimation)



## **CHAPTER 6**

### **SUMMARY AND CONCLUSIONS**

1. Two neural network models for two phase flow through chokes were developed. The first model for choke size prediction and the second for flow rate estimation.
2. The existing empirical correlations were evaluated three times, using their original coefficients, after linear/nonlinear regression and after robust regression.
3. Several statistical and graphical techniques were made to check the accuracy of the new models and to compare them with the existing correlations.
4. All the existing correlations have provided a lower error after regression compared to using the original coefficients.
5. The new models have outperformed all the existing empirical correlations, and have provided the lowest error.
6. The newly developed models can be used with high confidence within the range of the data used for developing the models.
7. The new models apply for a wide range of choke sizes and flow rates.
8. Neural network models proved to be more effective in the analysis of multiphase flow through chokes.

## REFERENCES

1. Tangren, R.F., Dodge C.H. and Seifert H.S.: "Compressibility Effects in Two-phase Flow," Journal of Applied Physics (July 1949) 637-645.
2. Gilbert, W.E.: "Flowing and Gas-Lift Well Performance," API Drilling and Production Practices (1954) 143.
3. Ros, N.C.J.: "An Analysis of Critical Simultaneous Gas-liquid Flow Through a Restriction and its Application to Flow Metering," Appl. Sci. Res. (1960) 374.
4. Ros, N.C.J.: Letter to Editor "Flowmeter Formula for Critical Gas-liquid Flow Through a Restriction," Appl. Sci. Res. (1961) 295.
5. Ros, N.C.J.: "Simultaneous Flow of Gas and Liquid as Encountered in Well Tubing," Journal of Petroleum Technology (October 1961) 1037.
6. Poetmann, F.H., and Beck, R.L.: "New Charts Developed to Predict Gas-Liquid Flow Through Chokes," World Oil (March 1963) 95-101.
7. Omana, R., Houssier C., Brown K.E., Jmnes P.B. and Richard E.T.: "Multiphase Flow Through Chokes," Paper SPE 2682 Presented at the 1969 SPE Annual Meeting, Denver CO., 28<sup>th</sup> September to 1<sup>st</sup> October.
8. Fortunati, F.: "Two-phase Flow Through Wellhead Chokes," Paper SPE 3472 Presented at 1972 SPE European Meeting, Amsterdam, May.
9. Ashford, F.E. and Pierce, P.E.: "Determining Multiphase Pressure Drops and Flow Capacities in Downhole Safety Valves," Journal of Petroleum Technology (September 1975) 45-52.

10. Pilehvari, A.A.: "Experimental Study of Critical Two-Phase Flow Through Wellhead Chokes," Tulsa, OK, University of Tulsa Fluid Flow Projects Report, (June 1981).
11. Abdul\_Majeed, G.H.: "Correlation developed to Predict Two Phase Flow Through Wellhead Chokes," Paper SPE 15839, May 1986.
12. Sachdev, A.R., Schmidt, Z., Brill J.P. and Blais, R.M.: "Two-phase Flow Through Chokes," Paper SPE 15657 Presented at the 1986 SPE Annual Technical Conference and Exhibition, New Orleans, LA, 5-8 October.
13. AL-Attar, H.H. and Abdul\_Majeed, G.H.: "Revised Bean Performance Equation for East Bagdad Oil Wells," Paper SPE 13742 Presented at 1987 Middle East Oil Show and Conference, Bahrain, 11-14 March.
14. Osman, M.E. and Dokla, M.E.: "Gas Condensate Flow Through Chokes," Paper SPE 20988, July 1988.
15. Surbey, D.W., Kelkar, B.G. and Brill, J.P.: "Study of Multiphase Critical Flow Through Wellhead Chokes," SPE production Engineering Journal (May 1989) 142-146.
16. Freeman, J.A. and David, M.S.: "Neural Networks: Algorithms, Applications, and Programming Techniques," Addison-Wesley Publishing Company, (1991).
17. Al-Towailib A.I. and Al-Marhoun, M.A.: "New Correlation for Two-phase Flow Through Chokes," M.S. Thesis, King Fahd University of Petroleum and Minerals, Dhahran, Saudi Arabia (1992).
18. Perkins, T.K.: "Critical and Subcritical Flow of Multiphase Mixture Through Chokes," SPE Drilling and Completion Journal (December 1993) 271-276.
19. Al-Towailib A.I. and Al-Marhoun, M.A.: "New Correlation for Two-phase Flow Through Chokes," Journal of Canadian Petroleum Technology (May 1994) 40-43.

20. El-Gibaly, A.M. and Nashawi, I.S.: "Prediction of Two Phase Flow Through Chokes For Middle East Oil Wells," Paper SPE 36274 Presented at 1996 Abu Dhabi International Petroleum Exhibition and Conference, UAE, 13-16 October.
21. Haykin, S. "Neural Network A comprehensive Foundation Second Edition ", Pearson Education Inc, (1999).
22. Abdul-Majeed, G. and Abual-Soof, N. "Estimation of Oil and Gas Surface Tension," Journal of Petroleum Science and Engineering (April 2000) 197-200.
23. Guo, B., Bemani, A. S. And Ghalambor, A.: "Application of Sachdeva's Choke Flow Model in Southwest Louisiana Gas Condensate Wells," Paper SPE 75507 Presented at 2002 SPE Gas Technology symposium, Calgary Alberta, Canada, 30<sup>th</sup> April to May 2.
24. Al-Rumah, M. and Al-Bizanti, M. "New Choke Correlation For Sabriyah Field Kuwait," Paper SPE 105103 Presented at 2007 Middle East Oil and Gas Show and Conference, Bahrain, 11-14 March.
25. AL-Attar, H. "Performance of Wellhead Chokes During Sub-Critical Flow of Gas Condensates," Journal of Petroleum Science and Engineering (August 2007) 205-212.
26. Ghareeb, M. and Shedid A.S.: "A New Correlation For Calculating Wellhead Production Considering Influences of Temperature GOR, and Water Cut for Artificially Lifted Wells," Paper IPTC 11101 Presented at 2007 International Petroleum Technology Conference, UAE, 4-6 December.
27. Al-Safran, E.M. and Kelker, M. "Prediction of Two-Phase Critical Flow Boundary and Mass Flow Rate Across Chokes," Paper SPE109243 Presented at 2007 SPE Annual Technical Conference, USA, 11-14 November.
28. Mesallati, A., Bizanti, M. and Mansouri, N.: "Multi Phase Choke Correlations for Offshore Bouri Oil Field," Paper 758966, National oil Corporation, Tripoli, Libya.

# VITAE



Name: Mohammed Abdul Jaleel Al-Khalifa

State of Origin: Saudi Arabia

Nationality: Saudi

Email: [mohammed.khalifah.3@aramco.com](mailto:mohammed.khalifah.3@aramco.com)

Address: Saudi Aramco Box# 2157, Dhahran 31311,  
Eastern Province, Kingdom of Saudi Arabia

Education: **MS (Petroleum Engineering), June 2009**  
King Fahad University of Petroleum & Minerals  
Dhahran, Saudi Arabia

**B.Sc. (Petroleum Engineering), June 2006**  
King Fahad University of Petroleum & Minerals  
Dhahran, Saudi Arabia

Experience: Joined Saudi Aramco and worked as a facility engineer for 30 months and as a reservoir engineer in reservoir management department for 6 months. He is also a member of several technical societies and has an active role in the society of Petroleum Engineers (SPE). He served in 2004 as the secretary of SPE-KFUPM student chapter and as the treasurer in 2007 for the SPE first Young Professional Technical Symposium.